AD-A098 733 CHARLES STARK DRAPER LAB INC CAMBRIDGE MA F/G 7/2
EFFECTIVE VISCOSITY OF LIQUID HELIUM4 - WITH MINUTE HE3 IMPURIT--ETC(U)
MAR 81 R C PANDORF N00014-77-C-0295
UNCLASSIFIED R-1403 ONR-CR-007-003-1F NL

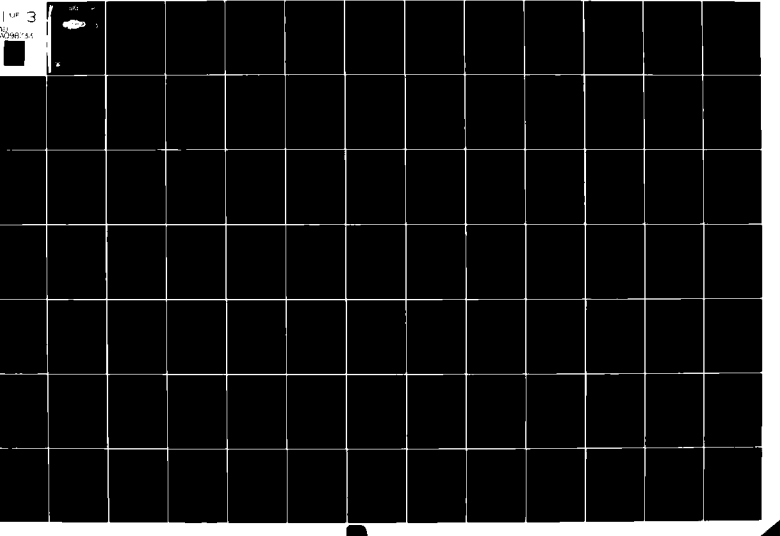

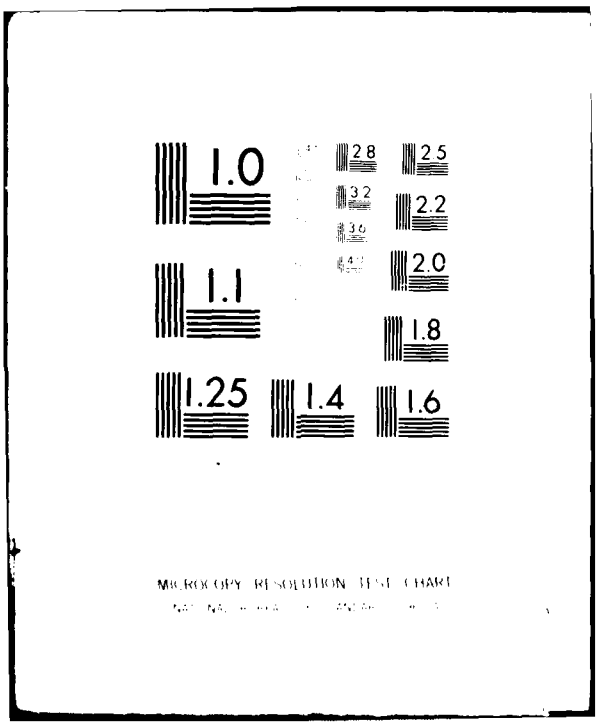
1.0
1.1
1.25
1.4
1.6
1.8
2.0
2.2
2.5
2.8
3.2
3.6
4.0
MICROCOPY RESOLUTION TEST CHART

LEVEL II

REPORT ONR CR-007-003-1F

EFFECTIVE VISCOSITY OF LIQUID HELIUM^4

WITH MINUTE He^3 IMPURITY AT TEMPERATURES FROM 0.05K TO 2K AND AT VELOCITIES SPANNING THE CRITICAL VELOCITIES

R. C. PANDORF, Ph.D
THE CHARLES STARK DRAPER LABORATORY, INC.
CAMBRIDGE, MASSACHUSETTS 02139

CONTRACT N000014-77-C-0295
ONR TASK 007-003

MARCH 1981

PREPARED FOR THE
OFFICE OF NAVAL RESEARCH • 800 N. QUINCY ST. • ARLINGTON, VA. 22217

SECURITY CLASSIFICATION OF THIS PAGE *(When Data Entered)*

REPORT DOCUMENTATION PAGE

READ INSTRUCTIONS BEFORE COMPLETING FORM

1. REPORT NUMBER: ONR CR-007-003-1F	2. GOVT ACCESSION NO.: AD-A098 733
3. RECIPIENT'S CATALOG NUMBER:	
4. TITLE *(and Subtitle)*: Effective Viscosity of Liquid Helium^4 - With Minute He^3 Impurity at Temperatures From 0.05K to 2K and at Velocities Spanning the Critical Velocities	5. TYPE OF REPORT & PERIOD COVERED: Final Report,
	6. PERFORMING ORG. REPORT NUMBER: R-1403
7. AUTHOR(s): Robert C. Pandorf, Ph.D.	8. CONTRACT OR GRANT NUMBER(s): N00014-77-C-0295
9. PERFORMING ORGANIZATION NAME AND ADDRESS: The Charles Stark Draper Laboratory, Inc., 555 Technology Square, Cambridge, MA 02139	10. PROGRAM ELEMENT, PROJECT, TASK AREA & WORK UNIT NUMBERS
11. CONTROLLING OFFICE NAME AND ADDRESS: Cdr. Roger A. Nichols, Office of Naval Research, 800 N. Quincy Street, Washington, DC 22217	12. REPORT DATE: March 1981 13. NUMBER OF PAGES
14. MONITORING AGENCY NAME & ADDRESS *(if different from Controlling Office)*: Dr. David C. Lewis, Office of Naval Research, 800 N. Quincy Street, Washington, DC 22217	15. SECURITY CLASS. *(of this report)*: Unclassified 15a. DECLASSIFICATION/DOWNGRADING SCHEDULE

16. DISTRIBUTION STATEMENT *(of this Report)*

17. DISTRIBUTION STATEMENT *(of the abstract entered in Block 20, if different from Report)*

Approved for public release; distribution unlimited.

18. SUPPLEMENTARY NOTES

19 KEY WORDS *(Continue on reverse side if necessary and identify by block number)*

normalfluid; superfluid; turbulence; viscosity; liquid He^4; liquid He^3 impurity; critical velocity; mean free path; specular reflection; Couette viscometer; unperturbed rotor; precision gyroscope; neutrally buoyant rotor; frictionless rotor; principle of equivalence; Eötvös experiment; inertial sensor; cryogenics; low temperatures

20. ABSTRACT *(Continue on reverse side if necessary and identify by block number)*

This report presents a comprehensive analy s of three Experimental Series on the measurements of the effective viscosity of liquid He^4 with minute He^3 impurity taken with a Couette viscometer at temperatures between 0.05K and 2K, and at viscometer velocities which span the liquid helium critical velocities. A comprehensive theory of the velocity independent effective viscosity of liquid He^4 with minute He^3 impurity is developed for parallel plate geometry and is found to well represent the experimental measurements.

DD FORM 1 JAN 73 1473 EDITION OF 1 NOV 65 IS OBSOLETE

SECURITY CLASSIFICATION OF THIS PAGE *(When Data Entered)*

20. Abstract (cont.)

The velocity independent viscosity measurements taken at temperatures above 0.8K were in agreement with the experimental measurements of the coefficient of viscosity made by Woods and Hollis Hallet. As the temperature T was lowered below 1.8K, the viscosity rose rapidly, approaching a T^{-9} temperature dependence. Then below 0.8K the rapid rise quickly diminished. Near the temperature 0.65K the observed viscosity reached a maximum value between 220 and 300μP depending upon the viscometer's fluid gap, d, and then fell at a rate somewhat greater than T^4 by over three orders of magnitude to values below the sensitivity of the viscometer. Within the sensitivity of the viscometer of 0.1μP, no measurable viscosity was observed below 0.1K for liquid He^4 of high purity. With the presence of minute amounts of He^3 impurity the observed viscosity approximated a $T^{\frac{1}{2}}$ temperature dependence below about 0.2K.

Two distinct regions of velocity dependent effective viscosity were observed. In the temperature region above the maximum effective viscosity peak near 0.65K, velocity dependent viscosity was initiated above the critical velocity $v_{n,c}$ where $v_{n,c}\, d \simeq 10^{-2}$. However, this velocity dependent viscosity component vanished below the viscosity peak near 0.65K. On the other hand, in the temperature region below the maximum in the effective viscosity peak, the velocity dependent viscosity was initiated above the critical velocity $v_{s,c}$ where $v_{s,c}\, d^{\frac{1}{4}} \simeq 1$. This latter velocity dependent viscosity component was observed to diminish rapidly with falling temperatures as T^4. Phenomenological equations for these velocity dependent viscosity components are developed in this report.

The diminution in the effective viscosity of liquid He^4 of high purity is so rapid that it extrapolates to a nearly frictionless fluid at temperatures below 0.1K. This nearly frictionless property of liquid He^4 should provide unprecedented opportunities for the development of inertial instruments of the highest precision.

This report includes a discussion of the application of a neutrally buoyant spherical rotor in liquid helium to an experimental test of the Principle of Equivalence and to an ultraprecision gyroscope.

R-1403

EFFECTIVE VISCOSITY OF LIQUID HE^4 With Minute He^3 Impurity at Temperatures From 0.05K to 2K and at Velocities Spanning the Critical Velocities

By

R. C. Pandorf, Ph.D.

139 Winchester Street
Newton Highlands, MA 02161

March 1981

Approved: Forrest E. Houston
Forrest E. Houston

The Charles Stark Draper Laboratory, Inc.
Cambridge, Massachusetts 02139

ACKNOWLEDGEMENTS

It should be pointed out that this work rests upon the foundations built by the Helios Program (Experimental Series I) and the people who contributed to that program. Special recognition must go to Paul R. Kerrigan, Helios Program Manager; Charles R. Dauwalter and Erwin Schowengerdt, mechanical engineering; James R. Clow, cryogenics; and Burton Boxenhorn, electronics. Robert F. Strong laid out the cryogenic systems which not only functioned with efficiency, but were a work of art.

Mr. Dauwalter's contribution to these programs has been considerable. During the Experimental Series I and II, he provided substantial engineering talent to the programs. His contributions go beyond any normal expectations. During experimental test periods he spent many all day and night sessions for days on end working on the apparatus and recording experimental data. Although he was not a part of the staff during Experimental Series III, he provided valuable advice and assistance to this program. He also provided valuable suggestions for improving this report and assisted in the editing. Mr. Schowengerdt was on the Helios Program staff and made a substantial contribution to that program. Although he was not on the staff during Experimental Series II and III, his time, talents, expertise and knowledge of the instrument was extensively utilized.

Robert W. Barden, with 20 years of work experience at Draper Laboratory, joined the program for Experimental Series III. It was due

to his talents and skills that substantial progress was made in improving the experimental apparatus. His careful, meticulous and well thought out designs and work brought excellent solutions to our many electrical and mechanical problems. He is a gifted person with many talents for working in research and development. His keen interest and enthusiasm for his work and this program went far beyond any normal job expectations or requirements. Many a time he would start a difficult project and at the end of the day would take his books and materials home only to return the next morning with the project completed.

The contribution by the technician staff was indispensible and special tributes go to Alfred U. Bilunas, John J. McLean, George Lauzon and Philip Lerman. Project technician Mr. Bilunas worked throughout all three programs. Mr. McLean, now age 75, worked half time with the vigor of a man half his age. From the beginning in 1971 he contributed a vast reservoir of technical experience.

It is difficult to imagine these cryogenic programs at Draper Laboratory without Benjamin M. Hildebrant. Being familiar with the problems facing inertial instrumentation, he immediately saw the role cryogenics could play in the development of ultra precision inertial instruments. He enthusiastically worked for the support of these cryogenic programs and was a constant source of encouragement to its staff. Also he has contributed many suggestions and ideas to this report and has been an endless source of encouragement during its writing.

The support by Robert A. Duffy, the President of Draper Laboratory, made Independent Research and Development (IR&D) funds available for Experimental Series II.

This report could not have been written without the support provided by Eleanor M. Pandorf, the author's wife.

We wish to acknowledge Helen M. Hobson for her contribution of typing and coordinating many of the tasks of this report and Jane Bisbee for the final typing.

We wish to thank Dr. David Lewis for his helpful comments and suggestions on this report and for his interest and assistance as our ONR representative.

Space does not permit the naming of all the talented people who have contributed to these programs, but their efforts are remembered and this report is dedicated to all the people who have contributed.

This report was prepared by The Charles Stark Draper Laboratory, Inc. under contract N000014-77-C-0295 with the Office of Naval Research. Publication of this report does not constitute approval by the U. S. Navy of the findings or the conclusions contained herein.

TECHNICAL SUMMARY

This report presents a comprehensive analysis of three Experimental Series on the measurements of the effective viscosity of liquid He^4 with minute He^3 impurity. The measurements were taken with a Couette viscometer at a constant density of 0.146 gm/cm^3, and at temperatures between 0.05K and 2K. The viscometer's inner cylinder, suspended from a tungsten torsion fiber, measured the viscous torques. Measurements were made with the outer cylinder rotating at tangential velocities from 0.04 cm/s to 21 cm/s. Three different fluid gap/inner/outer cylinder configurations were investigated: 0.0498 cm/Be/Mg; 0.152 cm/Glass/Al; and 0.125 cm/Glass/Al. The inner cylinder's heights were in the range of 8 to 10 cm and the radius approximately 5 cm.

The velocity independent viscosity measurements taken at temperatures above 0.8K were in agreement with the experimental measurements of the coefficient of viscosity made by Woods and Hollis Hallet. As the temperature was lowered below 1.8K the viscosity rose rapidly, approaching a T^{-9} temperature dependence, and then below 0.8K the rapid rise quickly diminished. Near 0.65 the observed viscosity reached a maximum value between 220 and 300μP, depending upon the fluid gap (d), and then fell at a rate somewhat greater than T^4 by over three orders of magnitude to values below the sensitivity of the viscometer. Within the sensitivity of the apparatus of 0.1μP no measurable viscosity was observed below 0.1K for liquid He^4 of high purity. With the presence of minute amounts of He^3 impurity the observed viscosity approximated a $T^{\frac{1}{2}}$ temperature dependence below about 0.2K.

A comprehensive theory of the velocity independent effective viscosity of liquid He^4 with minute He^3 impurity is presented for parallel plate geometry. Although the complete expression for the effective viscosity can be written in closed form, it is much too long and complex to rewrite in this abstract. At high temperatures where the mean free path (l_{ph}) of the phonon excitations is much less than the fluid gap (i.e. $l_{ph} << d$) this equation reduces to an expression similar to that developed by Zharkov. For pure He^4 at low temperatures where $l_{ph} >> d$ the phonon component of the effective viscosity η_{ph} reduces to an equation analogous to the Knudsen equation for a gas. In this case the effective viscosity η_o becomes equal to the phonon component η_{ph} which is proportional to the product of the phonon density $\rho_{ph} \simeq 1.78\ 10^{-5}\ T^4$ gm/cm^3, the velocity of sound $c \simeq 2.38\ 10^4$ cm/s and the fluid gap d, but with the added feature that the long wavelength nature of the phonon excitations permits extensive specular reflection. This specular reflection causes an augmentation of the rapid diminution of the phonon component of the effective viscosity with decreasing temperature. It was found that $\eta_{ph} = \frac{1}{4}\ \gamma\ f\ \rho_{ph} c\ d$. Using a simple surface model, γ was found to approximate the fractional surface area over which the phonons are diffusely scattered. The term f is a function of the temperature T. At the highest temperatures $f \simeq 1$, while at the very lowest temperatures the theoretical function f decreases very rapidly with temperature: $f \simeq (30/4\pi^4)\ x^3\ e^{-x}$ for $x \simeq 114/(T\ \delta) << 1$. In the simple surface model, δ represents the overall surface roughness dimension or asperity in dimensional units of angstroms and the function f represents the fractional density of diffusely scattered phonons. In the higher temperature regions where the effective viscosity was large enough to measure, a comparison between the theoretical equation and the experimental measurements was made. For the three experimental configurations mentioned above, γ = .316/.285/.310 and δ = 150Å/100Å/130Å provided a good representation of the experimental measurements.

At tangential velocities above the velocity $v_{n,c}$ and at temperatures above the maximum in the effective viscosity near 0.65K, the

viscosity became velocity dependent. The observed values of $v_{n,c}$ were consistent with the empirical equation for the onset of turbulence: $v_{n,c}\, d \simeq 10^{-2}$. The velocity dependent part of the effective viscosity $\eta_{n,t} = \eta - \eta_o$ measured above $v_{n,c}$ could be well represented by the phenomenological relation: $\eta_{n,t} = 3.7\ 10^{-4}\, \rho\, d\, (v - v_{n,c})$ where η_o is the velocity independent viscosity, ρ is the total density, and v the tangential velocity of the viscometer's outer cylinder where $v > v_{n,c}$.

At temperatures <u>below</u> the maximum in the effective viscosity, the effective viscosity η became velocity dependent above the tangential velocity $v_{s,c}$ where $v_{s,c}$ was consistent with the empirical equation for the critical velocity: $v_{s,c}\, d^{\frac{1}{4}} \simeq 1$. The velocity dependent part of the effective viscosity $\eta_{s,t} = \eta - \eta_o$ is well represented by the phenomenological equation $\eta_{s,t} \simeq 3.1\, \rho_{ph}\, d^{\frac{1}{4}}\, (v - v_{s,c})$, P, where ρ_{ph} is the normal fluid density and at low temperatures $\rho_{ph} \simeq 1.78\ 10^{-5}\ T^4$ gm/cm^3.

The velocity dependent component of the effective viscosity that occured <u>above</u> the viscosity maximum near 0.65K; namely, $\eta_{n,t}$ is thought to be due to turbulence initiated in the normal fluid or phonon excitations. <u>Below</u> the temperature 0.65K where $\ell_{ph} >> d$, the turbulence in the phonon excitations is suppressed with the result that $\eta_{n,t} \to 0$. The velocity dependent effective viscosity component $\eta_{s,t}$ which occured at temperatures <u>below</u> the effective viscosity maximum is thought to be due to turbulence in the superfluid. As one can see, this turbulent viscosity component $\eta_{s,t}$ is rapidly diminishing with temperature as T^4.

The diminution in the effective viscosity of liquid He^4 of high purity is so rapid that it extrapolates to a nearly frictionless fluid at temperatures below 0.1K. This nearly frictionless property of liquid He^4 should provide unprecedented opportunities for the development of inertial instruments of the highest precision.

This report includes a discusssion of the application of a neutrally buoyant spherical rotor in liquid helium to an experimental test of the Principle of Equivalence and to an ultra precision gyroscope. The implications of an ultra precision gyroscope for the strategic submarine fleet are outlined.

Structure Diagram of Comprehensive Analysis

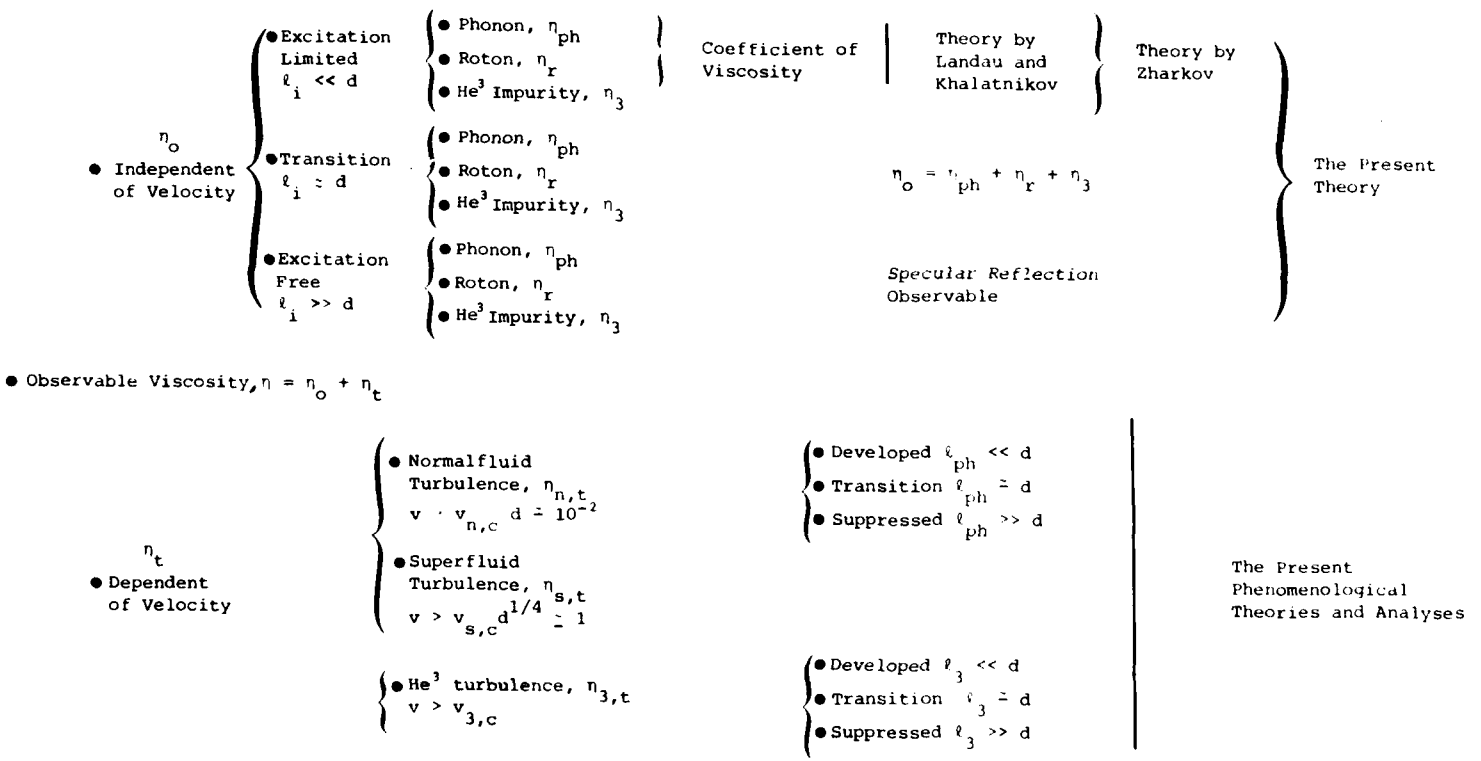

TABLE OF CONTENTS

TABLE OF CONTENTS (Cont.)

SECTION 1

POTENTIAL

1.1 INTRODUCTION

The errors in initial position, velocity and heading of an inertially guided ballistic missile at launch give rise to associated targeting errors. Land based missiles, with well surveyed launch sites, are near ideal in reducing these errors. For obvious reasons, it would be of great value if a nuclear submarine could navigate submerged for several months without dependence upon external fixes, and at any time during that period know its position, velocity and heading accurately enough to launch missiles with a targeting accuracy comparable to silo launched systems.

The weakest link in the submarine navigation system that precludes achieving the desired navigational accuracy is the gyroscope. Gyros with sufficient performance capability to meet the goals of the FBM navigation system do not exist today. The present instruments are characterized by inaccuracies that tend to grow unacceptably with time. At present this limitation is circumvented by frequently updating the inertial navigation system with inputs from external sources. Resets can be made by using sonar or by surfacing or nearly surfacing and using radio aids or satellites or some combination of these. Operations of this type tend to decrease the mission effectiveness or compromise the mission to some degree.

The development of a gyroscope based on the physical phenomena discussed in this report will strengthen the inertial guidance technology to the degree that launch coordinates comparable to land based systems could be obtained on a vheicle operating completely submerged over a period of months.

1.2 The Role of the Unperturbed Gyro Rotor

An inertial navigation system consists of the following components:

a) A frame of reference which is established by the use of gyroscopes

b) Measurements of acceleration or specific force with respect to the reference frame by accelerometers

c) Knowledge of the gravitational field which is obtained by gradiometers and/or augmented when possible by prior survey information

d) A computer system to perform the analytic computations of velocity, position and heading.

Accelerometers, gradiometers and computers either exist or are in the development stage which could possibly meet most of the desired performance goals. However, it is generally agreed that gyro performance must be considerably improved in order to achieve an ultraprecision inertial navigation system.

The question should be asked whether such a high performance gyro goal is possible. The laws of physics tell us that angular momentum if left unperturbed (i.e. with no applied torques) will be fixed in inertial space with no drift, the perfect gyro. This tells us that a straight forward solution to the ultraprecision gyro lies with a device which best approximates the unperturbed angular momentum. The performance of the free electrostatic gyro (ESG) which is not torqued bears out this notion. Yet the ESG is not as unperturbed as it could be. First, the strong electrostatic support forces couple to the asphericity of the rotor to produce torques. Second, the viscous drag of the residual gas requires the rotor to be continually torqued (driven). Both of these torques contribute significantly to the uncertainty in the drift of the angular momentum of the ESG's gyro rotor.

The gyro which is probably the least perturbed is the ESG type of free spherical rotor proposed by the Stanford University Group[1] for use in a satellite to measure relativity effects. This gyro has been predicted to have the remarkably small uncertainty of 0.001 $\widehat{sec}$ per year. Both of the above mentioned torque sources are virtually eliminated in this gyro. First, the satellite gyro is in free fall so the support forces are negligible. Second, this gyro rotor operates in a vacuum at cryogenic temperatures (~4K) and will be in a near drag free environment so that the continuous drive torquer can be eliminated. Furthermore, the cryogenic temperatures impart dimensional stability and provide opportunities for optimum control of the environmental perturbations not available for a room temperature instrument.

The next best thing to free fall for maintaining the position of the free rotor is neutral buoyancy. Neutral buoyancy in an incompressible fluid has the property that the position of the center of buoyancy or the center of support for any arbitrary shape is independent of its orientation. In other words, the support force is spherically symmetric about a fixed center of support. The torque couple created by the lever arm between the center of mass and the center of support can be made arbitrarily small by balancing. Any remaining residual torque would then lead to a predictable gyro drift.

The problem with fluids, however, is their viscous drag. That brings us to the present concept of the neutrally buoyant, frictionless rotor. On the basis of our theoretical and experimental work on liquid He^4 over nearly the last decade, we have concluded that liquid He^4 has the desired properties of this ideal frictionless gyro fluid. Our studies indicate that a gyro rotor under suitable conditions of low temperature will have a run down or relaxation time of many years. This should eliminate the need to continuously drive the rotor and thus eliminate a significant source of torque which causes gyro drift error.

The best shape for an unperturbed gyro rotor is spherical. This is because any radial forces F(r) such as gravitational, electrostatic,

etc. which act on a spherical rotor of homogeneous and isotropic material (i.e. one with spherical symmetry) will be independent of the orientation of the rotor and thus cannot apply a torque to the rotor. Also because liquid He^4 is a somewhat compressible fluid, the desire for spherically symmetric buoyancy requires the rotor to be spherical.

As for the best material for an unperturbed gyro rotor, there is no single and simple answer. Briefly, the material needs to have a high strength to density ratio, be physically and chemically stable, be highly polishable in its surface finish and in general be unperturbed by external force fields. To a great extent, shortcomings in the stability of the rotor material will be significantly mitigated by the cryogenic temperatures. Also, the cryogenic temperatures provide opportunities for enhanced magnetic shielding, temperature control and precision instrumentation not available near room temperature.

1.3 An Approach to the Unperturbed Gyro

In Figure 1.1 is presented an artist's view of a gyro instrument. This instrument would be about 20cm across and would be immersed in a dewar of liquid helium at 4K along with any other required sensors.

In Figure 1.1 the various parts are labeled for the gyro instrument, however, other kinds of sensors might look similar since most of the details have to do with the cryogenics. The ultra-low temperature liquid He^4, which provides the neutral buoyancy without friction, is located in the gap between the rotor and the gyroscope instrument case. This figure visualized a 360 degree of freedom angular pickoff. However, on an inertially stabilized instrument platform, a null reading type of angular pickoff would be used.

The parts labeled still, heat exchangers and mixing chamber depict parts of a refrigeration system which has the capability of providing continuous cooling to below 0.01K, which is well below the gyro working temperature.

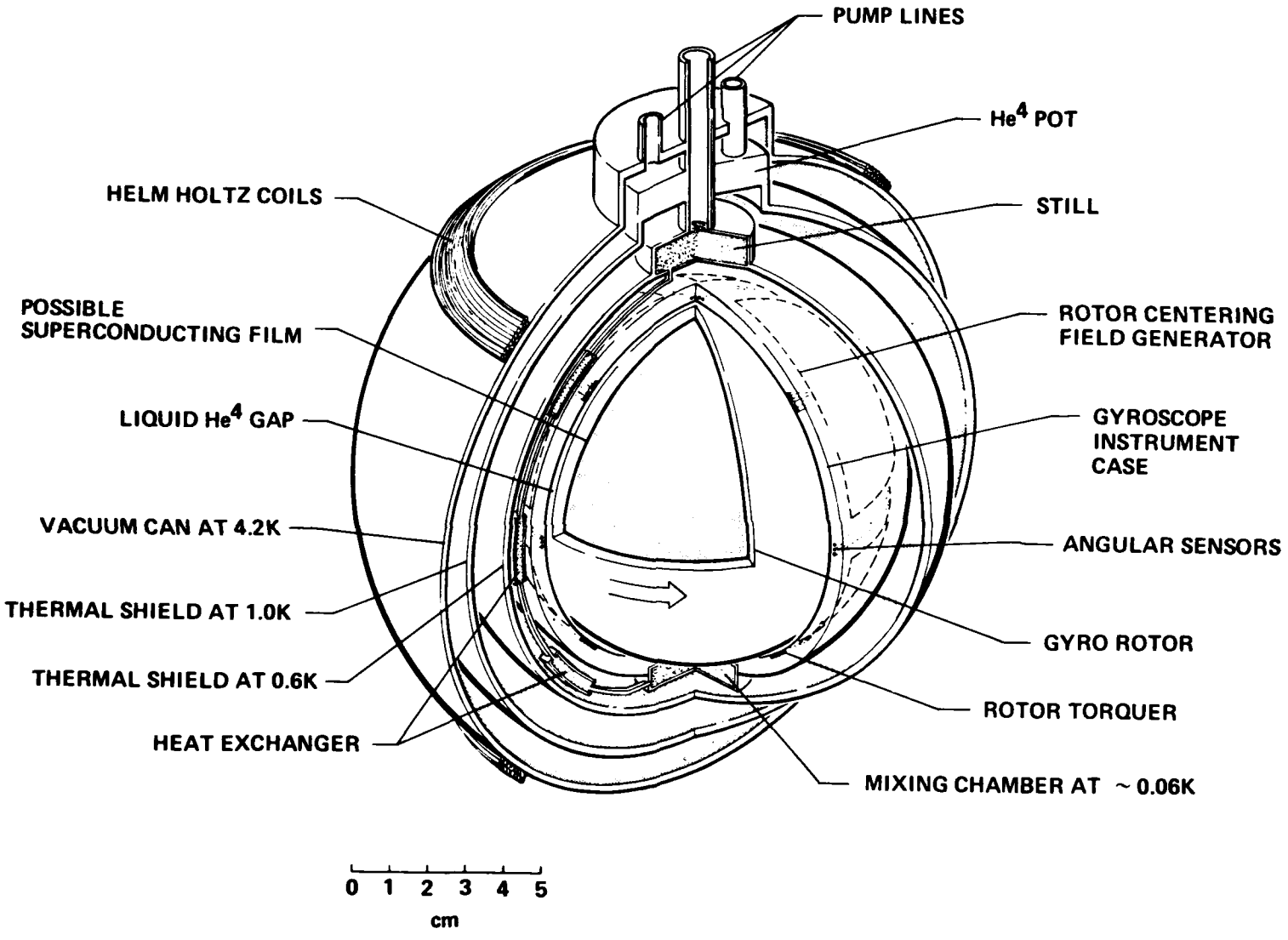

Figure 1.1 Liquid He^4 Neutrally Buoyant Frictionless Rotor Cutaway

The three outer spherical shells depict the vacuum can and thermal shells. The gyroscope instrument case contains the spin angular momentum pickoff sensors, the rotor centering capacitance plates, and the rotor spin up system.

If the gyro rotor runs at high angular velocities, perhaps the Stanford University relativity gyro technique of using the London moment as the angular momentum reference vector could be utilized. In that case, a superconducting film could be placed on the inside or outside of the rotor shell. However, an optical or capacitive pickoff could be utilized and indeed would be required for low angular momentum gyros. Patterns for optical sensing or capacitive pickoff could be placed on the outside of the shell, but there might also be some advantage to utilizing the inside of the shell if it is made of a dielectric material like quartz.

Spin up torquing of the spherical rotor could be accomplished by induced eddy currents on a metal film in the normal state on the inside of a quartz rotor or a mechanical method could be used if the temperature is raised above 0.2K where viscous coupling to the rotor can be established through the liquid He^4 surrounding the rotor. On the other hand, the torquing could be accomplished as in the ESG by having the rotor slightly oblate and torquing it capacitively. For a dielectric rotor made of quartz, the oblateness could be on the inside surface with a metal film coating while the outside surface was nearly spherical.

Because liquid He^4 is somewhat compressible, the achievement of neutral buoyancy of the rotor is made quite simple. The final adjustment of neutral buoyancy is accomplished by adjusting the density of the fluid by adjusting its pressure. Also, a spherical rotor is self centering under an acceleration or gravitational field. An acceleration or gravitational field establishes a small density gradient in the liquid He^4 which keeps the neutrally buoyant sphere centered. A centering force system would be required to oppose any electromagnetic forces which might off center the spherical rotor.

As can be seen, there are a number of options for sensing and torquing the spherical rotor. A thorough study of the gyro design, as well as other low temperature sensors, is now called for.

1.4 Low Temperature Inertial Sensors

The precision of other types of inertial instruments would also benefit from the use of liquid He^4 as the buoyant fluid. Ultraprecision accelerometers, gradiometers and vertical reference instruments are all conceivable. In Section 6 an outline of a proposal for applying this new approach to a relativity experiment is presented. The technological possibilities provided by a neutrally buoyant, free rotor in a nearly frictionless fluid could be very significant. One can only begin to imagine some of the forms that low temperature inertial sensors could take in the hands of creative design and development engineers and scientists. The implications of this work go beyond just developmental improvements in gyro performance because what this work is introducing is a medium with certain properties resembling a "gravity free vacuum". The forces of gravity and acceleration are opposed and "cancelled" on a neutral buoyant sphere while the nearly frictionless fluid has the drag free property of a vacuum.

1.5 Summary

As we have suggested above, the submarine launched missile system is becoming the principal strategic deterrent force of the triad. Moreover, this deterrent force could be further enhanced by the submarine utilizing an ultraprecision inertial navigation system. The weakest link in developing an ultraprecision inertial navigation system now appears to be the performance of the gyroscopes. Moreover, there is serious doubt whether or not normal temperature environmental operating conditions with its various perturbations will ever permit any gyro to perform with the desired precision. On the other hand, we can visualize an approach to an ultraprecision gyro based upon an

unperturbed stabilized rotor. The unperturbed rotor is envisioned as a spherical rotor neutrally buoyant in a virtually frictionless fluid and operating at very low temperatures to promote stability in the rotor material. Fortunately, nature has provided us with this near ideal fluid, liquid He^4, and at the desired very low temperatures as we will show in this report.

1.6 Recommendations

If the U. S. Navy decides to continue development along the lines outlined above, we would recommend the following:

a) An overview design study of the ultraprecision inertial navigation system. The purpose of this study would include:

   1) an examination and critique of the various approaches

   2) an examination of the overall navigation requirements to ensure that the various components of the system are properly configured to give the desired results.

b) A detailed model design study of the prototype gyro using the above concept of the unperturbed rotor. This study would include:

   1) materials, their stability and fabrication requirements for the spherical rotor

   2) mass balancing schemes for the rotor

   3) possible error torques

   4) angular sensor pick off scheme

   5) rotor centering scheme

   6) spin up and torquing method

7) further considerations and studies of the properties of liquid He^4

8) a design of the ship board prototype cryogenic system

9) interfacing with the ship board navigation system.

c) Based on the prototype design study, an experimental prototype gyro and cryogenic system would be built, tested and evaluated.

SECTION 1

REFERENCES

1. Everett, C. W. F., Fairbank, W. M., and Schiff, L. I., Theoretical Background and Present Status of the Stanford Relativity-Gyroscope Experiment, ESRO Colloquium on the Significance of Space Research for Fundamental Physics, Interlaken, Switzerland, 4 September 1969 (AD 701 555).

SECTION 2

HISTORY OF THE HELIUM VISCOSITY PROGRAMS

2.1 HELIUM VISCOSITY PROGRAMS

The U. S. Navy became interested in the potential gyro application of the work done by D. L. Ensley[1,2] at the Lawrence Livermore Laboratory. Ensley envisioned a spherical rotor, neutrally buoyant in liquid helium. The position of the rotor was to be controlled by a spherically symmetric sound field generated in the liquid helium by a spherical acoustic generator.

At that time the scientific literature on the viscosity of liquid He^4 indicated that the minimum viscosity occurred at 1.8K with a viscosity of 12.8μP. In order to maintain the spin angular momentum in the viscous fluid near 1.8K, Ensley envisioned synchronously co-rotating the gyro rotor case with the gyro rotor in order to approximate zero drag between the case and the rotor. The U. S. Navy then sponsored the Helios Program[3], contract N00030-71-C-0165, at the C. S. Draper Laboratory, Inc. to investigate Ensley's gyro concept. The Helios Program began in April 1971 and terminated in August 1973.

R. C. Pandorf came to Draper Laboratory in the spring of 1971 in anticipation of the Helios Program and began to develop the theoretical point of view that the effective viscosity of liquid He^4 would become vanishingly small at ultra-low temperatures. This work provided the impetus to direct the Helios Program into investigating the viscous properties of liquid He^4 at very low temperatures. In the present report, the viscosity measurements taken during the Helios Program are referred to as Experimental Series I.

The results of Experimental Series I were encouraging, and the helium viscosity measurements were continued by C. S. Draper Laboratory under its own Independent Research and Development (IR&D) funds until the spring of 1977. The experimental results done under IR&D are referred to in this report as Experimental Series II.

The program was then given new life in April 1977 by the Cryogenic Gyro Program sponsored by the Office of Naval Research, contract N00014-77-C-0295. The Cryogenic Gyro Program was a two part program. The first part was to complete the helium viscosity measurements. Part two was to build and test a prototype gyro. The helium viscosity measurements performed under this program are referred to as Experimental Series III. This program was terminated after one year, near the end of part one.

A preliminary final report on the Cryogenic Gyro Program was submitted July 31, 1978. With the termination of the Cryogenic Gyro Program, C. S. Draper Laboratory discontinued work on this program and the cryogenic facilities which were built up over the preceeding seven years were dismantled.

A great deal of effort has been expended on these facilities and on the three Experimental Series. While each of these series has been reported on separately, it was felt that without an overall in-depth analysis, much of the significance and meaning of this work would have been lost. For the next year the author, on his own initiative, worked on this comprehensive analysis of the experimental results and developed the theory presented in Section 3.

In March 1980 the Office of Naval Research, under contract N00014-77-C-0295, sponsored the completion of the analysis and the preparation of this comprehensive report on the viscosity of liquid He^4.

SECTION 2

REFERENCES

1. Ensley, D. L. Sound Supported Sphere in He II, Lawrence Radiation Laboratory Report UCRL-50514, Rev. 1.

2. Ensley, D. L., A New Superfluid Relativity Gyroscope, Lawrence Radiation Laboratory Report UCRL-71918, Rev. 1 (21 April 1970); also printed in the J. Appl. Physics 41, 12 November 1970.

3. Helios Program Final Report, R-833, by Dauwalter, C.R., Kerrigan, P.R. and Pandorf, R. C.; C. S. Draper Laboratory, Inc., Cambridge, MA.

SECTION 3

THE THEORETICAL EFFECTIVE VISCOSITY OF LIQUID He^4

3.1 INTRODUCTION

3.1.1 General Background

There has been a great deal of experimental and theoretical work done on the viscosity of liquid He^4. This work has spanned over forty years and has occupied scientists in over ten nations to bring to us our present understanding of the nature of the viscosity of liquid He^4. So many contradictions appeared in the earlier results, that it was necessary to measure the viscosity, then remeasure it and then verify it by every classical method known plus several methods unique to helium. Finally, the contradictions were beautifully explained by the two fluid model which later was supported by basic theory.

The following discussion cannot begin to touch on this extensive literature and the reader is referred to the excellent books by Wilks[1], Atkins[2], Keesom[3] and Keller[4] for references to this extensive literature.

In the early history of these measurements there was a great deal of conflicting results and controversy over just what the viscosity actually was, until it was realized that liquid helium below the temperature called the lambda point ($T \simeq 2.14K$) acts like a mixture of two nonseparable, interpenetrating fluids. One of these fluids is called a normal fluid and has properties similar to an ordinary fluid. The other

fluid is called a superfluid and has extraordinary properties such as zero viscosity and zero entropy. The density of the fluid, ρ, is the sum of the normal fluid density, ρ_n, and the superfluid density, ρ_s.

$$\rho = \rho_n + \rho_s \tag{3.1}$$

Figure 3-1 presents the relative densities of the normal and superfluid components as a function of temperature. The superfluid density, ρ_s, goes to zero at and above the lambda (λ) point ($T \simeq 2.14K$), while at absolute zero it becomes equal to the total density, ρ. The normal fluid density, ρ_n, becomes equal to the total density, ρ, at and above the lambda point and at low temperature ($T < 0.5K$) goes to zero as T^4.

Figure 3-2 presents the specific heat of liquid helium which demonstrates the reason why the transition to He II, the superfluid phase of helium beginning at $T \simeq 2.14K$, is called the lambda (λ) point.

The Landau theory of liquid He II proposes that the normal fluid density is a manifestation of quantized elementary excitations of sound waves in the superfluid background. These elementary excitations are grouped into two kinds: the lower energy, lower momentum excitations are called phonons; and the higher energy, higher momentum excitations are called rotons. With each of these excitations, a mass density may be associated. The normal fluid density then becomes the sum of the phonon density, ρ_{ph}, and the roton density, ρ_r.

$$\rho_n = \rho_{ph} + \rho_r \tag{3.2}$$

Presented in Figure 3-3 is depicted the energy-momentum excitation spectrum for the elemetary excitations, phonons and rotons. At low momentum the phonons obey the energy (E) - momentum (P) excitation equation $E = cP$, where c is the velocity of sound. At He II temperatures most of the roton excitations are centered about the minimum point

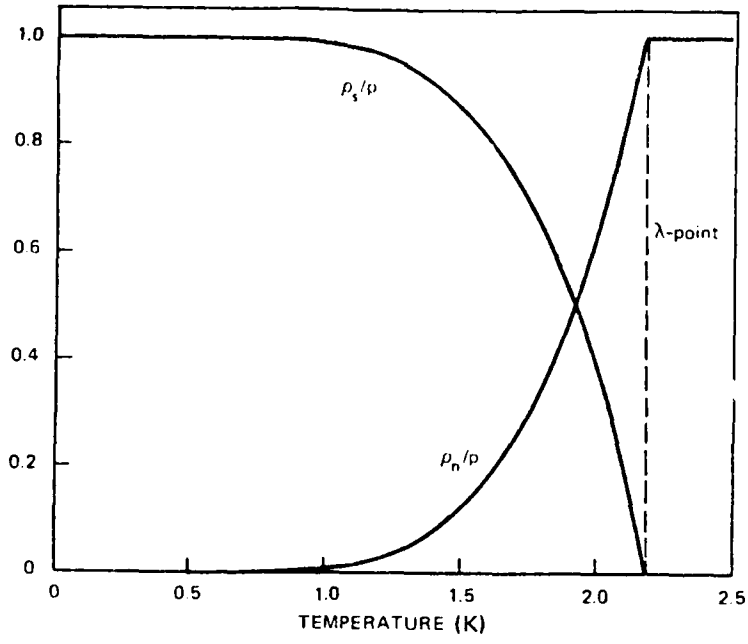

Figure 3-1. The relative densities of the normalfluid and the superfluid.

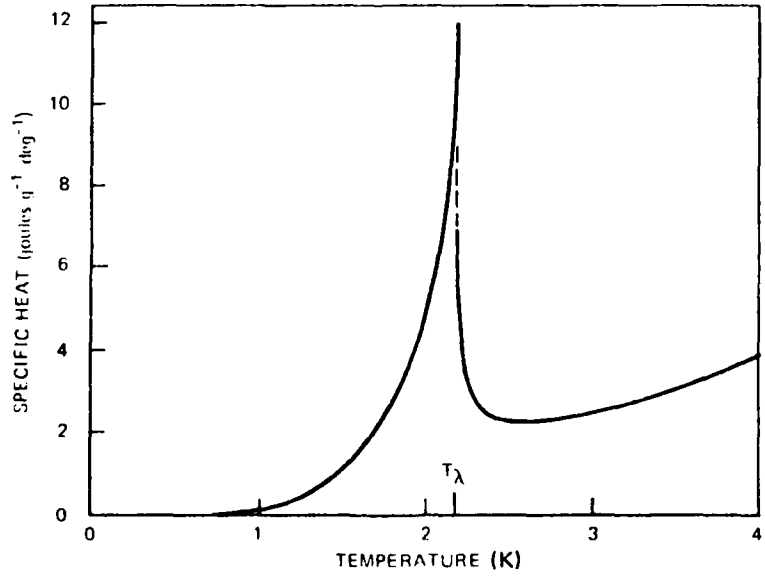

Figure 3-2. The specific heat of liquid He^4 in the neighborhood of the λ point transition.

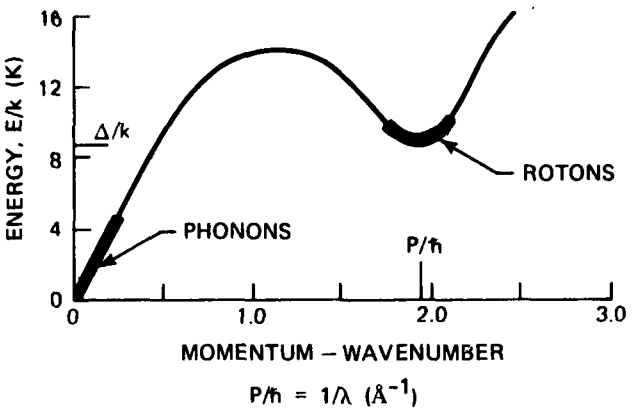

Figure 3-3. The energy-momentum excitation spectrum for He II.

$\Delta/k = 8.65$ and $P_o = 1.91 \times 10^8 \hbar$ in the excitation spectrum curve. Both the phonon and roton densities fall rapidly with decreasing temperature; the roton density falls as an exponential function of the temperature while the phonon density falls more modestly, going as T^4 at the lower temperatures. At the higher temperatures above 1.6K the rotons dominate while at temperatures below 0.5K the phonons dominate and the roton contributions can generally be ignored.

Figure 3-4 presents a phase diagram illustrating the region called He II over which the superfluid component exists. Note that even at absolute zero helium is a liquid and can be solidified only by increasing its pressure to about 25 atmosphere.

3.1.2 Experimental Measurements

Viscosity measurements which measured flow through capillaries usually gave zero and near zero values for the coefficient of viscosity because the superfluid would be the main fluid flowing. Viscosity experiments with oscillating disks which depend on the fluid density gave conflicting results until it was realized that the normal fluid density, ρ_n, was responsible for the viscosity and that ρ_n is a strong function of temperature, varying as the fourth power at low temperatures. Viscosity measurements with concentric rotating cylinders measured the viscosity of the normal fluid directly (independent of the density) and gave viscosity values of the order of the viscosity of He^4 gas at low temperatures.

For the most part, the two fluid model has reconciled the results from the various methods of measuring viscosity and it was concluded that objects rotating in liquid helium experience drag due to the normal fluid. Figure 3-5 presents the viscosity measurements by Hollis Hallett and co-workers[5,6] accomplished with a concentric cylinder (Couette) viscometer. These results well represent the now accepted behavior of helium viscosity as presently described in the literature. From this figure one sees that the viscosity reaches a minimum value near 1.82K and then begins to rise

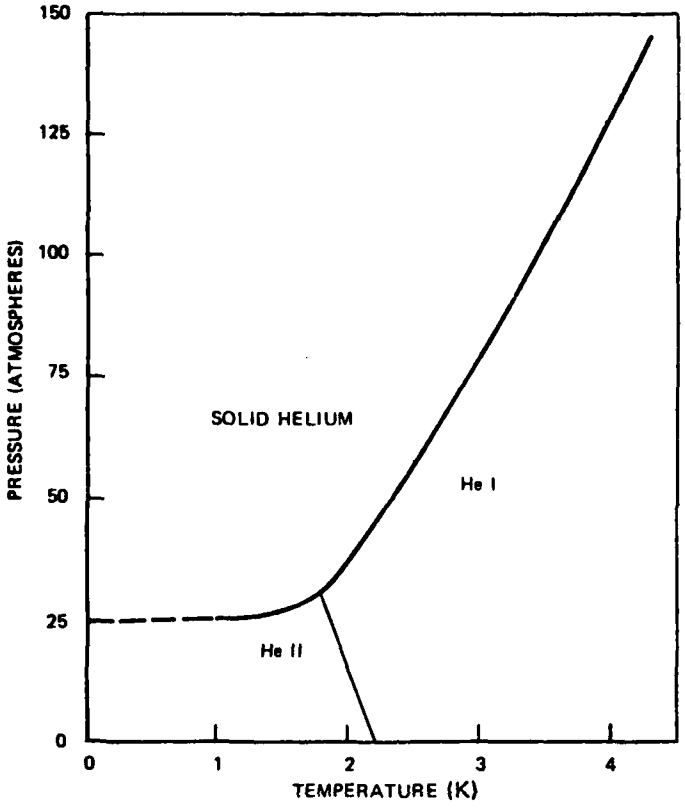

Figure 3-4. The phase diagram of He^4.

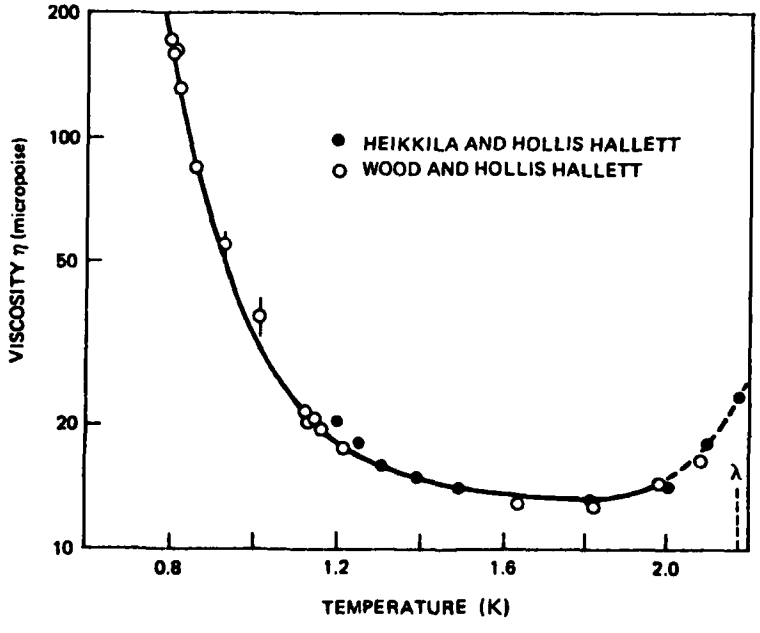

Figure 3-5. The coefficient of first viscosity of helium II.

quite steeply with decreasing temperature. Hollis Hallett and co-workers also observed the viscosity to be independent of rotational speed up to a certain critical speed; but above this critical speed the viscosity rose rapidly with speed. This critical speed was thought to be due to the onset of vorticity in the superfluid.

This points out one further complication in determining the viscosity which will now be illustrated. Consider an object, a cylinder or sphere, at rest in helium II. If the object is brought into slow rotation it will experience a viscous drag due to the normal fluid while the superfluid component simply acts as a non-interacting "vacuum" background. However, as the speed of rotation is increased, the superfluid is thought to break into a kind of turbulence or vortex excitation believed to be in the form of vortex rings (like smoke rings) or vortex lines (like whirlpools). The appearance of vorticity in the superfluid occurs at a certain critical velocity which depends upon the geometry. Turbulence in liquid He^4 will be more fully discussed in Section 5.

Returning to Figure 3-5, the 1962 viscosity measurements of Woods and Hollis Hallett[6] were made with a rotating cylinder viscometer and were taken in the temperature range 0.79 to 1.1K. These measurements along with those by Heikkila and Hollis Hallett in 1955 indicate that there is a minimum in the viscosity of 12.8 μP. 12.8 μP would lead to a relaxation time of a freely rotating 5 cm radius sphere just buoyant in liquid helium of less than an hour.

From this minimum the viscosity rises to 173 micro-poise at 0.79K, the lowest temperature at which measurements have been reported prior to the present work. The theory of Landau and Khalatnikov predicts that the viscosity increases as T^{-5} at temperatures below 0.5K. The Landau and Khalatnikov theory has, in general, provided excellent agreement with experimental measurements. In an elementary manner we will now look at the basic concepts of this theory in order to understand this rapid rise in viscosity.

3.1.3 The Theoretical Concept of Liquid He^4

Great insight into the underlying behavior of the viscosity, as well as many other properties of liquid He^4, was provided by the theoretical work of the two noted Russian physicists, L.D. Landau and I.M. Khalatnikov and amazingly, most of their work was accomplished prior to the experimental work.

To introduce the basic concept, let us consider a sample of liquid He^4 at absolute zero. The helium would be in its lowest energy state, called the ground state, meaning that no more energy could be removed from the helium. The helium would then be a pure superfluid having zero viscosity and acting very much like a vacuum, except that this helium "vacuum" has mass. Now, if we introduce a very small amount of energy into this liquid at absolute zero, what happens? The temperature will rise a little bit above absolute zero. Furthermore, this energy we placed in the helium would manifest itself in the form of collective modes of oscillation of the helium atoms, more commonly called sound waves. This situation is quite analogous to light waves or photons in a box containing a vacuum. The liquid He^4 sound waves are density waves also called first sound and are a manifestation of the elementary quantized excitations, photons and rotons. Phonons, like photons, have a dual nature in that they are both wave-like and particle-like. To the extent that they are particle-like, they act like a classical gas. On the other hand, to the extent they are wave-like, they act like light waves or sound waves and should exhibit diffraction and reflection properties of waves. Landau and Khalatnikov[7] recognized the gas-like nature of the helium phonon system and introduced a kinetic theory type of expression for the viscosity; namely,

$$\eta_{ph} = \alpha_{ph}\, \rho_{ph}\, c\ell_{ph} \qquad (3.3)$$

In this expression, α_{ph} is a numerical constant, ρ_{ph} is the phonon fluid density which varies as T^4 at low temperatures, c is the velocity of the phonons which is the velocity of sound and is nearly constant for

$T < 0.5K$, ℓ_{ph} is the mean free path which is the average distance traveled by the phonon between interactions or collisions, and was theoretically found by Khalatnikov to vary as T^{-9} at low temperatures $T < 0.5K$. This indicates that the viscosity, η_{ph}, is proportional to T^{-5} at low temperatures which gives a rapid rise in viscosity as the temperature falls. At higher temperatures $T > 0.7K$ the situation is more complex because of the influence of the rotons.

Figure 3-6 presents the values for the mean free path as a function of temperature as computed from equation 3.3.

There is, yet, one contradiction or paradox which has to be dealt with. First of all, both experiments and theory show the viscosity at low temperatures to be rising rapidly as the temperature is lowered, which means that as T approaches zero, η approaches infinity, that is infinitely large viscosity at absolute zero. On the other hand, both experiments and theory show that He^4 approaches a pure superfluid as T approaches zero (see Figure 3-1) and at absolute zero would be a pure superfluid. A pure superfluid has zero viscosity and so zero drag on a rotor. Obviously, viscosity is a real quantity and as absolute zero is approached, it must either become large, approaching infinity or must approach zero, not both. In the next sections theoretical considerations will be developed which will resolve this apparent paradox by showing that the viscosity will reach a maximum and then begin falling, going to zero at absolute zero. Atkins[8] discussed a similar situation as it applied to the thermal conductivity of liquid He^4.

3.2 The Phonon Free Effective Viscosity

3.2.1 The Role of the Mean Free Path

The first thing to note is that Khalatnikov's equation of the viscosity as expressed by Eq. (3.3) breaks down at some temperature which depends on the particular apparatus.* In order to see this,

*This does not diminish at all the correctness of the Landau and Khalatnikov theory, but only defines more clearly its applicability.

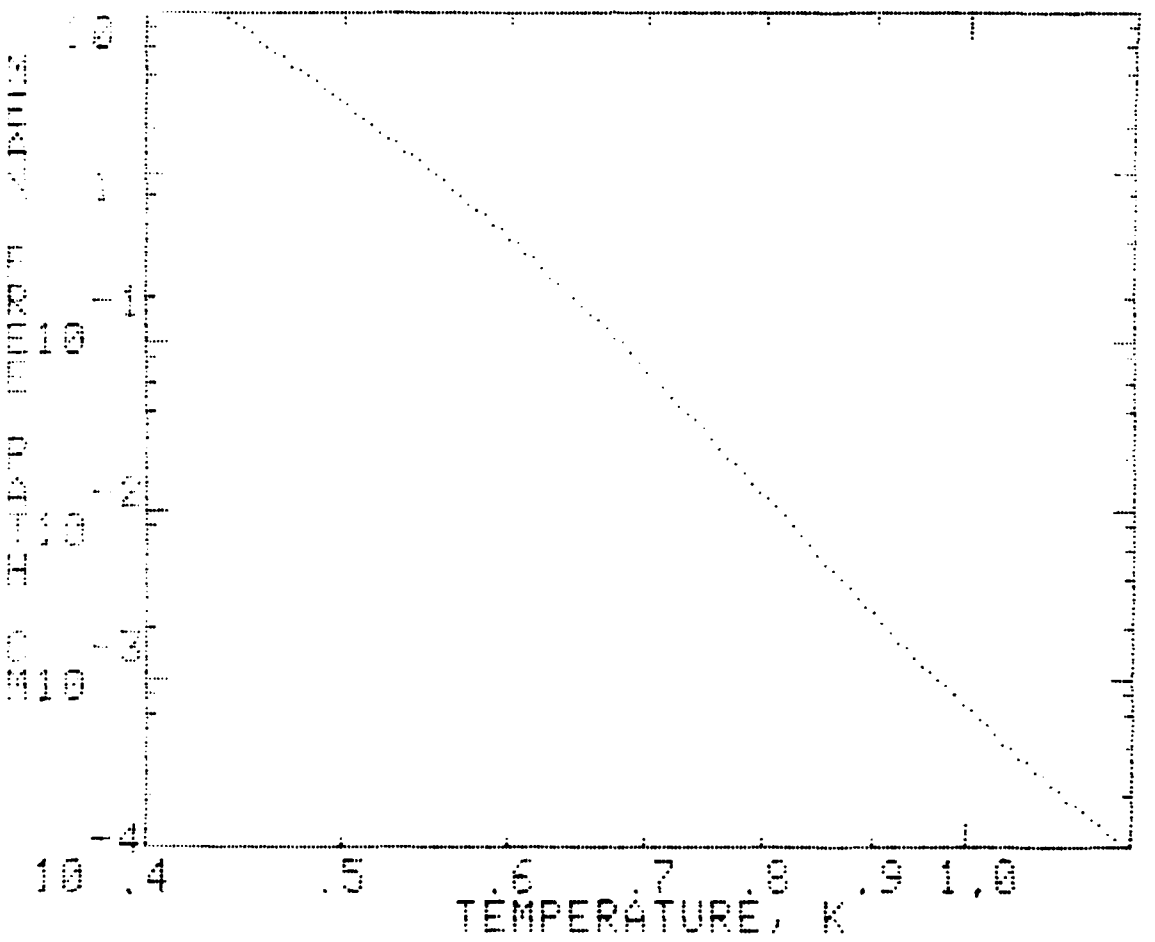

Figure 3-6. The mean free path of He II phonon.

consider a viscometer formed by two "infinite" parallel plates with a gap, d, between them which are immersed in pure liquid He^4. By Eq. (3.3), the measured viscosity due to the "gas-like" phonons should obey the equation $\eta_{ph} = \alpha \rho_{ph} c \ell_{ph}$. However, as the temperature is reduced the mean free path increases rapidly, $\ell_{ph} \sim T^{-9}$, being about 1cm at $T \sim 0.56K$ (see Figure 3-6), so that at some temperature the mean free path will eventually exceed the gap, d. This equation for the viscosity then breaks down because the phonons will travel for the most part from one viscometer plate to the other plate without collisions with other phonons. The magnitude of the mean free path between phonon to phonon collision will then have no bearing on the drag one plate exerts on the other.

Let us now compute how the phonons transfer a shear stress (force/unit area) F/A from a stationary parallel surface to a parallel surface moving with a uniform velocity v_o for the case $\ell_{ph} >> d$. For this case, the phonons move from one surface to the other without suffering collisions with other phonons. Imagine, if you like, particle-like phonons moving about the gap, d, "bouncing back and forth" between the moving surface and the stationary surface and creating a shear stress F/A. On the average, the phonons pick up drift momentum from interacting with the moving surface, then move to the stationary surface where, on the average, they give up their drift momentum. The mass incident per unit area per second on the surface can be shown to be $1/4\ \rho_{ph} c$ (see reference 17 or some standard text book on Kinetic Theory). If the mass incident upon the stationary surface has an average drift velocity, v_o, (the velocity of the moving surface) and if this drift momentum is <u>all</u> given up to the stationary surface, then the force per unit area on the stationary surface would be

$$F/A = 1/4\ \rho_{ph} c v_o \qquad (3.4)$$

Using the classical definition of viscosity for a parallel surface viscometer, $F/A = \eta\ v_o/d$ and comparing this to Eq. (3.4), then the phonon viscosity becomes

$$\eta_{ph} = 1/4\ \rho_{ph} cd \qquad (3.5)$$

The only temperature dependent term in this equation is ρ_{ph}, which is proportional to T^4. Therefore, the apparent or observed viscosity will go to zero at absolute zero.

What has been brought out here is the limitation in the applicability of the hydrodynamic-kinetic theory equation $\eta_{ph} = \alpha_{ph} \rho_{ph} c \ell_{ph}$ and not any problems with Landau and Khalatnikov's theory. This situation is quite analogous to the situation in gas dynamics where Poiseuille flow breaks down at very low pressures and the gas is described by Knudsen flow.

3.2.2 The Role of Specular Reflection

A phonon striking a surface is, in essence, a collision of the collective modes of motion of atoms of the liquid with the surface. As a phonon in the helium liquid approaches a surface, these vibrating helium atoms collide or interact with the surface atoms and give rise to a number of possibilities. The vibrating helium atoms which interact with the surface atoms may excite vibration in the surface atoms and thus create a phonon in the surface material by the helium giving up some of its own vibrational energy. This would be accomplished either by the helium phonon being completely annihilated and a new phonon being created in the wall to conserve energy and momentum or by two or more new phonons being created, one or more in the liquid helium and the others in the surface material in order to conserve energy and momentum. This type of process exchanges both momentum and energy (heat conduction) with the surface. It is also possible for the helium phonon interacting with the wall to be scattered elastically, i.e. without any energy exchange with the wall. Indeed, experimental results on the thermal boundary resistance (Kapitza resistance) indicate that at low temperatures energy exchange between liquid helium and its container becomes increasingly difficult. This indicates that at low temperatures the

dominant scattering process at the surface wall must be elastic (no energy exchange) with only the momentum direction being changed.

The helium phonon incident upon a surface could in general be elastically scattered back into the helium at any angle. Those phonons incident upon a surface and elastically scattered back into the helium, such that the incident plane and angle are equal to the reflected plane and angle are called specular reflected, and they will only transfer momentum (pressure) perpendicular to the surface. That is, there will be no transfer of momentum tangential (shear stress) to the surface. Those phonons which are scattered back into the helium with different incident and reflected angles will transfer momentum tangential as well as perpendicular to the surface, and thus will give rise to a shear stress and pressure at the surface. Those phonon collisions which, on the average, transfer all the phonon drift momentum to the surface are said to be diffusely scattered. The diffusely scattered phonons obey the cosine law of scattering, as well as having an isotropic directional distribution. The point to be emphasized here is that the elastically scattered phonons which are specularly reflected from a surface cannot contribute to drag on the surface whereas the diffusely scattered phonons do.

Obviously, in order to reduce drag on a surface one would like to see the phonons specularly reflected. The question then arises, what conditions can make the phonons specularly reflect? In the case of light, which is an electromagnetic wave and made up of photons, we know that a highly polished mirrored surface will specularly reflect light whereas a frosted surface will diffuse light. Likewise, in the case of phonons we may expect phonons whose wavelength is longer than the surface irregularities to be specularly reflected from the surface.

The phonons in He II (liquid He^4 below T_λ) range in wavelength all the way from the size of the container (centimeters) to the interatomic spacing of the order of a few angstroms. The phonon wavelength density distribution is a strong function of temperature and is given by

the Bose-Einstein statistical distribution function. When the He II phonons interact or collide with a surface we would expect some of the phonons to be specularly reflected and some to be diffusely reflected. In phonon-surface collisions, in which the phonon wavelength is long compared to the dimension of the surface roughness in the region of interaction, one expects specular reflection. Conversely, one expects on the average, diffuse scattering if the dimensions of the surface roughness is large compared to the phonon wavelength because there occurs a non-uniform, non-coherent interaction between the phonon wavefront and the surface as well as possible multi-surface phonon reflection, all of which tend to randomize the direction of the reflected phonon.

At this point we would like to compute the fractional density of phonons with wavelength less than some wavelength λ_D which is denoted as $f'(\lambda_D) = \rho_{ph,D}/\rho_{ph}$. The quantity ρ_{ph} includes the entire spectrum of phonons with wavelength $(0 \leq \lambda < \infty)$ and so is the phonon density. The quantity $\rho_{ph,D}$ represents the density of phonons with wavelength $0 \leq \lambda \leq \lambda_D$. Thus $f'(\lambda_D)$ represents the fractional density of phonons with wavelength less than λ_D.

Let us now look into just how long are the wavelengths of the phonons. The phonon density was computed by Landau using quantum statistical theory and found to be

$$\rho_{ph} = \frac{4\pi k^4}{3h^3c^5} T^4 \int_0^\infty \frac{e^x x^4 dx}{(e^x-1)^2} \tag{3.12}$$

where

$$x = ch/(kT\lambda)$$

After integrating one gets,

$$\rho_{ph} = \frac{16\pi^5 k^4}{45h^3c^5} T \tag{3.13}$$

where Boltzmann's constant $k = 1.381 \times 10^{-16}$ ergs/deg, Planck's constant $h = 6.626 \times 10^{-27}$ erg sec and the velocity of sound $c = 2.382 \times 10^{4}$ cm/sec ($T < 0.5K$). Evaluation of ρ_{ph} gives,

$$\rho_{ph} = 1.78 \times 10^{-5} T^4 \text{ gm/cm}^3$$

Calculations based on thermodynamic properties of liquid helium as reported by Bendt, et al[9] are in agreement with this theoretical value for $T < 0.5K$ where the roton contributions to the normal fluid density is negligible.

In order to get some insight into equation (3.12) let us rewrite it in the form

$$\rho_{ph} = \int_0^\infty \Delta\rho_{ph}\, d\lambda = \lim_{\Delta\lambda \to 0} \sum_i \Delta\rho_{ph} (\Delta\lambda)_i \tag{3.14}$$

where $(\Delta\lambda)$ is an increment of wavelength and $\Delta\rho_{ph}$ is the phonon density of the phonons whose wavelengths range from λ to $\lambda + \Delta\lambda$. Expressing Eq. (3.12) above in this form we find

$$\Delta\rho_{ph}/T^4 = \frac{4\pi h^4}{3h^3c^5} \frac{e^x x^5}{\lambda(e^x-1)^2} \tag{3.15}$$

where $x = ch/(kT\lambda)$. A plot of $\Delta\rho_{ph}/T^4$ versus wavelength, λ, is given in Figure 3-7 for three values of temperature. The total area under each curve is the same and this area times T^4 gives the phonon density for that temperature. The important thing to note in this plot is that as the temperature is lowered, the distribution of wavelengths over which the phonons are distributed become longer and longer. For example, at $T = 0.5K$ the phonons are clustered around the wavelength of 40 Å; while on the other hand, at $T = 0.05K$ the phonons are centered around 400 Å.

This means that for a given surface smoothness, as the temperature is lowered, there will be a larger fraction of the phonons whose wavelength is longer than the surface irregularities. Consequently, there

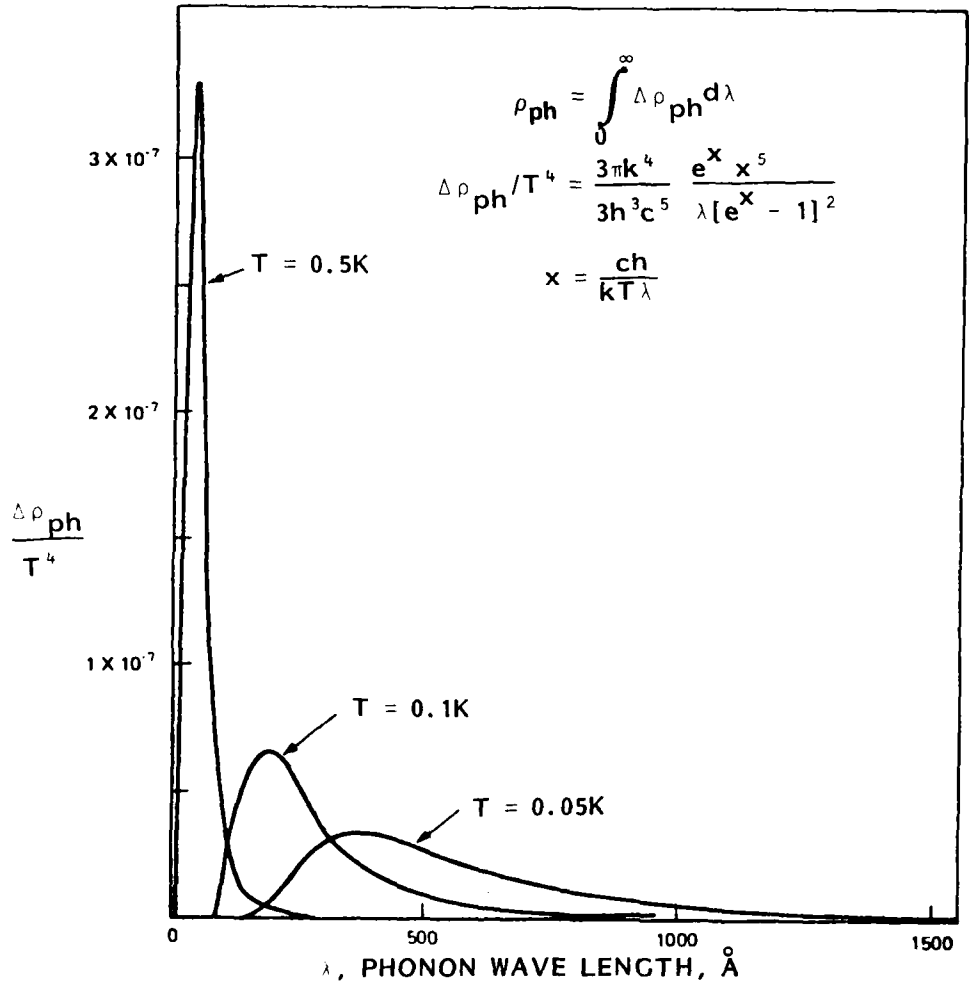

Figure 3 -7. The phonon wavelength distribution in Helium II. The density distribution function $\Delta\rho_{ph}$ has been normalized by the temperature function T^4.

will be a larger and larger fraction of phonons which are specularly reflected as the temperature is lowered as well as a lower number of phonons due to the T^4 temperature dependence of the phonon density. Both of these facts rapidly reduce the drag producing phonons.

The integral in Eq. (3.12) represents an integration or summation of all the phonons from zero to infinite wavelength. The density of the phonons, $\rho_{ph,D}$ whose wavelength, λ, is less than λ_D is, from this equation:

$$\rho_{ph,D} = \frac{4\pi}{3h^3} \frac{k^4}{c^5} T^4 \int_{x_D}^{\infty} \frac{e^x x^4}{(e^x-1)^2} dx \tag{3.16}$$

where $x_D = \frac{ch}{k} \frac{1}{\lambda_D T} \simeq 114/(\lambda_D T)$ for λ_D in units of angstroms, Å.

We can now compute the fractional density, f', by substituting $\rho_{ph,D}$ and ρ_{ph} from Eqs. (3.16) and (3.13) into equation $f' = \rho_{ph,D}/\rho_{ph}$ to get,

$$f'(x_D) = \frac{15}{4\pi^4} \int_{x_D}^{\infty} \frac{e^x x^4}{(e^x-1)^2} dx \tag{3.17}$$

A computation of f' as a function of x_D is presented in Table 3-1.

For x_D greater than 10, i.e., for small λ_D and very low temperatures the above integral can be approximated.

$$\int_{x_D}^{\infty} \frac{e^x x^4}{(e^x-1)^2} dx \simeq x_D e^{-x_D} (1 + 4/x_D + 12/x_D^2 + 24/x_D^3 + 24/x_D^4) \tag{3.19}$$

Within an accuracy of about 0.2% we find that $f'(x_D)$ can be represented for all values of x_D by

Table 3-1. Fraction density of phonon with $\lambda < \lambda_D$.

$f'(X_D)$	X_D	$f'(X_D)$	X_D
0.9955	0.7	0.408	5.0
0.9935	0.8	0.332	5.5
0.9908	0.9	0.264	6.0
0.9876	1.0	0.206	6.5
0.961	2.0	0.124	7.5
0.850	2.5	0.092	8.0
0.772	3.0	0.686	8.5
0.681	3.5	0.0507	9.0
0.586	4.0	0.0372	9.5
0.496	4.5	0.0271	10.0

$$f'(X_D) = \frac{1}{25.98} \int_{X_D}^{\infty} \frac{e^x x^4}{(e^x-1)^2} dx$$

$$X_D = \frac{114}{\lambda_D T}, \quad \lambda_D(\mathring{A})$$

$$f'(X_D) \simeq \frac{30}{8\pi^4} x_D^4 e^{-x_D} (1 + 4/x_D + 12/x_D^2 + 24/x_D^3 + 24/x_D^4) + 0.079\, e^{-0.1633\, x_D^2} \quad (3.20)$$

Furthermore, for $x_D > 40$ we may drop the second order terms and substitute the first order terms of Eq. (3.19) into Eq. (3.18) to get,

$$f' = f'(x_D) \simeq \frac{1}{25.98} x_D^4 e^{-x_D} \simeq 6.50 \times 10^6\, \lambda_D^{-4}\, T^{-4}\, e^{-114/\lambda_D T} \quad (3.21)$$

3.2.2.1 A Surface Model for Specular Reflection and the Fraction of Diffuse Phonons, f

We now wish to relate diffuse scattering and specular reflection to a simple surface model. We assume that an ideal perfectly smooth and flat surface will specularly reflect all the phonons. However, a real fabricated surface is generated by machining, grinding and polishing through various grit sizes and will physically deviate from the perfect surface. If the actual surface deviates from the ideal surface by a uniform and regular surface roughness with a maximum characteristic roughness of dimension δ, then we expect and assume that those phonons with wavelength less than this characteristic surface δ will be diffusely scattered. How rough the surface appears to the phonons depend upon the angle of incidence of the phonon. A phonon arriving at the surface at a grazing angle will have very little interaction with the "valleys" of the surface (ignoring diffraction) because the "valleys" are "shaded" by the "hills" or high points. A phonon incident normal to the surface, on the other hand, will interact with the "valleys" and "hills" equally and will experience the full surface roughness δ. Using this simple geometric argument, we assume that the phonons incident on the surface with an angle θ to the normal and with wavelength $\lambda_D \leq \delta \cos\theta$ will be diffusely scattered. Those phonons which are not diffusely scattered are assumed to be specularly reflected.

Let us now compute the fractional density of diffusely scattered phonons using the above discussed assumptions and surface model. Equation

(3.17) gives the fractional density of phonons with wavelengths less than λ_D. The cosine law states that for a homogeneous distribution of phonons, $(1/\pi \cos\theta\, d\Omega)$ fraction of the phonons would be found moving within a solid angle $d\Omega$ toward the surface at an angle θ to the normal. Combining equation (3.17) and the cosine law, we get

$$f(X) = \frac{30}{8\pi^5} \int_0^{2\pi} \int_{X_D}^{x=\infty} \frac{e^x x^4 \cos\theta}{(e^x - 1)^2} \, dx \, d\Omega \tag{3.22}$$

as the fractional density of diffused scattered phonons. The solid angle is integrated over a hemisphere and the lower limit of the x integral is $X_D = ch/(kT\,\delta\cos\theta)$. The limits on the x integral were determined from the assumption that all the phonons incident at angle θ to the surface with wavelengths less than $\delta\cos\theta$ would be diffusely scattered. $f = f(X)$, equation (3.22), is a function of X which we write in the form $X = ch/(kT\,\delta)$; namely, X is inversely proportional to the temperature T and the surface roughness factor δ. Integrating equation (3.22) with respect to x we can use the result of eq. (3.17)

$$f(X) = \frac{1}{\pi} \int f'(X_D) \cos\theta \, d\Omega \tag{3.23}$$

where $X_D = ch/(kT\,\delta\cos\theta) = X/\cos\theta$ and $f'(X_D)$ is approximated by equation (3.20). To prepare for integration over the hemisphere we set $d\Omega = 2\pi \sin\theta\, d\theta$, (the limits of integration are from $\theta = 0$ to $\pi/2$), substitute the approximate form for $f'(X_D)$ from equation (3.20) and change variables $x/\cos\theta = y$ to find

$$f(X) = \int_X^\infty \left[\frac{30x^2}{4\pi^4} ye^{-y} (1 + 4/y + 12/y^2 + 24/y^3 + 24/y^4) + 2\beta \frac{x^2}{y^3} e^{-\alpha y^2} \right] dy \tag{3.24}$$

where $\beta = .079$ and $\alpha = .1633$.

The first term on the left can be integrated using a table of integrals

$$\int_X^\infty ye^{-y} \, dy = e^{-x} (x + 1)$$

Then other integrals can be put in the form of the exponential integral[10]

$$E_n(Z) = \int_1^\infty \frac{e^{-Zt}}{t^n} dt$$

The 2nd through 5th term can be put into the form of the above exponential integral by the variable change $y = xt$ while the 6th and last term requires the variable change $y^2 = x^2 t$. After using the recurrence relation[10]:

$$E_{n+1}(Z) = \frac{1}{n}\left(e^{-Z} - ZE_n(Z)\right)$$

equation (3.24) reduces to the form,

$$f(X) = \frac{30}{4\pi^4} X^3 e^{-X}\left(1 + 5/X + 12/X^2 + 12/X^3\right) + \beta\left(e^{-\alpha X^2} - \alpha X^2 E_1(\alpha X^2)\right) \qquad (3.25)$$

where $\beta = .079$, $\alpha = .1633$ and $X = ch/(kT\delta)$.

If we express δ in units of angstroms, then $X \simeq 114/T\delta$. The exponential integral $E_1(Z)$ is approximated[10] for $0 \leq Z \leq 1$ as,

$$E_1(Z) = -.57722 - \ln Z - .2499 Z^2 + .0552 Z^3 - .0098 Z^4 + .0011 Z^5 \qquad (3.26)$$

and for $1 \leq Z < \infty$,

$$E_1(Z) = \frac{e^{-Z}\left(Z^2 + 2.335Z + .2506\right)}{Z\left(Z^2 + 3.3307Z + 1.6815\right)}$$

In Figure 3-8 the function, f, equation 3.25 is plotted against T for various values of δ, the surface roughness parameter.

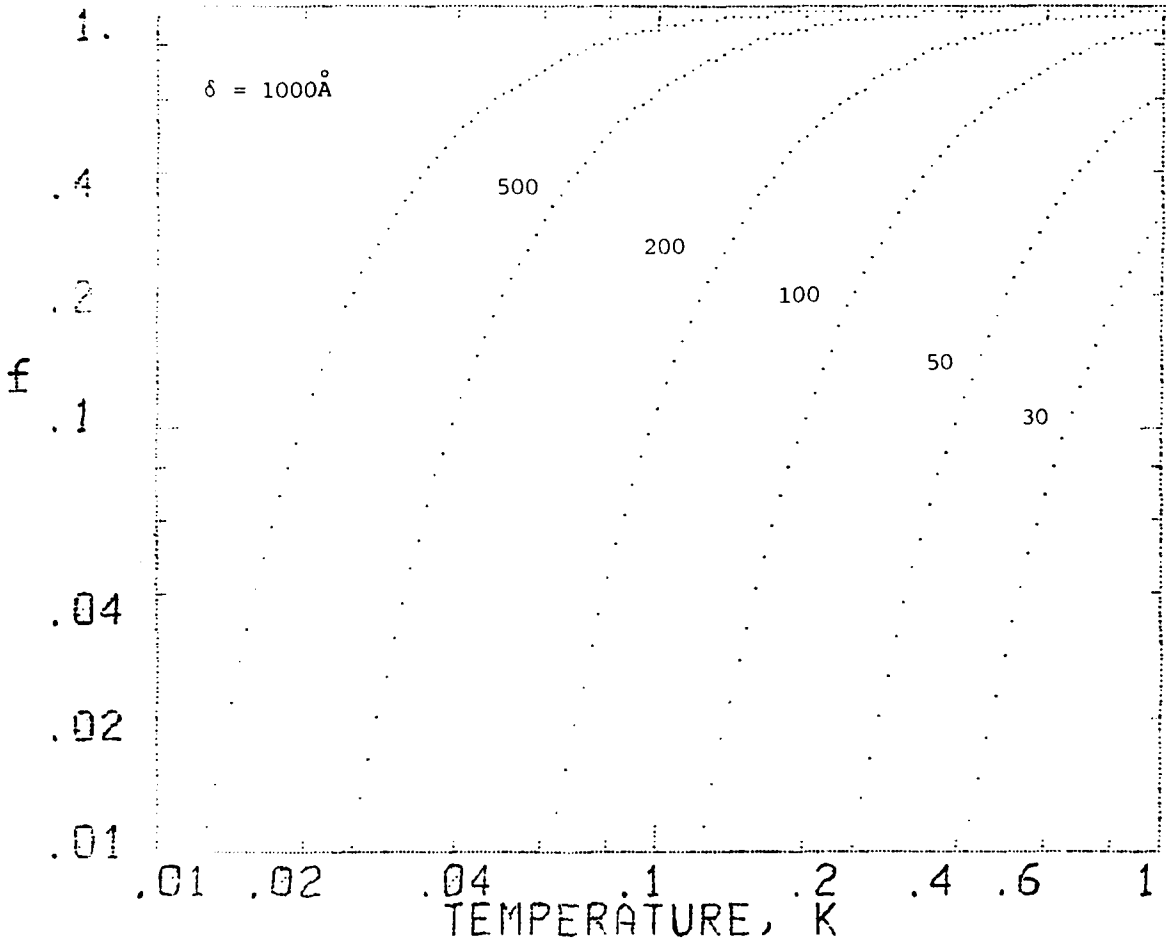

Figure 3-8. The fractional density of diffusely scattered phonons from a uniformly rough surface characterized by maximum roughness δ (units angstroms).

3.2.2.2 Extension of the Surface Model and the Super-Smoothness Ratio, γ

In the previous section we proposed a surface model which would diffusely scatter all phonons with wavelengths less than $\delta \cos \theta$ and specularly reflect all phonons with wavelengths greater than $\delta \cos \theta$. We would like to carry this model one step further by allowing for the possibility that the surface may contain numerous small spots or regions distributed throughout the surface which are "supersmooth." By "supersmooth" we mean a spot on which the local surface roughness δ_s is much much less than the overall or general surface roughness δ. As an example, see Fig. 3-9 which is an idealized illustration of our proposed surface profile.

This surface profile contains surface irregularities which are no greater than δ, yet there are minute areas $\Delta A_1 \sim \ell_1^2$, $\Delta A_2 \sim \ell_2^2$ and $\Delta A_3 \sim \ell_3^2$ which would support specular reflection of phonons with wavelengths less than $\delta \cos \theta$. For example, the figure depicts small areas, ΔA_i, which would specularly reflect phonons in the wavelength range between $\ell_i \cos \theta$ and $\delta_{si} \cos \theta$, $(i = 1, 2, 3)$ where ℓ_i is the order of the square root of the area ΔA_i of the i^{th} spot and δ_{si} is the surface roughness of this i^{th} supersmooth spot.

For the case of the parallel plate viscometer, let us assume for the moment that all the phonons are diffusely scattered from the upper surface moving at velocity v_o and that the lower surface has the characteristics of the surface model we are here proposing.

We now wish to write the force, F, or momentum transferred per second by the phonons to an area, A, of the stationary lower surface. From eq. (3.22) or (3.25) recall the $f(\delta)\rho_{ph}$ represents the assumed density of diffusely scattered phonons for a surface of uniform surface roughness of characteristic maximum roughness δ. Putting this result into eq. (3.5), the drag force on such a surface would become, $F = \frac{1}{4} f(\delta)\rho_{ph} c v_o A$. However, by the surface model as represented by Fig. 3-9 this equation overcounts the momentum transferring phonons by those phonons in $f(\delta)\rho_{ph}$ which are specularly reflected from the "supersmooth spots. The overcounted spots have a density approximated by

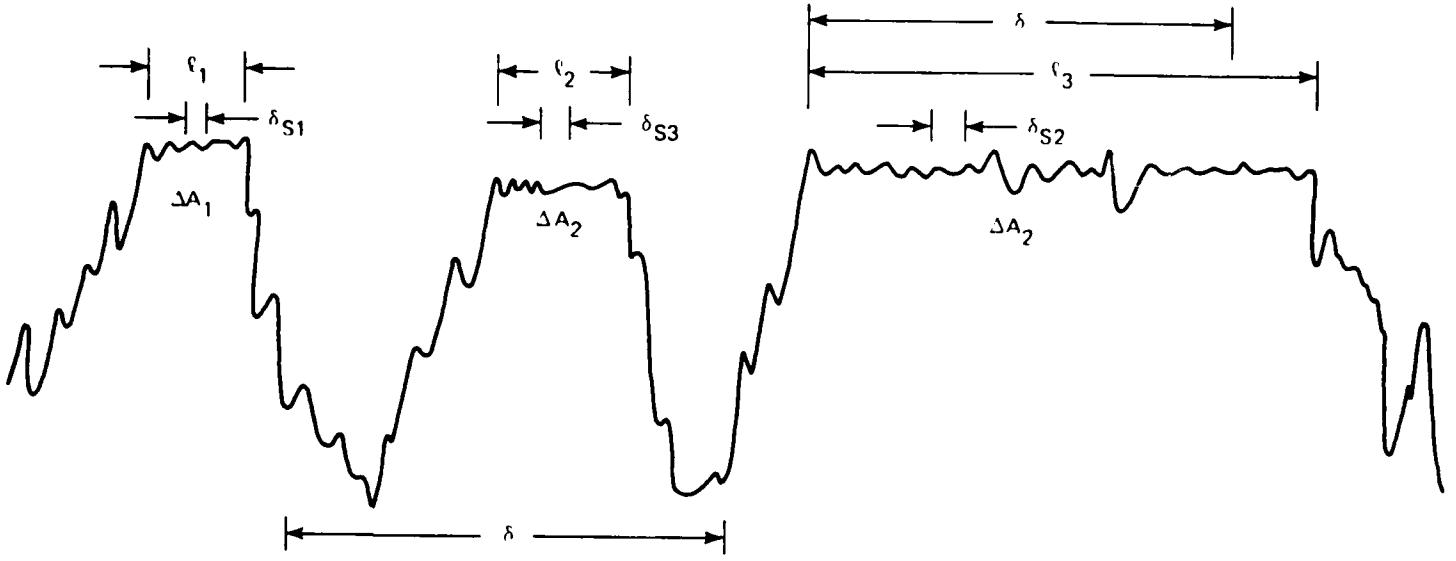

δ = THE OVERALL CHARACTERISTIC SURFACE ROUGHNESS OR ASPERITY DIMENSION

ℓ_i = THE ORDER OF THE SQUARE ROOT OF THE AREA OF THE i^{th} SUPERSMOOTH "SPOT"

δ_{Si} = THE CHARACTERISTIC SURFACE ROUGHNESS OF THE i^{th} SUPERSMOOTH "SPOT"

ΔA_i = AREA OF THE i^{th} SUPERSMOOTH "SPOT"

Figure 3-9. An idealized illustration of the assumed model of a surface profile.

$[f(\ell_i) - f(\delta_{si})]\rho_{ph}$. Therefore, the drag force, F, on an area, A, is written,

$$F = \frac{1}{4} f(\delta)\rho_{ph} A c v_o - \frac{1}{4}\sum_i [f(\ell_i) - f(\delta_{si})]\Delta A_i \rho_{ph} c v_o \tag{3.27}$$

The summation is over all the incremental areas ΔA_i which have a local roughness $\delta_{si} < \delta$. Because we are assuming that all the phonons with wavelengths $\lambda > \delta \cos\theta$ are specularly reflected, the equation (3.27) is only concerned with those phonons whose wavelengths $\lambda < \delta \cos\theta$ therefore in any cases where $\ell_i > \delta$ we must set $\ell_i = \delta$ in the function $f(\ell_i)$; otherwise, we would subtract out a second time phonons which had already been removed by the first term in eq. (3.27). The second term in eq. (3.27) can then be written as,

$$\frac{1}{4}\sum [f(\ell_i) - f(\delta_{si})]\Delta A_i \rho_{ph} c v_o \tag{3.28}$$

$$= \frac{1}{4}\sum_{A_i > \delta^2} [f(\delta)\Delta A_i - f(\delta_{si})\Delta A_i]\rho_{ph} c v_o$$

$$+ \frac{1}{4}\sum_{A_i < \delta^2} [f(\ell_i) - f(\delta_{si})]\Delta_i \rho_{ph} c v_o$$

where the first summation is over those supersmooth spots whose area ΔA_i is larger than the square of the overall surface roughness, δ^2 and the second summation is over those areas which are smaller. Setting,

$$\sum_{\Delta A_i > \delta^2} \Delta A_i = A_s \tag{3.29}$$

then A_s represents the total area of supersmooth spots whose individual spot area is larger than the square of the overall roughness δ^2.

Substitute these results into eq. (3.27) and divide through by A to get,

$$F/A = \frac{1}{4}(1 - A_s/A + S)\, f(\delta)\rho_{ph} c v_o \tag{3.30}$$

where

$$S = \sum_{\Delta A_i < \delta^2} f(\delta_{si})/f(\delta) \cdot \Delta A_i/A - \sum_{\Delta A_i > \delta^2} [f(\ell_i)/f(\delta) - f(\delta_{si})/f(\delta)]\ \Delta A_i/A \qquad (3.31)$$

Under the circumstance where supersmooth spots exist $\delta_{si} << \delta$ and for suitable low temperatures where $X = ch/(kT\ \delta_{si}) >> 1$ then $f(\delta_{si})/f(\delta) << 1$ as is readily illustrated in Table 3-2. The first and third term of eq. (3.31) then becomes negligible compared to 1. Considering the second term, with $\Delta A_i \quad \ell_i^2$, the second summation is over those areas $\ell_i < \delta$; and again at low temperatures $f(\ell_i)/f(\delta) << 1$ for that part of the summation where ℓ_i is much less than δ. The only contribution we get from this second term is for those values of ℓ_i near the value of δ. For these latter values, one would expect that $\sum \Delta A_i/A << 1$. However, if there should be a non-negligible contribution from this term from supersmooth spots of size $\ell_i < \delta$, we expect for any reasonable uniform distribution in area of the supersmooth spots that the term $\sum [f(\ell_i)/f(\delta)]\Delta A_i/A$ will be small compared to 1 and will decrease with decreasing temperatures. This, in turn, would cause the term $(1 - A_s/A + S)$ to slowly increase with decreasing temperature. For convenience, we denote γ as

$$\gamma = 1 - A_s/A + S \qquad (3.32)$$

The value of γ depends, of course, on the microscopic details of the surface profile as defined within the surface model by eq. (3.29) and (3.31).

Without first hand knowledge of the surface profile one cannot predict with any degree of accuracy the value of γ or how it varies with temperature, but estimates suggest that γ will not be a strong function of temperature. Substitute eq. (3.32) into (3.30) to get,

Table 3-2. Ratios of the fractional density function f(δ) equation (3.25) for various surface roughness factors δ as a function of temperature T (T in units of Kelvin and δ in units of anstroms.

T	f(95)/f(100)	f(90)/f(100)	f(80)/f(100)	f(60)/f(100)	f(40)/f(100)	f(20)/f(100)
0.06	0.363	0.118	0.008	3×10^{-6}	4×10^{-13}	
0.08	0.464	0.198	0.026	7×10^{-5}	4×10^{-10}	1×10^{-25}
0.1	0.537	0.270	0.053	4×10^{-4}	3×10^{-8}	1×10^{-20}
0.2	0.712	0.490	0.205	0.016	1×10^{-4}	6×10^{-11}
0.4	0.805	0.637	0.373	0.085	0.006	3×10^{-6}
0.6	0.833	0.685	0.480	0.135	0.018	9×10^{-5}
0.8	0.845	0.707	0.472	0.165	0.029	4.5×10^{-4}
1.0	0.852	0.718	0.490	0.183	0.038	0.001
1.2	0.855	0.725	0.501	0.194	0.045	0.002

$$F/A = \frac{1}{4} \gamma \, f(\delta) \rho_{ph} \, cv_o$$

and from the definition of viscosity,

$$\eta = \frac{1}{4} \gamma \, f(\delta) \rho_{ph} \, v_o d \tag{3.33}$$

as the shear force and viscosity for the phonon free region when only one of the parallel surfaces specularly reflects phonons while the adjacent parallel surface is taken as a "rough" surface which only diffusely scatters the phonons. We would now like to generalize this equation to include the case where both surfaces specularly reflect phonons.

Suppose the two parallel surfaces (1) and (2) would be characterized by the surface parameters δ_1, γ_1 and δ_2, γ_2. Let us first of all consider the overall surface roughness parameter δ. In the present model of the phonon-surface interaction, it was first assumed that the surface has an overall surface roughness δ such that all phonons with wavelengths greater than $\delta \cos \theta$ are specularly reflected. This has the effect of reducing the drag producing phonon density by the fraction $f(\delta)$. If $\delta_1 < \delta_2$ then the drag producing phonon density will be $f(\delta_1)\rho_{ph}$. Those phonons with wavelengths between $\delta_1 \cos \theta$ and $\delta_2 \cos \theta$ are diffusely scattered by surface (2) but are specularly reflected from surface (1) and therefore will not transfer momentum. Therefore, in the case $\delta_1 < \delta_2$, $f(\delta_1)\rho_{ph}$ is the appropriate density of the drag producing phonons.

Second, the present surface model assumed that there might exist small localized areas or spots throughout the surfaces which are supersmooth and it was pointed out that at lower temperatures all the phonons would be specularly reflected from these supersmooth spots. From eq. (3.32) we can write with good approximation $\gamma \simeq 1 - A_s/A = (A - A_s)/A$ where A_s is the total area of the supersmooth spots. Within this

approximation γ has the interpretation of being the fraction of non-supersmooth areas over which diffuse scattering of phonons with wavelength less than $\delta \cos \theta$ takes place.

The density of momentum transferring phonons which travel between the non-supersmooth areas of surface (1) and surface (2) is then $\gamma_1 \gamma_2 f(\delta)\rho_{ph}$. However, there are some momentum transferring phonons which travel to, say, the rough area on surface (1) from the supersmooth area on surface (2) by having picked up their average drift velocity by some prior collision with the rough area of surface (2). A more exact expression for the momentum transferring phonon density would then be

$$f(\delta)\rho_{ph}\,[\gamma_1\gamma_2 + (1-\gamma_2)(1-\gamma_1)\gamma_1\gamma_2 + (1-\gamma_2)^2(1-\gamma_2)^2\gamma_1\gamma_2 + \ldots]$$

$$= f(\delta)\rho_{ph}\,\gamma_1\gamma_2\,[1 + (1-\gamma_1)(1-\gamma_2) + (1-\gamma_1)^2(1-\gamma_2)^2 + \ldots$$

$$= f(\delta)\rho_{ph}\,\gamma_1\gamma_2/(\gamma_1 + \gamma_2 - \gamma_1\gamma_2) \qquad (3.34)$$

The shear force transferred by free phonons between two parallel surfaces of the viscometer then becomes,

$$F/A = \frac{1}{4}\,\gamma_1\gamma_2\,(\gamma_1 + \gamma_2 - \gamma_1\gamma_2)^{-1}\,f(\delta)\rho_{ph}\,cv_o \qquad (3.35)$$

where the characteristic surface roughness dimension δ is equal the lesser of δ_1, δ_2 and $f(X)$ is given by eq. (3.24) where $X \simeq 114/T\delta$ (δ in units of angstroms). $\gamma_1\ \gamma_2$ are near constants which approximate the fractional area of the super-smooth area of surface (1) and surface (2), respectively.

v_o is the velocity of the moving parallel surface,

c is the velocity of sound 2.38×10^4 cm/sec,

ρ_{ph} is the phonon density $1.78 \times 10^{-5}T^4$, $K^{-4}gm/cm^3$.

The corresponding phonon free effective viscosity becomes

$$\eta_{ph} = \frac{1}{4} \gamma_1 \gamma_2 (\gamma_1 + \gamma_2 - \gamma_1\gamma_2)^{-1} f(\delta)\rho_{ph} cd \qquad (3.36)$$

We have glossed over an extremely complex quantum mechanical scattering problem with a simple model which ignores most of the details of the scattering phonomena. However, the momentum transfer problem is very forgiving of this neglect because it depends on statistical behavior. Therefore, even though we expect this surface model to have some validity for the momentum transfer problem and for other transport problems, it may not hold up for those problems which are more structured and detail dependent, such as in scattering experiments.

For some additional discussion of specular reflection of phonons in liquid He^4, one should refer to the reference books already cited and the article by Whitworth.[11]

3.3 Interpretive Theory

3.3.1 The Interpretive Theory for the Complete Viscosity of He^4 with Minute He^3 Impurity

By the complete effective viscosity of He II we mean a theoretical description of the apparent viscosity that one would observe between parallel plates in relative subcritical motion, in the presence of He^3 impurity and where the influence of geometric and surface effects have been taken into account.

In the previous section we developed an expression for the apparent or effective viscosity for pure He II as would be observed for a parallel surface viscometer for temperatures less than 0.5K (where the roton contribution to the viscosity is neglectible) and where the phonon mean free path is larger than the fluid gap. For this case, the phonon-phonon interactions are neglectible and the phonon-surface interaction determine the apparent viscous properties.

As mentioned in earlier sections, Landau and Khalatnikov developed the fundamental viscous theory of He II. They developed the phonon and

roton excitation concepts and used this theory to compute the coefficient of first viscosity of He II. The coefficient of first viscosity is what one generally means when the word viscosity is used and this is the viscosity measured for the case where the interaction between the phonons and roton dominate the viscosity properties and where any effects due to surface interactions or impurity are neglectible. The viscosity measured by Woods and Hallet as presented in Figure 3-5 represents the coefficient of first viscosity. Implicit in the discussions in these sections is the understanding that the viscometer measurements are taken at low enough velocity to permit the superfluid to remain vortex free (i.e., non turbulent) and the normal fluid to be in an equivalent laminar flow regime (i.e., non turbulent).

At this point, the two above mentioned viscosities, the free phonon viscosity and the coefficient of viscosity, seem to stand alone as separate entities. In the next section we would like to bring these two viscosities together into one form. Also, since the isotope He^3 occurs naturally ir helium sources, we will also want to include the effect of the He^3 impurity in the complete viscosity of He II.

There is a quite extensive literature on liquid He^3 - He^4 mixtures and much of this work is listed in books already mentioned. For very dilute solutions of He^3 in He^4 the system acts like a gas mixture of He^3 atoms, phonons and rotons moving through the "vacuum" background of the superfluid.

I.M. Khalatnikov and V.N. Zharkov[12] theoretically investigated the diffusion and thermal conductivity of dilute solutions of He^3 in He II. Their work was based on Landau's theory of He II. In their paper many of the interaction laws between He^3 impurity atoms and phonons and rotons were developed. Using many of the results of that paper, Zharkov[13] theoretically investigated the influence of He^3 impurity on the viscosity of He II. The present discussion uses many of the results of these two papers. Zharkov's paper has been included in the appendix. The present discussion expands Zharkov's paper to include the boundary surface effects

and also includes the more up to date work of Hollis Hallet and colleagues. The discussion has also been cast on a more elementary level in order to make the basic ideas more clear to the non-specialist.

The viscosity η_0 of liquid He^4 with minute He^3 impurity can be written as the sum of the phonon viscosity, η_{ph}, the roton viscosity η_r and the He^3 impurity viscosity, η_3:

$$\eta_0 = \eta_{ph} + \eta_r + \eta_3 \tag{3.38}$$

Each of these viscosity components (phonon, roton and minute He^3 impurity) behave like a gas particle system such that

$$\eta_j = \alpha_j \rho_j \bar{v}_j \ell_j , \quad j = (ph, r, 3) \tag{3.39}$$

where α_j = constant to be determined by the nature and type of interaction. ρ_j = density of the excitation, $\bar{v}_j$ the average velocity of the excitation, and ℓ_j the mean free path.

An alternate approach of expressing the mean free path is to write it in terms of the collision time, t (time between collisions) where $\ell_j = \bar{v}_j t_j$. The inverse of the collision time is the collision frequency (the number of collisions per second), $\theta = t^{-1}$, thus $\ell_j = v_j \theta_j^{-1}$. Equation (3.39) above can be rewritten as,

$$\eta_j = \alpha_j \rho_j \bar{v}_j^2 t_j$$

or

$$\eta_j = \alpha_j \rho_j \bar{v}_j^2 \theta_j^{-1} \tag{3.40}$$

Let us consider the phonon contribution to the complete viscosity. The phonons collide with other phonons and Landau and Khalatnikov have identified two predominant phonon-phonon types of collisions. Above 0.7K the five phonon $[P_1 + P_2 \rightleftarrows P_3 + P_4 + P_5]$ collision process dominates and below 0.7K the four phonon $[P_1 + P_2 \rightleftarrows P_3 + P_4]$ collision process dominates. The phonons also collide with the higher energy and higher momentum

elementary excitations called rotons. In pure He^4 under conditions where the mean free path of the phonon is determined by collision with other phonons and rotons, Landau and Khalatnikov have computed the coefficient of first viscosity and we will denote the phonon component as $\eta_{ph - ph, r}$. Below 1.8K it can be written in the ideal gas form

$$\eta_{ph - ph, r} = \alpha_{ph - ph, r} \rho_{ph} c^2 \theta^{-1}_{ph - ph, r} \qquad (3.41)$$

where $\alpha_{ph - ph, r}$ is a numerical constant of the phonon to phonon and roton collision, ρ_{ph} the phonon density, c the phonon velocity, and thus the velocity of sound and $\theta_{ph - ph, r}$ is the collision frequency of the phonon collisions with other phonons and rotons.

If He^3 impurity atoms are added to pure He^4, the phonons will collide with these impurity atoms. The phonon mean free path due to collision with other phonons and rotons increased rapidly with decreasing temperature (see Figure 3-6), while the phonon mean free path due to collision with the He^3 impurity atoms remains nearly constant for a given concentration. Therefore, as the temperature is lowered, a temperature will be reached where the phonon collisions with the He^3 impurity atoms will dominate over the ph → ph, r collisions. Furthermore, if the fluid gap is large enough so that the collision frequency with the wall is negligible in comparison with the collision frequency with the He^3 impurity then the phonon viscosity would be determined entirely by phonon - He^3 impurity collisions (ph - 3) and will be denoted by $\eta_{ph - 3}$. For minute concentrations the viscosity can be written in the ideal gas form,

$$\eta_{ph - 3} = \alpha_{ph - 3} \rho_{ph} c^2 \theta^{-1}_{ph - 3} \qquad (3.42)$$

For relatively small fluid gaps and very minute concentrations of He^3 impurity, the phonon collisions with the surface walls of the viscometer will dominate the phonon to phonon collisions as the temperature is lowered. Also in this region where the phonon-wall (ph - w) collisions dominate all

other phonon collisions, the phonon viscosity is denoted as $\eta_{ph - w}$ and is written in the ideal gas form as,

$$\eta_{ph - w} = \alpha_{ph - w} \rho_{ph} c^2 \theta^{-1}_{ph - w} \tag{3.43}$$

The next step is to compute the phonon viscosity for the general case where the phonon collisions with other phonons and rotons, with the He^3 impurity atoms and with the surface wall are all of nearly equal importance. In these overlap regimes the total phonon viscosity can still be written in the kinetic theory form,

$$\eta_{ph} = \alpha_t \rho_{ph} c^2 \theta^{-1}_t \tag{3.44}$$

Provided that the three different types of collisions are independent of each other as would be the case for low densities, the total collision frequency θ_t is the sum of the individual frequencies

$$\theta_t = \theta_{ph - ph, r} + \theta_{ph - 3} + \theta_{ph - w} \tag{3.45}$$

and the numerical constant α_t would follow from a rigorous theory. Because the mean free path due to phonon collisions with other phonons and rotons changes so rapidly with temperature, the transition or overlap regions between the ph - ph, r and the ph - w collisions are very narrow. Furthermore, for minute concentrations of He^3 impurity the ph - 3 collisions play only a minor role. The numerical constants $\alpha_{ph - ph, r}$, $\alpha_{ph - 3}$ and $\alpha_{ph - w}$ should all be the same order of magnitude and so α_t would be of this same order of magnitude.

With these statements in mind, we then approximate the phonon contribution to the complete viscosity as

$$\eta_{ph} = \rho_{ph} c^2 \left[\frac{\theta_{ph - ph, r}}{\alpha_{ph - ph, r}} + \frac{\theta_{ph - 3}}{\alpha_{ph - 3}} + \frac{\theta_{ph - w}}{\alpha_{ph - w}} \right]^{-1} \tag{3.46}$$

When only one of the collision processes dominate, we see that this expression will reduce to the appropriate equation; either (3.41), (3.42), or (3.43). Furthermore, this equation provides an interpretive equation for the overlap or transition region because it is a good approximation to equation (3.44) with (3.45).

In terms of collision times ($t^{-1} = \theta$), equation (3.46) can be rewritten as

$$\eta_{ph} = \rho_{ph}\, c^2 \left[\frac{t^{-1}_{ph - ph,\, r}}{\alpha_{ph - ph,\, r}} + \frac{t^{-1}_{ph - 3}}{\alpha_{ph - 3}} + \frac{t^{-1}_{ph - w}}{\alpha_{ph - w}} \right]^{-1} \qquad (3.47)$$

Taking $\rho_{ph}\, c^2$ inside the bracket and using equations (3-41), (3-42), and (3-43), the phonon contribution η_{ph} to the complete viscosity can be rewritten in the form

$$\eta_{ph} = \left[\frac{1}{\eta_{ph - ph,\, r}} + \frac{1}{\eta_{ph - 3}} + \frac{1}{\eta_{ph - w}} \right]^{-1} \qquad (3.48)$$

Let us now evaluate the individual terms in this equation.

For T < 0.7K Khalatnikov concluded that the dominant scattering process was the 4 phonon process together with the scattering of the phonons by the rapidly vanishing rotons. He computed the phonon viscosity for this type of scattering to be

$$\eta_{ph - ph,\, r} = 1.63 \times 10^{-4}\, T^{-5} \left[\frac{2.15 \times 10^{-5}\, T^{9/2}\, e^{\Delta/kT}}{1 + 2.15 \times 10^{-5}\, T^{9/2}\, e^{\Delta/kT}} \right] \qquad (3.49)$$

The presently accepted value of $\Delta/k = 8.65K$.

For T > 0.8 the 5 phonon scattering process dominates along with the phonon-roton scattering. Woods and Hollis Hallet[6] have recalculated Khalatnikov's original equation making minor adjustments to some

constants and obtained excellent agreement with their experimental measurements. They found for $T > 0.8K$:

$$\eta_{ph - ph, r} = 3.5 \times 10^{-8}\ T^{-\frac{1}{2}}\ e^{8.65/T} \left[\frac{1 + 2.66 \times 10^{-4}\ T^{9/2}\ e^{8.65/T}}{1 + 4.26 \times 10^{-3}\ T^{9/2}\ e^{8.65/T}} \right] \tag{3.50}$$

There appears to be some uncertainty in the appropriate value of $\alpha_{ph - ph, r}$ but we will follow Atkins[2] and take $\alpha_{ph - ph, r} = .07$.

Let us now consider the term $\eta_{ph - 3}$. In an extended liquid helium medium where wall effects can be ignored we would qualtitatively expect the phonon mean free path to become limited by the He^3 impurity atoms as the temperature is lowered i.e., the phonon component of the viscosity η_{ph} would approach $\eta_{ph - 3}$ at low temperatures.

Khalatnikov and Zharkov[12] have calculated the mean free path for the phonon - He^3 collision,

$$\ell_{ph - 3} \simeq 8 \times 10^{-6}/(T^5\ X_3 \delta) \tag{3.51}$$

where X_3 is the He^3 impurity concentration and δ is a complicated function, reported to be of the order of unity. Ptukha[14] has estimated from her conductivity measurements that $\delta \simeq 10/T$.

Again, assuming the equation

$$\eta_{ph - 3} = \alpha_{ph - 3}\ \rho_{ph}\ c\ \ell_{ph - 3}$$

and taking $\rho_{ph} = 1.78 \times 10^{-5}\ T^4$ gm/cm^3, $c = 2.38 \times 10^4$ cm/sec. $\alpha_{ph - 3} = .17$ we find after substitution,

$$\eta_{ph - 3} \simeq 2.37 \times 10^{-8}/X_3$$

If one assumes the form of this equation is correct, i.e., $\eta_{ph-3} = \text{constant}/X_3$, then using equation (3.48) and the experimental viscosity data of Strass, Taconis and Fokkens[21] at 1K on dilute solution of He^3 in He II we find that

$$\eta_{ph-3} = 3.3 \times 10^{-8}/X_3 \tag{3.52}$$

as $X_3 \to 0$, a value quite close to the above calculated value. The above expression η_{ph-3} differs somewhat in temperature dependence from the corresponding equation developed by Zarkhov[13]; however above about 0.8K they both give values of η_{ph-3} of the same order of magnitude. For temperatures much less than 0.8K, Zharkov's expression for η_{ph-3} implies a much stronger scattering of the phonons by the He^3 impurity atoms and thus a much more rapid attentuation of η_{ph} than equation (3.52) would give. This is a question which should be more thoroughly investigated; however in order not to be unduly delayed in presenting this material we will adopt equation (3.52). The phonon contribution to the complete viscosity is then obtained by substituting equation (3.49) or (3.50) and (3.52), and equation (3.36) from Section (3.2.2) into equation (3.48).

Let us next consider the roton contribution η_r to the complete effective viscosity. The roton mean free path is limited by collisions with other rotons, the He^3 impurity atoms and the surface walls of the viscometer. The roton carries much more momentum than the phonons; consequently, the phonons have little effect on limiting the roton mean free path and this interaction can be ignored.

In the same manner as was done for the phonon contribution, we introduce the roton-roton collision frequency t_{r-r}^{-1}, the roton - He^3 impurity atom collision frequency t_{r-3}^{-1}, and the roton-surface wall collision frequency t_{r-w}^{-1}. As in equation (3.47), the roton contribution η_r to the complete viscosity becomes,

$$\eta_r = \rho_r v_r^2 \left[\frac{t_{r-r}^{-1}}{\alpha_{r-r}} + \frac{t_{r-s}^{-1}}{\alpha_{r-3}} + \frac{t_{r-w}^{-1}}{\alpha_{r-w}} \right]^{-1} \tag{3.53}$$

or in terms of the viscosities,

$$\eta_r = \left[\frac{1}{\eta_{r-r}} + \frac{1}{\eta_{r-3}} + \frac{1}{\eta_{r-w}} \right]^{-1} \tag{3.54}$$

The roton-roton viscosity term η_{r-r} has been computed by Khalatnikov. His value is quite close to the experiment value of Heikkila and Hollis-Hallet. The experimental value is,

$$\eta_{r-r} = 12.6 \times 10^{-6}, \text{ poise} \tag{3.55}$$

Zharkov[15], in his article, computed the viscosity η_{r-3} associated with the roton - He^3 impurity collision,

$$\eta_{r-3} = 5.0 \times 10^{-5} \quad X_3^{-1} \, e^{-8.65/T}, \text{ poise} \tag{3.56}$$

The viscosity η_{r-w} associated with the roton collision with the surface walls of the viscometer is assumed to have the same form as the equation (3.36) in Section 3.2.2 developed for the phonons; namely,

$$\eta_{r-w} = \frac{1}{4} \gamma_r \rho_r v_r d \qquad (3.57)$$

γ_r is the specular reflection term for the rotons at the surfaces. The terms $\rho_r v_r$ can be written as a product of the number density N_r and the roton momentum P_o. The roton number density is given by Landau and Khalatnikov and P_o is obtained from the phonon-roton spectrum E versus P. Substituting these values into equation (3.57) gives,

$$\eta_{r-w} = 3.6 \times 10^3 \gamma_r d T^{1/2} e^{-8.65/T}, \text{ poise} \qquad (3.58)$$

Substitution of equations (3.55), (3.56), and (3.58) into equation (3.54) gives the roton contribution to the complete viscosity.

Let us now compute the He^3 impurity contribution η_3 to the complete effective viscosity. The mean free path of the He^3 impurity atoms is limited by collisions with other He^3 impurity atoms, the rotons and the surface walls of the viscometer. Like the rotons, the He^3 impurity atoms are little affected by the phonons because the phonons carry a much lower effective mass than either the He^3 atoms or the rotons. For not too large a concentration, X_3, the He^3 atoms lose their gas-atoms move like an ideal gas through the superfluid background of the He II. For large concentrations X_3, the He^3 atoms lose their gas-like quality because the He^3 atoms are in near continuous interaction with each other and thus behave like a liquid. At low concentration the He^3 atoms move freely between interactions and thus behave like a gas. The He^3 gas atoms obey the Fermi-Dirac distribution function which become degenerate (non-classical) below the Fermi temperature T_F where

$$T_F \simeq 2.57 X_3^{2/3}, \text{ (K)} \qquad (3.59)$$

For temperatures much greater than the Fermi temperature T_F, the Fermi Dirac distribution reduces to the classical Boltzman distribution. Therefore, for minute concentrations where the He^3 atoms behave like an

ideal gas (i.e. a non-interacting gas except for collisions) and for temperatures greater than the Fermi temperature, the He^3 impurity atoms behave like an ideal classical gas with the one understanding that the He^3 atoms are moving through a superfluid "vacuum like" medium and not the voidless vacuum of empty space. This latter condition only requires that the mass of He^3 impurity atoms be adjusted to a larger value m*. The value of m*, the effective mass of the He^3 impurity atom, increases slowly with the concentration X_3, but for $X_3 \to 0$, $m^*/m_3 = 2.34$.[15]

Following the classical gas approach, as was done by Zharkov, we may write the viscosity η_{3-3} associated with the He^3 impurity atoms collision with other He^3 impurity atoms as

$$\eta_{3-3} = \alpha_{3-3} \rho_3 v_3^2 t_{3-3} \tag{3.60}$$

with

$$\alpha_{3-3} \simeq 1/3$$

$$v_3 = \frac{8}{3} \left(\frac{2kT}{\pi m^*}\right)^{1/2}$$

$$\rho_3 = N_3 m^*$$

and from Zharkov

$$t_{3-3}^{-1} = 2.9 \times 10^{11} \, a \, T^{1/2} X_3 \tag{3.61}$$

where, a, is a constant reported to be of the order of unity. The He^3 impurity number density N_3 can be written in terms of the concentration X_3 where

$$X_3 = \frac{N_3 m_3}{N_4 m_4 + N_3 m_3}$$

and for minute concentration X_3, $N_4 m_4 >> N_3 m_3$,

$$X_3 \simeq N_3 m_3 / N_4 m_4 = N_3 m_3 / \rho_4$$

therefore,

$$N_3 = \rho_4 X_3 / m_3 \tag{3.62}$$

Substituting the above equations into equation (3.60) for the viscosity η_{3-3} to get,

$$\eta_{3-3} = 1.5 \frac{kT}{m_3} \rho_4 X_3 t_{3-3} \tag{3.63}$$

Then substitute numerical values to get,

$$\eta_{3-3} = 2.07 \times 10^{-5} T^{1/2}/a, \text{ poise} \tag{3.64}$$

which is the same value as obtained by Zharkov.

We can estimate the value of, a, in the low temperatue region ~0.1K using the theoretical computation by William E. Keller[16] for the viscosity of gaseous He^3 at low temperatures. From equation (3.60) we conclude that the viscosity of He^3 impurity in liquid He^3 is larger by the factor $(m^*/m_3)^{1/2}$ than the viscosity of gaseous He^3 would be.

By extrapolating Keller's theoretical results to 0.1K, we estimate that $\eta_{3-3} \simeq 5.3 \times 10^{-6} T^{1/2}$ assuming a $T^{1/2}$ temperature dependence. Comparing this value to equation (3.64) we conclude that $a \approx 3.9$, which is of the order of magnitude of 1 as Khalatnkiov and Zharkov predicted.

In a similar manner we find, using Zharkov's results, that the viscosity associated with the He^3 impurity atom collision with the rotons is

$$\eta_{3-r} = 7.2 \times 10^{-7} X_3 e^{8.65/T}, \text{ poise} \tag{3.65}$$

The viscosity η_{3-w} associated with the He^3 impurity atoms' collision with the surface walls of the viscometer is written in a manner similar to that for the phonon as,

$$\eta_{3-w} = \frac{1}{4} \gamma_3 \rho_3 v_3 d \tag{3.66}$$

taking

$$\rho_3 = \rho X_3 m^*/m_3$$

and

$$v_3 = \frac{8}{3} \left(\frac{2}{\pi} \frac{kT}{m^*}\right)^{1/2}$$

then

$$\eta_{3-w} = \frac{2}{3} \gamma_3 \rho X_3 m^*/m_3 \left(\frac{2}{\pi} \frac{kT}{m^*}\right)^{1/2} d \tag{3.67}$$

Substituting numerical values to get

$$\eta_{3-w} = 6.2 \times 10^2 \gamma_3 X_3 d T^{1/2}, \text{ poise} \tag{3.68}$$

The He^3 impurity contribution η_3 to the complete effective viscosity is found by substituting equations (3.64), (3.65), and (3.66) into the equation:

$$\eta_3 = \left[\frac{1}{\eta_{3-3}} + \frac{1}{\eta_{3-r}} + \frac{1}{\eta_{3-w}} \right]^{-1} \tag{3.69}$$

3.3.2 Summary of the Interpretative Equation

In summarizing the equation for the complete effective viscosity of He II in the presence of minute concentration X_3 of He^3 impurity as would be observed by a parallel surface viscometer at subcritical velocities, we write

$$\eta = \eta_{ph} + \eta_r + \eta_3 \tag{3.70}$$

where the phonon component of the viscosity η_{ph} is

$$\eta_{ph} = \left[\frac{1}{\eta_{ph - ph, r}} + 9.8 \times 10^{7} X_3 + \frac{9.44 (\gamma_1 + \gamma_2 - \gamma_1 \gamma_2)}{\gamma_1 \gamma_2 f d T^4} \right]^{-1} \tag{3.71}$$

with the pure He II coefficient of viscosity $\eta_{ph - ph, r}$ given, for $T < 0.8K$:

$$\eta_{ph - ph, r} = 1.63 \times 10^{-4} T^{-5} \left[\frac{2.15 \times 10^{-5} T^{9/2} e^{8.65/T}}{1 + 2.15 \times 10^{-5} T^{9/2} e^{8.65/T}} \right] \tag{3.72}$$

and for $T > 0.8K$:

$$\eta_{ph - ph, r} = 3.5 \times 10^{-8} T^{-1/2} e^{8.65/T} \left[\frac{1 + 2.66 \times 10^{-4} T^{9/2} e^{8.65/T}}{1 + 4.26 \times 10^{-3} T^{9/2} e^{8.65/T}} \right] \tag{3.73}$$

and where the roton component of the viscosity η_r is

$$\eta_r = [7.94 \times 10^{4} + 2.0 \times 10^{4} X_3 e^{8.65/T} + 2.8 \times 10^{-4} e^{8.65/T}/(\gamma d T^{1/2})]^{-1} \tag{3.74}$$

and where He^3 impurity component of viscosity η_3 is

$$\eta_3 = [1.9 \times 10^{5} T^{-1/2} + 1.4 \times 10^{6} e^{-8.65/T}/X_3 + 1.6 \times 10^{-3}/(\gamma_3 X_3 d T^{1/2})]^{-1}$$

The unit used for viscosity is poise and the other parameters are, as well, in the CGS units. The following parameters then determine the value of the complete effective viscosity:

d = fluid gap between the parallel plates

X_3 = concentration of He^3 impurity atoms

T = the absolute temperature, K

γ_r, γ_3 are the specular reflection and slip terms of the roton and He^3 impurity atoms.

$f = f(\delta)$ the fractional density of diffusely scattered phonons from a surface of overall roughness δ given by tion (3.25).

δ is the overall surface roughness factor (an asperity dimension) in units of Å, see Section 3.2.2.

γ_1, γ_2 are the phonon surface smoothness ratios for surfaces (1) and (2) defined by equations (3.32), (3.29), and (3.31).

Remarks on γ_r and γ_3

If one compares equation (3.36), to (3.57) and (3.66), it will be seen that γ_1 and γ_2 are not directly comparable to γ_r and γ_3. Whereas γ_1 and γ_2 have an interpretation in terms of the area of the supersmooth spots, as discussed in the later part of Section 3.2.2. The terms γ_r and γ_3 are sort of "catch all" parameters to correct the viscosity of the roton and He^3 atoms for specular reflection of what ever form it may take. We did not go into a detailed analysis of γ_r and γ_3 because the rotons and He^3 impurity atoms play only a secondary role to the phonons in contribution to the complete viscosity in the region of interest of the present report.

Since the wavelength of the roton and the He^3 impurity atoms are very short one would not expect to observe a great deal of specular reflection of the kind discussed for the phonon.

3.3.2.1 Some Clarifying Remarks on the Notation

Perhaps a few clarifying remarks on the use of subscript will be helpful.

As applied to the physical quantities η, α, ℓ, t, θ, etc. the symbol $S_{i-j,\,k,\,l}$ means the $i^{\underline{th}}$ component of the physical quantity S due to interaction of the $i^{\underline{th}}$ quantity with the j, k, and l quantities. As an example, the symbol $\eta_{ph\,-\,ph,\,r}$ means the phonon component of the viscosity due to the phonon collisions with other phonons and rotons. This particular quantity $\eta_{ph\,-\,ph,\,r}$ also happens to be the phonon contribution to the coefficient of first viscosity.

The symbol $\ell_{ph\,-\,ph,\,r,\,3,\,w}$ denotes the phonon mean free path due to collisions with other phonons (ph), rotons (r), He^3 impurity atoms (3) and the surface walls (w) of the viscometer. As another example the symbol ℓ_{3-3} denotes the mean free path of the He^3 impurity atom due to collision with other He^3 impurity atoms.

In order to shorten the notation, we will write $S_i = S_{i\,-\,j,\,k,\,l}$ for the particular case where $S_{i\,-\,j,\,k,\,l}$ is the $i^{\underline{th}}$ component of the physical quantity S where <u>all</u> the significant collisions or interactions have been included. For example, in the present dicussion a complete list of interactions of the phonons are the interactions of the phonon with other phonons, rotons, He^3 impurity atoms and the surface wall of the viscometer; therefore, the symbol $\eta_{ph\,-\,ph,\,r,\,3,\,w}$ is considered to include all significant collisions of interest and will therefore be shortened to η_{ph}. Furthermore, in certain circumstances the interaction of the phonons with the He^3 impurity atoms and/or the surface walls may be of no consideration; therefore, in such cases the symbol $\eta_{ph\,-\,ph,\,r}$ may also be shortened to η_{ph}.

3.4 A More Exact Study of the Complete Effective Viscosity

3.4.1 The Effective Viscosity of the Phonons with a More Exact Emphasis on the Transition Region

In the study of flow of gases through a pipe, the flow obeys the Poiseuille formula when the mean free path of the molecules is much smaller than the diameter of the pipe. Furthermore, the gas flow resistance can be

characterized by the coefficient of viscosity. This type of flow is also called Poiseuille flow or viscous flow. In liquid He^4 this region is analogous to that theoretically investigated by Khalatnikov and experimentally measured by Hollis Hallet and coworkers as well as many others. The gas flow obeys Knudsen's formula when the mean free path of the molecules is much larger than the diameter of the tube. This type of flow is called Knudsen flow, free molecular flow, or just molecular flow. In liquid He^4 this region is analogous to the theoretical investigation in Section 3.2.

The gas flow in the region where the mean free path of the molecule is of the same order of magnitude as the diameter of the tube is called intermediate or transition flow. There appears to be no quantitative kinetic theory treatment of this flow. Poiseuille's formula can be extended to some degree into the transition region by adding correction terms for the incomplete momentum transfer of the molecules at the surface (commonly called slip). An interpretive equation for this analogous (transition) region in liquid He^4 was developed in Section 3.3. In the next section we would like to develop a more exact expression for the effective viscosity of liquid He^4 in the transition region.

As in all the previous calculations, we assume the geometry of parallel surfaces with liquid He^4 filling the gap, d, between the surface. A tangential force per unit area (a shear stress), F/A, is applied to one parallel surface to bring it to a subcritical (non-turbulent) steady state velocity v_o and an identical tangential force per unit area, F/A, must be applied to the other parallel surface to maintain it at zero velocity. This stress is transferred from the moving plate to the stationary plate by the liquid He II's system of excitation: phonons, rotons and He^3 impurity. For very minute concentrations of He^3 impurity and for moderately large fluid gaps, the roton and He^3 impurity atom contributions to the complete effective viscosity within the transition region is a small fraction of the phonon contribution as can be verified from equations (3.71) of Section 3.3.2. Within these limitations, therefore, we will consider in this section the stress F/A transferred by the

phonons only between the moving and stationary parallel plates. Qualitatively, the phonon which has interacted with the moving surface acquires, on the average, a drift velocity in the direction of the moving surface. This phonon then moves toward the stationary surface and one of two things will happen: it will travel between the surfaces without colliding with another phonon or it will collide with one or more other phonons. The phonons which travel between the plates without collisions with other phonons act like "free" phonons while the phonons which endure one or more collisions act like a "viscous" phonons.

Since the free phonons (by definition) do not interact with the other phonons they act independently of the viscous phonons and so the stress $(F/A)_{ph}$ at the parallel surface can be written as the sum of the stress due to the free phonons $(F/A)_{F,\,ph}$ and the stress due to the viscous phonon $(F/A)_{V,\,ph}$, i.e.,

$$(F/A)_{ph} = (F/A)_{F,\,ph} + (F/A)_{V,\,ph} \tag{3.76}$$

If $\rho_{F,\,ph}$ is the phonon density of the free phonons then using the results of Section 3.2, equation (3.35), the stress $(F/A)_{F,\,ph}$ due to the free phonons becomes,

$$(F/A)_{F,\,ph} = \frac{1}{4}\,\gamma_1\,\gamma_2\,(\gamma_1 + \gamma_2 - \gamma_1\,\gamma_2)^{-1}\,f\,\rho_{F,\,ph}\,c\,v_o \tag{3.77}$$

On the other hand, the density of the viscous phonons $\rho_{V,\,ph}$ is defined as

$$\rho_{V,\,ph} = \rho_{ph} - \rho_{F,\,ph} \tag{3.78}$$

where ρ_{ph} is the (total) phonon density. The viscous phonon density $\rho_{V,\,ph}$ is the density of the phonons which experience one or more collisions with other phonons (or rotons) between successive collisions with the surface walls of the parallel surface viscometer. The stress $(F/A)_{V,\,ph}$ due to the viscous phonons is written in terms of the kinetic theory equation as

$$(F/A)_{V,\,ph} = \alpha_{ph}\,\rho_{V,\,ph}\,c\,\ell'_{V,\,ph}\,v_o/d \qquad (3.79)$$

where $\ell'_{V,\,ph}$ is the mean free path of the viscous phonons. For the case where $\ell'_{V,\,ph} << d$ we would normally take $\ell'_{V,\,ph} = \ell_{V,\,ph}$ to be the mean free path of the viscous phonon due to collision with other phonons and rotons.* However, since we are specifically considering the case where the mean free path approaches the fluid gap, d, then the surface collisions become an appreciable fraction of the total collisions of the viscous phonons and therefore the surface collisions can no longer be ignored as is normally done in computing the mean free path. Another way of looking at the same thing is that when the coefficient of viscosity is computed, only collisions between the excitation are considered while in reality a viscosity measurement requires the excitations to interact with the surface walls of the viscometer. Consequently the coefficient of viscosity and the measured viscosity will only be in agreement when the rate of collisions of the excitations with each other completely dominates over the rate of collisions with the surface walls of the viscometer. This is certainly not the case when $\ell_{ph} \sim d$.

Let us now consider how the viscous phonons transfer the stress $(F/A)_{V,\,ph}$ from one surface wall to the surface interacting phonons; then, across the gap, d, occupied by phonons and rotons to the opposite surface interacting phonons which in their turn transfers the stress to the second surface wall.

In Figure 3-10 is depicted the parallel surface viscometer, with the upper surface moving with a steady state velocity v_o in response to an externally applied stress F/A. Focusing entirely on the viscous component at

---

*Even though we are assuming the roton viscosity to be small, the rotons still have a profound effect on the mean free path of the phonons which cannot be ignored. A more precise notation for the viscous mean free path which we are using here would be $\ell_{V,\,ph\,-\,ph,\,r}$, however, we will use the shorter notation in this section. Also in this section we will use the shorter notation η_{ph} for $\eta_{ph\,-\,ph,\,r}$ and $\eta_{V,\,ph}$ for $\eta_{V,\,ph\,-\,ph,\,r}$, etc.

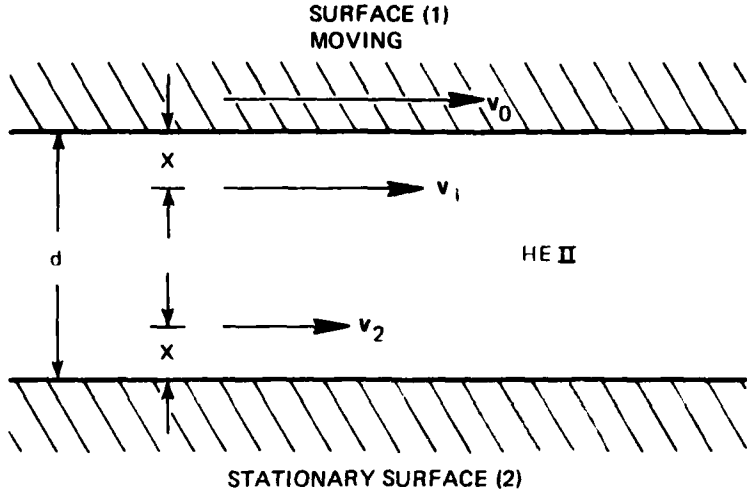

Figure 3-10. The parallel surface viscometer illustrating variables used in computation in section 3.4.1.

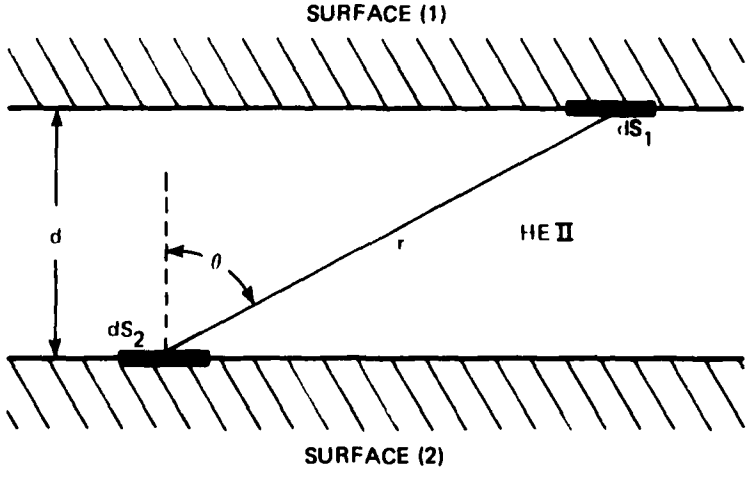

Figure 3-11. The parallel surface viscometer illustrating variables used in computations in Section 3.4.1.

this point, then the viscous stress $(F/A)_{V,\,ph}$ applied to the moving plate is transferred to the surface interaction viscous phonons by imparting to them some average drift velocity. The surface interacting viscous phonons travel on the average an assumed distance X away from the surface (1) where on the average they collide with other phonons (and rotons) and impart to the viscous phonon system the stress $(F/A)_{V,\,ph}$.

We denote v_1 as the average drift velocity of the viscous phonons system at a distance X from the surface (1) where it is assumed that due to phonon-phonon collisions the surface interacting viscous phonons have on the average established a drift equilibrium with the other neighboring viscous phonons. The shear stress $(F/A)_{V,\,ph}$ is then transferred through the remainder of the fluid gap to within a distance X of surface (2) through phonon-phonon and phonon-roton collisions. The average drift velocity of the viscous phonons at this point is denoted as v_2. At the distance X from surface (2) the phonons travel on the average to surface (2) without collisions with other phonons or rotons. The distance X that the viscous phonons travel on the average from a surface to a collision with another phonon or roton is of course proportional to its mean free path and by a simple calculation is found to be

$$X = \frac{2}{3}\,\ell_{V,\,ph} \tag{3.80}$$

Since the viscous phonons travel from surface (1) to a distance X from this surface on the average before having a collision, they therefore travel over this distance on the average as free phonons. The shear stress $(F/A)_{V,\,ph}$ across this boundary layer can then be written using the results of Section 3.2 and equation (3.33)

$$(F/A)_{V,\,ph} = \frac{1}{4}\,\gamma_1\,f_1\,\rho_{V,\,ph}\,(v_o - v_1) \tag{3.81}$$

The shear stress across the fluid from a distance X from surface (1) to a distance X from surface (2) is obtained from the common equation relating the shear stress to the coefficient of viscosity; namely,

$$(F/A)_{V,\ ph} = \eta_{V,\ ph} \frac{v_1 - v_2}{d - 2X} \tag{3.82}$$

Likewise, the stress is delivered to the surface (2) by the viscous phonons which travel from a distance X from surface (2) to the surface as though they were on the average free phonon and so as in equation (3.81).

$$(F/A)_{V,\ ph} = \frac{1}{4} \gamma_2\ f_2\ \rho_{V,\ ph}\ c\ (v_2 - 0) \tag{3.83}$$

Substituting equations (3.83), (3.81), and (3.80) into equation (3.82) to eliminate v_2, v_1, and X we get,

$$(F/A)_{V,\ ph} = \frac{\eta_{V,\ ph}\ v_o/d}{1 + \frac{4}{3} \frac{\ell_{V,\ ph}}{d} \left[3\ \alpha_{ph} \left(\frac{\gamma_1\ f_1 + \gamma_2\ f_2}{\gamma_1\ f_1\ \gamma_2\ f_2} \right) - 1 \right]} \tag{3.84}$$

which represents the shear stress at the surface walls of the viscometer due to the viscous phonons in terms of the viscosity $\eta_{V,\ ph}$. We see that for the case $\ell_{V,\ ph}/d \ll 1$ the above equation (3.84) reduces to the customary equation which relates the coefficient of viscosity to the shear stress; namely, $F/A \rightarrow \eta\ v_o/d$. For the case where the surfaces (1) and (2) have identical specular reflection terms γ, f, equation (3.84) reduces to

$$(F/A)_{V,\ ph} = \frac{\eta_{V,\ ph}\ v_o/d}{1 + \frac{4}{3} \frac{\ell_{V,\ ph}}{d} \left(\frac{6\ \alpha_{ph} - \gamma f}{\gamma f} \right)} \tag{3.85}$$

For a system of gas particles $\alpha_{ph} = 1/3$ and the above expression reduces to the classical gas expression for the coefficient of viscosity corrected by Maxwell's theory of slip where we identify γf as the momentum transfer ratio.[17]

From equation (3.76), (3.84), and (3.77) it is seen that in order to complete the calculation for the shear stress $(F/A)_{ph}$ due to the phonons in the transition region we need to compute the viscous phonon viscosity $\eta_{V,\,ph}$, the mean free path $\ell_{V,\,ph}$ and the free phonon density $\rho_{F,\,ph}$. Let us now compute the viscous phonon mean free path, $\ell_{V,\,ph}$.

Let us define several terms. The phonon mean free path is equal to the average of the distances traveled by each of the phonons between collisions with other phonons. If we let ℓ_i be the free path of the i^{th} phonon, then the mean free path is

$$\ell_{ph} = \frac{1}{N_{ph}} \sum_{i=1}^{N_{ph}} \ell_{ph\,i} \tag{3.86}$$

where N_{ph} is the total number of phonons.

Some of the phonons would have free path lengths which are long enough to travel from one parallel surface of the viscometer to the adjacent parallel surface. Let us label each of these phonon path lengths $\ell_{F,\,ph\,i}$ and the remainder shorter free path length as $\ell_{V,\,ph\,i}$ then

$$\sum_{i}^{N_{ph}} \ell_{ph\,i} = \sum_{i}^{N_{F,\,ph}} \ell_{F,\,ph\,i} + \sum_{i}^{N_{V,\,ph}} \ell_{V,\,ph\,i} \tag{3.87}$$

We denote the mean free path of the free phonons as $\ell_{F,\,ph}$

$$\ell_{F,\,ph} = \frac{1}{N_{F,\,ph}} \sum_{i}^{N_{F,\,ph}} \ell_{F,\,ph\,i} \tag{3.88}$$

where the sum is over the free phonons. The mean free path of the viscous phonons $\ell_{V,\,ph}$ is

$$\ell_{V,\,ph} = \frac{1}{N_{V,\,ph}} \sum_{i}^{N_{V,\,ph}} \ell_{V,\,ph\,i} \tag{3.89}$$

where the sum is over the viscous phonons.

The total number of phonons N_{ph} is

$$N_{ph} = N_{F,\,ph} + N_{V,\,ph} \tag{3.90}$$

Substitute equations (3.87), (3.88), and (3.89) into equation (3.86) to get

$$\ell_{ph} = \frac{N_{V,\,ph}}{N_{ph}} \ell_{V,\,ph} + \frac{N_{F,\,ph}}{N_{ph}} \ell_{F,\,ph} \tag{3.91}$$

Solving this equation for $\ell_{V,\,ph}$,

$$\ell_{V,\,ph} = \frac{N_{ph}}{N_{V,\,ph}} \ell_{ph} - \frac{N_{F,\,ph}}{N_{V,\,ph}} \ell_{F,\,ph} \tag{3.92}$$

Substituting from equation (3.80) $N_{V,\,ph} = N_{ph} - N_{F,\,ph}$ then

$$\ell_{V,\,ph} = \frac{N_{ph}}{N_{ph} - N_{F,\,ph}} \left[\ell_{ph} - \frac{N_{F,\,ph}}{N_{ph}} \ell_{F,\,ph} \right] \tag{3.93}$$

The above equation (3.93) relates $\ell_{V,\,ph}$ to $\ell_{F,\,ph}$ and we will compute $\ell_{F,\,ph}$ using an integral form of equation (3.88). Since we cannot really count the individual phonons as suggested in equation (3.88), we will write a free path distribution function in terms of descriptive macroscopic variables. Figure 3-11 helps to illustrate how the problem can be set up.

Taking cognizance of the fact that the free path of a phonon may depend upon its momentum or wavelength it is necessary to introduce the number density of phonons (Reference 18) with wavelengths between λ and $\lambda + d\lambda$, as $N'_{ph}(\lambda)$ then

$$N_{ph} = \int_0^\infty N'_{ph}(\lambda)\, d\lambda = 4\pi \int_0^\infty \frac{\lambda^{-4}}{(e^{-Ch/kT\lambda} - 1)}\, d\lambda \tag{3.94}$$

where N_{ph} is the number of phonons per unit volume.

Assuming a homogeneous spatial distribution and an isotropic momentum distribution of phonons one can write the incident flux of phonons with wavelengths between λ and $\lambda + d\lambda$ upon surface (2) as $1/4\ N'_{ph}\ (\lambda)\ c$. By the cosine law, the fraction of incident phonons whose incident direction of travel are within the solid angle $d\Omega$ at angle θ, is $1/\pi \cos\theta\ d\Omega$ (see Figure 3-11).

Furthermore, from the above assumptions one can show that the probability, $F(y, \ell_\lambda)\ dy\ d\lambda$* that the phonons with wavelength between λ and $\lambda + d\lambda$ will have a mean free path length between y and y + dy is

$$F(y, \ell_\lambda)\ dy\ d\lambda = \frac{1}{\ell_\lambda} e^{-y/\ell_\lambda} dy\ d\lambda \qquad (3.95)$$

where ℓ_λ, which in general is a function of wavelength λ, represents the mean free path of the phonons with wavelength λ to $\lambda + d\lambda$ due to collision with other phonons and rotons.

We can now write the incident flux of phonons onto surface (2) between wavelength λ and $\lambda + d\lambda$ with incident direction θ within the solid angle $d\Omega$ and with a free path length between y and y + dy as

$$\frac{1}{4} N'_{ph}\ c \frac{\cos\theta}{\pi} \frac{1}{\ell_\lambda} e^{-y/\ell_\lambda} d\Omega\ dy\ d\lambda \qquad (3.96)$$

The incident flux of free phonons is obtained by integrating this expression over $\lambda = 0$ to ∞, $y = r$ to ∞, and $\Omega = 0$ to 2π. Where $N_{F,\,ph}$ is the free phonon number density, the incident flux of free phonons is $\frac{1}{4} N_{F,\,ph}\ c$ then,

$$\frac{1}{4} N_{F,\,ph}\ c = \int_{\Omega=0}^{2\pi} \int_{y=r}^{\infty} \int_{\lambda=0}^{\infty} \frac{1}{4} N'_{ph}\ c \frac{\cos\theta}{\pi} \frac{1}{\ell_\lambda} e^{-y/\ell_\lambda} d\Omega\ dy\ d\lambda \qquad (3.97)$$

---

*Present, reference 19, develops a similar but less general expression.

Also, the mean free path of the free phonons $\ell_{F,\,ph}$ can be immediately written as

$$\ell_{F,\,ph} = \frac{1}{\frac{1}{4} N_{F,\,ph}\, c} \int_{\Omega=0}^{2\pi} \int_{y=r}^{\infty} \int_{\lambda=0}^{\infty} \frac{1}{4} N'_{ph}\, c\, \frac{\cos\theta}{\pi} \frac{1}{\ell_\lambda} e^{-y/\ell_\lambda}\, y\, d\Omega\, dy\, d\lambda \tag{3.98}$$

We emphasize that what makes this the free phonon mean free path is that the lower limit on y is r. If this lower limit is set to y = 0 then the result of the integration should be the phonon mean free path ℓ_{ph},

$$\ell_{ph} = \frac{1}{\frac{1}{4} N_{ph}\, c} \int_{\Omega=0}^{2\pi} \int_{y=0}^{\infty} \int_{\lambda=0}^{\infty} \frac{1}{4} N'_{ph}\, c\, \frac{\cos\theta}{\pi} \frac{1}{\ell_\lambda} e^{-y/\ell_\lambda}\, y\, d\Omega\, dy\, d\lambda \tag{3.99}$$

Considering the integration over λ, then if

$$\int_{\lambda=0}^{\infty} N'_{ph} \frac{1}{\ell_\lambda} e^{-y/\ell_\lambda}\, d\lambda = N_{ph} \frac{1}{\ell_{ph}} e^{-y/\ell_{ph}} \tag{3.100}$$

one can immediately show by integration that equation (3.99) is self consistent in that the right side of equation (3.99) yield ℓ_{ph},

$$\ell_{F,\,ph} = \frac{N_{ph}}{N_{F,\,ph}} \frac{1}{\pi} \int_{\Omega=0}^{2\pi} \int_{y=r}^{\infty} \frac{\cos\theta}{\ell_{ph}} e^{-y/\ell_{ph}}\, y\, d\Omega\, dy \tag{3.101}$$

Integrating with respect to y

$$\int_{r}^{\infty} y\, e^{-y/\ell_{ph}}\, dy = \ell^2_{ph}\, (r/\ell_{ph} + 1)\, e^{-r/\ell_{ph}} \tag{3.102}$$

$$\ell_{F,\,ph} = \frac{N_{ph}}{N_{F,\,ph}}\ \ell_{ph}\ [(a+1)\ e^{-a} - a^2 - E_1(a)] \qquad (3.109)$$

Substituting this result into equation (3.93) to get,

$$\ell_{V,\,ph} = \frac{N_{ph}}{N_{ph} - N_{F,\,ph}}\ \ell_{ph}\ [1 - (a+1)\ e^{-a} + a^2\ E_1(a) \qquad (3.110)$$

The quantity $N_{F,\,ph}$ is computed from equation (3.97), i.e.,

$$N_{F,\,ph} = \frac{1}{r} \int_{\Omega=0}^{2\pi} \int_{y=r}^{\infty} \int_{\lambda=0}^{\infty} N'_{ph}\ \frac{\cos\theta}{\ell_\lambda}\ e^{-y/\ell_\lambda}\ d\Omega\ dy\ d\lambda \qquad (3.111)$$

and again making the approximation of equation (3.100) we get

$$N_{F,\,ph} = \frac{N_{ph}}{\pi} \int_{\Omega=0}^{2\pi} \int_{y=r}^{\infty} \frac{\cos\theta}{\ell_{ph}}\ e^{-y/\ell_{ph}}\ d\Omega\ dy \qquad (3.112)$$

Integrating over y we get

$$N_{F,\,ph} = \frac{N_{ph}}{\pi} \int_{0}^{2\pi} \cos\theta\ e^{-r/\ell_{ph}}\ d\Omega \qquad (3.113)$$

Again setting $d = \frac{\cos\theta}{r^2}\ dS_1$; $dS_1 = 2\pi\ a^2\ \sin\theta/\cos^3\theta\ d\theta$ and then changing variable to $a = d/\ell_{ph}$ and $x = 1/\cos\theta$ we get

$$N_{F,\,ph} = 2N_{ph} \int_{1}^{\infty} \frac{1}{x^3}\ e^{-ax}\ dx \qquad (3.114)$$

which again is the form of the exponential integral

$$N_{F,\,ph} = 2N_{ph}\ E_3(a) \qquad (3.115)$$

Substitute this result into equation (3.110) for $\ell_{V,\,ph}$, and use the recurrence relationship to get,

Then substitute this result into equation (3.101) to get

$$\ell_{F,\,ph} \simeq \frac{N_{ph}}{N_{F,\,ph}} \frac{\ell_{ph}}{\pi} \int_0^{2\pi} \left(\frac{r}{\ell_{ph}} + 1\right) e^{-r/\ell_{ph}} \cos\theta \, d\Omega \qquad (3.103)$$

Expressing $d\Omega$ in terms of dS_i (see Figure 3-11) we see $d\Omega = \frac{\cos\theta}{r^2} dS_1$ where dS_1 is an element of area of surface (1). In turn, the surface area element can be written as $dS_1 = 2\pi\, r \sin\theta\, d(r \sin\theta)$. After setting $r = d/\cos\theta$, (see Figure 3-11), then $dS_1 = 2\pi\, d^2 \sin\theta/\cos^3\theta\, d\theta$. Substituting these results in equation (3.103) we get,

$$\ell_{F,\,ph} \simeq \frac{N_{ph}}{N_{F,\,ph}} 2\ell_{ph} \int_{\theta=0}^{\pi/2} \left(\frac{d}{\ell_{ph}\cos\theta} + 1\right) e^{-d/(\ell_{ph}\cos\theta)} \times \cos\theta \sin\theta \, d\theta \qquad (3.104)$$

To integrate let us change variables by setting $a = d/\ell_{ph}$ and $x = 1/\cos\theta$ Equation (3.104) becomes

$$\ell_{F,\,ph} = \frac{N_{ph}}{N_{F,\,ph}} 2d \int_1^{\infty} (x^{-2} + x^{-3}\, a)\, e^{-ax}\, dx \qquad (3.105)$$

The integral is in the form of the exponential integral $E_n(a)$ where

$$E_n(a) = \int_1^{\infty} \frac{e^{-ax}}{x^n}\, dx \qquad (3.106)$$

therefore, we get

$$\ell_{F,\,ph} = \frac{N_{ph}}{N_{F,\,ph}} 2d\, [E_2(a) + E_3(a)/a] \qquad (3.107)$$

using the recurrence relation[10],

$$E_{n+1}(a) = \frac{1}{n}\, [e^{-a} - a\, E_n(a)],\ n = 1,\ 2,\ 3 \qquad (3.108)$$

to get,

$$\ell_{V,\,ph} = \ell_{ph}\,\frac{1 - aE_2(a) - E_3(a)}{1 - 2E_2(a)} \approx \ell_{ph}\,\frac{1 - (a+1)\,e^{-a} + a^2\,E_1(a)}{1 + (a-1)\,e^{-a} - a^2\,E_1(a)} \tag{3.116}$$

The final quantity we need to calculate is $\rho_{F,\,ph}$

As stated in Section 3.2.2 equation (3.15) the phonon mass density ρ_{ph} in integral form is given by Landau as

$$\rho_{ph} = \int \frac{4\pi\,k^4}{3h^3\,c^5}\,\frac{e^x\,x\,T}{\lambda(e^x - 1)^2}\,d\lambda, \text{ where } x = ch/kT\lambda \tag{3.117}$$

Furthermore, the phonon number density N_{ph} in integral form is given as

$$N_{ph} = \int 4\pi\,\left(\frac{kT}{\lambda c}\right)^3 \frac{x^3}{\lambda(e^x - 1)}\,d\lambda \tag{3.118}$$

writing N_{ph} in the form,

$$N_{ph} = \int N'_{ph}\,d\lambda \text{ then, } N'_{ph} = 4\pi\,\left(\frac{kT}{\lambda c}\right)^3 \frac{x^3}{\lambda(e^x - 1)} \tag{3.119}$$

If we write the mass density in the form

$$\rho_{ph} = \int N'_{ph}\,M_\lambda\,d\lambda \tag{3.120}$$

then we may define an effective phonon mass M_λ of the phonons between wavelength λ and $\lambda + d\lambda$ as

$$M_\lambda = \frac{k\,e^x\,x\,T}{3c^2\,[e^x - 1]} \tag{3.121}$$

where $x = ch/kT\lambda$

The mass density of the free phonons would then be written as

$$\rho_{F,\,ph} = \int N'_{F,\,ph}\, M_\lambda \, d\lambda \tag{3.122}$$

where $N'_{F,\,ph}$ has the form

$$N_{F,\,ph} = \int_0^\infty N'_{F,\,ph}\, d\lambda$$

and is obtained from equation (3.97) as

$$N'_{F,\,ph} = \int_{\Omega=0}^{2\pi} \int_{y=r}^{\infty} N'_{ph}\, \frac{\cos\theta}{\pi}\, \frac{1}{\ell_\lambda}\, e^{-y/\ell_\lambda}\, d\Omega\, dy \tag{3.123}$$

Substituting $N'_{F,\,ph}$ into equation (3.122) for $\rho_{F,\,ph}$

$$\rho_{F,\,ph} = \frac{1}{\pi} \int_{\Omega=0}^{2\pi} \int_{y=r}^{\infty} \int_{\lambda=0}^{\infty} N'_{ph}\, \frac{\cos\theta}{\ell_\lambda}\, e^{-y/\ell_\lambda}\, M_\lambda\, d\Omega\, dy\, d\lambda \tag{3.124}$$

Considering the integration over λ and if again we make the approximation

$$\int_{\lambda=0}^{\infty} N'_{ph}\, M_\lambda\, \frac{1}{\ell_\lambda}\, e^{-y/\ell_\lambda}\, d\lambda \simeq \int_{\lambda=0}^{\infty} N'_{ph}\, M_\lambda\, \frac{1}{\ell_{ph}}\, e^{-y/\ell_{ph}}\, d\lambda \simeq \rho_{ph}\, \frac{1}{\ell_{ph}}\, e^{-y/\ell_{ph}} \tag{3.125}$$

the equation (3.124) for $\rho_{F,\,ph}$ becomes

$$\rho_{F,\,ph} = \rho_{ph}\, \frac{1}{\pi} \int_{\Omega=0}^{2\pi} \int_{y=r}^{\infty} \frac{\cos\theta}{\ell_{ph}}\, e^{-y/\ell_{ph}}\, d\Omega\, dy$$

which is the same integral as in Equation (3.112) and becomes

$$\rho_{F,\,ph} = 2\rho_{ph}\, E_3(a) = 2\ell_{ph}\, [(1-a)e^{-a} + a^2\, E_1(a))] \tag{3.126}$$

Since

$$\rho_{V,\,ph} + \rho_{ph} = \rho_{F,\,ph}$$

then

$$\rho_{V,\ ph} = \rho_{ph}\ [1 - 2E_3(a)]$$

or in terms of $E_1(a)$,

$$\rho_{V,\ ph} = \rho_{ph}\ [1 + (a + 1)\ e^{-a} - a^2\ E_1(a)] \qquad (3.127)$$

The viscosity of the viscous phonon is given by the kinetic theory equation

$$\eta_{V,\ ph} = \alpha_{ph}\ \rho_{V,\ ph}\ c\ \ell_{V,\ ph} \qquad (3.128)$$

Substituting equation (3.127) and (3.116) for $\rho_{V,\ ph}$ and $\ell_{V,\ ph}$ we get

$$\eta_{V,\ ph} = \alpha_{ph}\ \rho_{ph}\ c\ \ell_{ph}\ [1 - (a + 1)\ e^{-a} + a^2\ E_1(a)] \qquad (3.129)$$

setting $\eta_{ph\text{ - }ph,\ r} = \alpha_{ph}\ \rho_{ph}\ c\ \ell_{ph}$ then

$$\eta_{V,\ ph} = \eta_{ph\text{ - }ph,\ r}\ [1 - (a + 1)\ e^{-a} + a^2\ E_1(a)] \qquad (3.130)$$

Substituting this equation (3.130) and equation (3.116) into equation (3.84) we obtain for the shear stress of the viscous phonons

$$(F/A)_{V,\ ph} = \frac{\eta_{ph\text{ - }ph,\ r}\ [1 - (a + 1)\ e^{-a} + a^2\ E_1(a)]\ v_o/d}{1 + \frac{4}{3}\frac{\ell_{ph}}{d}\left[\frac{1 - (a + 1)\ e^{-a} + a^2\ E_1(a)}{1 + (a - 1)\ e^{-a} - a^2\ E_1(a)}\right]\left[3\alpha_{ph}\left(\frac{\gamma_1\ f_1 + \gamma_2\ f_2}{\gamma_1\ f_1\ \gamma_2\ f_2}\right) - 1\right]} \qquad (3.131)$$

We next write the shear stress $(F/A)_{F,\,ph}$ due to the free phonons. Substituting $\rho_{F,\,ph}$ from equation (3.126) into equation (3.77) for $(F/A)_{F,\,ph}$ we get

$$(F/A)_{F,\,ph} = \frac{1}{4}\,\gamma_1\,\gamma_2\,(\gamma_1 + \gamma_2 - \gamma_1\,\gamma_2)^{-1}\,f\rho_{ph}\,[(1 - a)\,e^{-a} + a^2\,E_1(a)]\,cv_o \tag{3.132}$$

By equation (3.76) the total shear stress $(F/A)_{ph}$ is the sum of the shear stress due to the free phonons and the viscous phonons. The phonon effective viscosity $\eta_{ph\,-\,ph,\,r,\,w}$ as would be observed in a parallel surface viscometer then immediately follows as,

$$\eta_{ph\,-\,ph,\,r,\,w} = \frac{\eta_{ph\,-\,ph,\,r}\,[1 - (a + 1)\,e^{-a} + a^2\,E_1(a)]}{1 + \frac{4}{3}\,\frac{\ell_{ph}}{a}\left[\frac{1 - (a + 1)\,e^{-a} + a^2\,E_1(a)}{1 + (a - 1)\,e^{-a} - a^2\,E_1(a)}\right]\left[3\alpha_{ph}\left(\frac{\gamma_1 f_1 + \gamma_2 f_2}{\gamma_1 f_1 \gamma_2 f_2}\right) - 1\right]}$$

$$+ \frac{1}{4}\,\gamma_1\,\gamma_2\,(\gamma_1 + \gamma_2 - \gamma_1\,\gamma_2)^{-1}\,f\rho_{ph}\,cd\,[(1 - a)\,e^{-a} + a^2\,E_1(a)] \tag{3.133}$$

where $a = d/\ell_{ph}$ and where $E_1(a)$ is the exponential integral $E_1(a) = \int_1^\infty \frac{1}{x}\,e^{-ax}\,dx$ found in mathematical tables[10] or easily evaluated using programmable calculators or computers. $f = f(\delta)$ is the surface factor where δ is the smaller of the two surface smoothness parameters δ_1 and δ_2.

The coefficient of first viscosity component $\eta_{ph\,-\,ph,\,r}$ and the corresponding mean free path ℓ_{ph}, have been computed by Khalatnikov, so the only unknown parameters in the equation are the surface smoothness parameters δ_1 δ_2 γ_1 and γ_2 which in principle could be determined from a detailed examination of the surface profile.

In order to simplify the appearance of equation (3.133) let us set

$$W(a) = 1 - (a + 1)\,e^{-a} + a^2\,E_1(a)$$

and

$$Z(a) = (1 - a)\,e^{-a} + a^2\,E_1(a) \tag{3.134}$$

then equation (3.133) becomes

$$\eta_{ph\text{ - }ph,\ r,\ w} = \frac{\eta_{ph\text{ - }ph,\ r}\ W(a)}{1 + \frac{4}{3}\frac{1}{a}\left[\frac{W(a)}{1 - Z(a)}\right]\left[3\alpha_{ph}\left(\frac{\gamma_1 f_1 + \gamma_2 f_2}{\gamma_1 f_1 \gamma_2 f_2}\right) - 1\right]} \qquad (3.135)$$

$$+ \frac{1}{4}\gamma_1\gamma_2\ (\gamma_1 + \gamma_2 - \gamma_1\gamma_2)^{-1}\ f\rho_{ph}\ c\ d\ Z(a)$$

Presented in Figure 3-12 are the two function W(a) and Z(a). From this figure we see for a > 5 that Z(a) $\simeq$ 0 and W(a) $\simeq$ 1 and equation (3.125) reduces to

$$\eta_{ph\text{ - }ph,\ r,\ w} = \frac{\eta_{ph\text{ - }ph,\ r}}{1 + \frac{4}{3}\frac{\ell_{ph}}{a}\left[3\alpha_{ph}\left(\frac{\gamma_1 f_1 + \gamma_2 f_2}{\gamma_1 f_1 \gamma_2 f_2}\right) - 1\right]} \qquad (3.136)$$

For a >> 5 or ℓ_{ph} << d equation (3.125) reduces to

$$\eta_{ph\text{ - }ph,\ r,\ w} \rightarrow \eta_{ph\text{ - }ph,\ r}$$

That is, the observed viscosity $\eta_{ph\text{ - }ph,\ r,\ w}$ becomes equal to the coefficient of viscosity. Thus it is only for the case where the mean free path is much smaller than the fluid gap that the observed viscosity is equal to the theoretical coefficient of viscosity as computed by Khalatnikov.

On the other hand, for a << .05, W(a) ~ 0 and Z(a) $\rightarrow$ 1, equation (3.135), for the observed viscosity, reduces to

$$\eta_{ph\text{ - }ph,\ r,\ w} \rightarrow \eta_{ph\text{ - }w} = \frac{1}{4}\gamma_1\ \gamma_2\ (\gamma_2 + \gamma_1 - \gamma_1\ \gamma_2)^{-1}\ f\rho_{ph}\ c\ d$$

which is the phonon free viscosity equation developed in Section 3.2.

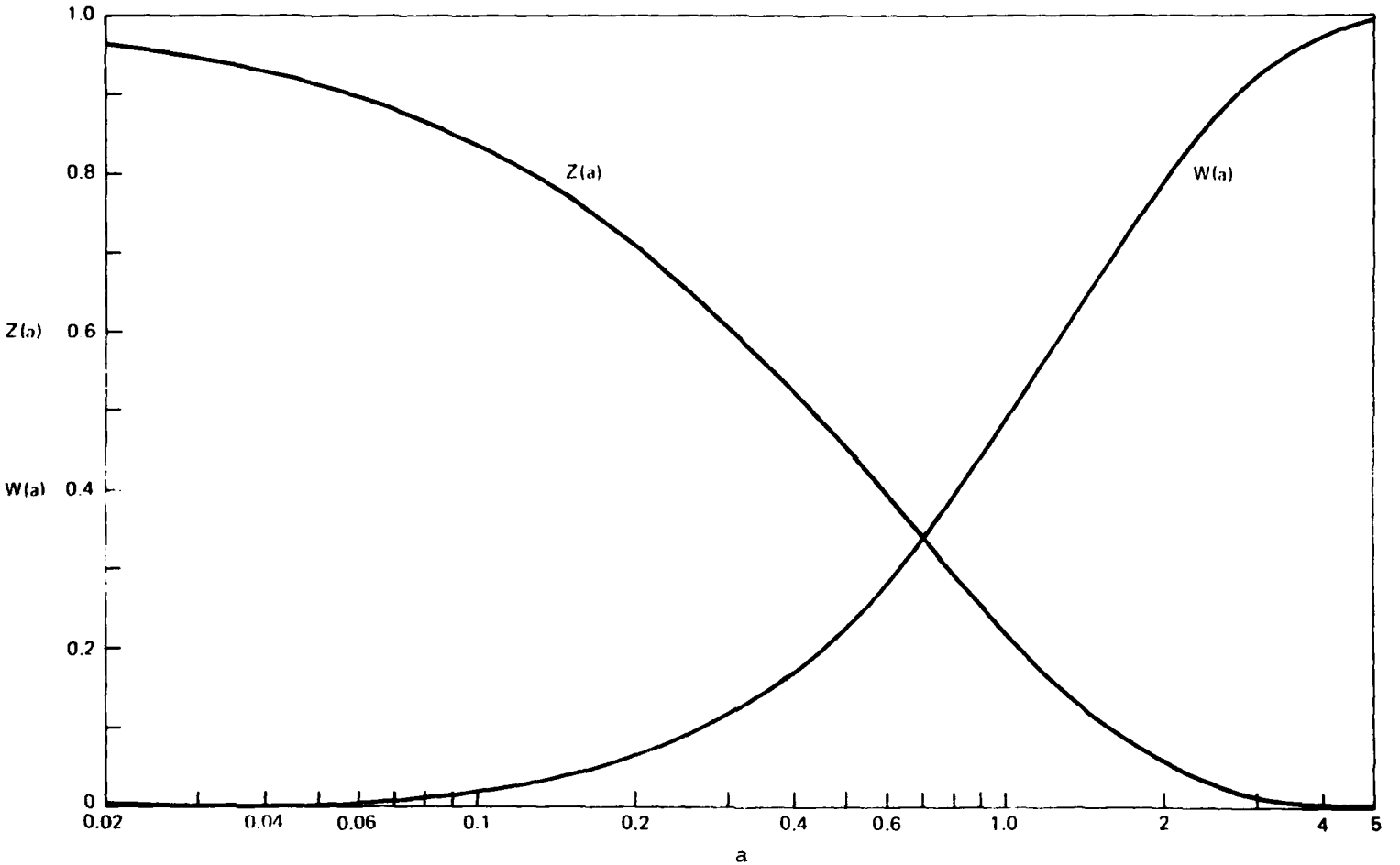

Figure 3-12. The functions W(a) and Z(a) versus a, $a = d/\ell_{Ph}$,

$Z(a) = (1-a)e^{-a} + a^2E,(a)$;

$W(a) = 1 - (1 + a)e^{-a} + a^2 E_1(a)$

3.4.2 The Equation for the Complete Effective Viscosity Using the More Exact Form

Equation (3.135) represents the phonon contribution to the viscosity and was particularly developed as a more exact equation for the transition region than the interpretive equation of Section 3.3. Surprisingly, it is found that the results obtained for the phonon contribution to the transition region viscosity using the interpretive equation of Section 3.3 are at most only about 15% smaller than the corresponding values found from the more rigorous equation (3.135). This suggests that the interpretive equations do indeed give a reasonably good estimation of the viscosity in the transition region.

For fluid gaps d > .001 cm the phonon contribution to the viscosity dominates in the transition region, for the most part, over the roton contribution, as well as over the contribution due to minute He^3 impurity. Therefore, it seems plausible that one loses little accuracy in extending equation (3.135) to include the roton contribution and the contribution due to minute He^3 impurity if the interpretive equation for the roton and He^3 impurity are used instead of a more exact form.

Recalling that in equation (3.38) the complete apparent viscosity η_o was written as the sum of the phonon contribution, the roton contribution, and the minute He^3 impurity contribution:

$$\eta_o = \eta_{ph} + \eta_r + \eta_3 \tag{3.137}$$

The phonon contribution is taken from equation (3.135), corrected for the He^3 impurity effect by equations (3.48) and (3.52) to become,

$$\eta_{ph} = \eta_{ph - ph,\, r,\, w,\, 3} = \left[1/\eta_{ph - ph,\, r,\, w} + 3.0 \times 10^7\, X_3\right]^{-1} \tag{3.138}$$

The roton contribution η_r is given by equation (3.74) and the minute He^3 impurity contribution by equation (3.75).

3.4.3 Summary of the Equations for the Complete Effective Viscosity for the Most Exact Form

In order to facilitate computations, let us bring together all the equations required to compute the complete effective viscosity: η_o (as would be observed for parallel surfaces where, by definition, the shear stress $F/A = \eta_o v_o/d$) as a function of temperature, T, the He^3 impurity concentration X_3, the phonon surface smoothness parameters δ_1, γ_1 and δ_2, γ_2 (let δ be the lesser of δ_1 and δ_2) and the roton and He^3 surface parameters γ_r, γ_3.

Again,

$$\eta_o = \eta_{ph} + \eta_r + \eta_3$$

The phonon contribution η_{ph} is given by equation (3.138)

where:

$$\eta_{ph\text{ - }ph,\,r,\,w} = \frac{\eta_{ph\text{ - }ph,\,r}\; W(a)}{1 + \frac{4}{a}\left[\frac{W(a)}{1 - Z(a)}\right]\left[3\alpha_{ph}\left(\frac{\gamma_1 f_1 + \gamma_2 f_2}{\gamma_1 f_1 \gamma_2 f_2} - 1\right)\right]} \qquad (3.139)$$

$$+ \frac{1}{4}\,\gamma_1\gamma_2\,(\gamma_1 + \gamma_2 - \gamma_1\gamma_2)^{-1}\; f\rho_{ph}\; c\; d\; Z(a)$$

with

$$f_1 = f(\delta_1);\; f_2 = f(\delta_2);\; f = f(\delta)$$

$$W(a) = 1 - (a + 1)\, e^{-a} + a^2\, E_1(a)$$

$$Z(a) = (1 - a)\, e^{-a} + a^2\, E_1(a)$$

$$a = d/\ell_{ph\text{ - }ph,\,r} \qquad (3.140)$$

for $0 \leqq a \leqq 1$ (reference 10) (3.141)

$$E_1(a) \simeq -.57722 - \ln a + a - .24991\, a^2 + .0552\, a^3 - .00976\, a^4 + .00108\, a^5$$

for $1 \leq a < \infty$

$$E_1(a) = \frac{e^{-a}}{a} \quad \frac{a^2 + 2.3347a + .2506}{a^2 + 3.3306a + 1.6815}$$

with $T < 0.8K$, the Khalatnikov 4 phonon equation is

$$\eta_{ph - ph,\, r} = \frac{3.50 \times 10^{-9}\ T^{-1/2}\ e^{8.65/T}}{1 + 2.15 \times 10^{-}\ T^{9/2}\ e^{8.65/T}} \tag{3.142}$$

$$\ell_{ph - ph,\, r} = \frac{\eta_{ph - ph,\, r}}{\alpha_{ph}\ \rho_{ph}\ c} \simeq 33.7\ T^{-4}\ \eta_{ph - ph,\, r} \tag{3.143}$$

after taking $\alpha_{ph} \simeq .07$, $\rho_{ph} = 1.78 \times 10^{-5}\ T^4$, $c = 2.38 \times 10^4$ (3.144)

then $a \simeq .03\ T^4\ d/\eta_{ph - ph,\, r}$

With $T > 0.8K$, the Khalatnikov 5 phonon theoretical equation modified by Woods and Hollis Hallet is

$$\eta_{ph - ph,\, r} = 3.5 \times 10^{-3}\ T^{-1/2}\ e^{8.65/T} \left[\frac{1 + 2.66 \times 10^4\ T^{9/2}\ e^{8.65/T}}{1 + 4.29 \times 10^{-3}\ T^{9/2}\ e^{8.65/T}} \right] \tag{3.145}$$

The specular reflection functions are

$$f_i = f(X_i) = \frac{30}{4\pi^4}\ X_i^{\,3}\ e^{-X_i}\ [1 + 5/X_i + 12/X_i^{\,2} + 12/X_i^{\,3}] + 0.079\ [e^{-.1633\ X_i^{\,2}} - .1633\ X_i^{\,2}\ E_1(.1633\ X_i^{\,2})] \tag{3.146}$$

$$X_i = 114/(\delta_i T) \qquad (\delta_i \text{ in units of } \mathring{A}) \text{ for } i = 1, 2$$

The roton contribution is

$$\eta_r = \left[7.94 \times 10^4 + 2.0 \times 10^4\ X_3\ e^{8.65/T} + 2.8 \times 10^{-4}\ e^{8.65/T}/(\gamma_r\ d\ T^{1/2}) \right]^{-1} \tag{3.147}$$

The He^3 contribution is

$$\eta_3 = [1.87 \times 10^5/T^{1/2} + 1.4 \times 10^3 \, e^{-8.65/T}/X_3 + 1.6 \times 10^{-3}/(\gamma_3 X_3 d \, T^{1/2})]^{-1} \quad (3.148)$$

In the Appendix is tabulated a computer program in BASIC language for computing the viscosity η_o for various temperatures, T.

3.4.4 Discussion of the Feature of the Complete Effective Viscosity

It is instructive to illustrate some of the main features of the effective viscosity equation (3.137) by several figures.* As noted by equation (3.137) the effective viscosity consists of three components; the phonon, the roton, and the He^3 components. Shown in Figure 3-13 are these three components for a He^3 concentration of 10^{-4} and 10^{-6}. The He^3 component, η_3, increases from low temperature as $T^{1/2}$ until the roton density, which is increasing rapidly with temperature, becomes large enough to severely limit the mean free path of the He^3 impurity atoms and thus causes a rapid drop in η_3 as the temperature continues to increase.

The roton component, η_r, contributes a constant viscosity at the higher temperatures. As the temperature is reduced, the roton effective mean free path is severely limited by the fluid gap size and by interaction with the He^3 impurity atoms at higher concentrations. Either or both of these effects cause the roton component, η_r, to drop rapidly as the temperature is lowered.

From 2K, the phonon component η_{ph} rises rapidly as the temperature is lowered due to the rapid increase in the phonon mean free path until the mean free path is severely limited by interaction with the He^3

*These figures were generated by an Apple II computer with an IDS-440G printer. The programs used are listed in the Appendix.

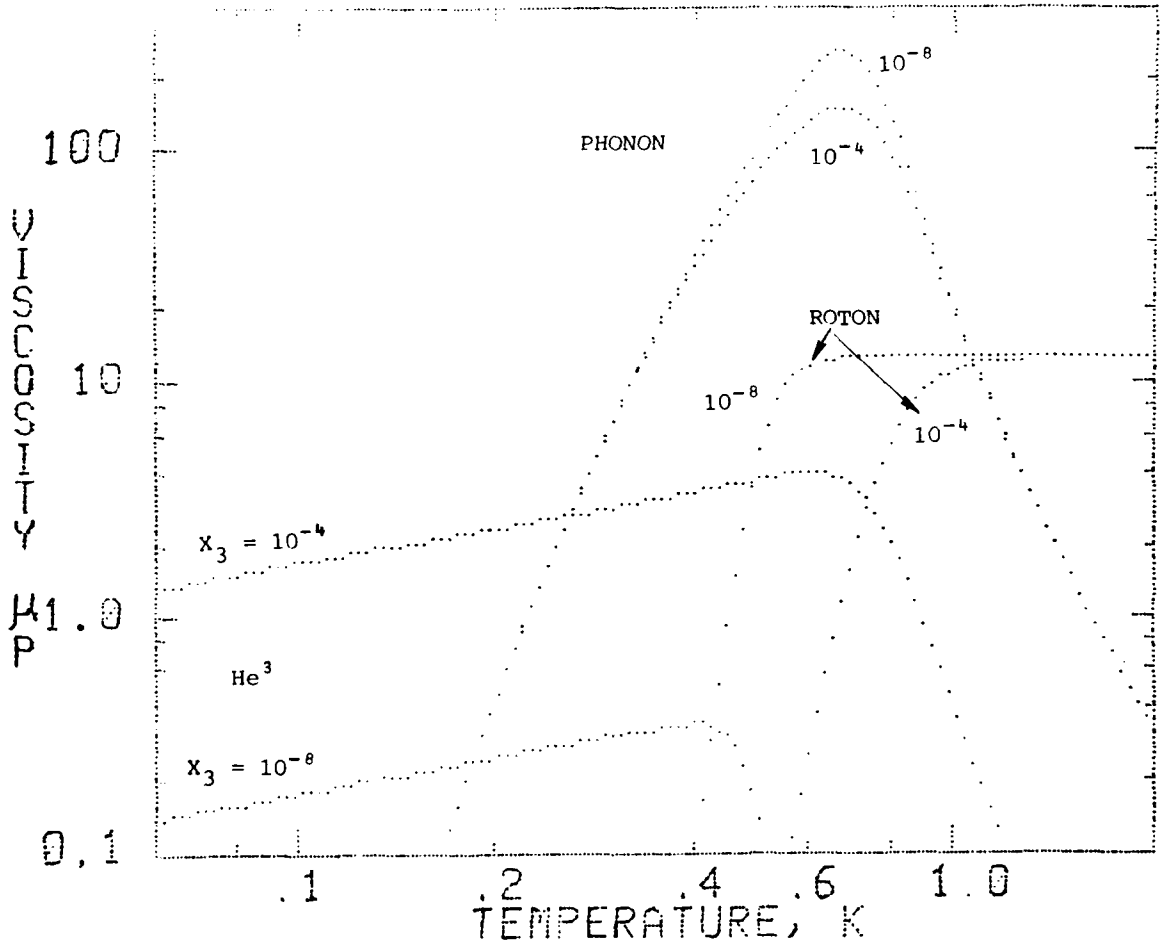

Figure 3-13. The components of the theoretical effective viscosity η_{ph}, η_3, η_r of liquid He^4 for concentrations of He^3 impurity of $X_3 = 10^{-8}$ and 10^{-4} with d = .1 cm, $\gamma_1 = \gamma_2 = .4$ and $\delta_1 = \delta_2 = 100\text{Å}$.

mpurity atoms and the fluid gap surface walls. In this latter region, he phonon component η_{ph} drops rapidly with decreasing temperature. e see from Figure 3-13 that for $X_3 = 10^{-4}$, η_{ph} in the region of its aximum value is strongly affected by the He^3 impurity. In this figure he surface smoothness parameters were somewhat arbitrarily given the alues indicated. It is reasonable to take $\gamma_r = 1$ since the roton wave- ength is about 0.5Å; $\gamma_3 = 1$ was also taken because of the small de Broglie avelength of the He^3 atoms.

Figure 3-14a, b depicts how the effective viscosity is influenced y the He^3 impurity. At the lower temperatures, the effective viscosity s nearly independent of concentration for $X_3 = 10^{-3}$ to 10^{-6} because the e^3 impurity atoms act like a viscous gas where viscosity is independent f density. For $X_3 << 10^{-6}$ the He^3 impurity atoms act like a molecular ree gas and so the effective viscosity decrease as X_3.

The present discussion is limited to minute He^3 concentrations of $_3 < 10^{-3}$; however, at concentrations larger than 10^{-3}, the He^3 impurity toms will become non-ideal and begin to strongly interact.[20] This oupling between the He^3 impurity atoms will cause the viscosity to ncrease. For pure He^3, $X_3 = 1$, the viscosity is proportional to T^{-2}.

For $X_3 < 10^{-7}$ we see from Figure 3-14a,b that the He^3 impurity as little effect upon the effective viscosity above the peak where the luid is in the viscous region. The higher concentrations $X_3 >> 10^{-6}$ owever can severely suppress the phonon peak and have a major influence n the viscosity. The theoretical work of Zharkov[13] deals mainly with his latter effect. Furthermore, this influence of the He^3 has been xperimentally observed by Staas, Taconis and Fokkens[21].

Presented in Figure 3-15 is the effective viscosity for various izes of the fluid gap. For temperatures above the peak (the phonon- honon interaction region) the viscosity is independent of the fluid gap ; it should be, while the viscous shear stress F/A is inversely propor- tional to the fluid gap.

AD-A098 733 CHARLES STARK DRAPER LAB INC CAMBRIDGE MA F/G 7/2
EFFECTIVE VISCOSITY OF LIQUID HELIUM4 - WITH MINUTE HE3 IMPURIT--ETC(U)
MAR 81 R C PANDORF N00014-77-C-0293
UNCLASSIFIED R-1403 ONR-CR-087-003-1F NL

2 OF 3
AD A098733

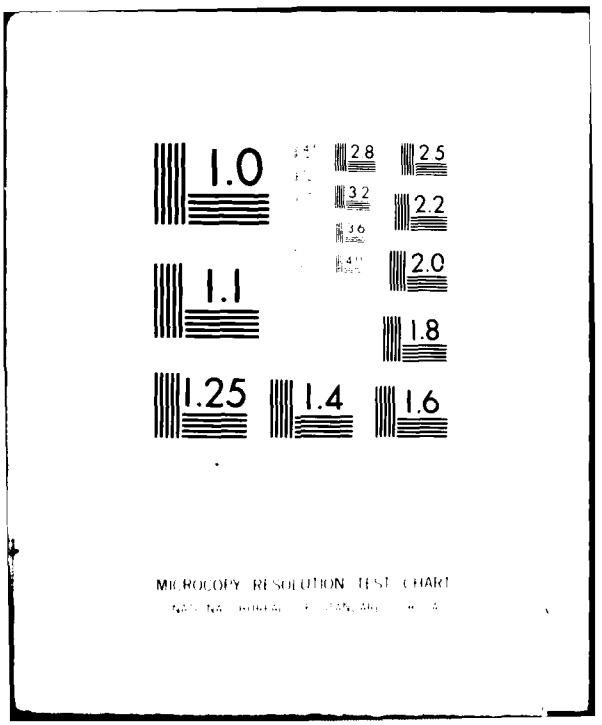
1.0
1.1
1.25
1.4
1.6
1.8
2.0
2.2
2.5
2.8
3.2
3.6
4.0
MICROCOPY RESOLUTION TEST CHART

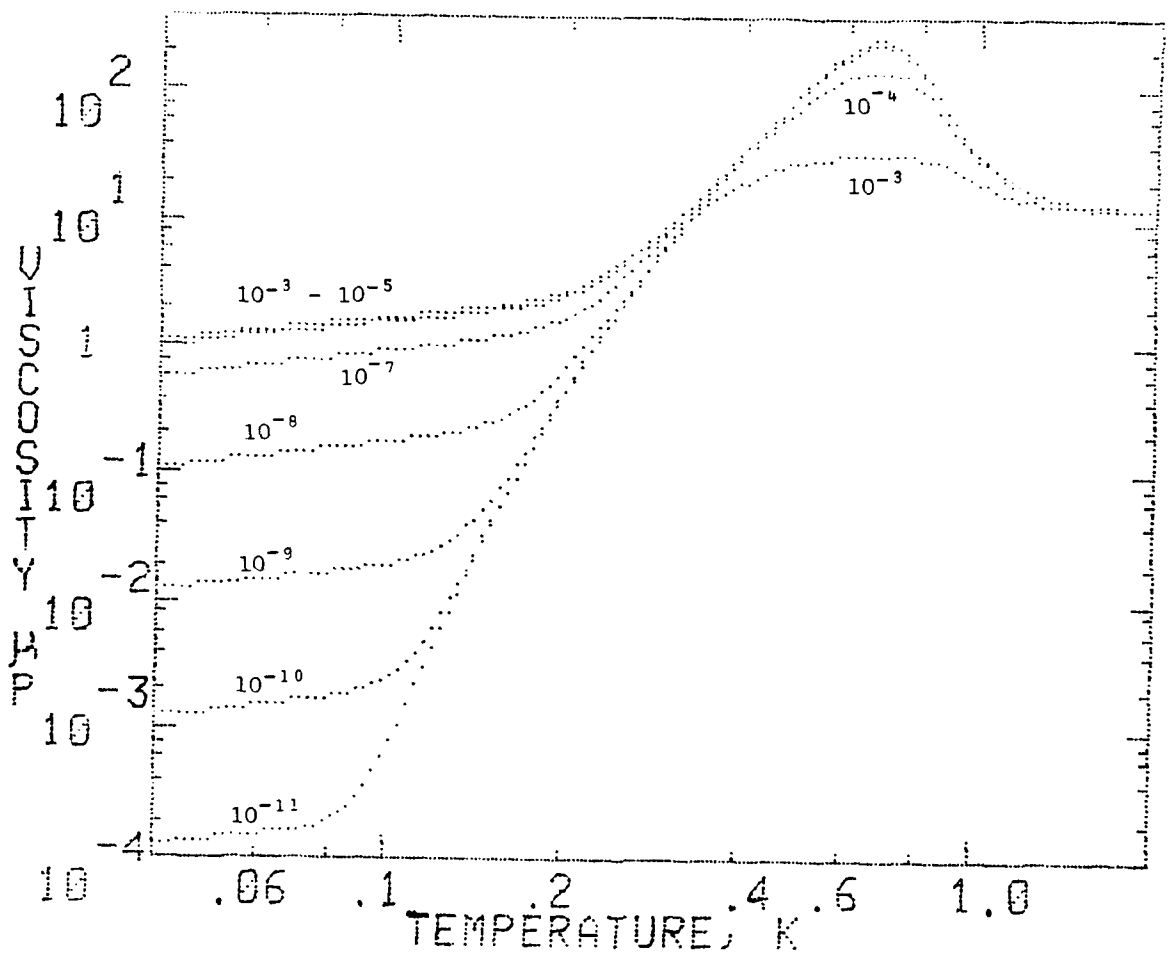

Figure 3-14a. The theoretical effective viscosity of liquid He^4 for various impurity concentrations X_3 of He^3 with d = .1 cm, $\gamma_1 = \gamma_2 = .4$ and $\delta_1 = \delta_2 = 100\text{Å}$.

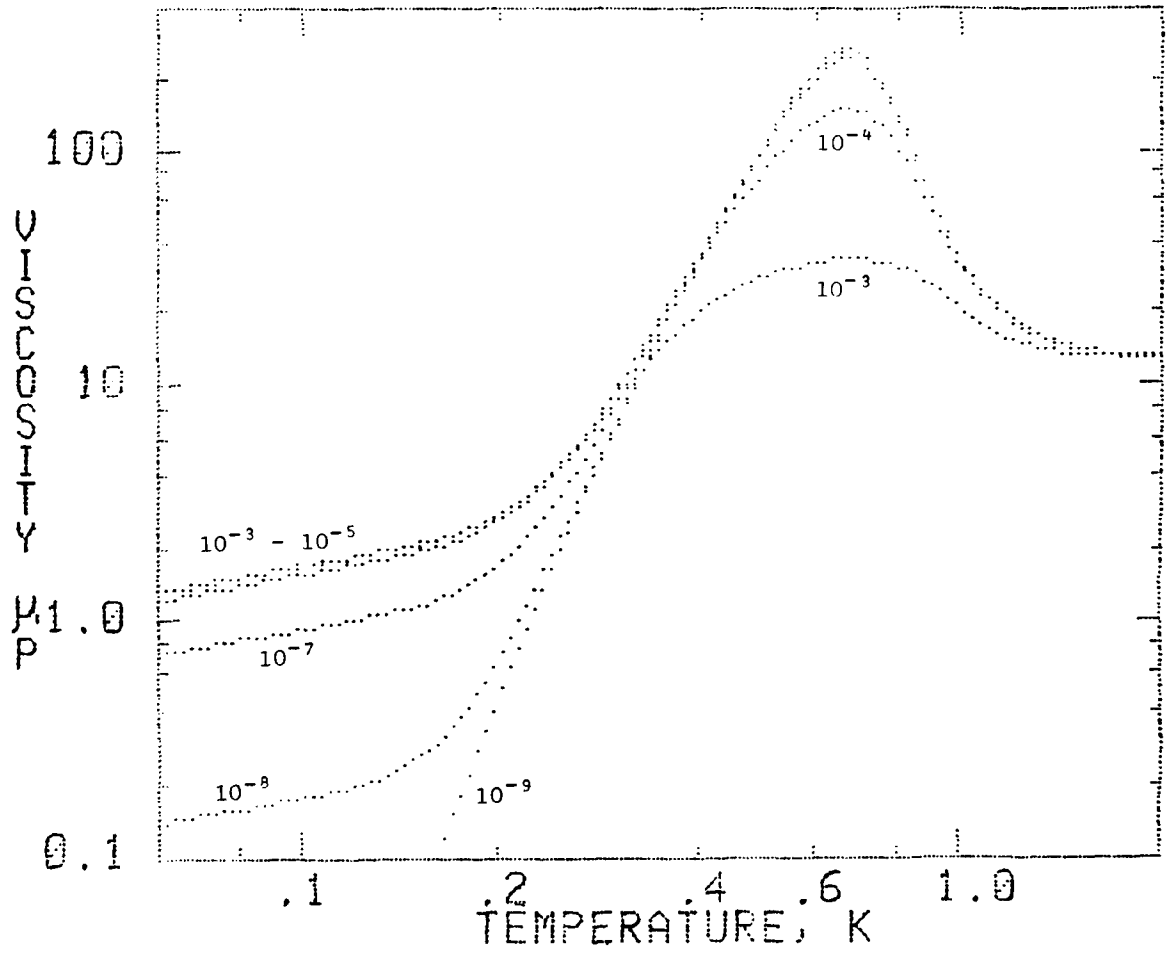

Figure 3-14b. The theoretical effective viscosity of liquid He^4 for various He^3 impurity concentrations X_3 with d = .1 cm, $\gamma_1 = \gamma_2 = .4$ and $\delta_1 = \delta_2 = 100\text{Å}$.

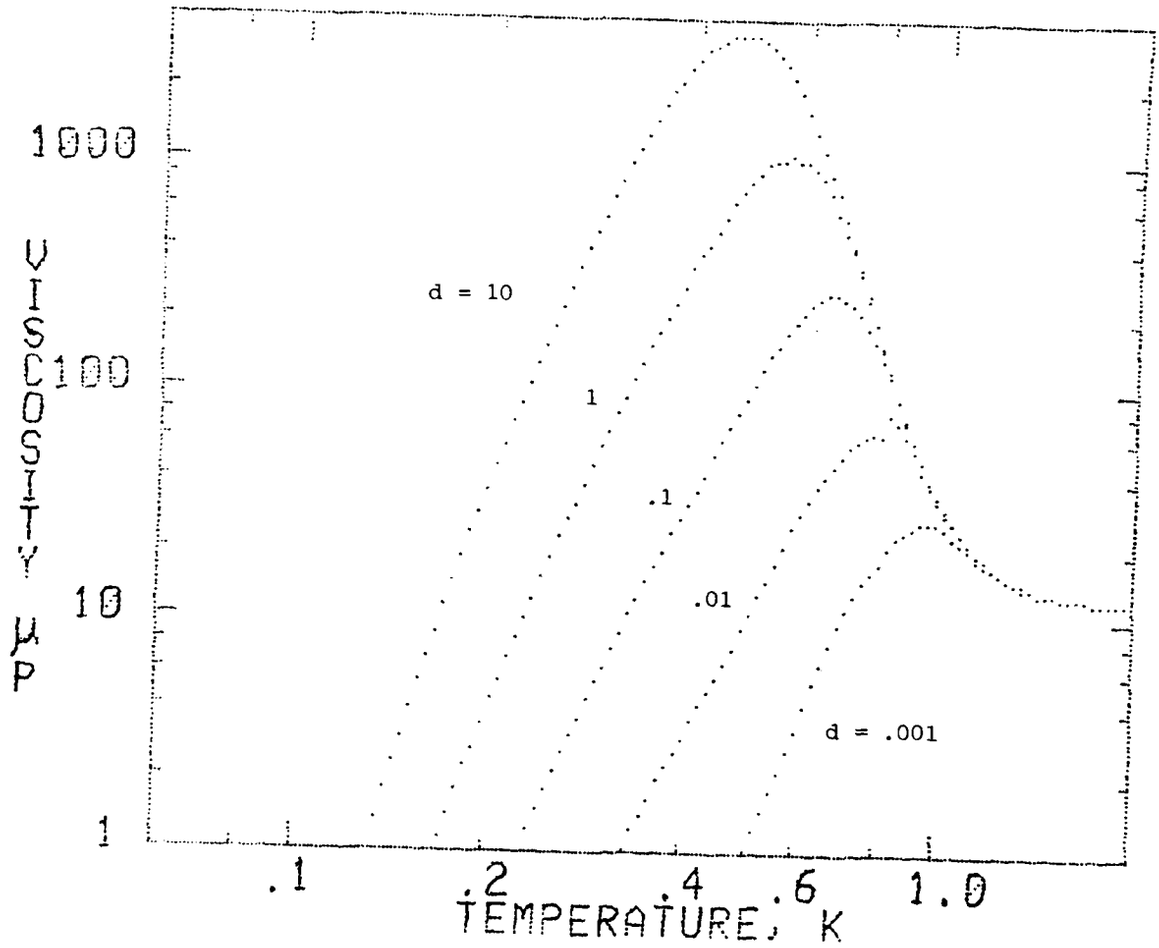

Figure 3-15. The theoretical effective viscosity of liquid He^4 for various fluid gaps d in cm, with $\gamma_1 = \gamma_2 = .4$, $\delta_1 = \delta_2 = 100\text{Å}$ and $X_3 = 10^{-12}$.

For temperatures below the peak, i.e., in the phonon free region, the effective viscosity is proportional to the fluid gap while the viscous shear stress F/A is independent of the fluid gap. In other words the coast down time of a free rotor in liquid He^4 would be independent of the fluid gap in the phonon free region! This is immediately apparent from the definition $F/A = \eta\, v/d$.

Figures 3-16a,b illustrate the effect of the surface smoothness ratio γ. Well into the phonon-phonon interaction region the γ ratio has no effect, while in the fully developed free phonon region the ratio shifts the effective viscosity by a constant multiple.

In Figures 3-17a,b is illustrated the effect of different values of the surface roughness parameter δ. The effective viscosity decrease with decreasing temperature is greatly accelerated by the smoother surfaces which have the smaller values of δ.

In comparing Figure 3-16b and 3-17a, it is seen that both γ and δ depress the peak viscosity values. However the parameter δ has its greatest effect in reducing the effective viscosity at the lower temperatures.

3.4.5 Discussions and Conclusions

The effective viscosity equations developed are for the particular geometry of the plane parallel surface viscometer which is a mathematically convenient but ficticious viscometer. However, the constant velocity concentric cylindrical and concentric spherical viscometers are suitable approximation to plane parallel surfaces provided that their fluid gap is much smaller than their radius.

For several reasons these effective viscosity equations are not applicable to flow type experiments even though the surfaces may be parallel. For one, flow experiments with He II do not depend upon the normal fluid viscosity, but involve mainly the flow characteristics of the superfluid. Second, even without the first problem, the physical conditions of motion are different.

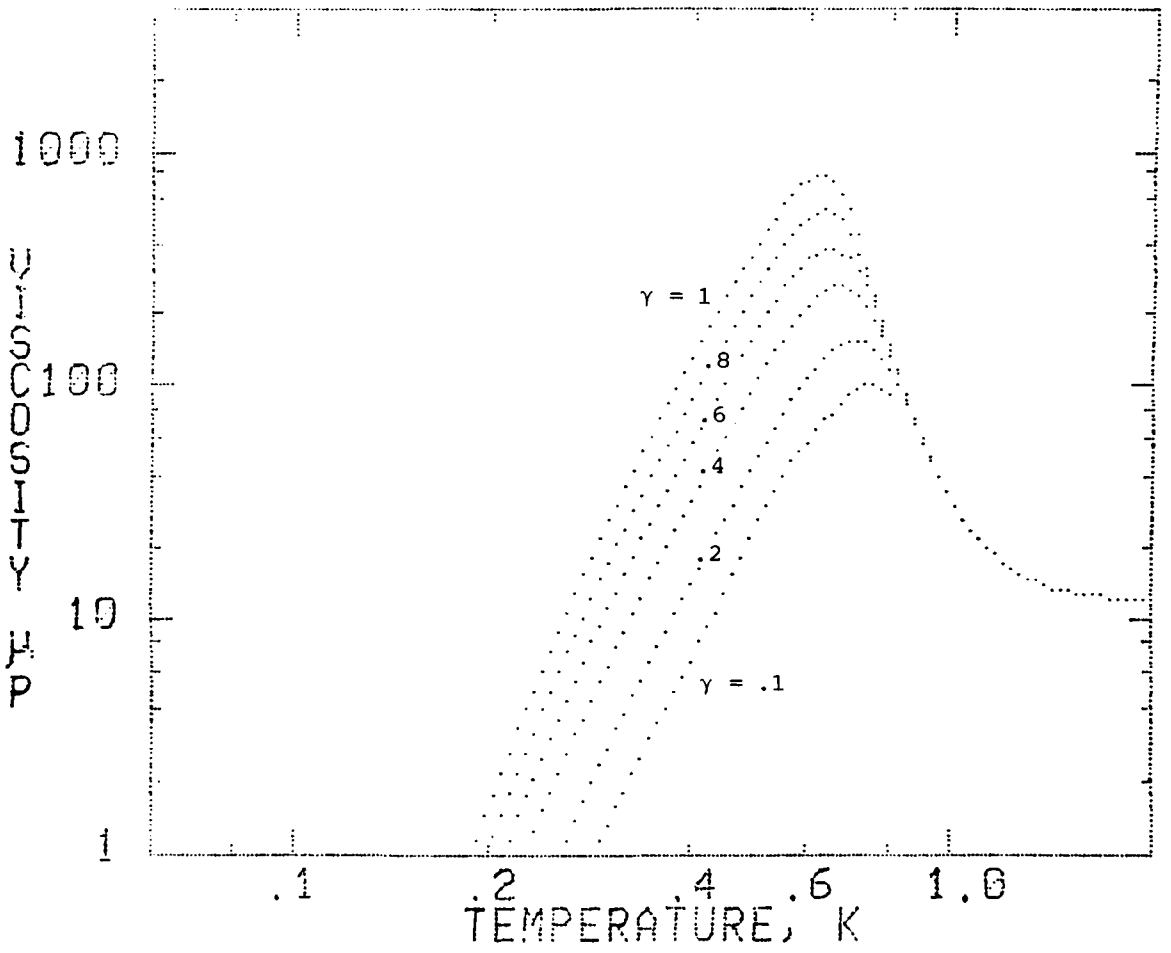

Figure 3-16a. The theoretical effective viscosity of liquid He^4 for various surface smoothness ratios $\gamma = \gamma_1 = \gamma_2$ with d = .1 cm, $\delta_1 = \delta_2 = 100\text{Å}$, and $X_3 = 10^{-12}$.

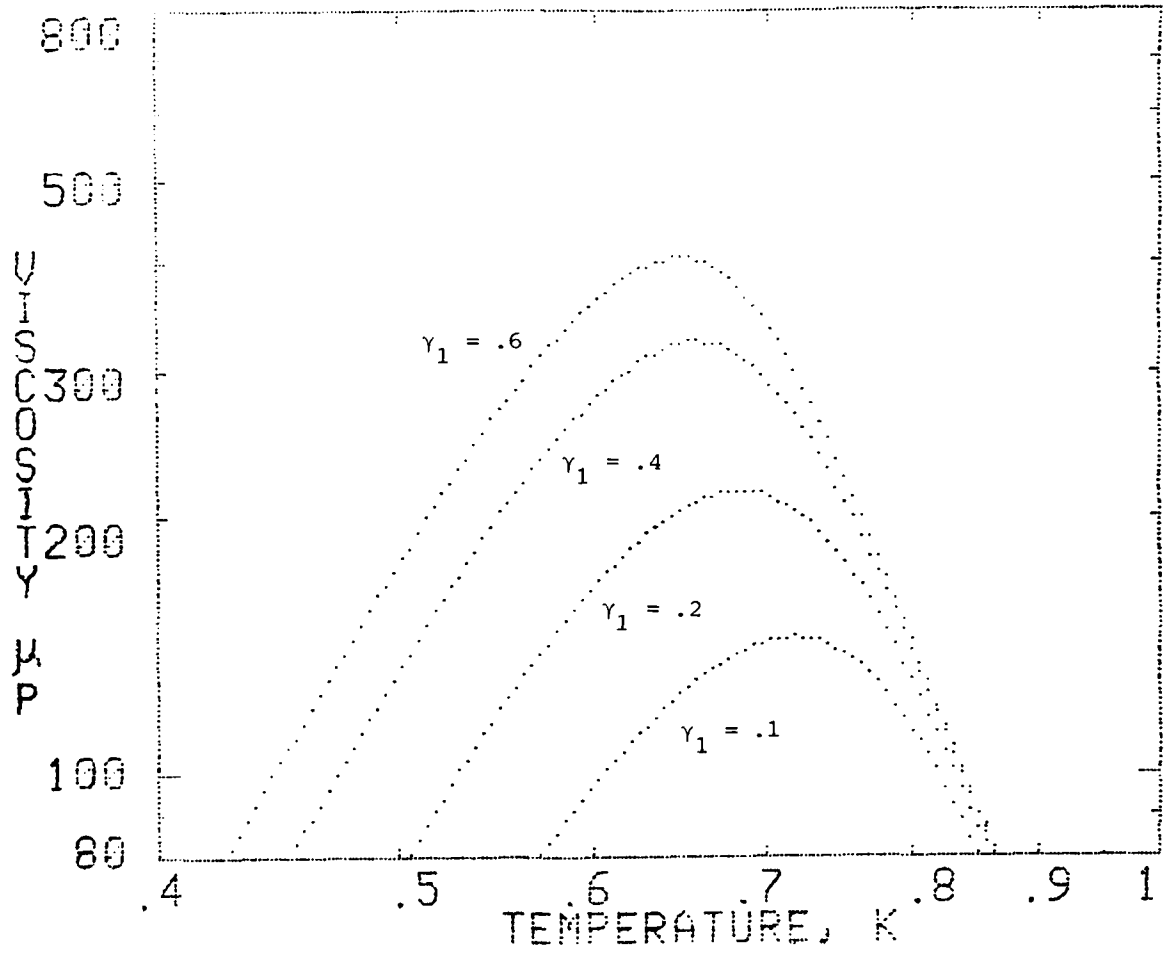

Figure 3-16b. The theoretical viscosity of liquid He^4 for various surface smoothness ratios γ_1 with d = .1 cm, γ_2 = .6, δ_1 = 100Å, δ_2 = 1000Å, and $X_3 = 10^{-12}$.

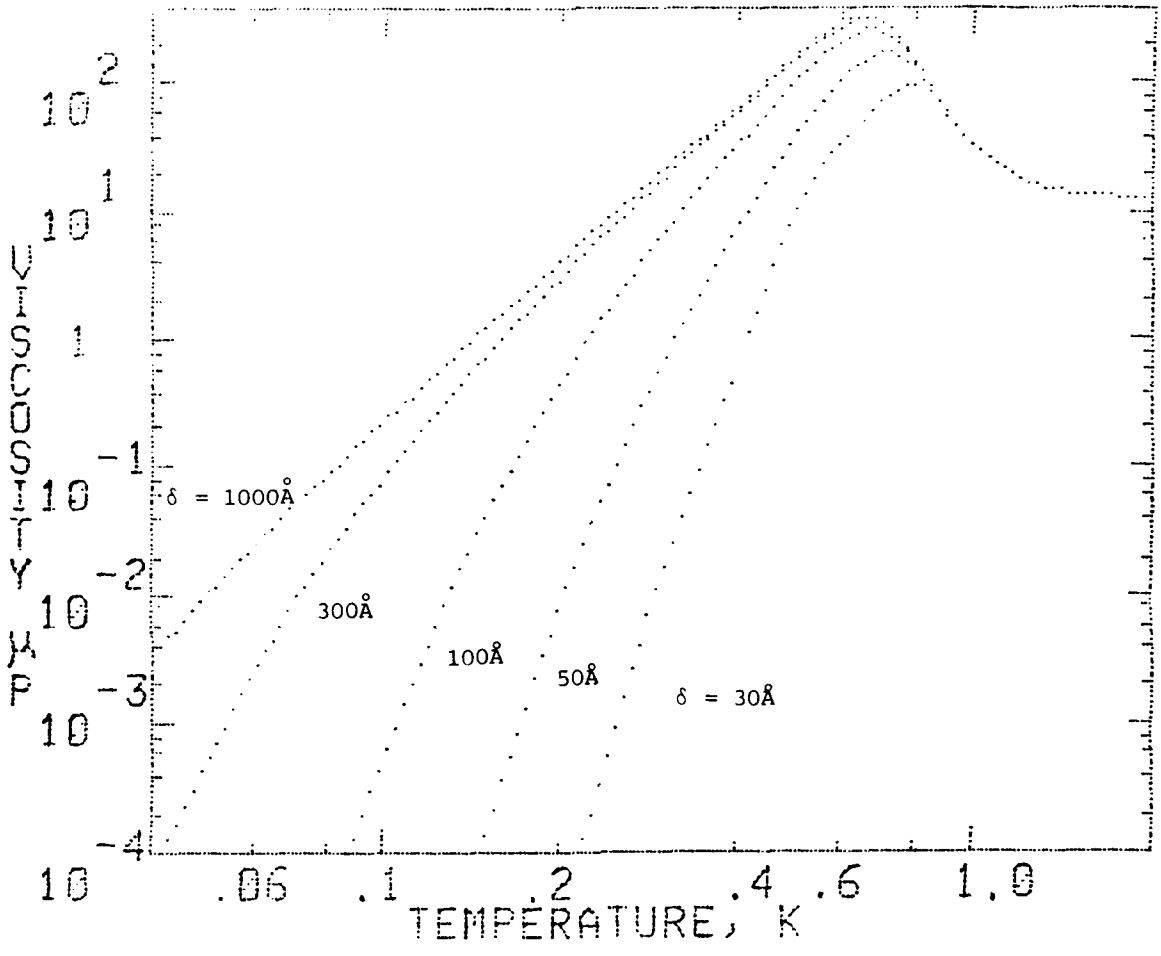

Figurre 3-17a. The theoretical effective viscosity of liquid He^4 for various surface roughness factors δ, in units of angstroms, with d = .1 cm, $\gamma_1 = \gamma_2 = .4$, $\delta = \delta_1 = \delta_2$, and $X_3 = 10^{-12}$.

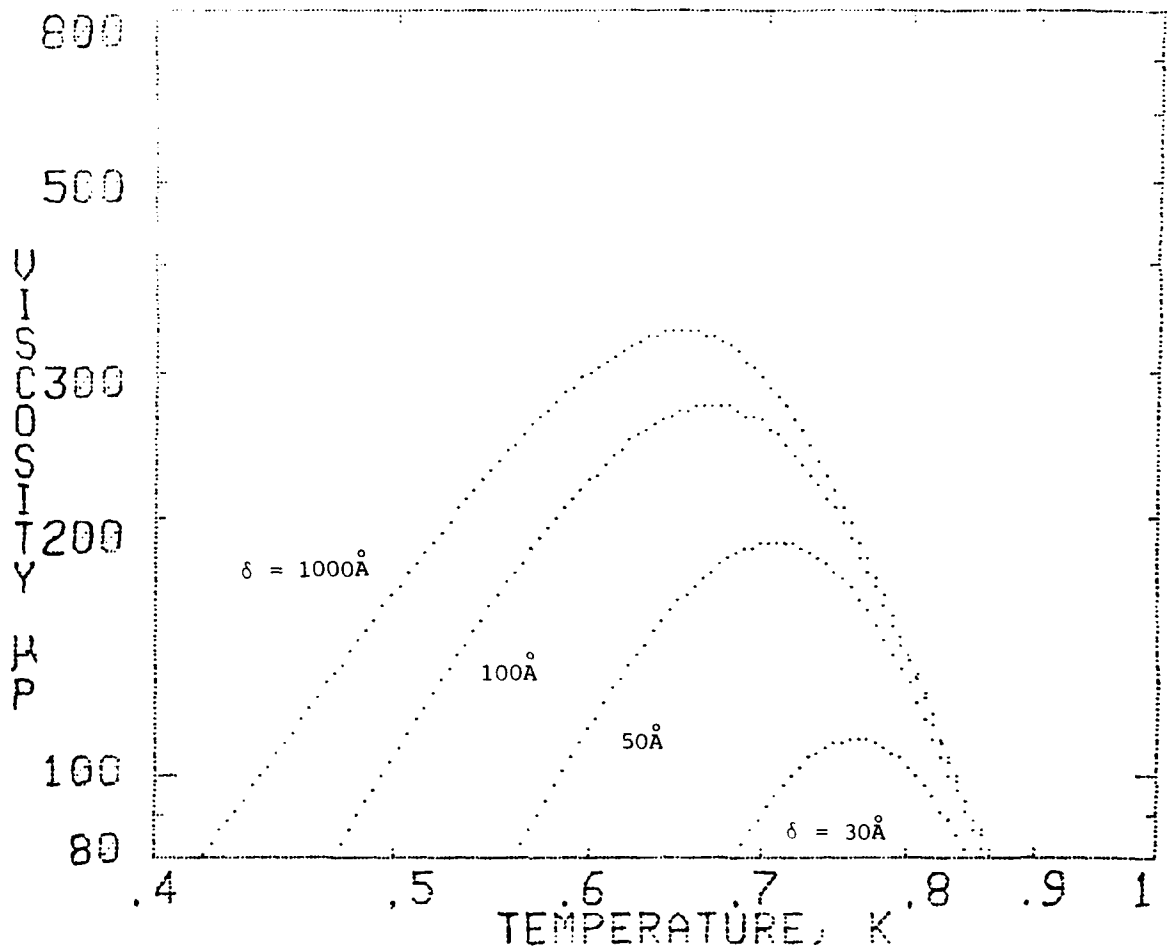

Figure 3-17b. The theoretical effective viscosity of liquid He^4 for various surface roughness factors δ, with d = .1 cm, $\gamma_1 = .3$, $\gamma_2 = .6$, $\delta_1 = \delta$, $\delta_2 = 1000Å$ and $X_3 = 10^{-12}$.

It should be emphasized that the effective viscosity equations apply only to steady state motion at subcritical velocities. By subcritical velocities is meant viscometer velocities for which the observed viscosity is independent of velocity. For classical fluids this would be analogous to the laminar flow region.

Specialists in the study of surface physics may find the surface model used for the present computations simplistic and perhaps too idealized. However, it was felt that for this first approach it was best not to get involved in detailed and complex surface computations which might obscure the more basic notions and also put us on a track where the mathematics could no longer be kept in convenient closed form. Also for these same reasons the more simple forms of kinetic theory were used. This leaves then numerous ways in which the present theory and model could be improved and made more rigorous.

Khalatnikov's 4-phonon equation for the coefficient of first viscosity was developed before there was much accurate experimental data available on He II. A review of his calculations using the newer improved data would be useful.

The general approach and methods developed in order to compute the effective viscosity of He II in this section have broad and immediate applications to other geometries and other transport properties of He II as well as applications to gaseous systems. At the present time gaseous systems are divided into three separate regions: Knudsen, transition and Poiseuille and only the Knudsen and Poiseuille regions have been adequately explained and described with an analytic expression. Using the general methods developed here, the flow and viscous properties as well, as other transport properties, can be described by a single expression applicable to all three regimes.

SECTION 3

REFERENCES

1. The Properties of Liquid and Solid Helium, J. Wilkes, Claredon Press, Oxford.
2. Liquid Helium, K.R. Atkins, Cambridge University Press.
3. Helium, W.H. Keesom, Elsevier, Amsterdam.
4. Helium-3 and Helium-4, W.E. Keller, Plenum Press, N.Y.
5. Heikkila, W.J. and Hollis-Hallet, A.C., Cam. J. Phys. 33, 420 (1955).
6. Woods, A.D.B., and Hollis-Hallet, A.C., Cam. J. Phys., 41, 596 (1962).
7. Introduction to the Theory of Superfluidity, I.M. Khalatnikov, W.A. Benjamin, Inc., N.Y.
8. Atkins, K.R., Phys. Rev. 104, 4, 1957.
9. Bendt, P.S., Cowan, R.D., and Yarnell, S.L., Phys. Rev., 113, 1386 (1959).
10. Handbook of Mathematical Functions, Edited by Abramovitz, M. and Stegus, I.A., NBS #55, U.S. Dept. of Commerce.
11. Whitworth, R.W., Proc. R. Soc. A246, 390 (1958).
12. Khalatnikov, I.M., and Zharkov, V.N., Soviet Phys., JETP 5, 905 (1957).
13. Zharkov, V.N.; Soviet Phys., JETP 6, 714 (1958).

14. Ptukha, T.P.; Soviet Phys. JETP 13, 1112 (1961).

15. Thermodynamic Properties of He^3 - He^4. Solutions with Applications to He^3 - He^4 Dilution Refrigerator, Radebaugh, R., NBS 362, U.S. Government Printing Office.

16. Keller, W.E., Phys. Rev. 105, 41 (1957).

17. Kinetic Theory of Gases, Kennard, E.H., McGraw-Hill Book Inc., 1938, Chapter VIII.

18. Experimental Superfluidity, Donnelly, R.J., University of Chicago Press, 1967; see page 79.

19. Kinetic Theory of Gases, Present R.D., McGraw-Hill Book Co, Inc., 1958.

20. Low Temperature Physics - LT12, edited by Timmerhaus, K.D., O'Sullivan, W.J., and Hammel, E.F.; vol. 1, (Section 9), Plenum Press, N.Y.

21. Staas, F.A., Taconis, K.W., and Fokkens, K., Physics 26, 669 (1960).

SECTION 4

APPARATUS

4.1 INTRODUCTION

The basic cryogenic laboratory was built for the Experimental Series I, the Helios Program, which has already been reported on in some detail.[1] This facility was quite sophisticated and considerable effort went into its planning and construction. During Series I, the ultra low temperature viscometer was built using a beryllium inner cylinder with torsion wires attached to both the top and bottom of the cylinder.

The next Experimental Series II replaced the beryllium inner cylinder with a glass inner cylinder, installed an eddy current dampener on the inner cylinder, installed a low pressure, low temperature pressure transducer on the instrument package, and installed a temperature controller for the mixing chamber.

The following Experimental Series III also used the glass inner cylinder. For this series a number of improvements were made in the apparatus. Many of the electronic circuits were upgraded and improved. The instrument package leads were replaced to give much improved signal to noise and reliability. The cryostat platform vibration isolation system was improved and a platform leveling system installed. The viscometer eddy current dampener was improved and the bottom torsion wire was removed.

The following section, for the most part, describes the facility and apparatus as it was during the Experimental Series III.

4.2 CRYOGENIC LABORATORY FACILITY

The cryogenic facility consisted of the following component areas:

a) The potting facility included an atmospheric oven, a vacuum oven, a storage refrigerator, a stirrer, scales and miscellaneous items. The potting facility was used mainly for making vacuum-superfluid tight electrical epoxy feed throughs and seals.

b) The metal fabrication facility consisted of a TIG and electric arc welder, spot welders, oxygen-acetelene welder, soldering torches, etc., lathe, miller, band saws, sander, cutoff wheel, drill press, tool grinder, sand blaster, sheet metal cutter and brake, and miscellaneous equipment. This facility was used for making non-precision parts, repairs, modifications and fabrication of required cryogenic components.

c) The cleanroom assembly area consisted of a controlled semi-clean room with a clean air laminar flow booth, exhaust hood, microscopes, de-magnetizers, and miscellaneous hand tools and equipment. This area was used for working on the viscometer apparatus and other instruments which required a clean (dust free) environment.

d) The electronic assembly facility consisted of the usual electronic instruments and equipment for fabricating, testing and repairing electronic circuits and equipment.

e) The cryogenic testing facility consisted of a small and a large cryostat capable of cooling instruments and individual components to 1.2K for testing and checkout.

f) The ultralow temperature laboratory facility provided the necessary environment and equipment for performing

experiments at ultralow temperatures. Experiments were conducted on a passive vibration isolation platform with active leveling inside a radio-frequency (RF) shielded room. Accessories like vacuum pumps and mechanical machinery were located outside the shielded room to reduce vibration, electrical interference and noise.

The cryostat insert, dewar, etc. was mounted on the vibration isolated platform over a pit which permitted the long dewar to be lowered and completely removed from the cryostat insert for working on the insert and instrument package. Above the platform an overhead space and trolley was provided so that the long insert could be lifted up and removed from the platform mounting.

Within the RF shielded room, the following systems were constructed:

a) The dilution refrigeration He^3-He^4 pumping, storage and handling system which, along with the dilution refrigerator, provided the cooling power for lowering the temperature of the experimental instrument from around 1K to below 0.1K.

b) The He^3 gas handling system provided the system for operating a He^3 refrigerator when required and for handling the He^3 exchange gas used during cool down.

c) The N^2 and He^4 gas distribution, handling and pumping system was used for flushing, monitoring and interconnecting the liquid He^4 bath spaces with other vacuum spaces and the manometer system.

d) The He^4 bath and inner pot pumping and gas handling system.

e) The ultra high vacuum pumping systems which provided the vacuum isolation required for cryogenics.

f) The leak detection system which consisted of a CVC leak detector and the interconnecting plumbing system so that the various spaces could be conveniently leak checked. The leak detector, which is a mass spectrometer, was also used to monitor the operation of the dilution refrigerator's still.

g) The pressure instrumentation system which measured the pressure at various points in the vacuum and gas systems and provided monitoring, testing and status condition of the various sections of the numerous vacuum and gas spaces. The system included 54 thermocouples, 10 ionization gauges, 3 capacitance pressure transducers, 2 manometers, 2 McLeod gauges and various mechanical pressure gauges. The system also provided pressure and overheat safety controls for the diffusion pumps.

h) The instrument package liquid and gaseous filling, emptying and pressurizing system was used for handling the gas and liquid inside the instrument package.

i) The dilution refrigeration control and temperature monitoring system included heater control circuits for various parts of the cryostat such as the bath, He^4 pot, still, still He^4 film suppressor tubes, superfluid pump, and mixing chamber, as well as a temperature controller for the mixing chamber and 14 temperature sensors for the various parts of the cryostat. The temperature values were based on two calibrated germanium thermometers.

Presented in Figure 4-1 is a photograph of the ultra low temperature system taken during Experimental Series I. In the middle of the picture is the cryostat platform set on three concrete pillars. Between the concrete pillars and the cryostat platform, the passive vibration isolators and active leveling devices are located (not shown in this

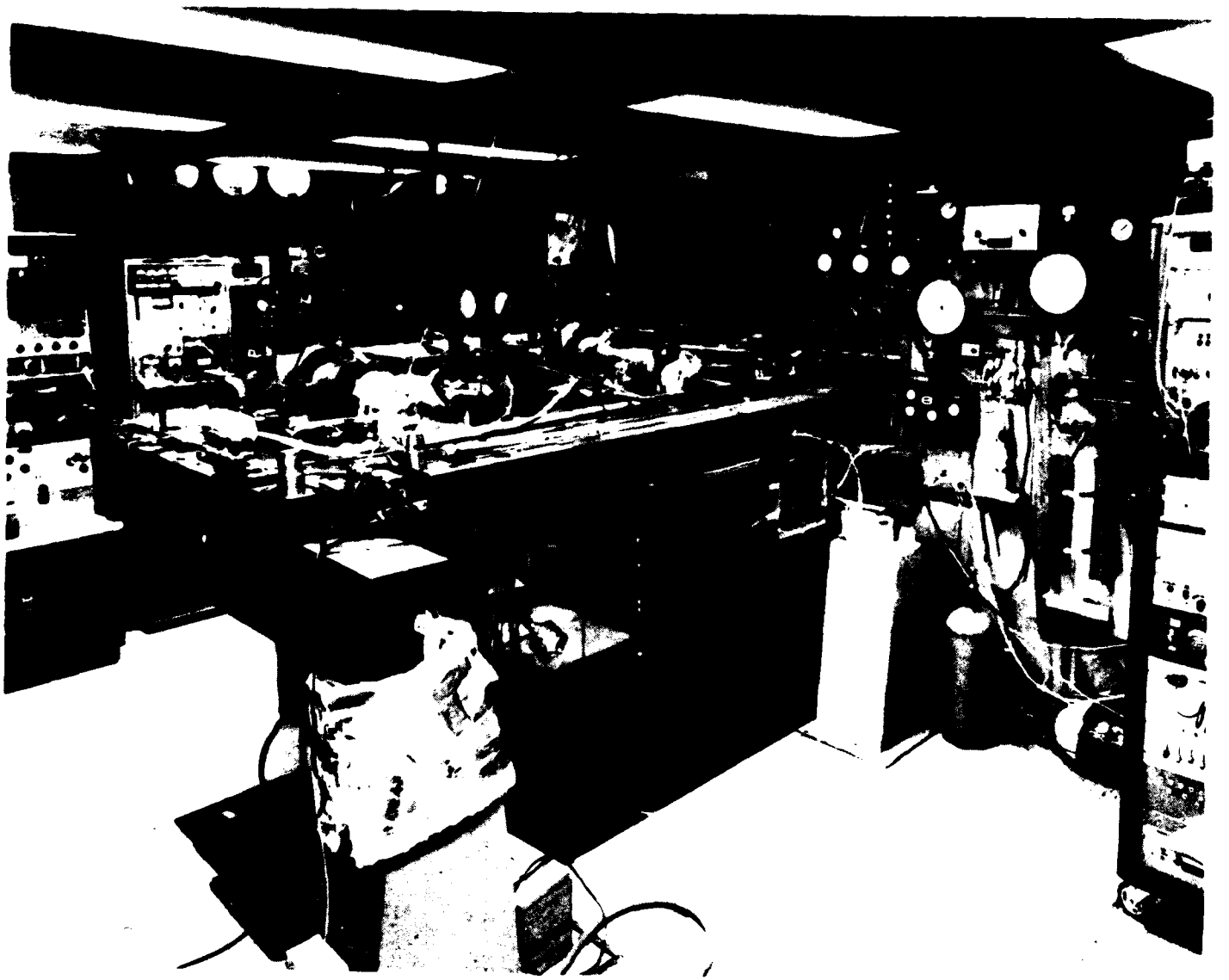

Figure 4-1. Photograph of ultra low temperature facility inside R.F. shielded room.

photograph). Hanging below the platform and extending into the pit area, one can see the cryostat insert. The dewar which surrounds the cryostat insert and instrument package has been lowered into the pit and is out of sight.

The three concrete pillars which support the platform are set on a concrete "boat" detached from the building, as is depicted in Figure 4-2. This particular arrangement is helpful in those cases where the major disturbing influences are being transmitted along the concrete floor of the building and not through the soil, which may not be the case for a laboratory next to a busy roadway.

Depicted in Figure 4-3a is a outline of the platform's passive vibration isolators and the active leveling system. The horizontal vibrations were isolated by means of air bearings. The major disturbing frequency was at 7.2 Hz and the air bearings reduce this disturbance by over two orders of magnitude.

The vertical vibrations were isolated by using a rolling diaphragm air cushion as depicted in Figure 4-3b. The major disturbing frequency in the vertical direction was at 7.8 Hz, and the rolling diaphragm air cushion system reduced the vertical motion at 7.8 Hz by again over two orders of magnitude.

The level of the platform was adjusted by bleeding air in or out of the rolling diaphragm cushion and attached auxiliary air tank. The electromechanical schematic for maintaining level is presented in Figure 4-4. This servo-leveled system could maintain a level within 0.2 arc seconds over a 12 hour period as monitored by a tilt meter placed on the platform.

The state-of-the-art of cryogenics is such that the achievement of low temperatures using conventional equipment is fairly straightforward and one can routinely use the dilution refrigerator for cooling to 10 millikelvin. The instrument package must be carefully designed to operate in the low temperature environment and it must do so in a manner

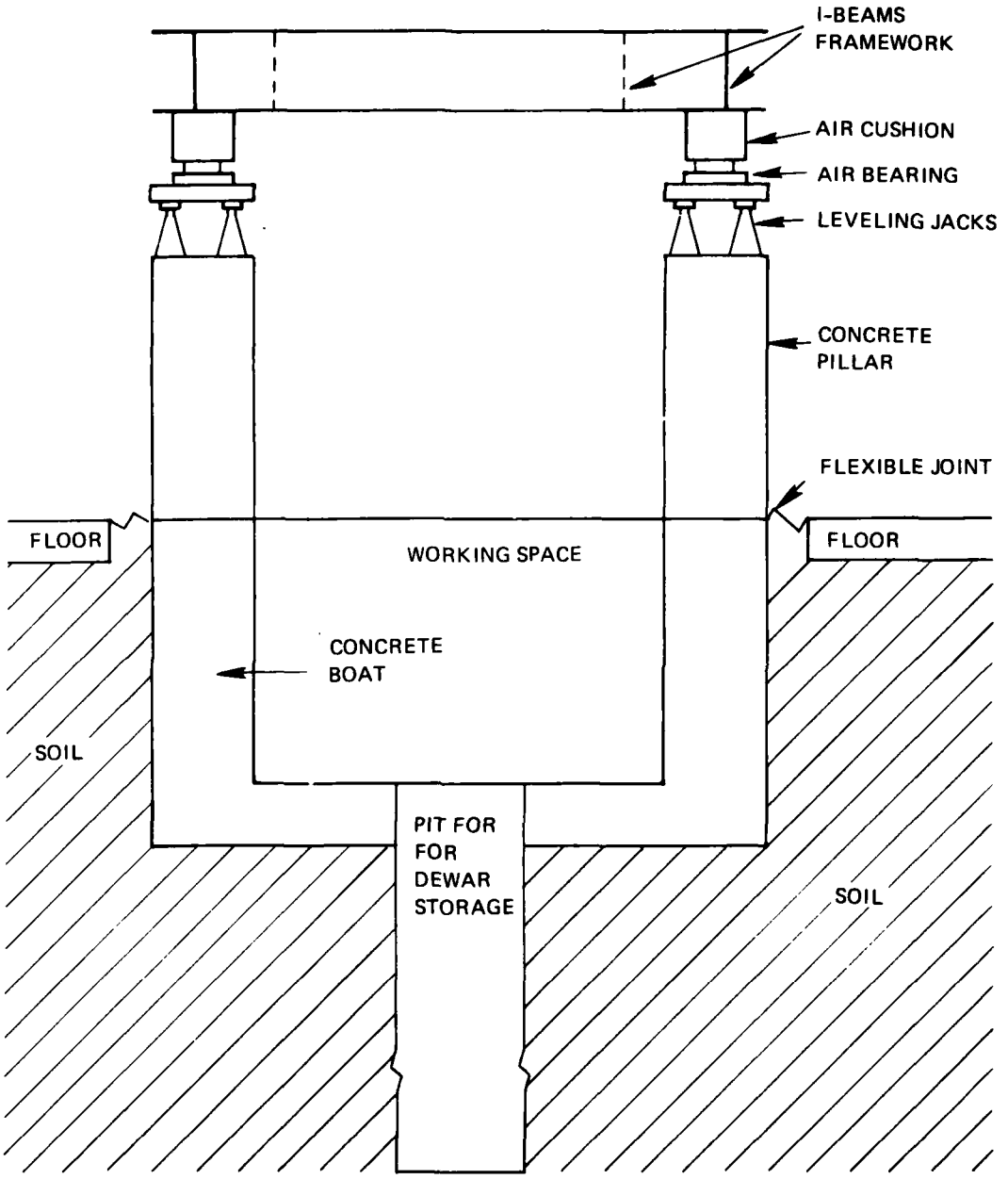

Figure 4-2. Schematic of cryostat pit and platform mounting arrangement.

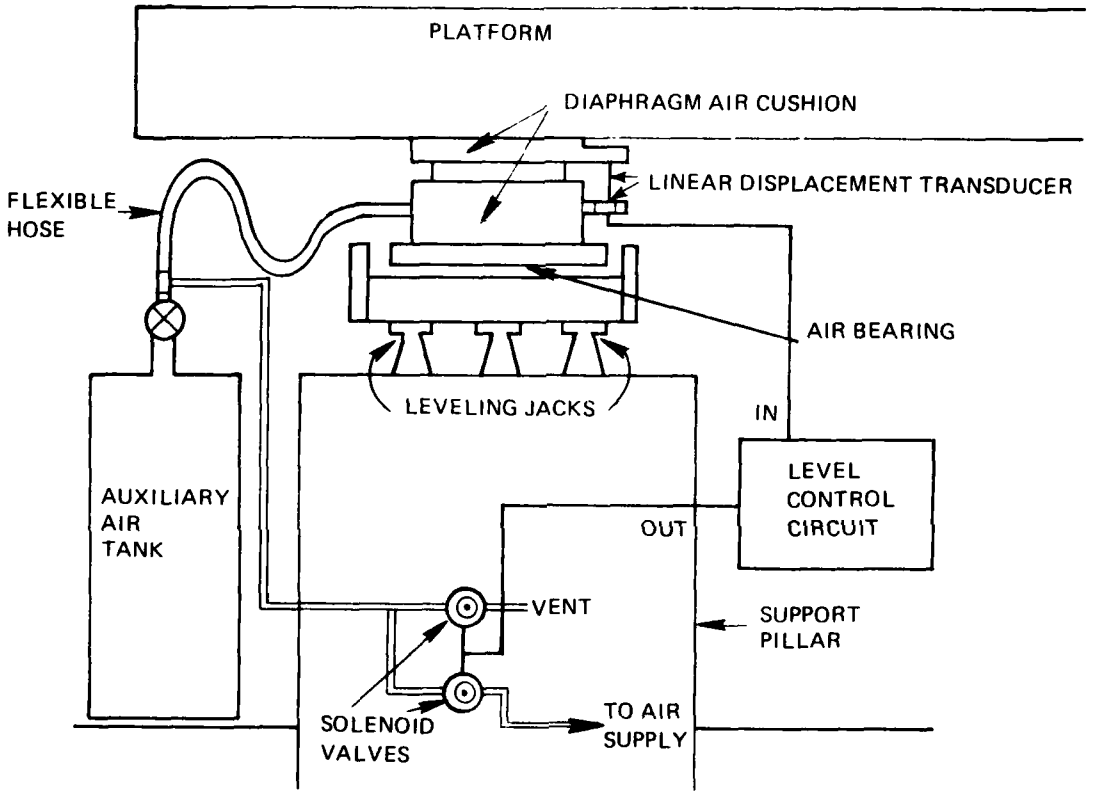

Figure 4-3a. Schematic outline of the platform vibration isolation and leveling system use in experimental Series III.

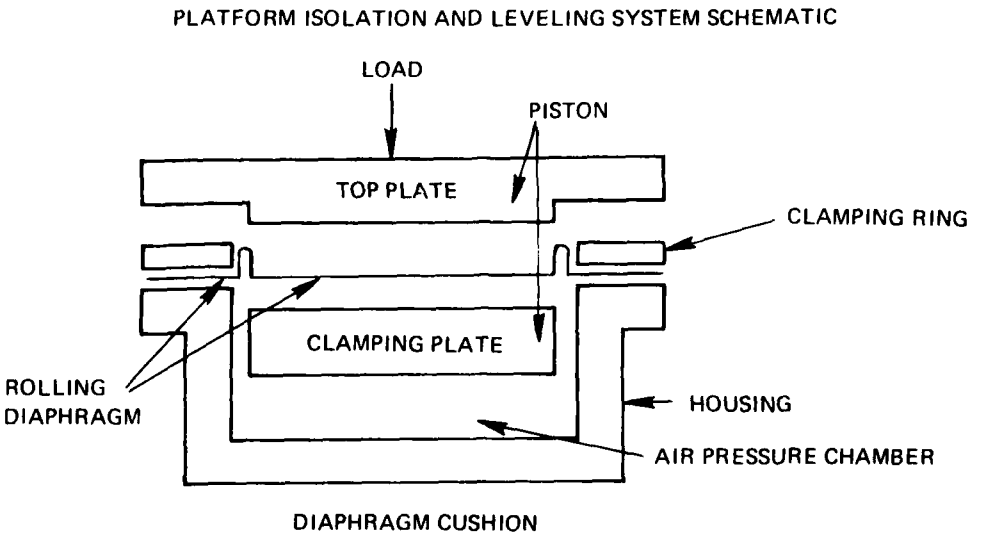

Figure 4-3b. Schematic details of diaphragm air cushion.

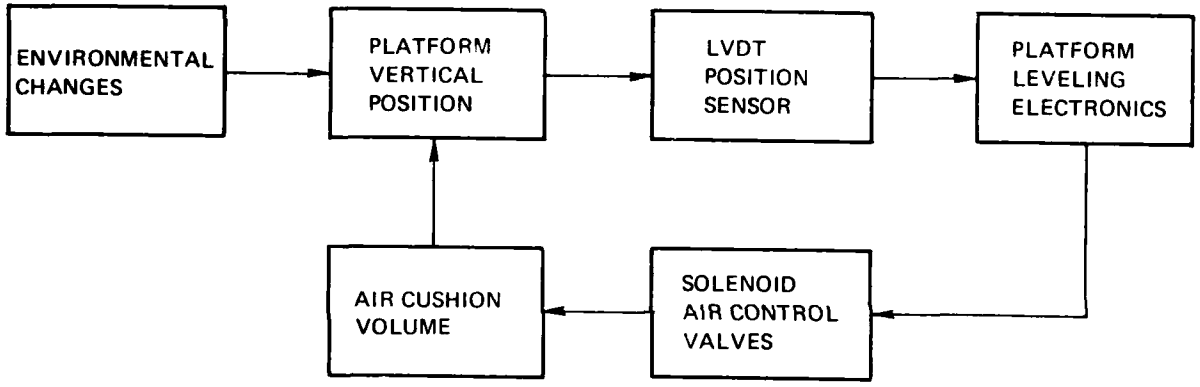

Figure 4-4. Schematic diagram of electro-mechanical loop for leveling the platform.

which is compatible with the cryogenic conditions. The purpose of the cryogenic insert with its auxiliary support systems is to provide the desired low temperature environment for the instrument package. Furthermore, since the instrument package must interface with room temperature instruments and equipment, the insert has to provide this interface. However, again the instrument package along with its interface requirements must be compatible with the cryogenic conditions.

The cryogenic conditions have to do with the physics and chemistry of matter at low temperatures and the engineering state-of-the-art of the cryogenic equipment.

Depicted in Figure 4-5 is the lower end of the cryogenic insert. This insert together with the Dewar, the other support systems and the cryogenic fluids, provides the means for cooling and maintaining the instrument package at the desired low temperatures. Also the insert provided the interface requirements which included bringing 38 fully shielded co-axial sensor and monitoring leads, numerous current leads and the liquid filling sytem to the instrument package.

The small superfluid tight needle valves on the instrument package and at the top of the vacuum can were actuated with rods which lead to room temperature outside the cryostat. This was part of the instrument package filling system. Not depicted in the figure was a small liquid helium pot attached to the mixing chamber used to speed up the cooldown from 4K.

4.3 VISCOMETER APPARATUS (EXPERIMENTAL SERIES III)

Basically, the viscometer is a Couette type (co-axial cylinders) viscometer adapted for use at ultralow temperatures. While the outer co-axial cylinder is driven at a constant rotational velocity, the inner co-axial cylinder experiences a torque due to the viscous coupling of the fluid in the gap between the cylinders. The measured torque on the inner cylinder is directly proportional to the effective viscosity of the fluid.

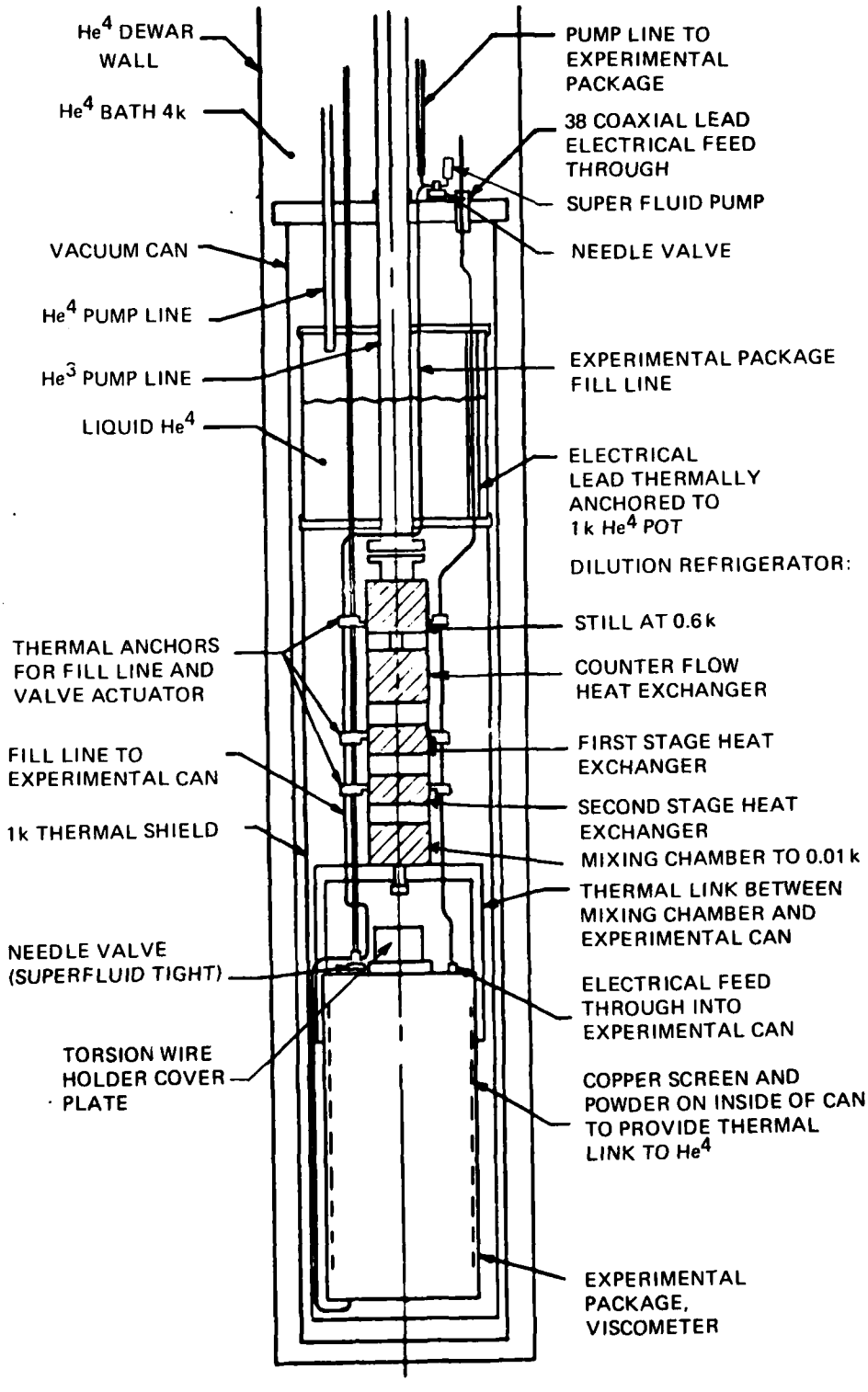

Figure 4-5. Cryostat - instrument package interface.

In Figure 4-6 is depicted the viscometer apparatus used for Experimental Series III. The driven outer cylinder is held in position by a ball bearing spindle shaft which permits the outer cylinder to rotate while holding alignment. To reduce the load placed on the bearing and the resultant frictional heating, a superconducting thrust bearing is used to support the weight of the outer cylinder assembly.

When the outer cylinder is rotated at a speed corresponding to the superfluid critical velocity of about 0.3 rad/sec, the bearings generate about 100 ergs/sec. The outer cylinder is driven by a six pole, two phase hysteresis-type synchronous motor with super conducting windings and provides rotational speeds between 0.001 rad/sec and 4 rad/sec. A capacitance-type angular velocity sensor is attached to the outer cylinder. This sensor was used to verify the speed and monitor the smoothness or constancy of rotation. The heat generated by the synchronous motor was mainly due to the hysteresis in the stator which was made from laminated silicon iron (transformer 58); the rotor was made from solid Simonds 73 iron. This hysteresis heating was several times larger than the heat generated by the bearings. However, the hysteresis heating could be reduced somewhat by reducing the motor excitation current after the outer cylinder had been brought up to speed. The heat extraction of the dilution refrigerator was about 38 ergs/sec at .05K and 500 erg/sec at 0.12K.

The inner cylinder consists of a section of true bore pyrex glass tube with attached truncated (120°) conical end capacitance plates made of titanium (see Figure 4-7). The end sections are epoxied (K-10) to the glass by small finger connections made of titanium. Each end section consists of six equally spaced 30° radial sectioned cutouts to form six equally spaced 30° radial sectioned capacitance plates. These inner cylinder capacitance plates are set opposite 12 stator capacitance plates which are utilized to measure the position of the inner cylinder (see Figure 4.c). The conic stator plates also guard the inner cylinder ends from the moving fluid created by the rotating outer cylinder.

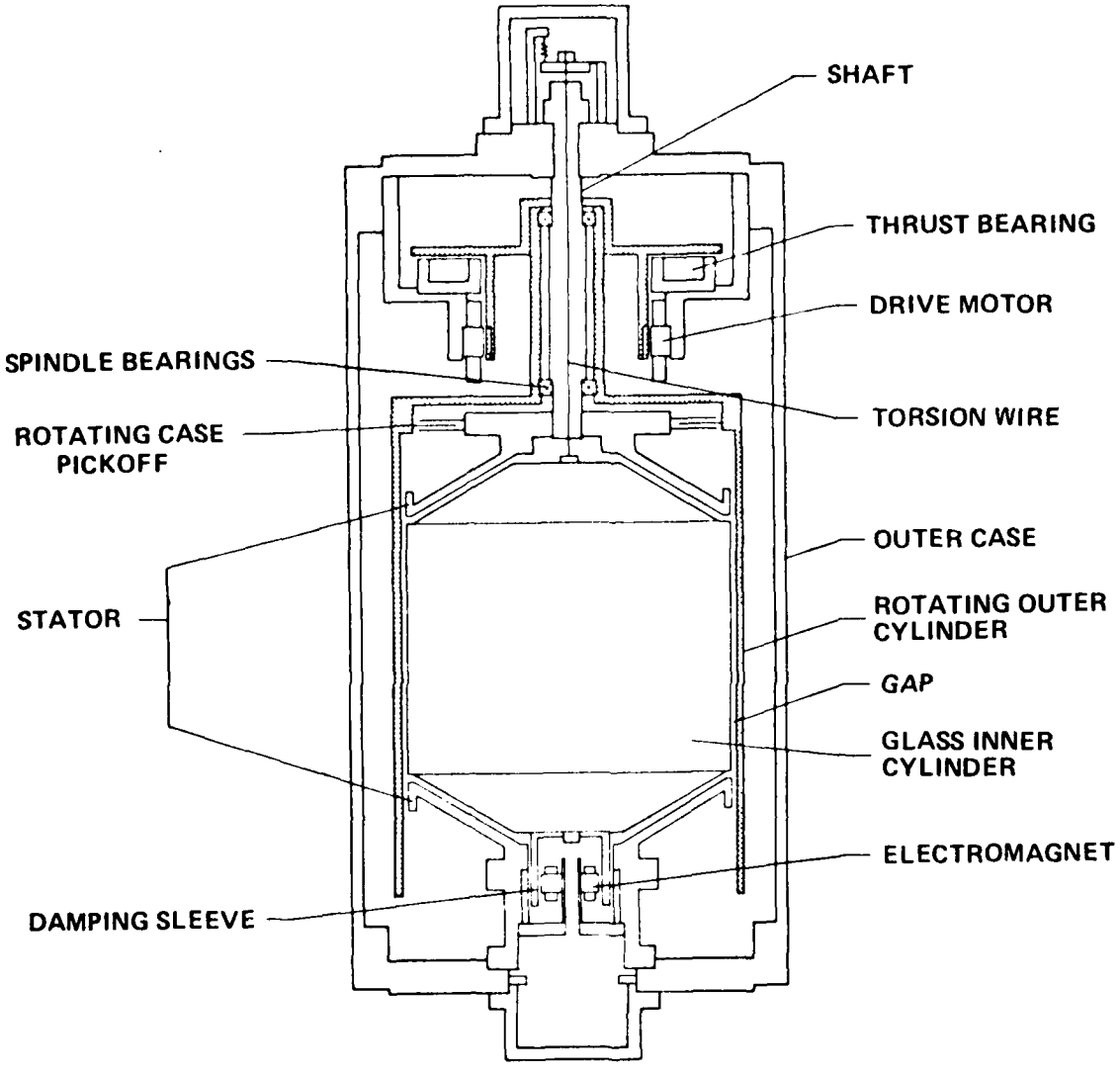

Figure 4-6. Schematic diagram of viscometer used in experimental Series III.

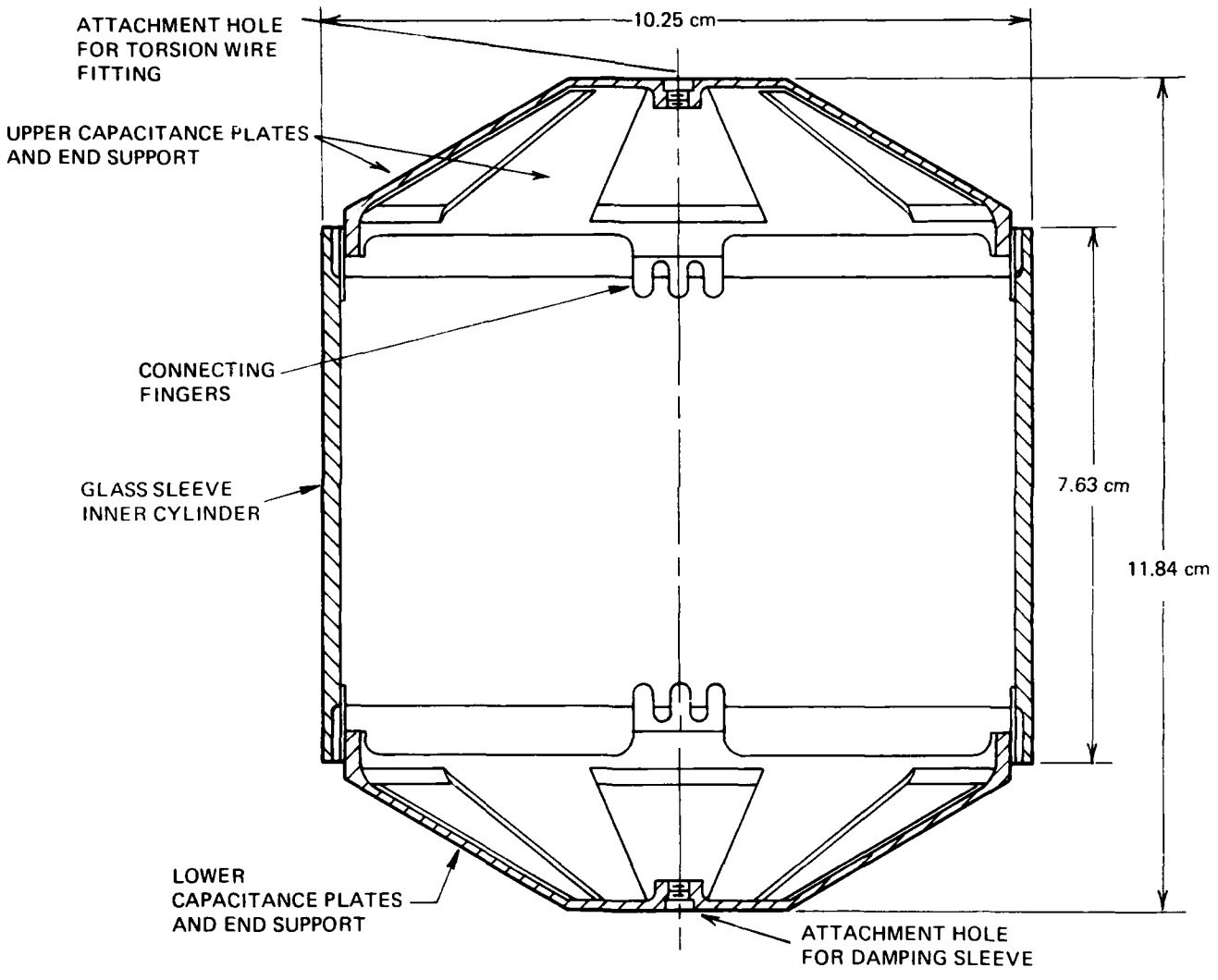

Figure 4-7. Inner glass cylinder of viscometer.

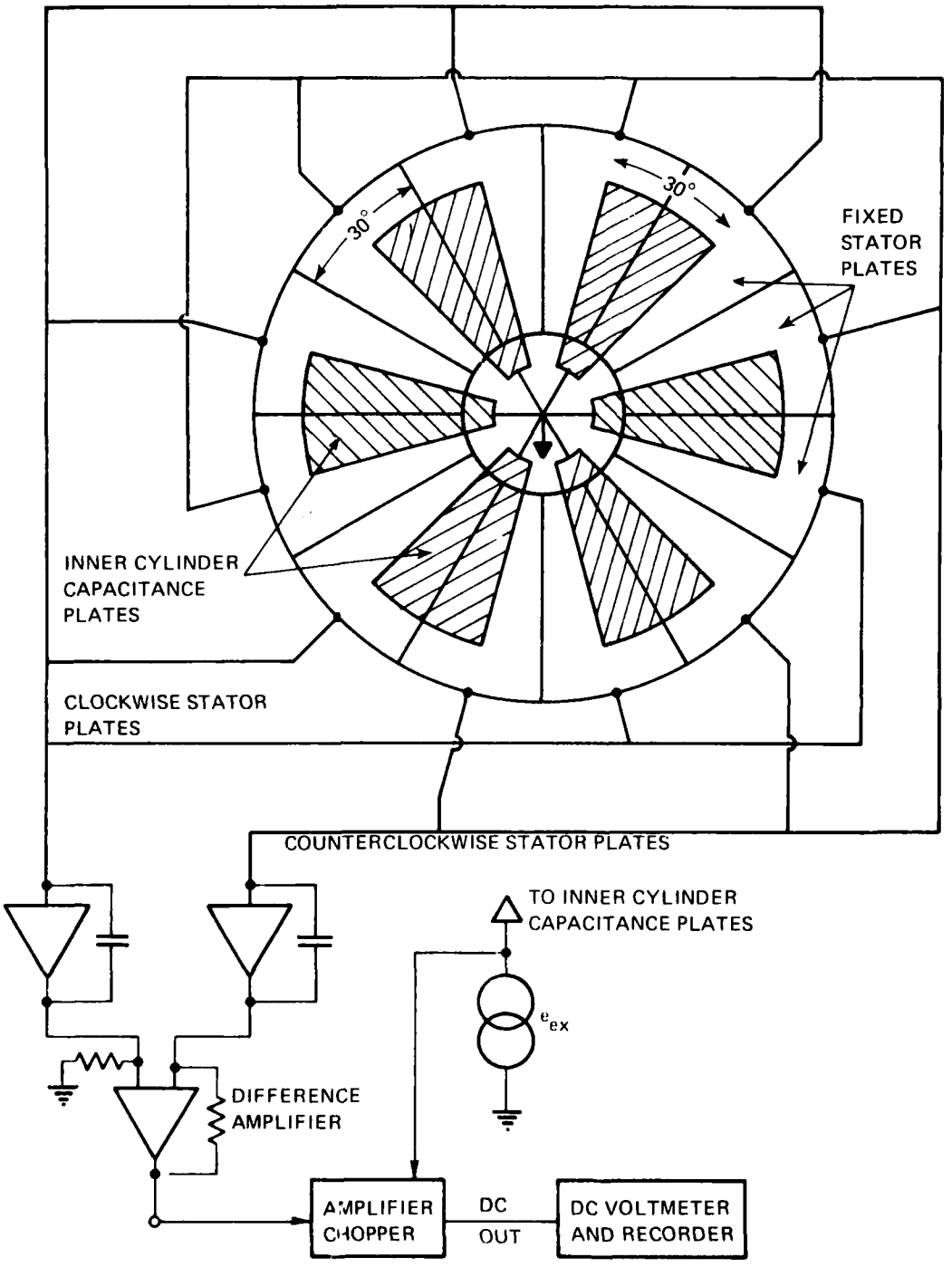

Figure 4-8. Schematic diagram of glass inner cylinder angular sensor.

The inner cylinder is suspended by a single tungsten torsion wire. The tungsten wire is hard soldered into a fitting which is, in turn, screwed into the inner cylinder. The torsion wire is attached at the top of the instrument package to a spring lever system which limits tension in the wire to some preset value. This prevents breaking of the small .003" torsion wire should the instrument package be jarred. The upper attachment point allows for adjusting the rotational position of the inner cylinder as well as positioning it up and down. This upper attachment point is electrically isolated from the instrument package so that a non-grounded electrical connection can be made to the inner cylinder capacitance plates.

Attached to the bottom of the inner cylinder is a pure copper damping sleeve. This damping sleeve is enclosed by a superconducting electromagnet. Since the damping is proportional to $(\text{field})^2/\text{resistivity}$, the required field can be minimized by minimizing the resistivity. Copper has one of the lower resistivities, and for zone refined copper which has been oxygen annealed[2], the resistance ratio between room temperature and helium temperature is about 10,000. The present copper sleeve was so made and annealed.

It is desired to keep all stray magnetic fields in the neighborhood of the inner cylinder at a minimum because these fields may apply unwanted torques to the inner cylinder. For this reason, superconducting shielding material was placed around the electromagnetic damper and the outer cylinder drive motor to reduce and divert such fields from the inner cylinder.

Experimental Series I and II were done with a torsion wire attached at the bottom of the inner cylinder as well as the top. This arrangement provided lateral restraint and kept the inner cylinder properly centered. However, it had the disadvantage that since the line of support did not pass through the center of mass, there was vibrational mode coupling which caused lateral vibrational motion of instrument package to induce rotational motion and, consequently, increased the unwanted noise

in the signal. By removing the bottom torsion wire, the inner cylinder hung freely and the unfavorable mode coupling link vanished. Without the bottom torsion wire the level of the instrument package had to be carefully controlled in order to maintain a uniform fluid gap. This level stabilization was accomplished by servo control of the level of the cryostat platform, as discussed in the previous section.

The vacuum seals in the instrument package case were "O-rings" made from .032" lead wire. Rings were made from the lead wire by soldering the ends of the wire. The instrument package contains approximately 12 "O-ring" seals and these seals were extremely reliable.

Thermal contact between the instrument package and the dilution refrigerator's mixing chamber was made by three thick (OFHC) copper bars. The joints along the thermal path were fastened with copper screws and then whenever possible furnace blazed. The copper link passed through the side wall of the instrument package and was directly furnace brazed to a copper heat exchanger, which covered the entire inside wall of the instrument package. The instrument package heat exchanger was a composite of an OFHC copper sheet, small mesh copper screens and copper powder sintered together and rolled into a cylinder to cover the entire inside wall of the instrument package.

Carbon resistance thermometers were placed on the upper stator and lower stator. Two calibrated germanium thermometers* were suspended in the liquid He^4 near the top of the instrument package. At the low temperature end of the cryostat the germanium thermometer leads were thermally anchored at the mixing chamber before passing through the instrument package feed-through, which provided additional thermal anchoring to the instrument package. Inside the instrument package the leads were over 10 cm long and were immersed in the liquid He^4 of the instrument package. The mixing chamber, the instrument package (when filled with liquid He^4) and the thermometers behaved as though they were in good thermal contact.

*By Scientific Instruments, Inc., Lakeworth, Florida.

The concentric cylindrical viscometer is a very usefull instrument for studying the basic viscous properties of liquid He^4. For this geometry the shear velocity is uniform and so critical velocities and turbulent viscosity can be much more easily analyzed. The geometric parameters which influence the viscosity, the critical velocity and the turbulent viscosity are well defined and can be changed by simple modifications of the viscometer.

The functions of the electronic instrumentation for the viscometer may be summarized as follows:

a) Position measurement of the inner cylinders' three degrees of displacement (x, y, z) and most importantly its angular displacement on the torsion wire.

b) Torquing of the inner cylinder about the torsion wire axis.

c) Control and monitoring of the angular velocity of the outer cylinder.

d) Control and monitoring of the inner cylinder eddy current damper.

e) Control of the outer cylinder thrust bearing.

f) Thermometry measurements and temperature control of the instrument package.

g) Storage and documentation of output information.

4.4 CALIBRATION EQUATIONS OF THE VISCOMETER

In order to make a viscosity measurement, the outer cylinder was brought into rotation with constant angular velocity ω. Because the drive motor was a six-pole, two-phase synchronous hysteresis motor, the angular velocity was

$$\omega = 2/3\ \pi f \qquad (4.1)$$

where f is the frequency of the drive motor excitation. This rotational motion of the outer cylinder, acting through viscous drag of the fluid between the inner and outer cylinders, causes a torque τ on the inner (torsion wire suspended) cylinder which results in an angular deflection θ given by

$$\tau = k\theta \tag{4.2}$$

The torsion wire constant k was determined from the natural period of oscillation P knowing the moment of inertia I of the inner cylinder by

$$k = \left(\frac{2\pi}{P}\right)^2 I \tag{4.3}$$

The angular deflection θ of the inner cylinder was measured by means of capacitive sensors (see Figure 4-8) located in the top and bottom of the inner cylinder which were coupled to appropriate electronics whose DC voltage output e_o was directly proportional to the angle θ. Presented in Figure 4-8 is a schematic of the capactive angular sensor readout system as viewed from one end of the cylinder. In Figure 4-8 the inner cylinder capacitance plates are shaded and positioned over the stator plate in a null position; that is, the capacitance between the clockwise stator plates and the inner cylinder equals the capacitance between the counter clockwise stator plates and the inner cylinder. From this figure it is seen that a clockwise rotation increases the clockwise capacitance and decreases the counter clockwise capacitance; this would continue until the inner cylinder is rotated 15° clockwise where the clockwise capacitance is a maximum and the counterclockwise capacitance is a minimum.

A similar situation occurs if the inner cylinder is rotated in the other direction. This feature is utilized in the calibration of the system; that is, by allowing the inner cylinder to oscillate more than ±15° one can observe e_o^+ at $\theta = +15°$ and e_o^- at $\theta = -15°$. This experimentally measured value is called e_{p-p} (e, peak to peak) and corresponds to a rotation of 30°. The inner cylinder is made to oscillate by temporarily using some of the capacitance plates as torquers.

For a fixed excitation voltage e_{ex} and amplifier gain G, and for a linear system the DC output voltage e_o is directly proportional to the angular displacement

$$e_o = \frac{de_o}{d\theta}\,\theta \tag{4.4}$$

Allowing for the case that the excitation voltage e_{ex} and amplifier gain G can be changed and that $de_o/d\theta$ may be measured at different values of G and e_{ex} we write equation (4.4)

$$\theta = \left[\frac{1}{\frac{1}{Ge_{ex}}\,de_o/d\theta}\right]_{cal}\frac{e_o}{Ge_{ex}} \tag{4.5}$$

where the term in the brackets represents a constant, determined by calibration and the terms G and e_{ex} represent the gain and excitation voltage at the time e_o is measured.

The calibration of the angular sensor now involves a measurement of the term in the brackets. As mentioned above, due to the geometry of the inner cylinder capacitance plates and stator plates, e_o reaches a peak at +15° and a minimum at -15°. However, due to fringing and edge effects the system is only linear out to about ±12°, and so a correction must be applied. C.R. Dauwalter* using a computer model of the capacitance sensor, determined for the glass inner cylinder that this correction to e_{p-p} to be 1.149. The peak to peak output voltage e_{p-p} is then related to the linear ratio $de/d\theta$ as,

$$\frac{de}{d\theta} = \frac{1.149\ e_{p-p}}{2(15°)}\ ,\ \text{volts/deg} \tag{4.6}$$

*private communication

Substitute equation (4.6) into (4.5) to get,

$$\theta = \frac{1}{2.194[e_{p-p}/Ge_{ex}]_{cal}} \frac{e_o}{Ge_{ex}} \tag{4.7}$$

It should be pointed out that the values of G and e_{ex} in the brackets are the values of G and e_{ex} at the time e_{p-p} is measured, while the values of G and e_{ex} outside the bracket are the values of G and e_{ex} when e_o is observed during a viscosity measurement

In making a viscosity measurement, the outer cylinder is first run in the forward direction and e_o^+ is measured and then it is run in the reverse direction and e_o^- is measured, thus,

$$e_o = \frac{e_o^+ - e_o^-}{2} \tag{4.8}$$

The viscosity η, for a concentric cylindrical viscometer of inner radius r, outer radius R, and height h of the inner cylinder, is given as,

$$\eta = \frac{(R^2-r^2)k\theta}{4\pi R^2 r^2 h\ \omega} \tag{4.9}$$

Using the above equations, one can then write the viscosity in the final form

$$\eta = \frac{3(R^2-r^2)I}{4R^2r^2P^2 2.194\ [e_{p-p}/Ge_{ex}]_{cal}} \frac{e_o^+ - e_o^-}{fGe_{ex}} \tag{4.20}$$

Presented in Tables 4-1, 4-2, and 4-3 are the viscometer parameters for the three Experimental Series.

Table 4-1. Experimental Series I Viscometer Parameters

Inner Cylinder	
Height:	h = 10.203 cm ±0.0013 cm
Outer Radius:	R = 5.065 cm ±0.0025 cm
Moment of Inertia:	I = 2753 gm cm² ±8 gm cm²
Material:	Beryllium S-200
Smoothness:	8μin.
Outer Cylinder	
Inner Radius:	r = 5.115 cm ±.0015 cm
Material:	Aluminum 2024T4
Smoothness:	8μin.
Fluid Gap:	d = .0498 cm ±.004 cm
Torsion Wire	
Height:	upper 12 cm, lower 2 cm
Diameter:	upper .0134 cm, lower .0089 cm
Material:	Tungsten
Calibration Data	
Inner Cylinder Period:	10.88 sec
Gain G:	G100/G10/G1 = 75.67/9.91/1
Viscosity:	$\eta = 6.46 \times 10^{-5} \frac{e_o^+ - e_o^-}{fGe_{ex}}$, poise

Table 4-2. Experimental Series II Viscometer Parameters

Inner Cylinder (dimensions computed to 4K)

Height:	7.634 cm ±.008 cm
Outer Radius:	4.974 cm ±.011 cm
Moment of Inertia:	3715.5 gm cm² ±30 gm cm²
Material:	Glass (Pyrex)
Smoothness:	As solidified from molten state

Outer Cylinder

Inner Radius:	5.0978 cm ±.002
Material:	Pure magnesium
Smoothness:	Polished to grit size 0.25 micron
Fluid Gap:	0.125 cm ±.013 cm

Torsion Wire

Length:	upper 12 cm, lower 2 cm
Diameter:	-
Material:	Tungsten

Calibration Data

Inner Cylinder Period:	P = 46.3 sec
Angular Sensor:	$[e_{p-p}/Ge_{ex}]_{cal} = 9.012$
Gain, G:	G100/G10/G1 = 74.22/10.03/1
Viscosity:	$\eta = 1.517 \times 10^{-5} \frac{e_o^+ - e_o^-}{fGe_{ex}}$, poise

Table 4-3. Experimental Series III Viscometer Parameters

Inner Cylinder	
Height:	$h = 7.638$ cm, $h_4 = 7.634$ cm ± 0.008*
Outer Radius:	$R = 4.975$ cm; $r_4 = 4.974$ cm $\pm .011$ cm
Moment of Inertia:	$I = 3721.5$ gm cm^2; $I_4 = 3716$ gm ± 30 gm cm^2
Material:	Pyrex Glass
Smoothness:	As solidified from molten state during forming
Outer Cylinder	
Inner Radius:	$r = 5.147$ cm; $r_4 = 5.126$ cm $\pm .002$ cm
Material:	Pure magnesium
Smoothness:	Polished to grit size 0.50 micron
Fluid Gap:	$d = 0.1727$ cm; $d_4 = 0.152$ cm $\pm .013$ cm
Torsion Wire	
Length:	12.05 cm; ± 0.2 cm
Diameter:	.00735 cm
Material:	Tungsten
Calibration Data	
Inner Cylinder Period:	$P_4 = 57.5$ sec
Amplifier Gain, G:	G100/G10/G1 = 100/10/1
Angular Sensor: Calibration:	$[e_{p\text{-}p}/e_{ex}G]_{cal} = 4.522$
Viscosity:	$\eta = 2.62 \times 10^{-5} \dfrac{e_o^+ - e_o^-}{fGe_{ex}}$, poise

*The subscript 4 denotes value at temperature 4K.

4.5 OUTLINE OF EXPERIMENTAL PROCEDURE (EXPERIMENTAL SERIES III)

a) With the viscometer package assembled and connected to the cryostat, all the wiring and electrical circuits were checked out. The various vacuum spaces were routinely checked for leaks.

b) The torsion wire cover plate on the top of the instrument package was removed and the upper torsion wire clamp was adjusted to bring the inner cylinder to its angular null position, i.e., so that the counterclockwise angular sensor capacitance equaled the clockwise capacitance (as depicted in Figure 4-8). The inner cylinder was also positioned vertically so that the inner cylinder would be centered between the top and bottom stator plates when the apparatus was at low temperatures (4K). The stator capacitance plates at the top and bottom were interconnected to measure the angular position of the inner cylinder while at the same time being insensitive to all other displacements when centered and near null.

c) The instrument package torsion wire cover was replaced and the instrument package was evacuated, leak hunted, and baked out at about 140°F for two days to "dry out" any moisture absorbed by the MoS_2 coating on the outer cylinder spindle bearings (frozen moisture in the bearing would degrade their performance).

d) The apparatus was cooled to liquid nitrogen temperature, leak checked, then cooled to 4.2K by transfer of liquid He^4. It usually required about two days to reach 77K and another eight hours for the He^4 transfer to bring the 14 Kg instrument package to 4K. The electronic circuits were also checked at low temperatures. The main bath was then pumped to just below the λ temperature which brought the instrument package and cryostat to about 2K.

e) The instrument package was then filled with liquid He^4 through a superfluid pump located in the main bath space. The superfluid pump provided high quality filtering of the fluid entering the instrument package as well as retarding the He^3 impurity from entering. Once the instrument package was filled, the small needle valve on the instrument package was closed, locking the He^4 in the package. The fill line was then evacuated to reduce heat leakage and the He^3 exchange gas in the vacuum can was removed.

f) The instrument package was then cooled to about 1K by the small He^4 pot on the package and by circulation of liquid and gas through the dilution refrigerator. The cooling to 1K took several days because of the extremely large specific heat of liquid helium near the lambda point.

g) After the instrument package reached about 1K, the small He^4 pot was pumped dry and the circulation of the liquid and gas through the dilution refrigerator cooled the package to about 0.6K in another couple of days. Sometimes the small He^4 pot was switched to a He^3 pot in order to reduce this cooling time. After phase separation was achieved in the dilution refrigerator, the package was cooled to below 0.1K. The instrument package was calibrated and the viscosity measurement begun.

h) The instrument package capacitance plates were interconnected in order to observe the lateral position of the (torsion wire) suspended inner cylinder with respect to the stator plates and thus to the outer cylinder. The platform level was then adjusted so that the suspended inner cylinder would hang in the center of the outer cylinder thereby giving a uniform fluid gap between the cylinders. After this procedure the platform leveling system maintained the platform at this desired level and the capacitance plates were again interconnected to measure angular displacement of the inner cylinder.

i) The inner cylinder damper and the outer cylinder vertical thrust bearing were energized. Viscosity measurements were taken by rotating the outer cylinder in the forward direction for periods between ten minutes and thirty minutes while the DC output voltage e_o^+ of the angular sensor electronic was being observed on a strip chart recorder. When it appeared that the output had reached a stable value the outer cylinder rotation was reversed and e_o^- was similarly observed.. During the measurement of a viscosity data point, the temperature of the instrument package was held constant by a temperature controller.

4.6 EXPERIMENTAL SERIES I, II, AND III INSTRUMENT PACKAGE MAJOR ERROR SOURCES AND IMPROVEMENTS

There was a minor problem in all three experimental series associated with mechanical hysteresis effects in the tungsten torsion wire which lead to angular null shifts in the suspended inner cylinder. Tungsten was used because of its great strength however there may exist more suitable materials.

The principal source of error in the viscosity measurements was due to the "noise" oscillations of the inner cylinder, which reduced the precision of the measurement of the angular displacement of the inner cylinder. These "noise" oscillations of the inner cylinder were excited by vibrational motion of the instrument package and by magnetic coupling to the rotating outer cylinder mechanism.

Vibrational oscillations of the instrument package along the axis of the inner cylinder could excite the inner cylinder through the torsion wire. Also lateral vibrational motion of the instrument package could couple to the oscillatory mode of vibration of the inner cylinder through a lateral moment arm between the center of mass and the center of support. A lateral moment arm between the center of mass and the center support was created by an out of balance inner cylinder restrained by both an upper and lower torsion wire.

Another source of inner cylinder oscillatory noise was due to magnetic coupling. The outer bearing housing had a small magnetic moment which coupled to the inner cylinder through some slightly magnetic materials on the inner cylinder torsion wire clamps, giving the inner cylinder an excitation with a period of the outer cylinder. Also the drive motor field, which had a frequency of 3 times the outer cylinder frequency, coupled to the inner cylinder.

These unwanted oscillations of the inner cylinder severely limited the accuracy of the lowest viscosity measurements. To minimize the effects due to vibrational oscillation required waiting for a quiet period. The lowest temperature points required several weeks of monitoring and measuring until usually between 3 and 6 a.m., the apparatus was quiet enough to make the lowest viscosity measurements. In Experimental Series I the inner cylinder oscillations were dampened out by torquing through the capacitance plates located at the ends of the inner cylinder. After torquing to rest, the position of the inner cylinder was measured to determine its displacement due to viscous drag. The beryllium inner cylinder was accurately machined and supported by the upper and lower torsion wire and the out of balance lateral moment arm was minimal. Consequently, when viscosity measurements were taken during the lowest vibrational noise period of the building (which occurred only a few hours in a month), the main driving source of noise oscillation of the inner cylinder was probably due to magnetic coupling.

For Experimental Series II an eddy current damper was installed to control the unwanted oscillation of the inner cylinder. This proved to be a step in the right direction; however, the eddy current damper also added its own set of errors. Due apparently to slight magnetism still on the inner cylinder torsion wire clamp and perhaps magnetic effects of the copper damping sleeve due to inhomogenous impurities and possible asymmetries in the copper sleeve, the inner cylinder null position was dependent upon the damping magnetic field, which required that the current generator for the damper field be very precisely controlled.

To reduce some of the magnetic coupling problems the entire instrument was demagnetized which reduced the magnetic moment on the outer cylinder bearing housing. Some stainless steel screws on the inner cylinder torsion wire clamp were found to be slightly magnetic and were replaced by non-magnetic ones. This reduced somewhat the magnetic coupling between the inner cylinder and the outer cylinder drive system.

However the vibrational problems were worse with the glass inner sleeve than with the beryllium sleeve. This apparently was due to the fact that the glass cylinder was out of balance somewhat due to its imprecise geometry. The resultant large lateral moment arm between the center of mass and the center of support allowed vibrational motion of the instrument package to cross-couple energy into the oscillatory mode of the inner cylinder which was supported by both an upper and lower torsion wire.

For Experimental Series III these problems were vigorously addressed. The vibration isolation system was rebuilt as described above in the apparatus Section 4.2.

The lower torsion wire was removed so that the inner cylinder would hang freely thereby putting the center of mass on the line of support so that the cross-mode coupling would be greatly reduced. The damping sleeve was carefully rebuilt with zone refined (ultra-pure) copper to minimize contamination, and then oxygen annealed to give high electrical conductivity so that only a minimal damping field would be required. The sensing electronics was extensively rebuilt and greatly improved by Robert Barden, and also new fully shielded co-axial leads were installed to the instrument package.

It was hoped, once and for all, that the "noise" problem would be greatly reduced. The damper worked beautifully and all its previous magnetic problem had been resolved. The inner cylinder was extremely quiet and it looked like we were going to be able to measure viscosity values as small as ±0.01 μP.

However as we took measurement at low temperatures we found yet a magnetic couple between the outer case drive system and the inner cylinder.

The problem was finally traced to a small screw on the inner cylinder made of beryllium copper. The beryllium copper screw behaved as a paramagnetic above about 0.3K and appeared to become ferromagnetic below that temperature. Needless to say this problem greatly worsened the "noise" problem. Unfortunately the program was terminated before the small screw could be replaced and the measurement remade with improvements which promised to extend the viscosity measurement another decade lower in magnitude. In spite of these problems some very useful measurements were taken as will be presented in Section 5.

REFERENCES

1. Helios Program Final Report, R-833, The Charles Stark Draper Laboratory, Inc., Cambridge, Massachusetts 02139.

2. Rosenblum, Steyert and Fickett, Cryogenics 17, 11, 645, (1977).

SECTION 5

EXPERIMENTAL RESULTS

5.1 VELOCITY INDEPENDENT VISCOSITY

5.1.1 Introduction

Prior measurements on the viscosity of liquid He^4 with Couette viscometers have indicated that it behaves as a Newtonian fluid at low shear velocities; which is to say, the viscosity is independent of the shear velocity. However, as the velocity is increased a value is soon reached where the fluid is no longer Newtonian and the viscosity begins to increase with the velocity. In classical fluids this increase of viscosity with velocity is associated with turbulence in the fluid. Since liquid He^4 has two components, the normal and the superfluid, there exists the possibility of each component becoming turbulent. There has been an enormous amount of research done on turbulence or vorticity in liquid He^4, yet it is still not completely understood and there still seems to be some confusion about identifying and distinguishing normal fluid from superfluid turbulence in wide channel experiments. For the Couette type viscometer the shear velocity v_c above which the viscosity is velocity dependent and below which the viscosity is velocity independent is called the critical velocity.

The results section is divided into two parts. In the first part 5.1 the velocity independent viscosity (Newtonian behavior) results will be presented, discussed and compared to the theory developed in Section 3. In the second part 5.2 the velocity dependent or "turbulent" viscosity results will be presented and discussed.

5.1.2 Velocity Independent Viscosity Results

Presented in Figure 5.1 are results from the Experimental Series, I, II and III, measurements made by J.R. Clow* during the Helios Program, and measurements by Woods and Hollis Hallet and Heikkila and Hollis-Hallet. The solid line represents the theoretical 5-phonon viscosity equation by Khalatnikov and near 0.75K has a T^{-9} temperature dependence. This equation has been reviewed and modified by Woods and Hollis-Hallet. The Experimental Series I, II, and III and the measurement by J.R. Clow were all taken at constant density of about .146 gm/cm^3. The short dashed line represents the theoretical 4-phonon equation by Khalatnikov. The other long dashed lines are drawn through the points to assist the eye in following the appropriate data point curves. The rise in the viscosity above 1.8K is thought to be due to the non-ideal gas behavior of the rotons and so Khalatnikov theory which treated the rotons as ideal particles is not expected to agree with experiment in this temperature region.

Within the experimental scatter and error (about ± 5%) in the present results (Experimental Series I, II, and III) there appears to be no significant difference between these results and those of Woods and Hollis Hallet and Heikkila and Hollis Hallet; except, those values of Woods and Hollis Hallet near T = 0.8K have a consistently larger value in viscosity. Their results are about 17% larger than the present results and are also larger than the values predicted by the theoretical 4 phonon interaction equation of Khalatnikov. Khalatnikov's theory indicated that below 0.7K the 4 phonon process would dominate the viscous properties of Helium II and thus the viscosity values should lie along the short dashed line of Figure 5.1. In the region of T = 0.75K the 4 phonon viscosity is changing approximately as T^{-7}; at somewhat lower temperature, this will go to a T^{-5} temperature dependence.

---

*Professor Clow is currently a member of the Department of Physics at Miami University, Oxford, Ohio. While at C.S. Draper Lab., Inc., he also built a proto-type-gyro using the superfluid persistent current of liquid He^4 as the angular momentum generator. This program was showing promising and interesting results but was terminated before the experimental results could be reported. For information on this concept see report: "Superfluid Persistent Current Gyroscope" by J.R. Clow; C-3983, (November 1975), C.S. Draper Lab., Inc., Cambridge, MA.

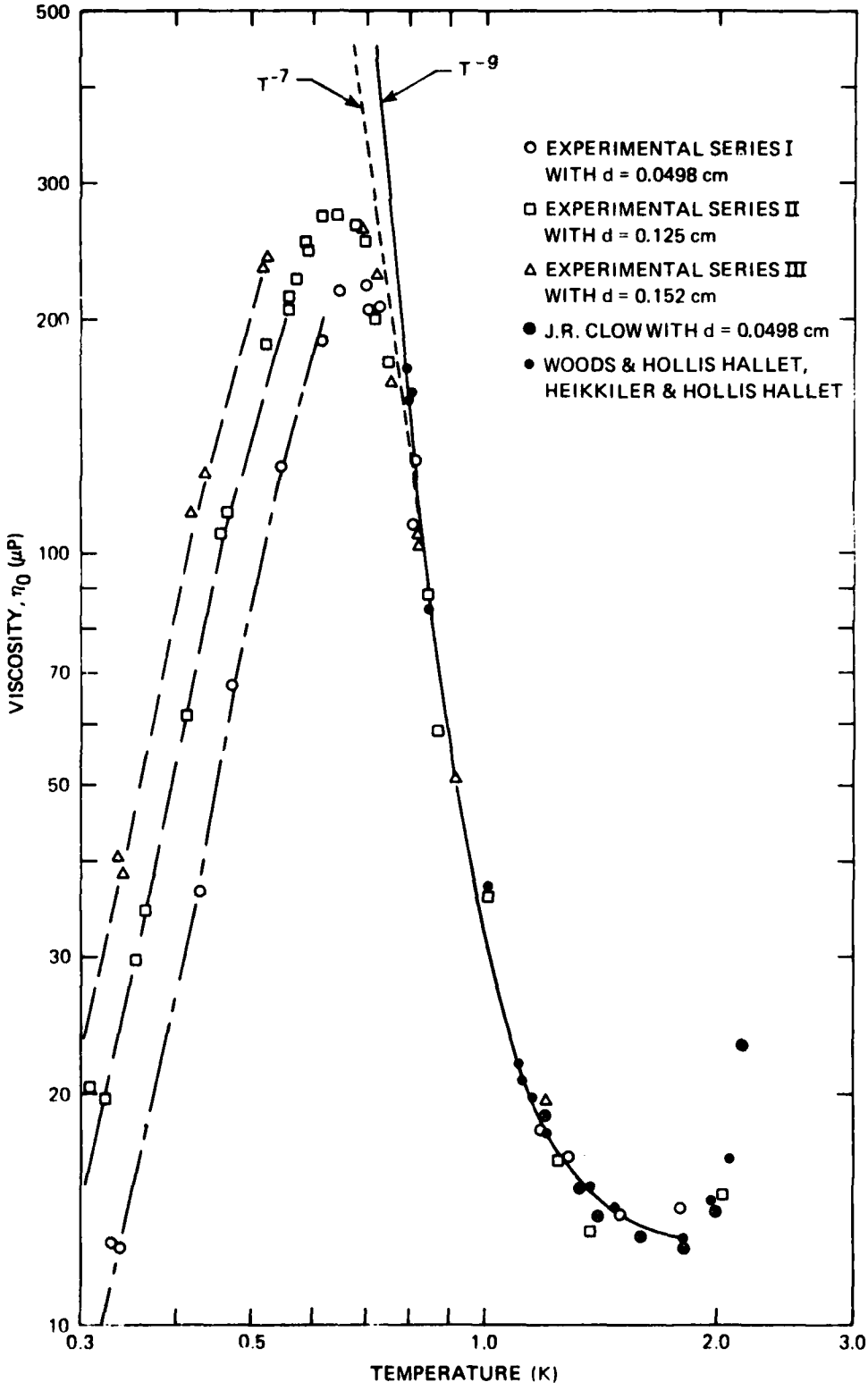

Figure 5-1. Experimental velocity independent viscosity measurements.

Below the temperature of 0.8K, the present results not only fall below the viscosity measurements of Woods and Hollis-Hallet but they also fall below the 4-phonon interaction equation of Khalatnikov. However, the present results contain both slip and specular reflection (wall effects) as the transition region is approached from higher temperatures and thus should fall below the "true" first viscosity values as the transition region is approached.

As presented in Figure 5-1 we see that as the temperature is lowered below 0.8K toward the transition region, the effective viscosity measurements fall away from the first viscosity values (as represented by Khalatnikov theory) reaching a maximum value in the same order as the fluid gap size, and then fall rapidly with temperature, while the coefficient of first viscosity values continue to rapidly increase with temperature.

As we see from Figure 5-1, at temperatures above the viscosity peak, the viscosity is independent of the fluid gap. Since the drag force per unit area is given as $F/A = \eta\, v/d$, the drag force is then inversely proportional to the fluid gap as one normally expects. On the other hand for temperatures below the viscosity peak the (effective) viscosity is proportional to the fluid gap; therefore, the drag force per unit area will be <u>independent</u> of the fluid gap.

Presented in Figure 5-2 are the Experimental Series I viscosity measurements. The numbers beside the points indicate the numbers of measured values averaged for the plotted points. For these measurements, the viscometer contained a beryllium inner cylinder of 8μin. finish which formed a fluid gap of 0.0498 cm. A line with a T^4 temperature dependence has been drawn through the points just below the peak. Except for the very lowest temperature points just above 0.1K, the points fall increasingly below the T^4 curve as the temperature is decreased from the peak. The point near 0.2K, for example, has a viscosity value about 45% less than the corresponding value on the T^4 curve. The unwanted

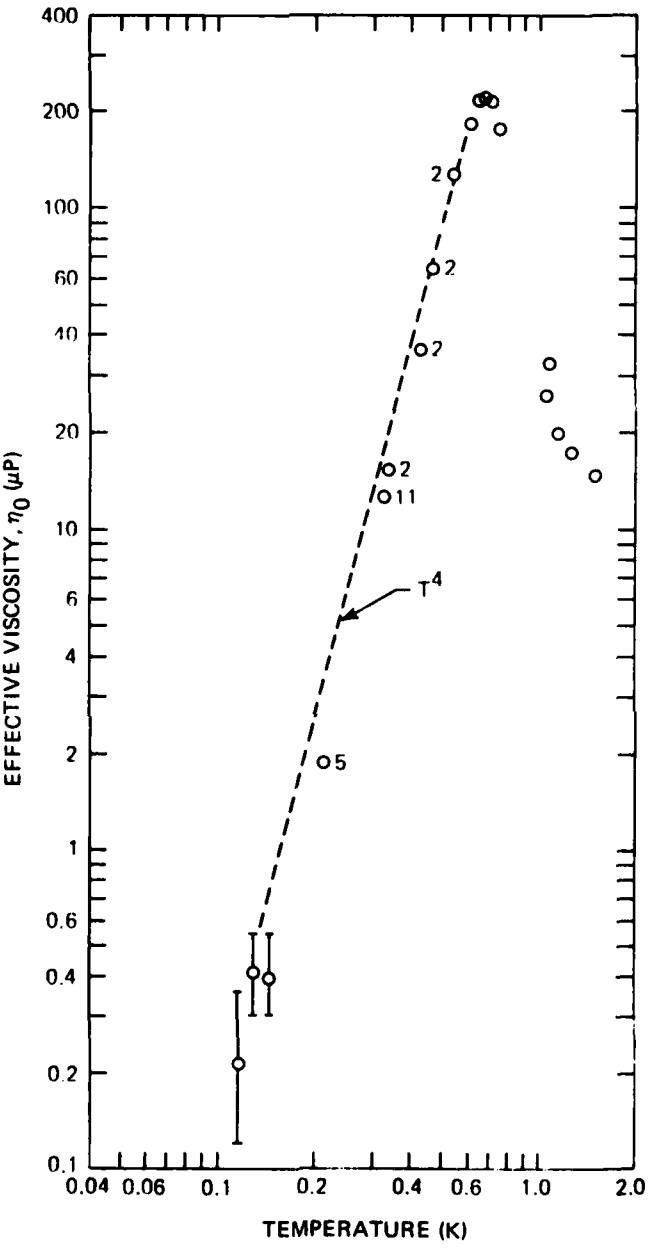

Figure 5-2. Experimental Series I, velocity independent viscosity results on liquid He^4.

oscillation of the inner cylinder discussed in Section 2 limited how small a value of viscosity could be measured. The unwanted oscillation caused an uncertainty of about ± 0.15μp under optimum conditions of lowest vibrational disturbance.

The measurements for Experimental Series II were taken with a true bore glass inner cylinder. The viscometer surface of the glass cylinder was the original surface formed during the fabrication process of the true bore tube where the surface solidified from the semi-molten state under influence of surface tension as it was being drawn over the "true bore" mantle. The viscometer surface of the glass inner cylinder was slightly out of round as well as slightly tapered making the OD vary about 0.04 cm from the minimum to the maximum diameter. The outer cylinder was made from pure magnesium, polished to a highly smooth finish with a final grit of 0.25μin. These cylinders gave an average fluid gap of 0.125 cm at 4K.

As presented in Figure 5-3, it is seen that as the temperature falls from the point of maximum viscosity the data points begin to fall below the T^4 curve and at T ≐ .25K the points have fallen about 35% below the corresponding value on the T^4 curve. The data points then cross over the T^4 curve and tend to level out with a viscosity just above 1μp. He^3 was then added to the instrument package in a series of steps, point A after the addition of 7×10^{-5} STP liters, point B after an additional 1.5×10^{-3} STP liters, and point C after another 5×10^{-3} STP liters, The total amount of He^3 added would have increased the concentration by approximately $X_3 \doteq 2 \times 10^{-6}$. The added He^3 caused only a small increase in the viscosity at temperatures just below 0.1K.

The triangular points were taken after the He^3 impurity had been added to the viscometer and while the viscometer was permitted to continuously and slowly warm up. Normally, the temperature was held constant or nearly so during a viscosity measurement. A later experiment was performed with the instrument package empty of liquid helium and the viscosity measurements in the neighborhood of 0.1K were found to be zero ± about 0.2μP.

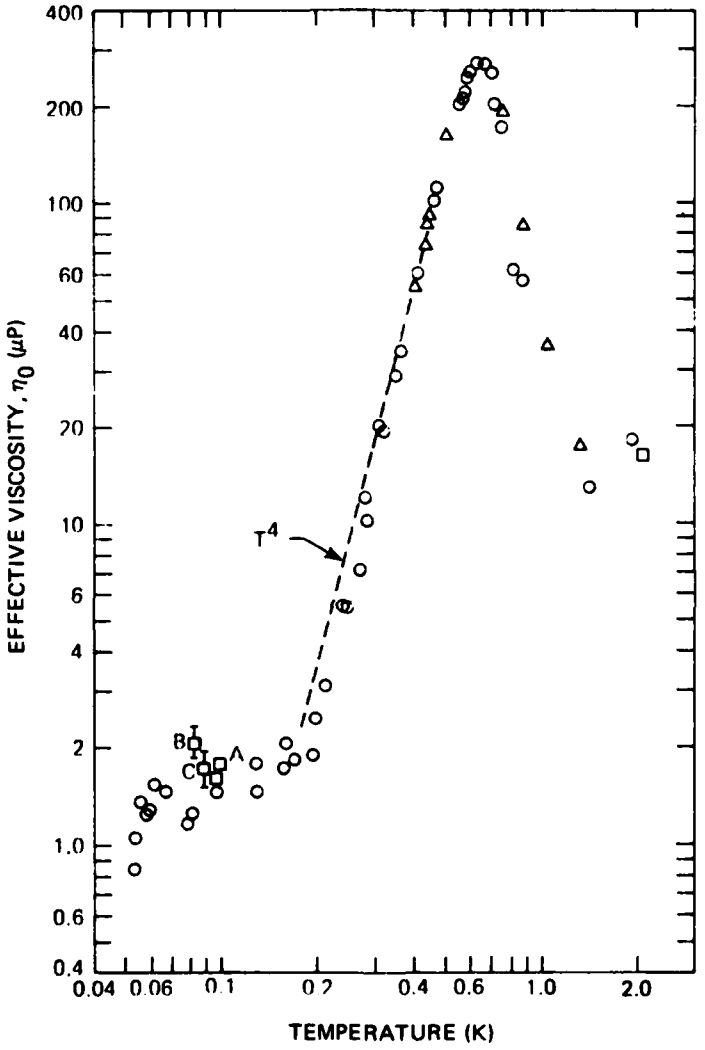

Figure 5-3. Experimental series II, velocity independent viscosity results on liquid He^4 with minute He^3 impurity. Glass inner sleeve, d = 0.125 cm.

Presented in Figure 5-4 are the velocity independent viscosity measurements taken in Experimental Series III with the same glass inner cylinder as in Experimental Series II, but with a slightly larger pure magnesium outer cylinder which gave an average fluid gap of 0.152 cm at 4K. The outer cylinder viscometer surface was polished with a final grit size of about 0.5μin. Again the number near the points indicate the number of measurements averaged into the plotted points.

The data below 0.3K has somewhat more scatter, yet it clearly shows a trend to fall below the T^4 line as the temperature is lowered.

5.1.3 Discussion of the Velocity Independent Viscosity Results and a Comparison with Theory

In Section 3, a theoretical expression for the velocity independent viscosity was developed using the Landau and Khalatnikov theory for the coefficient first viscosity, with Woods and Hollis Hallett's adjustments to the 5-phonon equation, with Khalatnikov and Zharkov's computation of the collision times and viscosity components and all of this brought together and modified by the present analysis to include the excitations' (phonons, roton and He^3 impurity atoms) mean free path effects and the viscometer surface effects.

Presented in the computer plotted Figures 5-5a,b,c, and d are experimental points from Experimental Series I for the beryllium inner sleeve with a fluid gap of 0.0498 cm at 4K. In order to avoid unclear clusters of plotted points, these computer plotted points usually represent an average of many data points. The dotted line represents a plot of the theoretical equation with the fluid gap d, the surface parameters δ_1, δ_2, γ_1, γ_2 and the He^3 impurity concentration X_3 as listed with the figure. The viscosity computed by the theoretical equation is left unchanged by an exchange of surface parameters (1) and surface parameters (2). Therefore, if the two surfaces are of different surface quality the surface parameters δ_1, δ_2, γ_1, γ_2 cannot be uniquely determined from a single experiment. The smaller of the two surface roughness

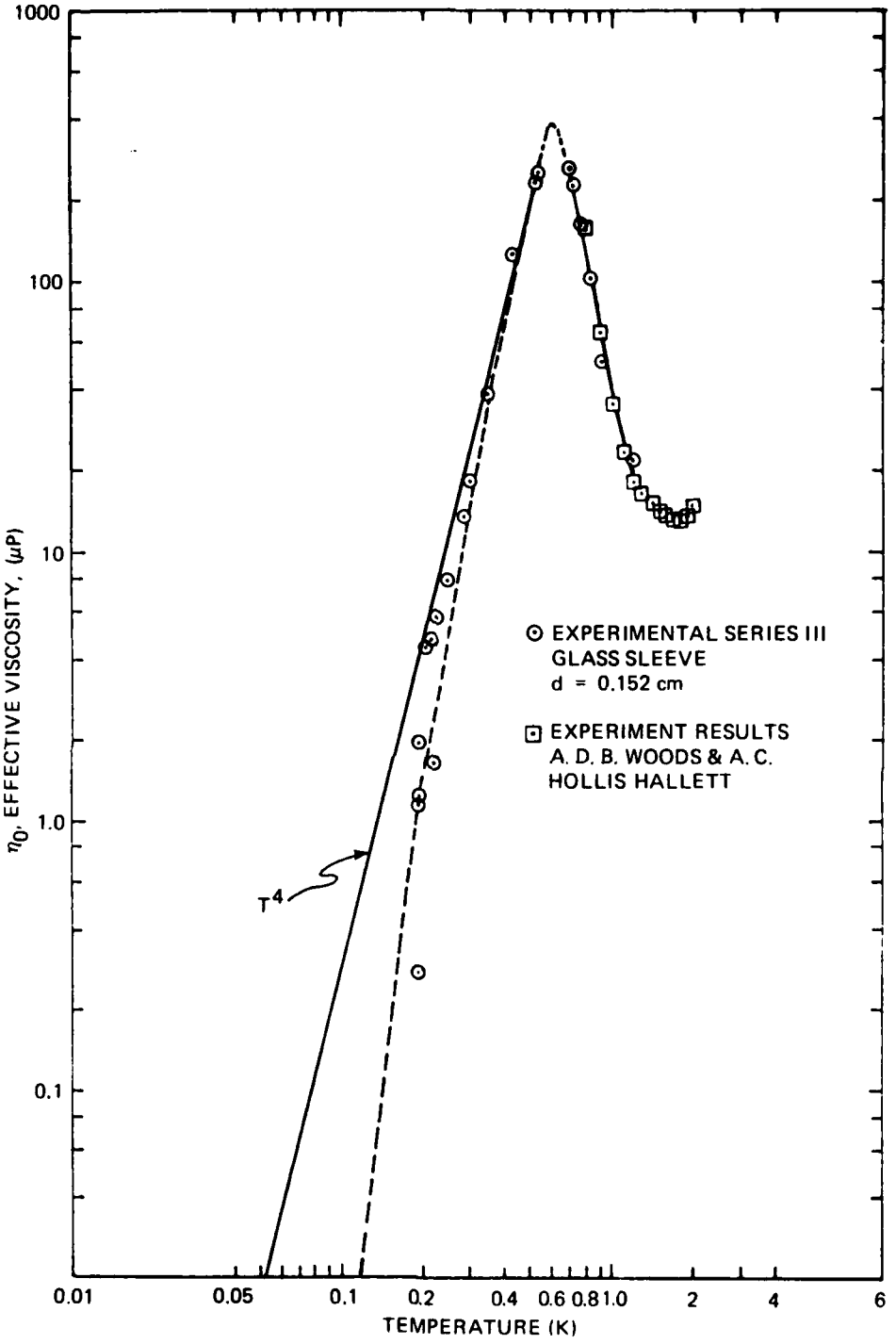

Figure 5-4. Experimental Series III, velocity independent viscosity results on liquid He^4.

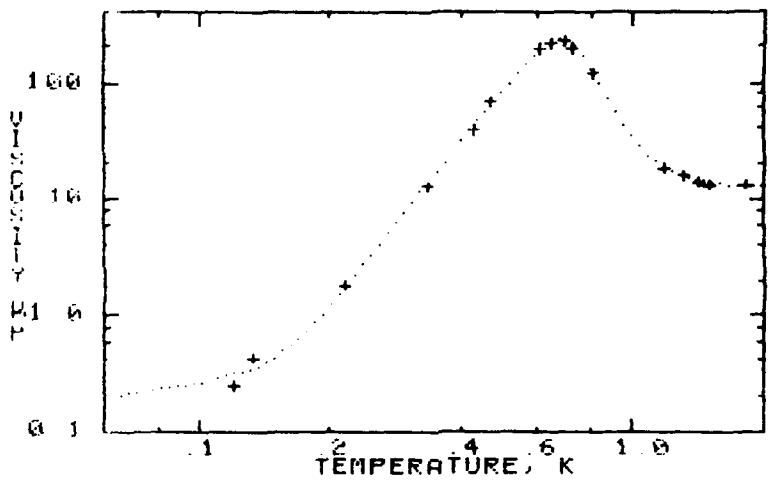

Figure 5-5a. Experimental Series I: Be sleeve, d = .0498 cm, $\gamma_1 = .6$, $\delta_1 = 300\text{Å}$, $\gamma_2 = .4$, $\delta_2 = 150\text{Å}$, $X_3 = 3 \times 10^{-8}$.

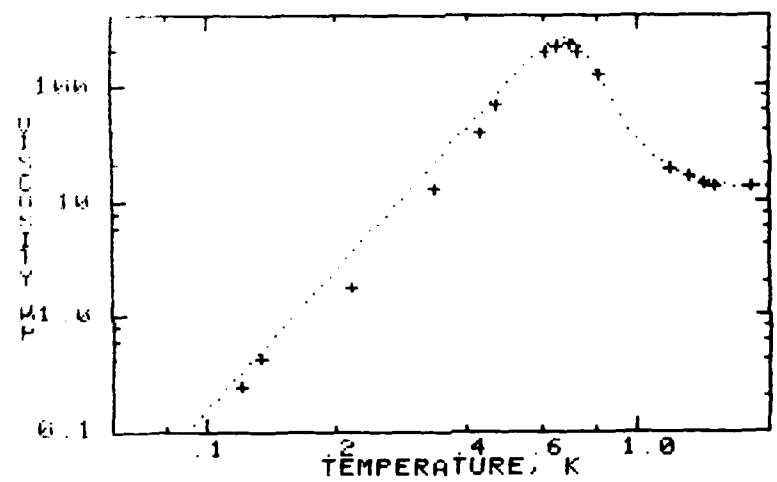

Figure 5-5b. Expeimental Series I: Be sleeve, d = .0498 cm $\gamma_1 = .6$, $\delta_1 = 2000\text{Å}$, $\gamma_2 = .4$, $\delta_2 = 2000\text{Å}$, $X_3 = 10^{-12}$.

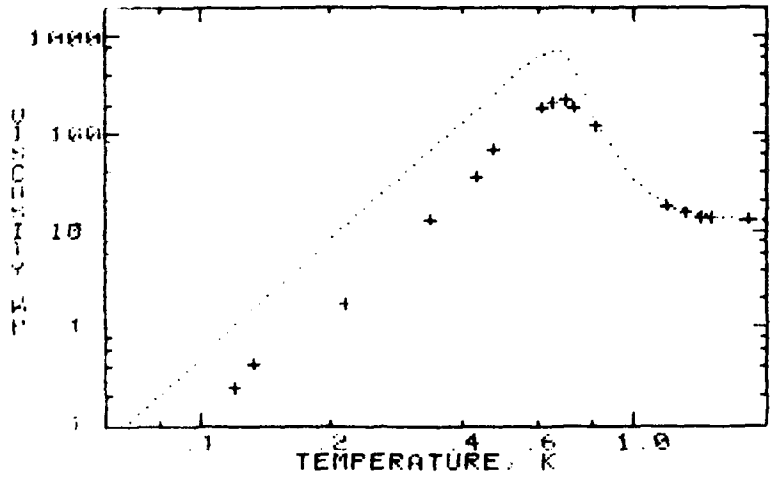

Figure 5-5c. Experimental Series I: Be sleeve, d = .0498 cm, $\gamma_1 = 1$, $\delta_1 = 2000\text{Å}$, $\gamma_2 = 1$, $\delta_2 = 2000\text{Å}$, $X_3 = 10^{-12}$.

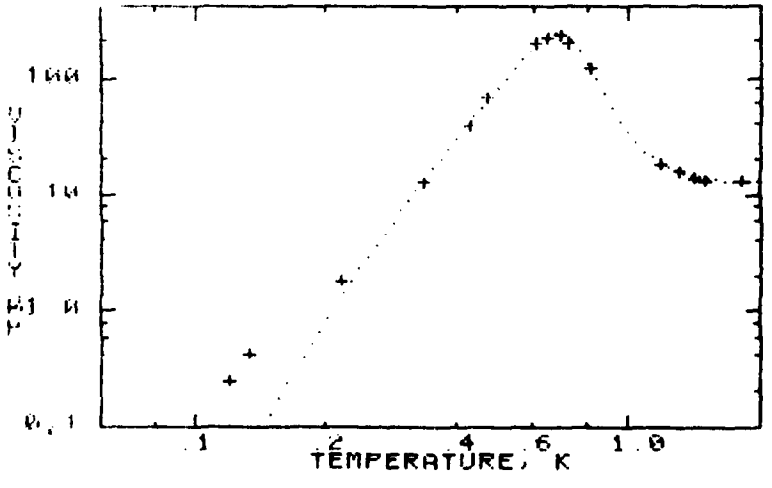

Figure 5-5d. Experimental Series I: Be sleeve, d = .0498 cm, $\gamma_1 = .6$, $\delta_1 = 300\text{Å}$, $\gamma_2 = .4$, $\delta_2 = 150\text{Å}$, $X_3 = 10^{-12}$.

parameters δ_1 and δ_2 determine the rapidity with which the viscosity falls away from the T^4 temperature dependence in the phonon free region. The larger of δ_1 and δ_2 has only a very minor effect. The surface smoothness parameters γ_1 and γ_2 cause a constant, temperature independent shift in the viscosity in the phonon free region, and this shift is approximately proportional to their product (γ_1 γ_2). Consequently if γ_1 is increased while γ_2 is decreased, leaving γ_1 γ_2 unchanged, the viscosity curve is little changed. The value of X_3, the He^3 impurity concentration, determines the values at which the viscosity changes to a $T^{1/2}$ temperature dependence. For larger concentrations where $X_3 > 10^{-7}/d$ (d, the fluid gap in cm), the He^3 impurity atoms enter the viscous flow region and the He^3 component of viscosity η_3 becomes independent of concentration. For $X_3 \gtrsim 10^{-3}$, the He^3 impurity atoms begin to strongly interact which causes the ideal gas equation to become invalid.

The beryllium inner cylinder was machined to an 8μin. finish as measured by a profilometer, which suggests a surface roughness of the order of 300Å. The data points when compared to the theoretical values suggests that δ_2 - 150Å; see Figure 5-5a. That figures also suggests that $X_3 = 3 \times 10^{-8}$ is the impurity concentration of He^3. It is reported (reference 2, Section 3) that He^3 impurity occurs naturally in gaseous He^4 with concentrations of 10^{-6} to 10^{-7}. Thus, a value of $X_3 = 3 \times 10^{-8}$ seems plausible.

The value of $\gamma_1 = .6$ and $\gamma_2 = .4$ suggests an appreciable fraction of supersmooth area on the viscometer surfaces. We have no independent verifications or checks on these values. The suggested value of $\delta_2 = 150$Å. indicates that the outer aluminum sleeve was quite smooth to the phonons.

Figure 5-5b presents the theoretical curve for the same surface smoothness parameters γ_1, γ_2 but with surface roughness parameters $\delta_1 = \delta_2 = 2000$Å which give a T^4 temperature dependence in the lower temperature range presented.

Figure 5-5c presents the theoretical curve for the case where there is no specular reflection, (i.e., $\gamma_1 = \gamma_2 = 1$, $\delta_2 = \delta_2 = 2000\text{Å}$) at the surface walls of the viscometer.

The theoretical curve in Figure 5-5d presents the viscosity for the same surface parameters as in Figure 5-5a but with a He^3 impurity of $X_3 = 10^{-12}$.

We can conclude that the experimental data fits well with the theoretical equation for the selected parameters in Figure 5-5a and these selected parameters indicate a great deal of specular reflection of the phonons.

Presented in Figures 5-6a,b,c, and d are experimental points from the Experimental Series II for the glass inner sleeve with an average fluid gap of 0.125 cm at 4K. The dotted line represents the plot of the theoretical equation for the parameters indicated with the figure. The theoretical equation for the selected parameters give a good fit as seen in Figure 5-6a except for the region near the viscosity peaks. A possible explanation for this discrepancy could be due to the fact that for the glass sleeve the fluid gap was not uniform due to the out of roundness of the glass and due to the fact that it is slightly tapered.

Figure 5-6b presents the theoretical curve for the surface roughness parameter increased to $\delta_1 = \delta_2 = 2000\text{A}$, and a He^3 impurity $X_3 = 10^{-12}$.

Figure 5-6c presents the theoretical curve for the case of no specular reflection where the phonons are diffusely scattered from the viscometer walls. The He^3 impurity atoms at concentrations $X_3 = 4 \times 10^{-7}$ dominates the low temperature viscosity. Figure 5-6d shows theoretically what the viscosity would have been for a concentration of $X_3 = 10^{-12}$.

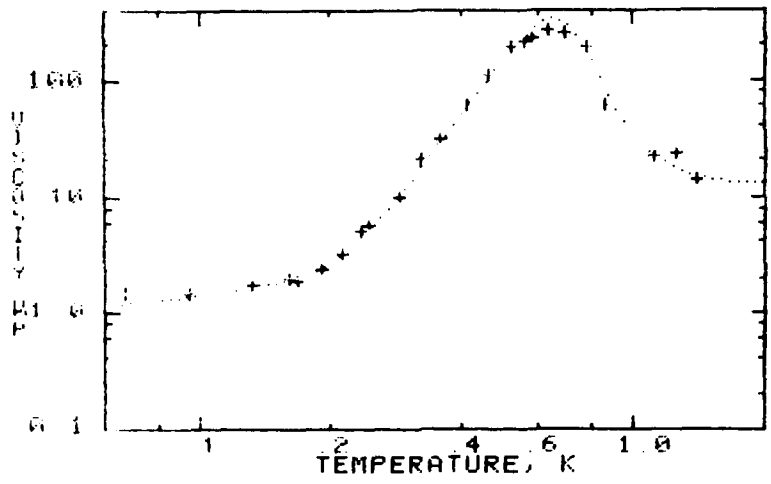

Figure 5-6a. Experimental Series II: Glass sleeve, d = .125 cm
γ_1 = .5, δ_1 = 130A, γ_2 = .4, δ_2 = 100Å, $X_3 = 4 \times 10^{-7}$.

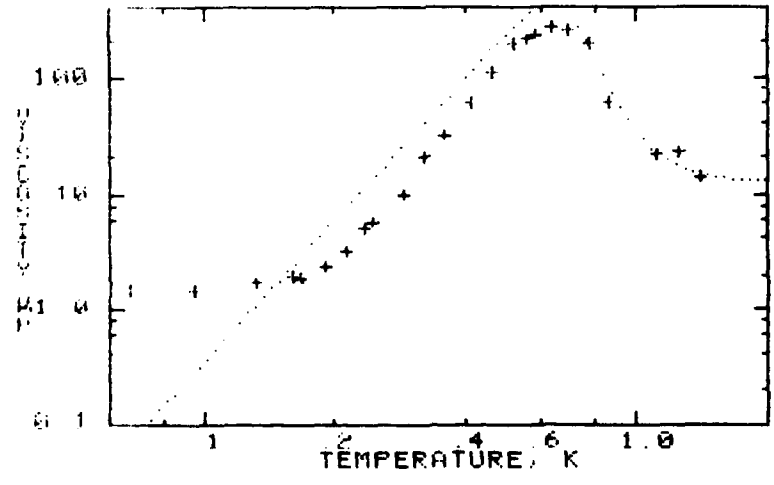

Figure 5-6b. Experimental Series II: Glass sleeve, d = .125 cm
γ_1 = .5, δ_1 = 2000Å, γ_2 = .4, δ_2 = 2000Å, $X_3 = 10^{-12}$.

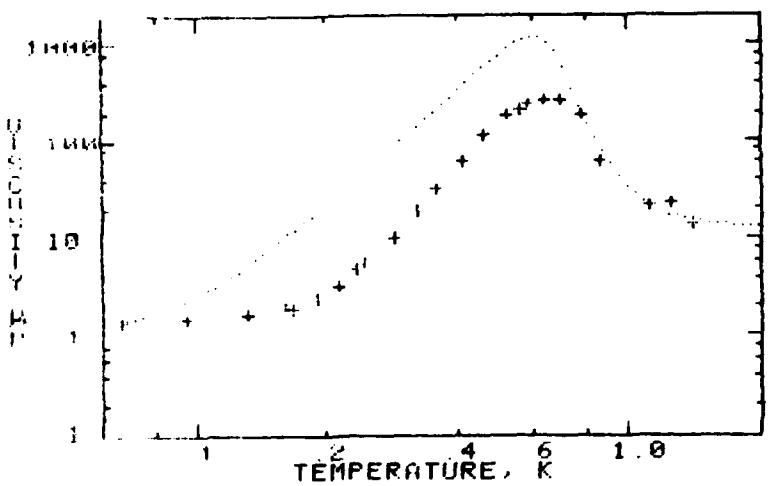

Figure 5-6c. Experimental Series II: Glass sleeve, d = .125 cm
$\gamma_1 = 1$, $\delta_1 = 2000\text{Å}$, $\gamma_2 = 1$, $\delta_2 = 2000\text{Å}$, $X_3 = 4 \times 10^{-7}$.

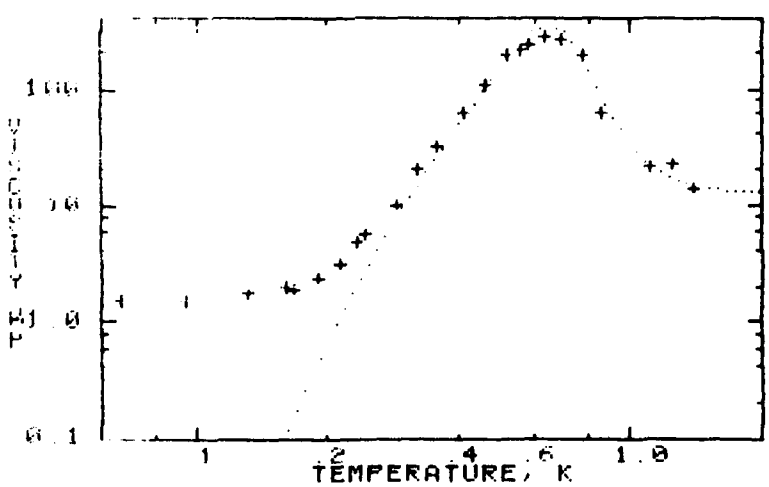

Figure 5-6d. Experimental Series II: Glass sleeve, d = .125 cm
$\gamma_1 = .5$, $\delta_1 = 130\text{Å}$, $\gamma_2 = .4$, $\delta_2 = 100\text{Å}$, $X_3 = 10^{-12}$.

Presented in Figures 5.7a and b, are data points from the Experimental Series III for the same glass inner sleeve as in Series II, but with an average fluid gap of .152 cm at 4K. The dotted line represents the theoretical curve for the parameter listed with the figure.

There is some scatter in the data and the agreement between the experimental data and theoretical curve also shows some discrepancy. The problem with the experimental data, as already discussed, was due to the viscometer. A small beryllium copper screw on the inner viscometer cylinder became magnetic at low temperature.

There is a significant discrepancy between the experimental data and the theory which appears to exist particularly in Experimental Series II and III. Namely, as the viscosity peak is approached from the higher temperature side, the experimental data points tend to fall below the theoretical curve. This is the same region in which Khalatnikov's 4-phonon viscosity equation is applied and it is also the region in which the phonons begin experiencing slip and specular reflection. If one assumes the experimental data to be correct, then either Khalatnikov's 4-phonon equation over estimates the first viscosity in this region, or the present theory has under estimated the magnitude of phonon slip and specular reflection.

If Khalatnikov's 4-phonon viscosity equation of Section 3, Equation (3.142) is adjusted by replacing the constant 3.50×10^{-9} by 4.34×10^{-9} and the constant 2.15×10^{-5} by 5.32×10^{-5}, then this discrepancy for the most part disappears. Also, the discrepancy in Experimental Series II at the viscosity peak is also resolved. Presented in Figures 5.8a, b, and c are the three Experimental Series with the adjusted 4-phonon equation. As can be seen, the fit to the data points is good. However, this does not necessarily prove a problem in Khalatnikov's 4-phonon equation, but it does add emphasis that the 4-phonon equation should be re-examined.

If it turns out that Khalatnikov's 4-phonon viscosity equation is correct, then this discrepancy may suggest some temperature dependence

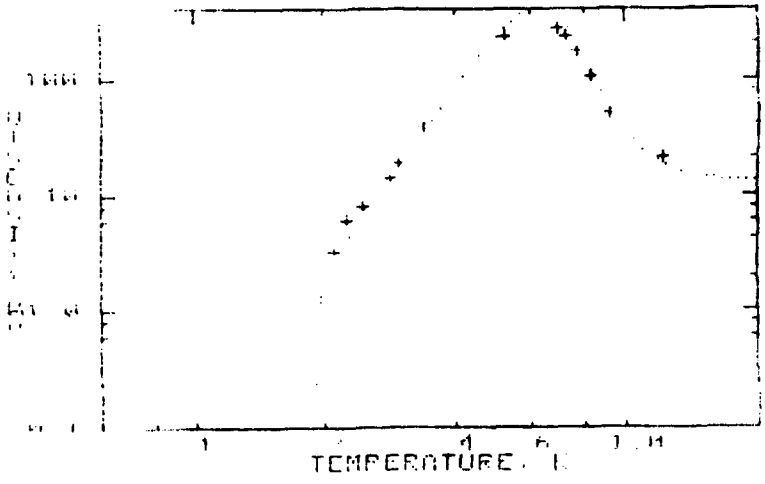

Figure 5-7a. Experimental Series III: Glass sleeve, d = .152 cm
γ_1 = .5, δ_1 = 130Å, γ_2 = .45, δ_2 = 130Å, $X_3 = 10^{-9}$.

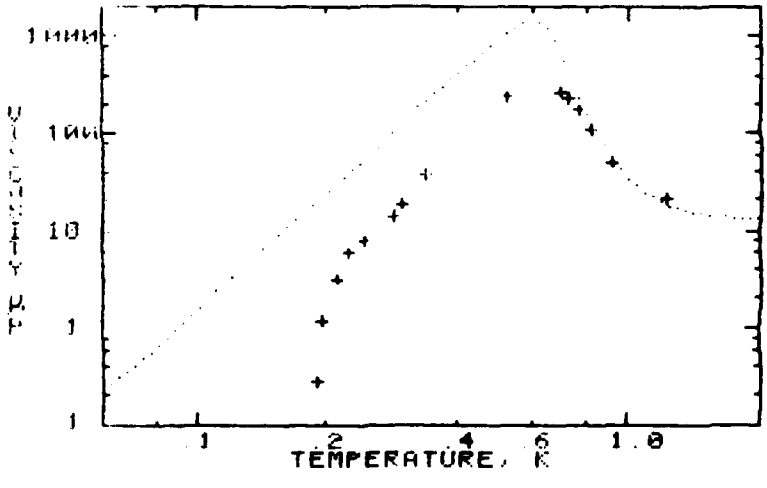

Figure 5-7b. Experimental Series III: Glass sleeve, d = .152 cm
γ_1 = 1, δ_1 = 2000Å, γ_2 = 1, δ_2 = 2000Å, $X_3 = 10^{-9}$.

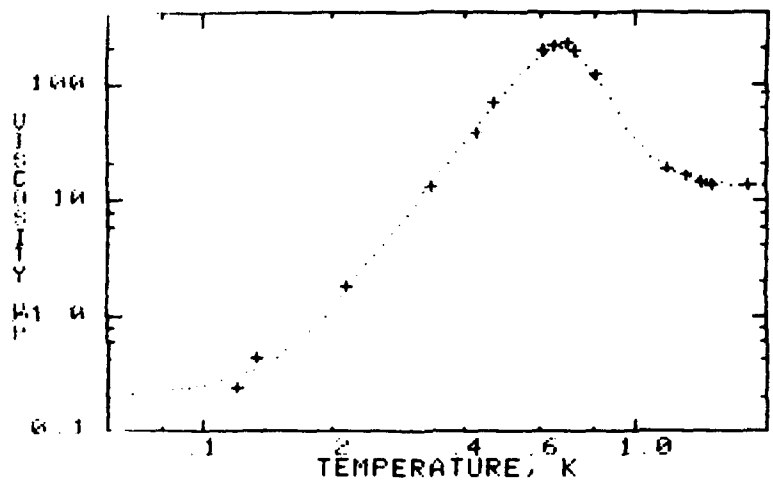

Figure 5-8a. Experimental Series I: Be sleeve, d = .0498 cm γ_1 = .7, δ_1 = 300Å, γ_2 = .4, δ_2 = 140Å, $X_3 = 3 \times 10^{-8}$ with adjusted 4-phonon equation.

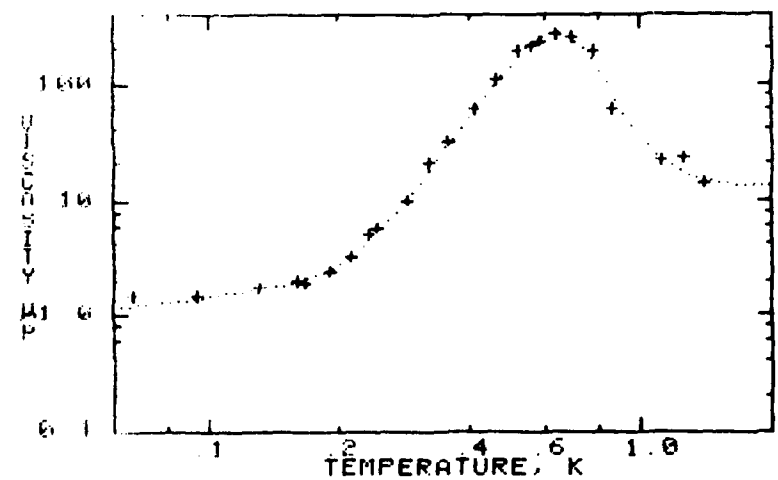

Figure 5-8b. Experimental Series II: Glass sleeve, d = .125 cm γ_1 = .5, δ_1 = 130Å, γ_2 = .4, δ_2 = 100Å, $X_3 = 4 \times 10^{-7}$ with adjusted 4-phonon equation.

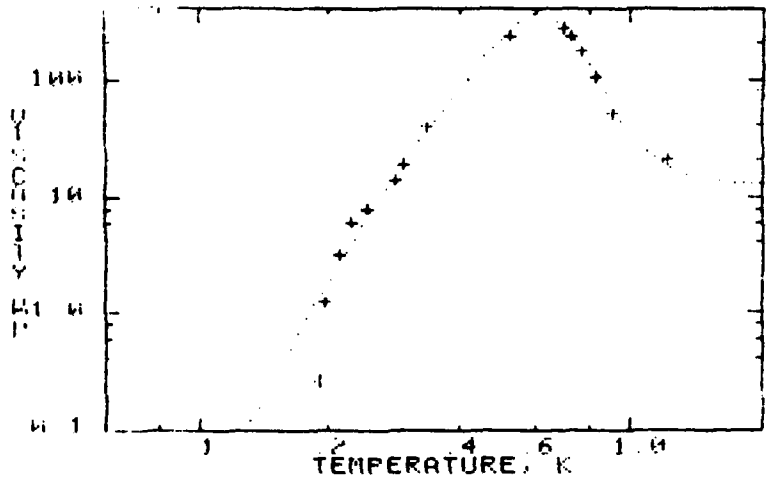

Figure 5-8c. Experimental Series III: Glass sleeve, d = .152 cm γ_1 = .5, δ_1 = 130Å, γ_2 = .45, δ_2 = 130Å, $X_3 = 10^{-9}$ with adjusted 4-phonon equation.

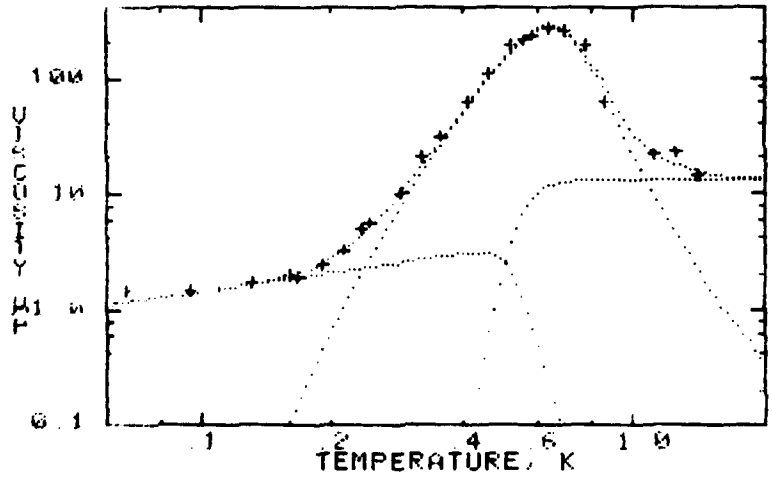

Figure 5-9. Experimental Series II: Glass sleeve, d = .125 cm γ_1 = .5, δ_1 = 130Å, γ_2 = .4, δ_2 = 100Å, $X_3 = 4 \times 10^{-7}$ components of viscosity, phonon, roton, and He^3 impurity.

in the surface smoothness parameter δ_1 or perhaps as we have pointed out it has to do with the large variation in the fluid gap in Series II and III. See also comment in addendum at end of this section.

Presented in Table 5.1 are results on the viscometer inner and outer cylinders (sleeve) and the values of parameters γ_1, δ_1, γ_2, δ_2, and X_3 which bring the theoretical curve and the data points into good agreement. Because the viscosity measurements do not indicate which cylinder is responsible for the viscous drag, then in reality, there are only three experimentally significant parameters: namely, the He^3 impurity concentration X_3, the lesser of the surface roughness factors δ_1 or δ_2, and a parameter approximated by the product of γ_1 and γ_2. Thus, the values of γ_1, δ_1, γ_2 and δ_2 contain some arbitrary choices. In Experimental Series I, δ_1 was selected to approximate the profilometer measurement. δ_2 was then estimated by the rapidity at which the low temperature viscosity data departed from the T^4 temperature dependence. γ_1 and γ_2 were partitioned from the requirement that the product $\gamma_1 \gamma_2 = 0.24$. In Experimental Series II and III the glass cylinder was given the values γ_1 and δ_1 to be consistent with the experimental data and with the fact that the same glass cylinder was used in both experiments. As it turned out δ_2 is the lesser of surface roughness parameters and because the greater of the surface roughness parameters (in this case δ_1) has only minor effects on the theoretical viscosity, the value of δ_1 presented in Table 5.1 is somewhat arbitrary. Even if δ_1 was ten times larger, only minor changes in the theoretical viscosity would occur. To determine the value of δ and γ for a given surface from viscosity measurements both viscometer surfaces should be identical so that $\gamma_1 = \gamma_2$ and $\delta_1 = \delta_2$.

The values of the He^3 concentrations X_3 given in Table 5.1 are plausible when one realizes that the He^4 gaseous sources contain impurity concentrations of 10^{-6} to 10^{-7} of He^3. The helium in the present viscometer instrument package can be expected to be somewhat purified by the liquification process and by filtering of the helium fluid through the superfluid pump before it entered the instrument package.

Table 5-1. Summary of the Surface Parameters of the Viscometer

Exper. Series	Fluid Gap d, cm	Inner Sleeve				Outer Sleeve				X_3
		Mat.	Finish	γ_1	δ_1, Å	Mat	Finish	γ_2	δ_2, Å	
I	.0498	Be	8 in.	.6	~300	Al	8μin.	.4	150	3×10^{-8}
II	.125	Gl	*	.5	~130	Mg	.25μin.†	.4	100	4×10^{-7}
III	.152	Gl	*	.5	~130	Mg	.5μin.†	.45	130	1×10^{-9}

$1\text{Å} = 10^{-8}$ cm, $1\mu\text{in.} = 2.54 \times 10^{-6}$ cm

* as solidified from molden state

† grit size of final polish

Presented in Figure 5.9 is an interesting result showing the theoretical viscosity components (phonon, roton and He^3 atoms) which make up the effective viscosity for Experimental Series II. Presented also are points from the Experimental Series II. For this figure adjustments to the 4-phonon equation of Khalatnikov as described above and as used in Figures 5.8a, b, and c were applied. In the theoretical section, equation (3.38) it was stated that the effective viscosity of liquid He II could be written as the sum of the viscosities due to the excitation components (phonon, roton and He^3 atoms). From Figure 5.9 it is seen that in the region of 1.8K the viscosity is mainly determined by the roton excitations. As the temperature is lowered the roton mean free path increases until the roton interactions are dominated by interactions with the walls which cause the roton component of the viscosity to fall rapidly (due to the rapid decrease in the roton density). In the temperature range between about 1.0K and 0.3K, the phonon excitation dominates the viscosity. Below 0.2K the He^3 impurity atoms dominate the viscosity. As the temperature is increased above 0.5K the roton density becomes large enough to dominate the He^3 interactions, which causes the He^3 component of viscosity to fall rapidly as the temperature increases.

Considering the complex interactions which determine the effective viscosity of liquid helium in the presence of He^3 impurity and under the influence of the surface walls, the present theory shows good agreement with the experimental data and an ability to quantitatively explain this rather complex problem.

5.1.4 The Phonon Mean Free Path

As noted in the theoretical Section 3, the phonon viscosity is related to the mean free path for a "gas like" system by the kinetic theory expression $\eta = \alpha \rho c \ell$. The phonons collide or interact with other phonons (through the 4-phonon process according to Khalatnikov below 0.7K and through the 5-phonon process above 0.7K)*. Using the

*The 4-phonons and 5-phonon equations join more smoothly at 0.8K than at 0.7K. Therefore, in all computations using these equations, a crossover temperature of 0.8K was used.

notation adopted in Section 3, the phonon mean free path $\ell_{ph - ph, r}$ due to collision with other phonons and rotons becomes $\ell_{ph - ph, r} = \eta_{ph - ph, r}/(\alpha_{ph - ph, r} \rho_{ph} c)$. Using this definition of the phonon mean free path and Khalatnikov's equations for the phonon viscosity with Woods and Hollis Hallet's modification to the 5-phonon equation, and $\alpha_{ph - ph, r} = .07$, $\rho_{ph} = 1.78 \times 10^{-5} T^4$ and $c = 2.38 \times 10^4$ cm/sec, resultant values of $\ell_{ph - ph, r}$ are presented in Figure 5.10 as the dotted line.

It is reasonable to assume that the peak in the viscosity data should occur at or very near the point where the mean free path is equal to the average distance traveled by a free phonon from one parallel surface to the other. Using the cosine law one can show that the average distance travelled by a free phonon from one parallel surface to the adjacent surface is twice the gap. The temperature of the viscosity peak was estimated by a straight line extrapolation of the data points on each side of the viscosity peak to the temperature where the lines crossed. A point from each of the three Experimental Series is presented in Figure 5-10. Also plotted are two points taken from thermal conductivity data* handled in the same manner.

The experimental data falls quite close to the theoretical curve, if not slightly above. However, when these data points are corrected for the affect of specular reflection, they fall to the left of the theoretical (dotted) curve having approximately a 20% to 50% smaller mean free path. Perhaps the 4-phonon equation may be over estimating the viscosity or the constant $\alpha_{ph - ph, r}$ in the above equation is not quite correct.

5.2 Velocity Dependent Viscosity

5.2.1 Introduction to Critical Velocities

The hydrodynamic properties of liquid helium are more complex than other fluids because it possesses an additional degree of freedom or mode of motion; namely superfluidity. This pure superfluid flow, however, is observed only for velocities below a certain value called the superfluid

*Fairbank, H.A. and Wilks, J., Proc. R. Soc. A231, 545 (1955).

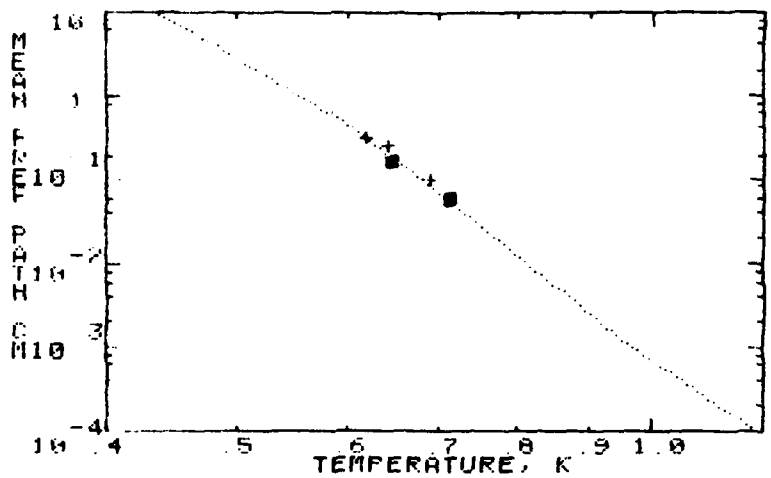

Figure 5-10. Phonon mean free path
+ present results, ■ Fairbank and Wilks.

critical velocity $v_{s,c}$. The superfluid critical velocity is ascribed to the onset of vortex excitations sometimes referred to as superfluid turbulence.

Since Helium II also possesses a normal fluid component, (which gives rise to the viscous properties we have spent so much time discussing), one also expects to observe a critical velocity $v_{n,c}$ associated with the onset of turbulence in the normal fluid. A great deal of experimental work has been done on measuring the critical velocities of liquid helium over the last three decades or so, and there is still some uncertainty and ambiguities in these results. However, those experiments which are done in a way which suppress the normal fluid motion while observing the superfluid motion indicate a geometric dependence generally believed to be approximated by $v_{s,c} d^{1/4} \simeq 1$ where d is the fluid gap or channel width.

The superfluid critical velocity $v_{s,c}$ is believed to be independent of temperature except near the lambda temperature. There exists a body of critical velocity measurements for wider channels $> 10^{-3}$ cm, which allow normal fluid motion and which suggests a geometric dependence given approximately by $v_c\, d \simeq 10^{-2}$. It is currently believed by some researchers[+] that this critical velocity is due to the normal fluid, i.e., $v_{n,c}\, d \simeq 10^{-2}$.

In Figure 5.11 is presented selected experimental results of the critical velocity versus the fluid channel width from 34 different experiments using 11 different methods taken over the last 25 years. These results are also presented in Table 5-1 and 5-2. The results of $v_{s,c}$ were taken from the text book "Helium-3 and Helium-4" by W.E. Keller and the results on $v_{n,c}$ from "Liquid and Solid Helium" by J. Wilks.

Presuming the above interpretation of the critical velocities to be correct, then Figure 5.11 suggests that there are possibly four regions of hydrodynamic flow; Region I, laminar and linear, i.e., no normal fluid or superfluid turbulence; Region II, with normal fluid turbulence

[+] W.M. van Alphen, G.J. van Haasteren, R. De Bruyn Ouboter and K.W. Taconis, Physics Letters, 20, 474 (1966).

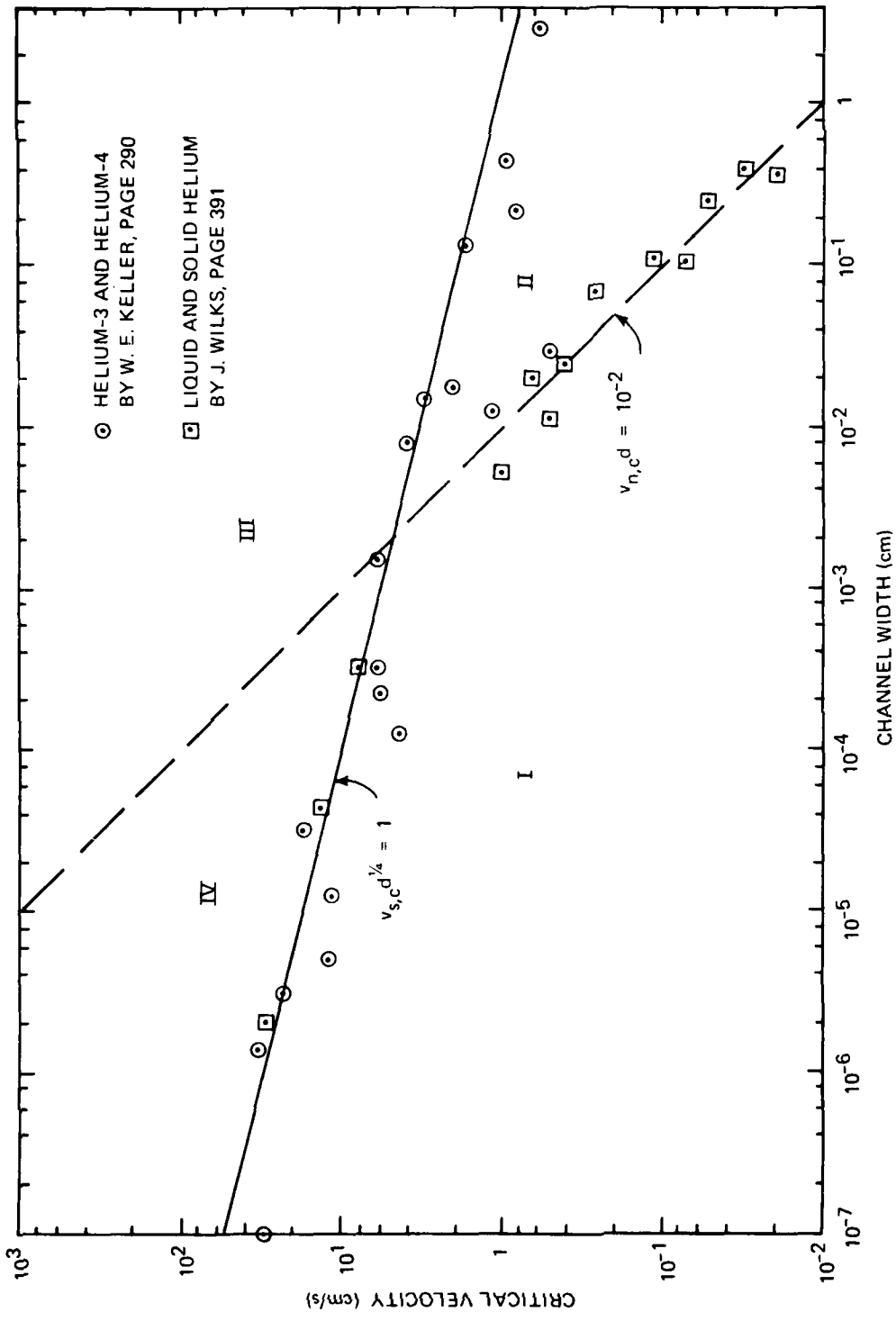

Figure 5-11. Experimental values of critical velocity for liquid He^4 vs. channel width.

Table 5-2 Experimental Values of $v_{s,c}$ vs. d Compared with Calculations Made From the Relation $v_{s,c} d^{1/4} = 1.$ **

Method	Reference	d (cm)	$v_{s,c}$(obs) (cm/sec)	$v_{s,c}$(calc) (cm/sec)
Superfluid wind tunnell	(55)	~3	0.6	0.76
Calorimeter	(39)	0.44	0.95	1.23
Rotating persistent current	(10)	0.22	0.81	1.47
Calorimeter	(39)	0.13	1.7	1.66
Adiabatic flow	(61)	1.74×10^{-2}	2	2.75
Calorimeter	(39)	1.5×10^{-2}	3.0	2.85
Adiabatic flow	(61)	8.2×10^{-3}	4	3.32
Calorimeter	(39)	1.5×10^{-3}	6.0	5.08
Heat flow	(57, 58)	3.4×10^{-4}	3.0	7.35
Isothermal channel flow	(51)	2.3×10^{-4}	5.8	8.13
Isothermal channel flow	(68)	1.2×10^{-4}	4.5	9.55
Isothermal channel flow	(51)	3.1×10^{-5}	18	13.4
Isothermal channel flow	(68)	1.2×10^{-5}	11	17.0
Isothermal channel flow	(68)	5.0×10^{-6}	12	21.2
Saturated film, H = 1 cm	*	3.0×10^{-6}	~25	24
Saturated film, H = 1 cm	(56)	3.0×10^{-6}	25	24
Saturated film, H = 10 cm	(56)	1.4×10^{-6}	35	29
Unsaturated film	(60)	1×10^{-7}	30	56
From the following experiments, $v_{s,c}$ depends upon d^{-1}				
Isothermal channel flow	(63)	0.11	0.10-0.14	1.74
Isothermal channel flow	(64)	2.9×10^{-2}	0.40-0.55	2.42
Isothermal channel flow	(64)	1.2×10^{-2}	1.15	3.02

*Value obtained from many film flow experiments

**From "Helium-3 and Helium-4," by W. E. Keller, p. 290.

From "Helium-3 and Helium-4," page 290, by W. E. Keller

10. P. J. Bendt, Phys. Rev., 127, 1441 (1962).

39. R. DeBruyn Ouboter, K. W. Taconis and W. M. van Alphen, in Progress in Low Temperature Physics (C. J. Gorter, ed), Vol. V, p. 44, Interscience Publishers, Amsterdam, New York (1967). This article contains references to recent Leiden work on superfluid flow.

51. W. E. Keller and E. F. Hammel, Physics, 2, 221 (1966).

55. P. P. Craig and J. R. Pellam, Phys. Rev., 108, 1109 (1957).

56. K. R. Atkins and K. Pickar, in Superfluid Helium (J. F. Allen, ed) p. 271, Academic Press, London (1966): LT-10, Vol. 1, p. 313, Moscow (1967).

57. W. E. Keller and E. F. Hammel, Ann. Phys. (NY), 10, 202 (1960).

58. E. F. Hammell and W. E. Keller, Phys. Rev., 124, 1641 (1961).

59. E. Long and L. Meyer, Phys. Rev., 98, 1616 (1955).

60. K. Fokkens, K. W. Taconis and R. DeBruyn Ouboter, Physica, 32 2129 (1966).

61. W. M. van Alphen, W. Vermeer, K. W. Taconis and R. DeBruyn Ouboter, in Low Temperature Physics LT-9 (J. G. Daunt, D. O. Edwards, F. J. Milford and M. Yaqub, eds), p. 323, Plenum Press, New York (1965).

63. J. N. Kidder and W. M. Fairbank, Phys. Rev., 127, 987 (1962).

64. J. N. Kidder and H. A. Blackstead, in Low Temperature Physics LT-9 (J. G. Daunt, D. O. Edwards, F. J. Milford and M. Yaqub, eds), 1. 331, Plenum Press, New York (1965).

68. J. F. Allen and J. D. Watmough, in Low Temperature Physics LT-9, (J. G. Daunt, D. O. Edwards, F. J. Milford, M. Yaqub, eds) p. 304, Plenum Press, New York (1965).

Table 5-3 Experimental Values of v_c vs d Where Mostly v_c d ~ 10^{-2}. *

"The critical velocity v_c at about 1.4°K, as a function at channel size d"

	Method	Authors	d	v_c
1	Flow	Staas & Taconis (48)	0.26 mm	0.42
2		Kidder & Fairbank (49)	1.1 mm	0.12
3	Heat flow	Winkel, Delsing & Poll (38)	0.43μ	13
4			3.1μ	8
5		Brewer & Edwards (19)	52μ	1.0
6			0.11 mm	0.5
7	Second sound	Vinen (20)	2.4 mm	0.051
8			4.0 mm	0.033
9		Peshkov & Stryukov (40)	3.8 mm	0.02
10	Film flow	See section 14.6	~ 200 Å	30
11	Oscillation expts	See Atkins (32) p. 199	0.21 mm	0.62
12			0.69 mm	0.26
13	Rotation viscometer	Heikkila & Hollis Hallett (30)	1 mm	0.07

19. Brewer, D.F. and Edwards, D.O., Phil. Mag. 6, 775 (1961)

20. Vinen, W.F., Proc. R. Soc. A240, 114 (1957)

30. Heikkila, W.J. and Hollis Hallett, A.C., Can. J. Phys. 33, 420 (1955)

38. Winkel, P., Delsing, A.M.G., and Poll, J.D., Physica 21, 331 (1955)

40. Peshkov, V.P. and Stryukov, V.B., Zh. eksp. teor. Fiz. 41, 1443 (1961)

48. Staas, F.A. and Taconis, K.W., Physica 27, 924 (1961)

49. Kidder, J.N. and Fairbank, W.M., Proc. 7th Int. Conf Low Temp Phys., editors Graham and Hollis Hallett (North Holland, 1961), p. 560

*From "Liquid and Solid Helium," p 391, by J. Wilks.

but no superfluid turbulence; Region III, with both normal and superfluid turbulence; and Region IV, with superfluid turbulence but no normal fluid turbulence.

Figure 5.11 also suggests the difficulties experimenters have had in measuring the superfluid critical velocity $v_{s,c}$ for the wider channels $d \cdot 10^{-3}$ for those experiments in which the normal fluid can move. In this case the experimenter would first observe $v_{n,c}$ as the velocity is increased from zero and that would overshadow $v_{s,c}$ because $v_{s,c}$ occurs at a higher velocity. Likewise, $v_{n,c}$ has not been observed in smaller channels $d < 10^{-3}$ because $v_{s,c}$ overshadows $v_{n,c}$.

5.2.2 Velocity Dependent Viscosity Results

Presented in Figures 5.12 through 5.15 are the velocity dependent viscosity results for the three Experimental Series (Series I, Be sleeve with d = .0498 cm; Series II, glass sleeve with d = .125 cm, and Series III, glass sleeve with d = .152 cm). The effective viscosity measurements were made for each curve by maintaining a constant temperature while the velocity of the outer cylinder was increased above the critical velocity. The results are presented for the various measurements as the effective viscosity versus the outer cylinder velocity for various fixed temperatures and includes all three experimental series.

Within the scatter of the data, the turbulent viscosity results are consistent with a linear velocity dependence as indicated by the straight line drawn through and near the data points. Indicated on each figure is the slope of the straight line given in dimensionless units of $\Delta\eta/\rho d\Delta v$.

In Figure 5.12 are presented results taken in the phonon free region (i.e., the region where the phonon mean free path is free of interactions with other phonons). In Figure 5.13 results taken in the neighborhood of the phonon viscosity peak (transition region) are presented. Figures 5.14 and 5.15 present results taken in the phonon mean

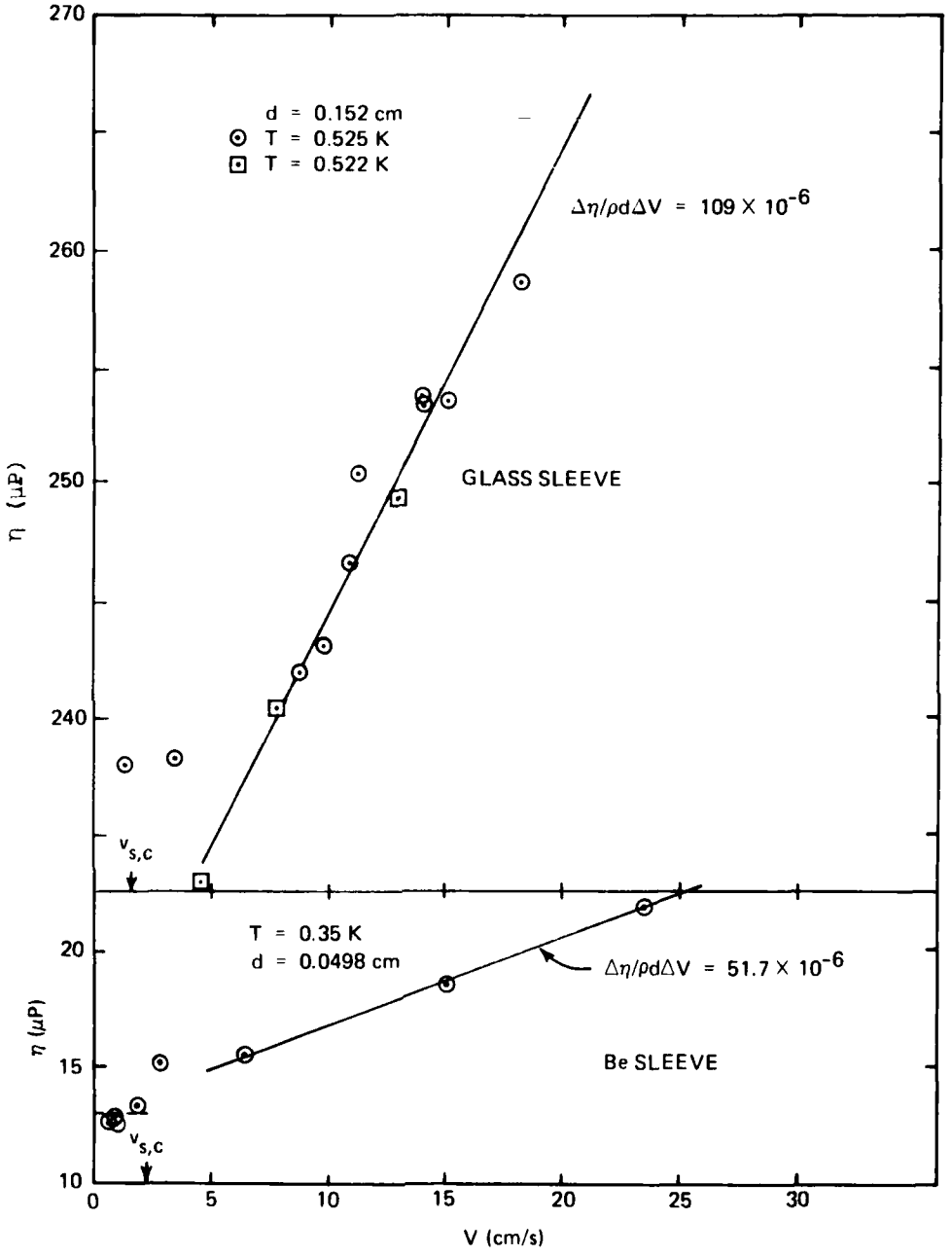

Figure 5-12. Effective viscosity vs. tangential velocity for liquid He^4 in phonon free region.

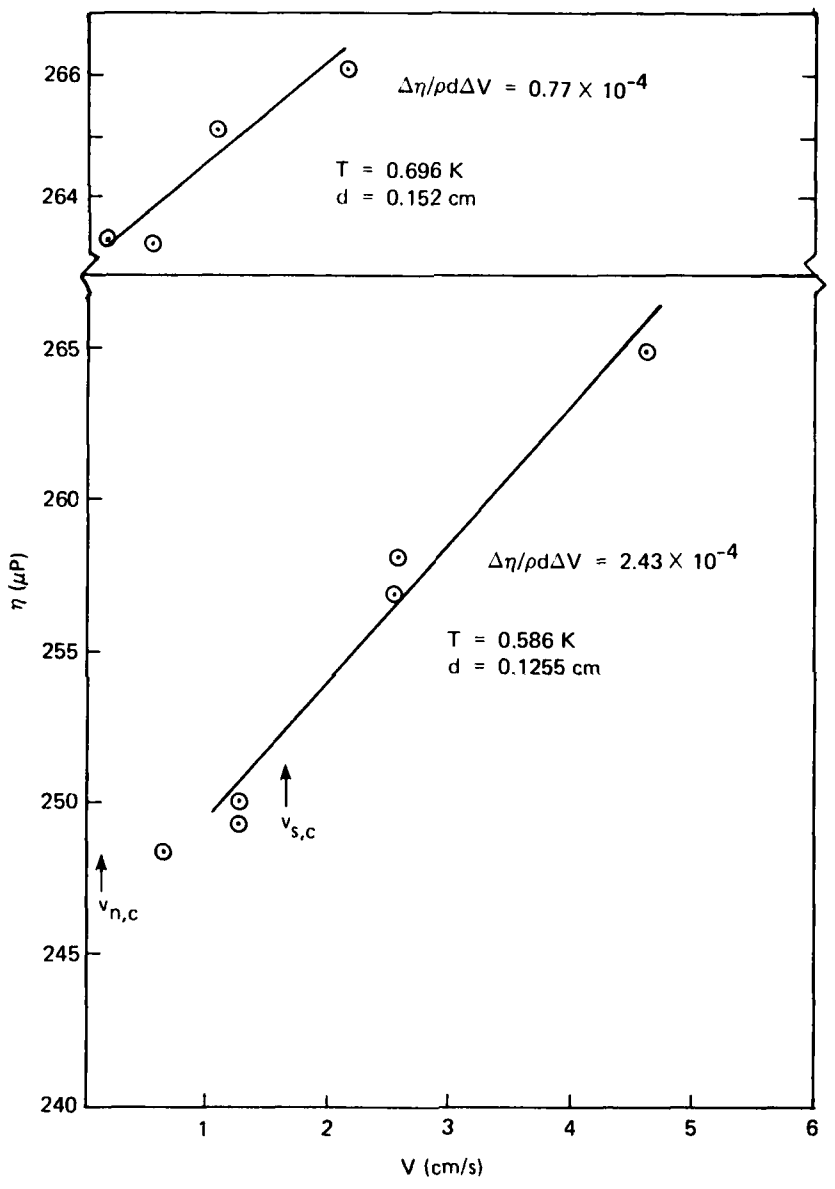

Figure 5-13. Effective viscosity vs. tangential velocity for liquid He^4 near phonon transition region.

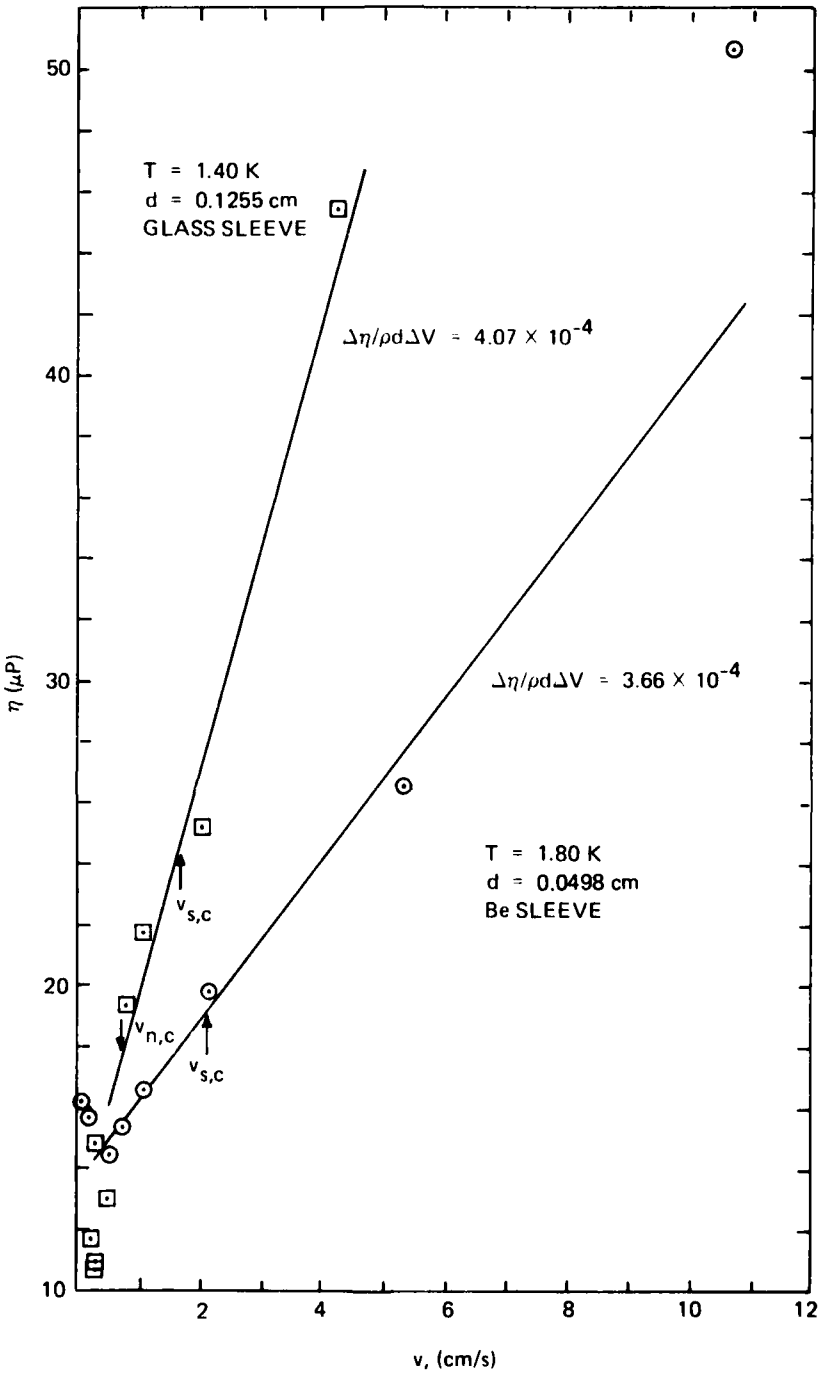

Figure 5-14. Effective viscosity vs. tangential velocity for liquid He^4 in phonon limited region.

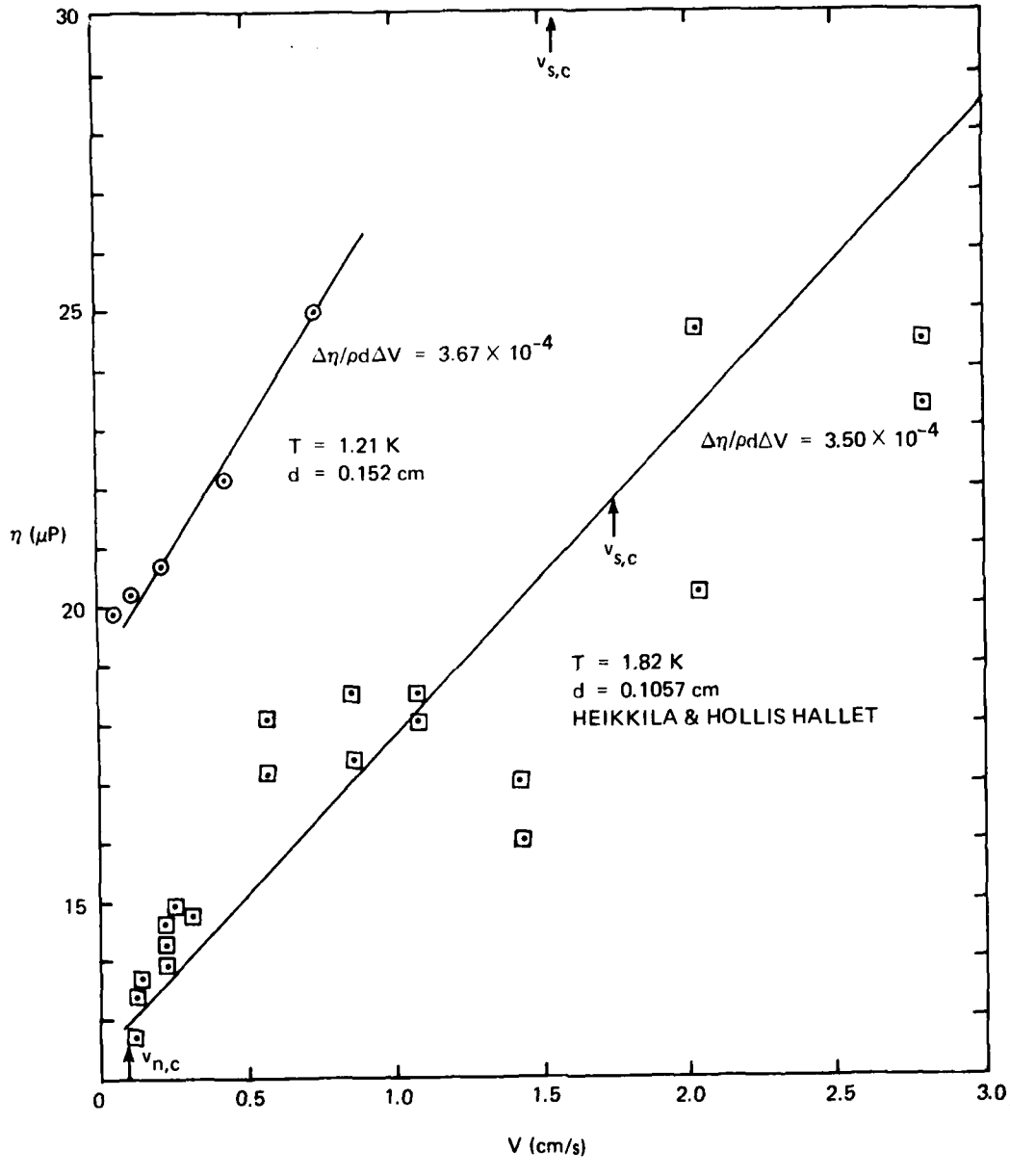

Figure 5-15. Effective viscosity vs. tangential velocity for liquid He^4 in phonon limited region.

free path limited region (i.e., the phonon mean free path is limited by interaction with other phonons). The small vertical arrows labeled $v_{s,c}$ and $v_{n,c}$ indicate the critical velocities for the appropriate fluid gap d taken from the empirical equations $v_{s,c}d^{1/2} \simeq 1$ and $v_{n,c}d \simeq 10^{-2}$ (cgs units) of Figure 5.11.

Presented in Figure 5.16 is a plot of some of the turbulent viscosity results plotted as $\nu - \nu_o$ versus the tangential velocity. For each set of data points ν_o is the velocity independent viscosity value. A set of data was selected from the phonon free region and from the phonon limited region. The small vertical arror labeled $v_{n,c}$ indicated the normal fluid critical velocity calculated from the relation $v_{n,c}d \simeq 10^{-2}$ with d = .125 cm and the arrow labeled $v_{s,c}$ is the superfluid critical velocity computed from the relation $v_{s,c}d^{1/4} = 1$ with d = .152 cm.

5.2.3 Discussion of the Turbulent Viscosity and the Critical Velocities Results

Figure 5.16 in conjunction with Figure 5.11 suggests an important result which has a far reaching implication. At a temperature of 1.40K or 1.21K the data is consistent with a critical velocity $v_{n,c}$ given by the relation $v_{n,c}d \simeq 10^{-2}$. On the other hand, with the same apparatus at a temperature of 0.52K a critical velocity is not observed until a velocity $v_{s,c}$ of nearly 30 times larger is reached where the value of $v_{s,c}$ is consistent with the relation $v_{s,c}d^{1/4} \simeq 1$.

We observe that in the phonon limited region, where the phonon mean free path is much shorter than the fluid gap, the phonon "gas" or normal fluid behaves as a hydrodynamic fluid and thus exhibits turbulence (in this case turbulent viscosity). On the other hand, in the phonon free region where the phonon-to-wall collisions dominate, the phonon "gas" or normal fluid no longer has a statistical density on the scale of the fluid gap great enough for a turbulent structure or excitation to be formed. To make this latter point in a more conceptual manner,

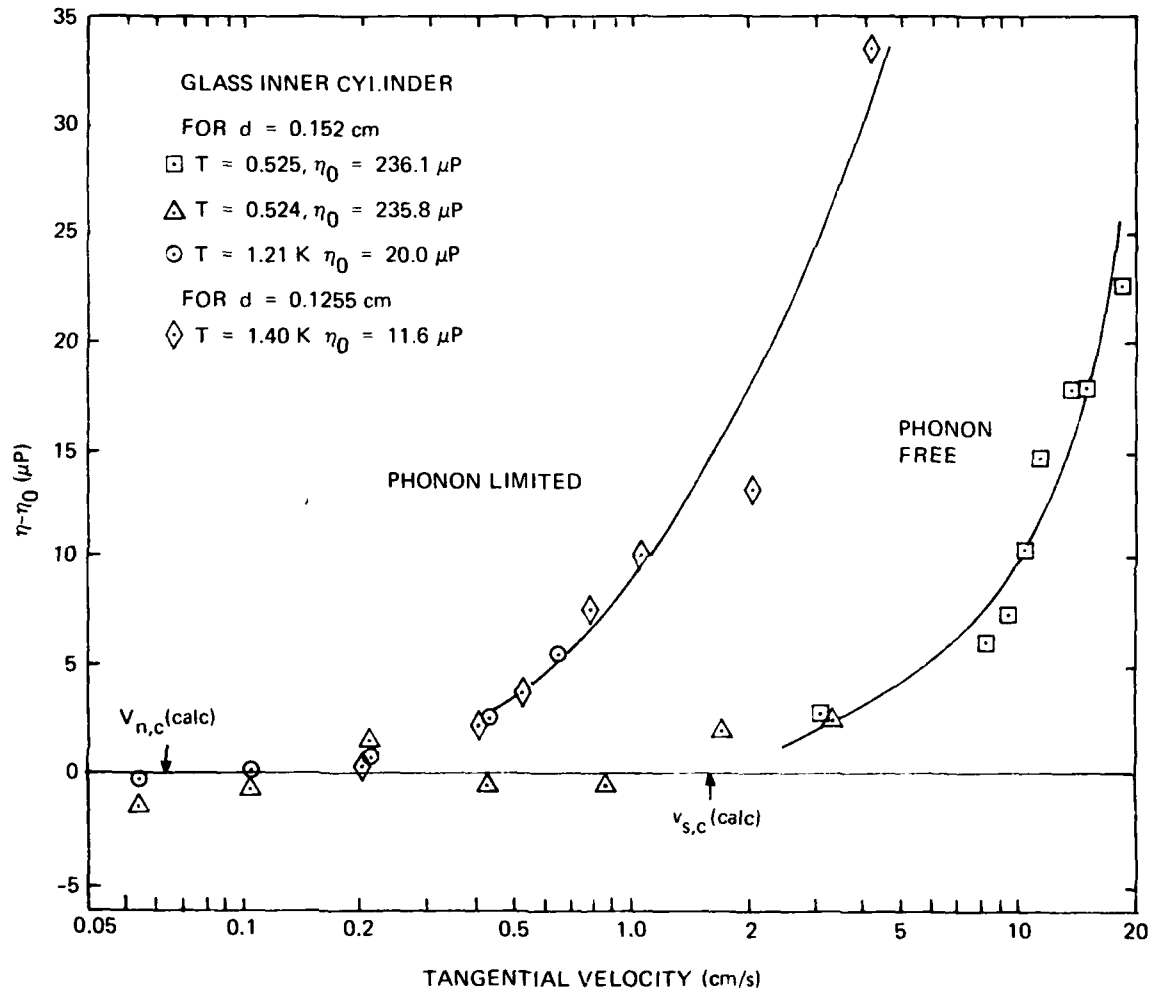

Figure 5-16. Turbulent viscosity vs. tangential velocity.

if the normal fluid turbulence represents a sort of vortex or eddy in the phonon "gas", then the density of the phonon "gas" must be great enough to structurally form an eddy within the confines of the fluid gap; this would require numerous interactions (collisions) between the phonons, which in the phonon free region are just not available. Continuing this gas analogy, clearly, turbulence in a gas vanishes as vacuum conditions are approached.

There are two main conclusions we can then make from the sample data of Figure 5.16. The first is that the data supports and is consistent with the point of view represented in Figure 5.11 and discussed in the introduction 5.5 concerning the geometric dependence of the normal fluid critical velocity ($v_{n,c}d \doteq 10^{-2}$) and the superfluid critical velocity ($v_{s,c}d^{1/4} \doteq 1$). The second point is that the hydrodynamic equations in general are no longer applicable to the normal fluid in the phonon free region where $\ell_{ph} >> d$; and more specifically, in this region normal fluid turbulence is suppressed.

5.2.4 Discussion of the Turbulent Viscosity Results and the Turbulence Number

The motion of a fluid is described by the hydrodynamic equations. The classic hydrodynamic equations describe an ordinary fluid, while liquid He^4 is described by the more complicated two fluid hydrodynamic equations. Little progress has been made in solving the classical hydrodynamic equations for the turbulent region, and consequently, the more complicated two fluid hydrodynamic equations of liquid He^4 will probably be even more intractable. Therefore, let us be modest and take a phenomenological approach which we will supplement with general physical arguments when possible.

Some progress has been made in analyzing the classical fluid behavior through the "Laws of Similarity." The introduction of the dimensionless Reynolds number $R = \rho vd/\eta$ is an example. The terms in the two fluid hydrodynamic equation include: ρ_s the superfluid density, ρ_n,

the normal fluid density, $\rho = \rho_s + \rho_n$ the fluid density, v_s the superfluid velocity, v_n the normal fluid velocity, η the normal fluid viscosity, the thermodynamic quantities like entropy, temperature, etc. and the boundary condition terms like channel width, d, channel length, time etc. If we could solve the two fluid hydrodynamic equations for the turbulent viscosity, it would have to 1) be a function of the hydrodynamic variables and 2) have the dimensions of viscosity:

$$\eta \sim \text{Mass}/(\text{Length} \cdot \text{Time})$$

Now let us summarize the experimental observations. The experimental data for the most part is consistent with the following statements:

a) At low velocities, v_o, of the outer cylinder of the viscometer, the viscosity is independent of velocity. This viscosity was theoretically studied in Section 3; it includes not only the coefficient of first viscosity, but also the phonon free and transition region viscosities described by equation (3.137). This viscosity is denoted by η_o.

b) In the phonon limited region where normal fluid hydrodynamics is applicable, the viscosity increased linearly with the velocity for velocities above the critical velocity $v_{n,c}$ where $v_{n,c}\, d \simeq 10^{-2}$. This increase of viscosity with velocity is interpreted as due to turbulence in the normal fluid. Where the observed viscosity is denoted by η, the part of the viscosity due to turbulence in the normal fluid is denoted by $\eta_{n,t}$ where $\eta_{n,t} = \eta - \eta_o$. For $v_o < v_{n,c}$, $\eta_{n,t} = 0$ and for $v_o > v_{n,c}$, $\eta_{n,t}$ is linear in v_o.

c) In the phonon free region where the usual normal fluid hydrodynamics is no longer applicable, the viscosity increases linearly with velocity for velocities above the

critical velocity $v_{s,c}$ where $v_{s,c} d^{1/4} \simeq 1$. The increase of viscosity with velocity is interpreted as due to turbulence in the superfluid. The part of the viscosity due to turbulence in the superfluid is denoted by $\eta_{s,t}$ where $\eta_{s,t} = \eta - \eta_o$. For $v_o < v_{s,c}$, $\eta_{s,t} = 0$ and for $v_o > v_{s,c}$, η_{st} is linear in v_o.

We would now like to use these statements and the requirement of a law of similarity to write an expression for $\eta_{n,t}$ and $\eta_{s,t}$ which is consistent with the experimental data. Specifically, we seek an expression for $\eta_{n,t}$ and $\eta_{s,t}$ from among the variables which could make up a solution of the two fluid hydrodynamic equations, which has the dimensions of viscosity and which is consistent with the known information and present experimental data on the turbulent viscosity.

Let us consider the normal fluid viscosity with turbulence represented by the phonon limited viscosity measurements presented in Figures 5-14 and 5-15, and the observation that $\eta = \eta_o$ when $v_o < v_{n,c}$. A plot of the experimental data as $\eta - \eta_o$ vs $(v_o - v_{n,c})$ should then make each of the experimental data curves pass through the origin. Since $v_{n,c}$ is a function of the fluid gap d, i.e., $v_{n,c} d \simeq 10^{-2}$ we may attempt to eliminate the d dependence in the expression by plotting $\eta - \eta_o$ vs $(v_o - v_{n,c})d$. Furthermore, in order to give the expression $(v_o - v_{n,c})d$ the dimensions of viscosity we multiply it by a density ρ_i to get the form

$$\eta - \eta_o = \alpha_n \rho_i (v_o - v_{n,c}) d \qquad (5.1)$$

where α_n is a dimensionless proportionality parameter. Assuming for the moment that this trial equation has the proper form, the question is, which density is appropriate ρ_n, ρ_s or $\rho = \rho_n + \rho_s$, or perhaps some combination. If the turbulence exists only in the normal fluid, then it would be plausible that the density ρ_i is the normal fluid density ρ_n.

If the turbulence in the normal fluid causes the superfluidity to break down and thus turbulence to develop throughout the entire fluid, it would be plausible that the appropriate density ρ_i would be the total density $\rho = \rho_n + \rho_s$.

In the present experiments where $d > 2 \times 10^{-3}$ cm we see from Figure 5-11 that $v_{n,c} < v_{s,c}$ so that a third possibility is that for velocities v_o between $v_{n,c}$ and $v_{s,c}$ only the normal fluid ρ_n participates in the turbulence and that above $v_{s,c}$ the superfluid then develops (perhaps independently) its own turbulence within the superfluid density ρ_s. In this latter case the turbulence viscosity for velocities $v > v_{s,c}$ would be a superposition of turbulent viscosity due to the normal fluid and the superfluid. We will come back to this possibility later but let us at this time see if the experimental data is consistent with the simpler point of view that $\rho_i = \rho$. Equation (5.1) then becomes

$$\eta_{n,t} = \eta - \eta_o = \alpha_n \rho (v_o - v_{n,c}) d \tag{5.2}$$

If this equation represents the experimental data in a proper similarity law, then α_n must be a dimensionless constant, independent of temperature, viscometer dimensions, etc. Taking the derivation of the above equation with respect to velocity v then,

$$\frac{d\eta_{nt}}{dv} = \frac{d\eta}{dv} = \alpha_n \rho d \tag{5.3}$$

so that the assumed dimensionless constant, α_n which we call the normal fluid viscosity turbulence number becomes

$$\alpha_n = \Delta\eta/(\rho d \Delta v) \tag{5.4}$$

Presented in Figure 5-17 is a plot of α_n versus temperature for the present experimental data and one point from Heikkila and Hollis Hallet as taken from Figures 5-13, 5-14, and 5-15.

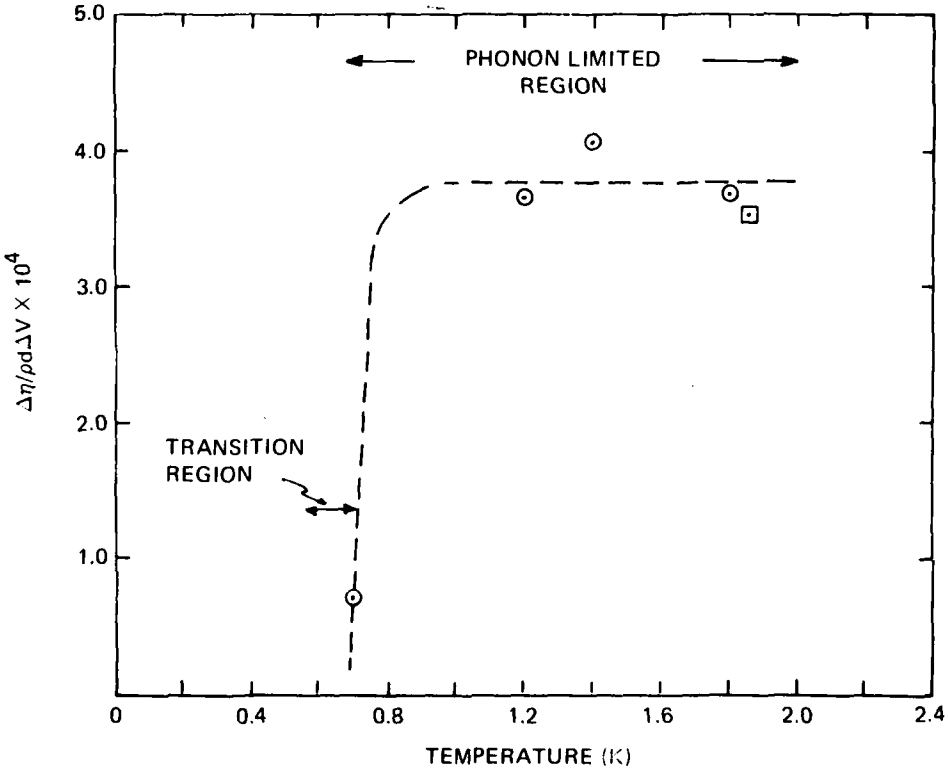

Figure 5-17. Normal fluid viscosity turbulence number vs. temperature. ⊙ Present results. ⊡ Heikkila and Hollis Hallet.

The value of lowest temperature point at T = .696K is somewhat below the value of the other high temperature points. This lowest temperature point occurs at the same temperature as the viscosity peak in η_o (see Figure 5-1). The point is, thus, in the transition region where where the phonon to wall collisions are dominating the collisions to such a point that the ability to maintain normal fluid turbulence is rapidly being lost. Therefore, we expect the turbulent viscosity to be suppressed and α_n to decrease and go to zero.

The average of the points in Figure 5-17 which are well within the phonon limited region is $\alpha_n = 3.73 \times 10^{-4}$ and it has a percentage standard derivation of ±6%. The experimental results are thus consistent with α_n being independent of temperature and fluid gap and thus suggest that α_n may indeed be a dimensionless constant.

The effective viscosity of liquid Helium II in the phonon limited region can then be written using Equation (5.2) with the above experimental value for α_n.

$$\eta = \eta_o + 3.73 \times 10^{-4} \rho d(v_o - v_{n,c}) \Delta_v, \text{ poise} \qquad (5.5)$$

where:

$$\Delta_v = \begin{cases} 0 \text{ for } v_o < v_{n,c} \\ 1 \text{ for } v_o > v_{n,c} \end{cases}$$

$$v_{n,c} d \doteq 10^{-2} \text{ (cgs)}$$

and $$\eta_o = \eta_{ph} + \eta_r$$

where η_{ph} is the phonon viscosity given by the theoretical equation (3.49) and (3.50) and η_r, the roton viscosity, equation (3.55), is $\eta_r = 12.5 \times 10^{-6}$ poise. Equation (5.5) for the effective viscosity is in agreement with the present experimental data to within about 5%.

The normal fluid turbulence viscosity number α_n in equation (5.4) was found to be a constant when the total fluid density was used for the density. This fact suggests that the normal fluid turbulence does indeed break down the pure superfluidity of the superfluid component and that turbulence develops in both the superfluid and normal fluid. The fact that α_n in Figure 5-15 for $v_o < v_{s,c}$ is approximately the same as α_n in Figure 5-14 for $v_o > v_{s,c}$ also supports this conclusion.

Let us now consider the effective viscosity in the presence of superfluid turbulence as presented in Figure 5-12. Recalling statements a) and c) above and using a similar approach as was used for the normal fluid, a plot of $\eta - \eta_o$ versus $(v_o - v_{s,c})$ should make each of the experimental curves pass through the origin. Since $v_{s,c}$ is a function of d, i.e., $v_{s,c} d^{1/4} \doteq 1$ then we may attempt to eliminate the $d^{1/4}$ dependence without changing the coincidence of curves at the origin by plotting the data as $\eta - \eta_o$ versus $(v_o - v_{s,c})d^{1/4}$.

In order to make $\eta_{s,t} = \eta - \eta_o$ into a properly dimensioned expression we write a trial function for the component of superfluid turbulence as,

$$\eta_{s,t} = \eta - \eta_o = \alpha_s L^{3/4} \rho_i (v_o - v_{s,c}) d^{1/4} \tag{5.6}$$

where ρ_i is a fluid density ρ_n, ρ_s or ρ and $L^{3/4}$ is an undefined length parameter to give the expression for η_{st} the correct dimensions. Taking the derivative of η_{st} with respect to v,

$$\frac{d\eta_{s,t}}{dv} = \frac{d\eta}{dv} = \alpha_s L^{3/4} \rho_i d^{1/4} \tag{5.7}$$

Solving for α_s we get:

$$\alpha_s = \frac{1}{L^{3/4} \rho_i d^{1/4}} \frac{\Delta n}{\Delta v} \tag{5.8}$$

If α_n is a constant independent of the parameters of the viscometer and the variables of the helium then a similarity law for superfluid turbulence will have been found and equation (5.6) will represent the effective viscosity component.

In order to establish α_s as a dimensionless constant and equation (5.6) as a similarity law for the superfluid turbulent viscosity, we must be able to identify the length term L and the density term ρ_i, and show that α_s is independent of the parameters of the viscometer and the variables of the helium. The unknown length parameter L entered equation (5.6) due to the form of the empirical equation for the superfluid critical velocity, $v_{s,c}\, d^{1/4} \cdot 1$. This critical velocity equation has withstood, so far, all efforts by theoreticians to understand it; so its form may only be approximate which in turn means that the $L^{3/4}$ term may be approximate.

Using the data presented in Figures 5-12 and 5-13 to develop Table 5.3 we see that the form for the superfluid turbulence number α_s which is nearly constant with respect to the different temperatures and fluid gaps is equation (5.8) with $\rho_i = \rho_{ph}$. The experimental data suggests that L is a near constant with respect to changes in temperature and fluid gap. Other than that the data offers no clues as to the meaning of L. The circumference of the viscometer used in the three experimental series was nearly the same, so that if L was a term like the circumference of the fluid gap, then one would not expect a difference. Any difference would have to be tested on a different size viscometer. On the other hand if L was an internal structure term of the turbulent excitation like the core radius of the vortex one would not expect L to vary.

Assuming the partially verified equation (5.6) with the empirical value of $\alpha_s\, L^{3/4} = 3.1$, then the effective viscosity in the phonon free region ($l_{ph} \gg d$) for the present viscometer can be represented by the relation $\eta = \eta_o + \eta_{s,t}$. After substitution,

$$\eta = 1/4\ \gamma_1\gamma_2(\gamma_1 + \gamma_2 - \gamma_1\gamma_2)^{-1}\ f(\delta)\rho_{ph}\ cd$$
$$+ 3.1\ \rho_{ph}(v_o - v_{s,c})\ d^{1/4}\ \Lambda_v \qquad (5.9)$$

Table 5-3. Experimental value of the superfluid turbulent number.

Exp. Series	d cm	Temp. K	$\Delta\eta/\Delta v_o$	$\Delta\eta/(\rho d\Delta v_o)$	$\Delta\eta/(\rho d^{1/4}\Delta v_o)$	$\Delta\eta/(\rho_{ph} d\Delta v_o)$	$\Delta\eta/(\rho_{ph} d^{1/4}\Delta v_o)$
I	0.0498	0.35	0.373×10^{-6}	0.571×10^{-4}	0.544×10^{-5}	28.1	2.96
II	0.152	0.522	2.41×10^{-6}	1.09×10^{-4}	2.63×10^{-5}	12.0	2.91
III	0.125	0.586	4.40×10^{-6}	2.43×10^{-4}	5.12×10^{-5}	16.8	3.53
Average			2.39	1.34×10^{-4}	2.76×10^{-5}	19.0	3.13
RMS Deviation			2.01	0.982×10^{-4}	22.9	8.26	0.34
% Deviation			84%	73%	83%	43%	11%

$\rho_{ph} \simeq 1.78 \times 10^{-5} T^4$ gm/cm^3

$\rho \simeq 0.145$ gm/cm^3

where

$$\Delta_v = \begin{cases} 0, \text{ for } v_o < v_{s,c} \\ 1, \text{ for } v_o > v_{s,c} \end{cases}$$

where η_o is the velocity independent viscosity for $l_{ph} >> d$ given be equation (3.36).

There was no experimental evidence that specular reflection of the phonons had an affect on the superfluid turbulence. The fact that $\eta_{s,t}$ is proportional to ρ_{ph} is very interesting and could have theoretical significance in that it may point the way for the development of a theoretical model for superfluid turbulence.

Equation (5.9) represents the lowest temperature form (the phonon free) of the effective viscosity. As discussed in Section 5.1.3 there was some discrepancy between the theoretical η_o values and the experimental values in the neighborhood of the viscosity peak, the theoretical value of η_o is nearly 40% larger then the experimental value of η_o in the neighborhood of the viscosity peak for Experimental Series II and III. Therefore equation (5.9) somewhat overestimates the viscosity η for the Glass Sleeve Curve of Figure 5-12. For the Be Sleeve Curve of Figure 5-12, Equation (5.9) gives values about 10% too large. Nonetheless, Equation (5.9) should be useful in extrapolating the effective viscosity of pure He^4 outside the experimental range of temperature and velocity.

5.2.5 Discussion of Turbulent Viscosity Associated with the He^3 Impurity Atoms

There is to be expected yet a third critical velocity and viscosity turbulence; namely, that associated with the He^3 impurity atoms. No attempt was made to examine the viscosity turbulence associated with the He^3 impurity, but it should exist for concentrations for which the He^3 mean free path is much less than the fluid gap ($X_3 > 10^{-6}$ in the present viscometer) and be most evident in the phonon free region where $\eta_3' >> \eta_{ph}$. In the region where the He^3 impurity behaves as an ideal gas

($X_3 < 10^{-3}$ and $T > T_F$), the He^3 impurity viscosity turbulence should behave as in a classical fluid, similar to the normal fluid turbulence and we would then expect $\eta_3' = \eta_{0,3} + \eta_{3,t}$ or:

$$\eta_3' = \eta_{0,3} + \alpha_3 \rho_3 d(v_o - v_{0,3}) \Delta_v \qquad (5.10)$$

where $v_{3,c}$ is the critical velocity associated with the onset of turbulence. $\eta_{0,3}$, the velocity independent viscosity, given by the theoretical equation (3.148), ρ_3 the He^3 impurity atom density and α_3 a constant.

As in the case for the normal fluid, we also expect the He^3 impurity turbulence to vanish at lower concentrations where its mean free path is much greater than the fluid gap ($X_3 << 10^{-6}$ for the present viscometer).

We would anticipate that a complete expression for the effective viscosity of liquid He^4 with minute He^3 impurity would be approximated by the equation,

$$\eta = \eta_{0,4} + \eta_{i,t} + \eta_{0,3} + \eta_{3,t} \qquad (5.11)$$

where i = n for $l_{ph} << d$ or i = s for $l_{ph} >> d$ and $\eta_{0,4}$ is the velocity independent viscosity of pure He^4. $\eta_{0,4} + \eta_{0,3} = \eta_{ph} + \eta_r + \eta_3$ and is given by the theoretical equation (3.137).

5.3 Miscellaneous Observations

In taking a viscosity measurement, the outer cylinder was brought to operating speed in a few seconds, and the inner cylinder had a period of oscillation of a minute or less. In the phonon free region, however, it seemed to take quite a number of minutes for the full steady state drag value of the helium to be realized. From the point of view of the phonon behavior this seems rather strange because the phonons in the phonon free region travel without collisions with other phonons from surface wall to surface wall at the speed of sound $c \doteq 2.38 \times 10^4$ cm/sec which one would

think would give a very short drag time response. Furthermore, after steady state was obtained and then the outer cylinder stopped, there appeared to be some lag in the decay of the viscous drag. These observations are only tentative and need more careful observation, but it would appear that the momentum carried by the superfluid may be playing a role in the drag time response through a weak link between the phonons and the superfluid.

On the question of observation of hysteresis effects in the turbulent viscosity measurements, there were no gross effects observed. However, due to experimental scatter, it would be difficult to rule out possible small hysteresis effects. There were isolated cases in which it appeared there might be some hysteresis effects between increasing and decreasing velocities, but it was not regular and so was attributed to noise, possible temperature drifts and other instrumentation problems.

No real effort, however, was spent to look for possible hysteresis effects. Furthermore, in order to observe a convincing hysteresis effect in the present apparatus with the present procedure would require this effect to be fairly stable and to endure several tens of minutes.

ADDENDUM TO SECTION 5.1.3

A critical factor in determining the exact position and magnitude of the theoretical viscosity peak in the transition region is the equation for $a = d/l_{ph\text{-}ph,\ r}$. $l_{ph\text{-}ph,\ r}$ was computed from the relation (equation 3.143 and 3.144): $\eta_{ph\text{-}ph,\ r} = \alpha_{ph}\rho_{ph}\ c\ \ell_{ph\text{-}ph,\ r}$. The value of $\alpha_{ph} = .07$ was taken from Atkins (reference 2, section 3) and was admittedly approximate. A source of the discrepancy between the theory and the experimental data in the transition region might also be due to possible error in this term.

In section 3.3.1 it was brought out in the development of the equation for $\eta_{ph\text{-}3}$, equation 3.52, that Zharkov's corresponding equation had a much stronger temperature dependence below 0.8K than equation 3.52. The present experimental results can be shown to clearly show that equation 3.52 is consistent with the present experimental results while Zharkov's corresponding expression for $\eta_{ph\text{-}3}$ causes the phonon effective viscosity to fall much too rapidly with temperature.

SECTION 6

A PROPOSED APPLICATION OF THE NEUTRALLY BUOYANT SPHERICAL ROTOR IN AN EXPERIMENTAL TEST OF THE PRINCIPLE OF EQUIVALENCE

The Eötvös beam experiment by Roll, Krotkov and Dicke[1] to test the principle of equivalence is probably one of the most precise laboratory measurements ever made of an inertial property. This carefully planned and executed experiment brings out many of the severe problems one must address when designing an ultraprecision inertial type instrument to operate at room temperature. It is quite instructive to study this experiment for those problems and to see how those problems may be mitigated by simple geometry and the use of cryogenics.

6.1 Introduction and Background

Einstein's principle of equivalence forms one of the basic postulates of General Relativity. This principle of equivalence is a very general principle which applies to all the laws of nature and, therefore, is commonly called the "strong" principle.

A more restricted and less general form of the principle of equivalence is the equivalence of inertial and gravitational mass, which is called the "weak" principle of equivalence. The weak equivalence principle requires that the acceleration of an object in a gravitational field not depend upon the kind of substance of the object (i.e. gold, lead, iron, etc.) but only upon its mass. For example, if some object of substance A is placed in a gravitational field, it will experience a force, F, given by Newton's gravitation law:

$$F = \frac{GM'}{r^2} M_A = g M_A \tag{6.1}$$

M´ is called the active gravitational mass because it "creates" so to speak, a gravitational field at the position of the mass, M_A. M_A is called the passive gravitational mass because one thinks of it as being acted upon by the field. This object (A) of passive gravitational mass, M_A, would experience an acceleration, a, as given by Newton's second law of motion:

$$F = m_A a \tag{6.2}$$

where m_A is the inertial mass of this object of substance A. When the force causing the acceleration, a, is the gravitational force, we may equate equations (6.1) and (6.2)

$$a = g \frac{M_A}{m_A} . \tag{6.3}$$

If $M_A/m_A - M_B/m_B = 0$ for any two (and all) substances A and B, we would then know the acceleration is independent of the substance and that the inertial mass and the passive gravitational mass are equivalent.

Very precise measurement of this ratio was made by Roll, Krotkov and Dicke[1] in 1964 and they found this ratio with 95% confidence to be less than 3×10^{-11} for gold and aluminum. It is customary to define the ratio η (A,B) as

$$\eta\ (A,B) = \frac{M_A/m_A - M_B/m_B}{1/2\{M_A/m_A + M_B/m_B\}} \tag{6.4}$$

for small values of η (A,B) this parameter reduces in first order to

$$\eta\ (A,B) \simeq M_A/m_A - M_B/m_B \simeq m_A/M_A - m_B/M_B \tag{6.5}$$

The question is whether or not the value of 3×10^{-11} is small enough to satisfy the equivalence principle. To answer this question, one must look at the makeup of matter. Matter is made up of the elementary particles (electrons, protons, neutrons) and because of the mass-energy equivalence ($E=Mc^2$) one must include the binding and interaction energy of the elementary particles.

The energy-mass Mc^2 of an atom is the sum of its constituents given as[2]

$$Mc = Z M_p c^2 + N M_n c^2 + Z M_e c^2 - B_e - B_s(A,A) - B_{er} - B_w - B_g \tag{6.6}$$

where Z = atomic number, M_p = proton mass, M_n = neutron mass. M_e = electron mass, N = neutron number, B_e = electronic binding energy. $B_s(Z,A)$ = strong-interaction binding-energy of the nucleus, B_{er} = electromagnetic repulsion energy of the protons, B_w = weak-interaction part of the binding energy, $B_w \simeq 2 \times 10^{-7}\ B(Z,A)$ and B_g = gravitational part of the binding energy.

In Table 6-1 is presented the mass-energy constituents for aluminum and gold. If we assume M in this table to be the passive gravitation mass, and if we assume that all the mass-energy constituents except the weak interaction contribute to the inertial mass, then $m = M + B_w/c^2$

$$\text{or} \qquad \frac{m}{M} = 1 + \frac{B_w/c^2}{M} \tag{6.7}$$

The parameter η (A,B) then becomes

$$\eta\ (A,B) = \left(\frac{m}{M}\right)_A - \left(\frac{m}{M}\right)_B = \left(\frac{B_w/c^2}{M}\right)_A - \left(\frac{B_w/c^2}{M}\right)_B \tag{6.8}$$

From the table we see that $|\eta\ (Al,Au)| \simeq 9 \times 10^{-11}$ if the weak interaction mass-energy contributes to the passive gravitation mass and <u>not</u> to the inertial mass (or vice versa).

Table 6-1. Mass-Energy Composition of Matter.

	Total Energy-Mass	Protons	Neutrons	Electrons	Electrons	Strong Interaction	Proton Repulsion	Weak Interaction	Gravitational
	$E^{*} = Mc^2 =$	$Z m_p c^2$ +	$N m_u c^2$ +	$Z M_e c^2$ -	B_e -	$B_s(Z, A)$ -	B_{er} -	B_w -	B_g
Al	25.13×10^9	12.2×10^9	13×10^9	6.6×10^9	6.2×10^3	2.25×10^6	3.2×10^7	45	5×10^{-29}
Au	183.5×10^9	74.1×10^9	110.9×10^9	4.037×10^6	4.18×10^5	1.56×10^9	6.35×10^8	312	1.4×10^{-27}
η(Al, Au)		.081	.081	2.4×10^{-4}	2.03×10^{-6}	4.5×10^{-4}	2.2×10^{-3}	9×10^{-11}	5×10^{-39}

*Energy units in electron volts

Eötvös parameter $\eta(A, B)$ if weak interaction mass-energy violates equivalence principal

$$\eta\,(\mathrm{Au, Al}) \simeq 9 \times 10^{-11}$$

$$\eta\,(\mathrm{Be, Al}) \simeq 4 \times 10^{-10}$$

$$\eta\,(\mathrm{Mg, Be}) \simeq 3.9 \times 10^{-10}$$

AD-A098 733 CHARLES STARK DRAPER LAB INC CAMBRIDGE MA F/G 7/2
EFFECTIVE VISCOSITY OF LIQUID HELIUM4 - WITH MINUTE HE3 IMPURIT--ETC(U)
MAR 81 R C PANDORF N00014-77-C-0295
UNCLASSIFIED R-1403 ONR-CR-007-003-1F NL

3 OF 3
AD
A098733

END
DATE FILMED
6-81
DTIC

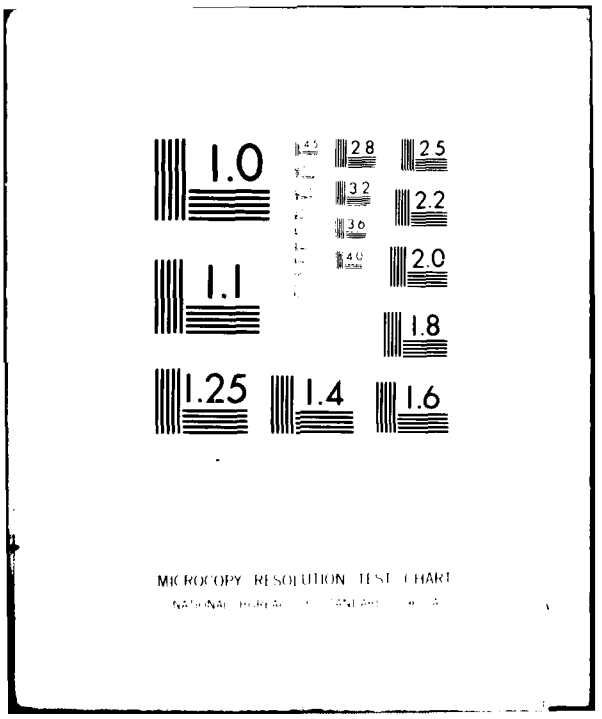
1.0
1.1
1.25
1.4
1.6
1.8
2.0
2.2
2.5
2.8
3.2
3.6
4.0
MICROCOPY RESOLUTION TEST CHART

Therefore, the Roll, Krotkov and Dicke measurement of η (Al, Au) $\lesssim 3 \times 10^{-11}$ is not precise enough to prove that the weak interaction mass-energy has an equivalent passive gravitation mass and inertial mass.

An experiment which showed that the weak interaction passive gravitational mass and inertial mass were equivalent to 1 part in 10^4 or better would be more convincing. This would require a measurement of η (A,B) $< 10^{-14}$.

The weak interaction is unique among the various interactions in that it is associated with the violation of parity conservation (Beta decay). This emphasizes the question of whether it is also unique enough that it violates the equivalence of inertial and gravitational mass.

6.1.1 The Basic Laboratory Method of Measuring η (A,B): The Eötvös Method

The parameter η (A,B) is measured using a torsion balance which consists of a beam supported by a torsion wire with a mass of substance A suspended from one end of the beam and another mass of substance B suspended from the other end as in Figure 6-1. The masses A and B are placed on the beam to give an approximate balance. The beam then bends and adjusts itself to give a perfect balance in the gravitation field, g, such that

$$M_A \, g \, l_A = M_B \, g \, l_B$$

or

$$l_B = M_A/M_B \, l_A \qquad (6.9)$$

If the torsion beam is then allowed to experience a lateral acceleration, a, (such as that caused by the horizontal component of the centrifugal acceleration due to the earth's rotation or its orbit around the sun), the torsion balance will experience a torque, L:

$$L = m_A \, a \, l_A - m_B \, a \, l_B \qquad (6.10)$$

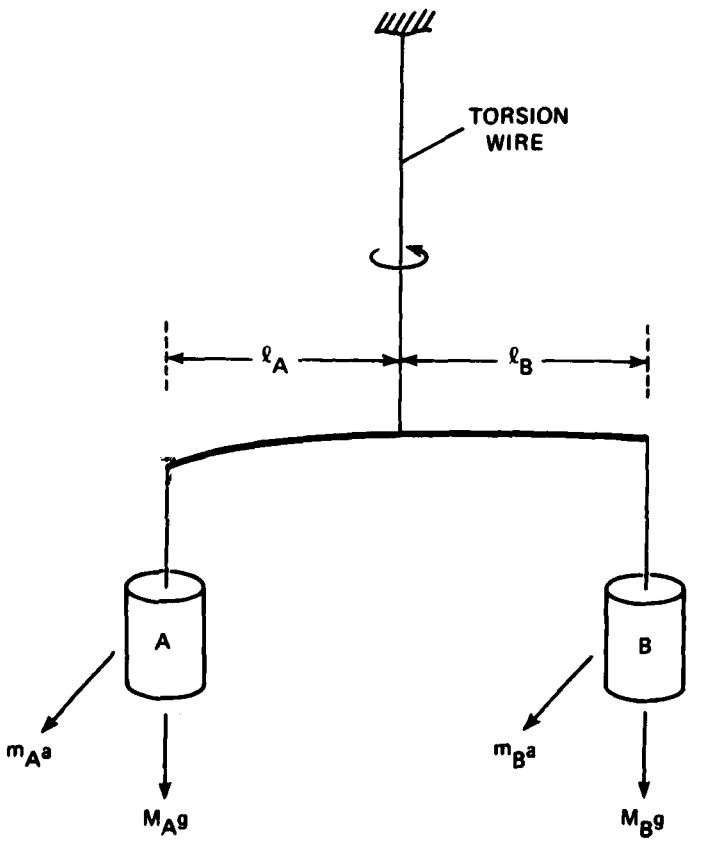

Figure 6-1. Simplified diagram of Eötvös torsion beam experiment.

Substituting from Equations (6.6) and (6.5)

$$L = M_A\, l_A\, a\, (m_A/M_A - m_B/M_B) = M_A l_A a\, \eta\, (A,B) \qquad (6.11)$$

Thus, we see by this simplified analysis that the parameter, η (A,B) is measured by the torque applied to the torsion wire.

Roll, Krotkov and Dicke made their measurements with a very well thought out, very carefully designed and controlled torsion balance type of apparatus. To give the reader an idea of the small effect they were measuring, Roll et al pointed out that for a gravitational force anomaly of η (A,B) = 10^{-11} the turning force on their beam was about 10^{-10} dynes which would produce an acceleration of 6×10^{-12} cm/sec^2, and after a whole year of acceleration (if one ignores the torsional constraint) would have led to a velocity of only 7 mm/hr.

There are two acceleration sources which can be utilized in performing earth laboratory experiments: the centrifugal acceleration due to the earth's daily rotation which has a horizontal component of 1.6 cm/sec^2 at the latitude of 45°, and the centrifugal acceleration due to the earth's orbit around the sun which has a value of 0.6 cm/sec^2 and which, of course, is along the line between the sun and earth.

In a torsion beam experiment performed by Eötvös around 1890, he utilized the centrifugal acceleration due to the earth's rotation. But in order to determine the torsion beam null, it was necessary to first measure the angular position in a north-south direction and then turn the apparatus 180° and measure the angular position again. The disadvantage of this method is that the turning of the apparatus disturbs the torsion wire and shifts the null.

Roll, et al utilized the acceleration due to the earth's orbit around the sun, which has a diurnal variation and so makes it unnecessary to rotate the apparatus. The disadvantage of this method is that the acceleration is less and the effect accumulates in a given direction for

no more than 12 hours. However, the significance of this last point depends upon the magnitude of the torsion constant, the moment of inertia, and the output sensitivity.

In order to measure η (A,B) = 10^{-11}, Roll et al had to deal with the following problems:

1. Gravitational gradient effects acting on the torsion balance. (They minimized this effect by using the masses suspended from the corners of a triangle and locating their experiment in a remote area 12 feet below ground and by operating the apparatus by remote control.)

2. Magnetic effects due to magnetic contaminant in the suspended masses acted upon by the earth's diurnal magnetic field variation. (This was a very great problem and required the most scrupulous care in selecting materials, fabricating and assembling the balance.)

3. Electrostatic effects which created varying potential differences between the suspended mass and their surroundings. Maximum variations in potential of only 10^{-5} volts could be tolerated. Variations in the potential were dealt with by temperature control to 10^{-3}°C and by temperature calibration of the output which was used to correct the results.)

4. Gas pressure effects which created torques due to non-symmetric outgasing and absorption on the torsion balance which in turn were augumented by temperature variations. (This effect was minimized by maintaining the apparatus in a vacuum, by having the entire balance well outgassed, by temperature control and by temperature correction of the results.)

5. Brownian motion effects. (Thermal fluctuation would normally represent a severe limitation on the precision

of the experiment. However, this problem was dealt with by artificial damping of the thermal fluctuation using electronic feedback which reduced the thermal fluctuation energy to much less than kT.)

6. The detection system for measuring the rotation of the torsion balance. (The Roll, et al experiment required them to measure an angular displacement of 3×10^{-9} rad, or a displacement of the masses of 10^{-8} cm. They accomplished this by the "old fashion" optical lever which has the advantage of separating angular displacement from the lateral motion. Furthermore, this required a very stable and drift-free detection system.)

7. Output signal noise. (The output signal noise was dealt with by three different methods. The Gaussian noise was narrow band filtered to pass the desired 24 hour signal period. The bandwidth of the filter was about 2×10^{-3} Hz or 0.3 cycles/day. The non-Gaussian noise pulses were handled by simply deleting the output information during the time period of the noise pulse. Finally, the output signal was corrected for temperature dependence by using prior calibration data of output-temperature dependence.)

8. Temperature effects. There were numerous temperature dependent effects throughout the apparatus. The most critical was the differential gas pressure mentioned above. Others had to do with the optics of the detection system, deflection of the balance, twist of the torsion fiber, potential differences etc. This problem was dealt with by control of the environment and by correction of the output results as mentioned above.)

9. Ground vibration effects. (Seismic disturbances contributed to the 24 hour signal noise problem mainly through

non-linear response mechanism which would permit 24 hour beats between higher frequency vibration. For those modes of vibrations which did not readily dampen out due to high Q, special provisions were made for damping.

In order to improve on the apparatus of Roll, Kratkov and Dicke, one would need to reduce the noise and increase the signal. Their experiment was so well done that it would be a monumental task to improve on it using the torsion balance approach.

What we propose is a different approach which will significantly (many orders of magnitude) reduce the noise and increase the signal, yet is fundamentally similar to the torsion balance.

6.2 The Cryogenic Spherical Rotor Experiment to Test the Weak Equivalence Principle*

This experiment would consist of a spherical shell composed of two hemispheres of different substances and made to be neutrally buoyant in liquid He^4. For materials which do not lend themselves well to making hemispheres, a spherical shell with opposing cutouts can be made into which different substances can be inserted as depicted in Figure 6-2. Or a third alternative would be to have a spherical shell of some suitable material and then place the test mass A and B as thick coatings on the inside of the hemispherical halves.

The two hemispherical shells play the same role as the two suspended masses in the torsion balance experiment and the neutral buoyancy in liquid He^4 provides the support that was provided by the torsion wire. One of the advantages of this type of support is that there are no vertical torsional restraints, so that any anomalous inertial torques can create an accumulated displacement.

* The author wishes to acknowledge and thank Prof. Ranier Weiss, Dept. of Physics, MIT for useful discussions on this new approach.

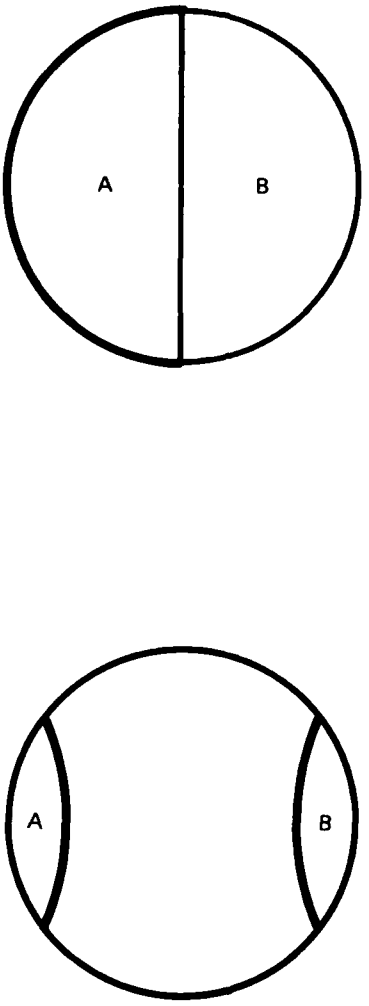

Figure 6-2. Possible arrangements of materials A and B in a neutrally buoyant spherical shell.

Let us now do a simplified analysis. The neutrally buoyant sphere depicted in Figure 6-3 will orient itself in a gravitational field such that the sum of the torques acting on the two masses are zero:

$$L = M_A \, l_A g - M_B \, l_B g = 0 \tag{6.12}$$

or

$$l_B = M_A / M_B \, l_A \tag{6.13}$$

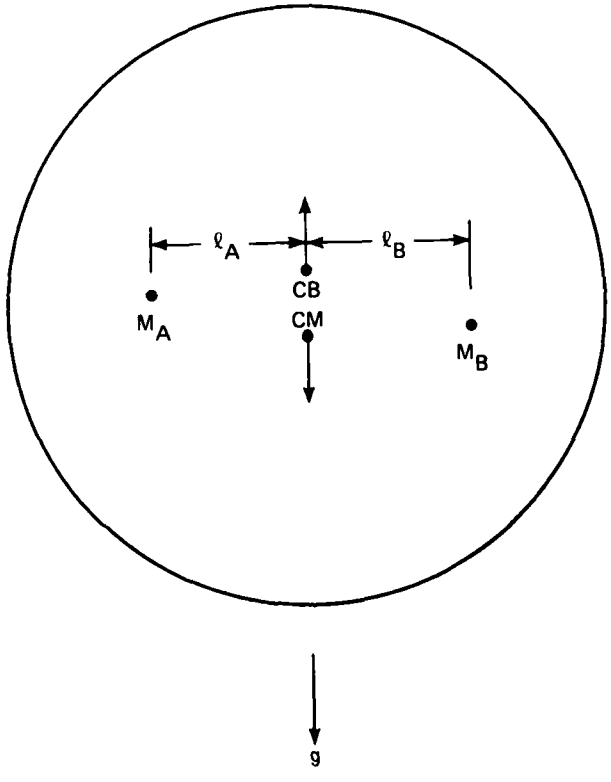

Figure 6-3. The spherical rotcr for testing the weak equivalence princple.

If an acceleration, a, is applied perpendicularly to the gravity vector, then the resulting torque becomes:

$$L_i = m_A\, l_A\, a - m_B\, l_B a \tag{6.14}$$

Substituting from the equation above,

$$L_i = M\, l_A a\, (m_A/M_A - m_B/M_B) \tag{6.15}$$

or

$$L_i = M l_A a\, \eta\, (A,B) \tag{6.16}$$

The torque would cause an angular acceleration $\dot{\omega}_0 = \frac{L_i}{I}$ and setting

$$I \simeq 2/3\, (M_A + M_B) r \simeq 4/3\, M_A r \quad \text{and} \quad l_A \simeq 1/2\, r \tag{6.17}$$

then $\dot{\omega}_0 = \frac{L_i}{I} = \frac{3}{8} \frac{a}{r}\, \eta\, (A,B)$

Integrating this expression to get the angular displacement θ,

$$\theta \simeq \frac{3}{16}\, t^2\, \eta\, (A,B) \tag{6.18}$$

where t is the time the acceleration is applied.

Taking r = 5 cm, a = 1.6 cm/sec^2, η (A,B) = 10^{-14}, we find for a 6 day observation that $\theta = 1.6 \times 10^{-4}$ rad, a value which is about 50,000 times larger than the least measurement by Roll, Krotkov and Dicke using the optical lever (i.e., to measure η (A,B) = 10^{-11} required Roll et al to measure the angular displacement to 3×10^{-9} rad).

There are several possible methods of conducting the experiment. As in Eötvös original experiment, one could orient the masses M_A and M_B in the initially fixed east-west direction and allow the horizontal component of the centrifugal acceleration of the earth's rotation to act on the free, neutrally buoyant rotor for any number of days to observe

whether or not the rotor is accelerating. Then repeat the procedure again with the rotor oriented initially 180° from the first test to see if the acceleration is reversed. Or as in Roll et al experiments, one could utilize the acceleration due to the sun and look for a diurnal period in the angular acceleration.

The liquid He^4 which provides the neutral buoyancy for the spherical rotor also has a viscosity which will limit the maximum angular velocity (i.e., a terminal velocity) the spherical rotor could achieve due to any anomalous inertial torques. For an anomaly η (A,B) = 10^{-14} and the liquid He^4 at a temperature of 1.8K the rotor would reach its maximum velocity after 13 minutes. However, at a temperature of 46mK it would require (even for a rough finish spherical rotor) one month to reach its maximum velocity, or 4.6 months at 10mK. The length of time would be considerably longer for a smooth rotor.

The problems discussed above which confronted Roll et al will be significantly reduced by the neutrally buoyant spherical rotor. Taking them one at a time:

1. The gravitational field gradients will be virtually eliminated by the spherical symmetry.

2. The magnetic contaminants problem would still require great care to be eliminated. However, superconducting shielding techniques could be utilized to provide virtually perfect shielding from the earth's magnetic field and its variations.

3. Electrostatic effects would be virtually eliminated by the spherical symmetry used with conducting surfaces.

4. Gas pressure effects would be virtually eliminated by the cryogenic temperature and the spherical symmetry.

5. Brownian motion effects would be negligible because of the cryogenic temperatures.

6. Rotation detection system even 1/100 as good as Roll et al would be adequate because the output signal can be time integrated.

7. Temperature effects would be virtually non-existent due to the experimental arrangement, the cryogenic temperatures and the good temperature control which is possible.

8. Noise and vibration effects will be significantly reduced due to the fact that the spherical rotor can be made as perfectly neutrally buoyant as desired (the fine tuning being done by adjusting the fluid density) and the lateral to rotational noise mode coupling can be virtually eliminated by Schuler tuning the sphere.

The neutrally buoyant Schuler tuned spherical rotor, in addition to having very low noise characteristics, also will have a relatively large signal output because the signal information will accumulate and will be integrated with time, because the near frictionless environment of the liquid He^4 allows unconstrained, undamped rotation in response to any amomaly in the mass equivalence.

REFERENCES

1. Roll, P.G., Krotkov, R. and Dicke, R.H., Ann Phys. 442, 517 (1964).

2. PR-8 "Studies of Space Experiments to Measure Gravitational Constant Variation and the Eötvös Ratio", Ed. by L.S. Wilk; Measurement System Laboratory, MIT, Cambridge, Massachusetts.

APPENDIX A

THE INFLUENCE OF A He^3 IMPURITY ON THE VISCOSITY OF HELIUM II

A Reprint of an Article

by

V. N. ZHARKOV

Institute of Terrestrial Physics

Academy of Sciences

U.S.S.R.

THE INFLUENCE OF A He^3 IMPURITY ON THE VISCOSITY OF HELIUM II

V. N. ZHARKOV

Institute of Terrestrial Physics, Academy of Sciences, U.S.S.R.

Submitted to JETP editor April 11, 1957

J. Exptl. Theoret. Phys. (U.S.S.R.) 33, 929-932 (October, 1957)

On the basis of the Landau theory of liquid helium, a determination is made of the coefficient of viscosity of a weak solution of He^3 in helium II as a function of temperature and concentration.

ACCORDING to the theory of Landau, a weak solution of He^3 in helium II can be regarded as a mixture of three gases of elementary excitations:[1] (1) a gas of rotons $\epsilon_r = \Delta_r + (p - p_0)^2/2m$, (2) a gas of phonons $\epsilon = sp$, and (3) a gas of impurity excitations $\epsilon_i = \Delta_i + p^2/2\mu$.

In order to solve the problem of the viscosity of the solution it is necessary to know how the elementary excitations interact with each other. The effective cross-sections for roton-roton, roton-phonon, and phonon-phonon scattering have been calculated by Landau and Khalatnikov[2] in their well known work on the theory of the viscosity of helium II. They have also discussed the question of the establishment of energy equilibrium in a phonon gas, which plays an important role in the study of kinetic effects in helium II. Effective cross-sections for the scattering of impurities by rotons and by each other, and for the scattering of phonons by impurities, have been calculated by Khalatnikov and the author[3] for an investigation of diffusion and of thermal conduction in solutions.

From the conservation laws it follows that, relative to the phonons, the rotons and the impurity excitations can be regarded as heavy particles. Moreover, the absolute values of the effective cross-sections for the scattering of the heavy particles by each other are much greater than the cross-sections for the scattering of phonons by these particles. These facts lead to the result that, for concentrations of He^3 atoms greater than $\sim 10^{-6}$ and for all temperatures, deviations of the roton and impurity distribution functions from their equilibrium values are determined only by processes which involve the scattering of the "heavy" excitations by each other. Furthermore, in solving the kinetic equations which determine the phonon distribution function, the rotons and impurities can be described by equilibrium Maxwellian distribution functions, since deviations of these functions from equilibrium are much smaller than deviations of the phonon distribution function from its equilibrium value. Both these circumstances make the calculations extremely simple and analogous to those carried out earlier in determining the thermal conductivity κ of a solution.[3]

The viscosity, as well as the thermal conductivity, of a solution is the sum of three parts: (1) the "roton viscosity" η_r, which depends on the transfer of momentum by rotons, (2) the "phonon viscosity" η_{ph}, which depends on the transfer of momentum by phonons, and (3) the "impurity viscosity" η_i, which depends on the transfer of momentum by the impurities. Analysis of the thermal conductivity of a solution of He^3 in helium II has shown that κ_r and κ_{ph}, the roton and phonon parts of the coefficient of thermal conductivity, differ from their corresponding values κ_{0r} and κ_{0ph} for pure helium only in that the scattering processes determining their effective times are modified by the presence of impurities. As we have shown,[3] κ_r is obtained from κ_{0r} by replacing the time t_{rr}^{-1} in the latter by the time $t_r^{-1} = t_{rr}^{-1} + t_{ri}^{-1}$, where t_{rr} and t_{ri} are quantities differing from the average times between roton-roton and roton-impurity collisions by temperature-independent factors of order unity. These times are[2,3]

$$t_{rr} = \hbar^4/4p_0m\,|V_0|^2N_r = 0.7\cdot 10^{-13}T^{-1/2}e^{\Delta_r/kT}, \tag{1}$$

$$t_{ri}^{-1} = \overline{v_i\sigma_{ir}N_i} = 3.3\cdot 10^{13}cT^{1/2}. \tag{2}$$

Here the usual notation is used: Δ_r and p_0 are the zero-point energy and momentum of a roton, m the effective mass of a roton, N_r the number of rotons per unit volume, v_i the velocity of an impurity

excitation, σ_{1r} the effective cross-section for the scattering of an impurity by a roton, N_i the number of impurity atoms per unit volume, $c = N_3m_3/(N_3m_3 + N_4m_4)$ the concentration; M_3 and m_4, N_3 and N_4 the masses and numbers of atoms of He^3 and He^4 per unit volume. The representation of t_r^{-1} in the form of a sum is justified in the limiting cases $t_{rr} \ll t_{ri}$ and $t_{rr} \gg t_{ri}$, i.e., when rotons are scattered only by other rotons or only by impurities.

Because of the fact that the quantity t_{rr}^{-1}, which is proportional to the number of rotons, decreases exponentially with decreasing temperature, the transition from the case $t_{rr} \ll t_{ri}$ to the case $t_{rr} \gg t_{ri}$ (for a given concentration) will take place in a temperature interval of the order of $\sim 0.1°K$. Analogously, in the case of phonons, κ_{ph} will be obtained from κ_{0ph} by replacing θ_{phr}^{-1} by $\theta^{-1} = \theta_{phr}^{-1} + \theta_{phi}^{-1}$, where θ_{phr} and θ_{phi} are times characterizing the scattering of phonons by rotons and by impurities, respectively:[2,3]

$$1/\theta_{phr} = \frac{6!N_r}{4\pi s}\left[\frac{p_0(kT/s)^3}{\hbar^3\rho}\right]^3 A, \tag{3}$$

$$1/\theta_{phi} = \frac{6!N_i}{8\pi s}\left[\frac{(3\mu kT)^{1/3}(kT/s)^3}{\hbar^3\rho}\right]^2 \delta. \tag{4}$$

Here s is the velocity of sound and ρ the density of helium. The quantities A and δ are temperature-independent constants of order unity.

The representation of θ^{-1} in the form of a sum $\theta_{phr}^{-1} + \theta_{phi}^{-1}$ is also justified only in the limiting cases $\theta_{phr} \ll \theta_{phi}$ and $\theta_{phr} \gg \theta_{phi}$, and the formula $\theta^{-1} = \theta_{phr}^{-1} + \theta_{phi}^{-1}$ represents an interpolation. Except for the replacement of t_{rr}^{-1} by t_r^{-1} and of θ_{phr}^{-1} by θ^{-1}, the form of the coefficients of thermal conductivity κ_{0r} and κ_{0ph} remains the same. It is, therefore, natural that the relation which exists between η_{0r} and η_{0ph}, on the one hand, and between κ_{0r} and κ_{0ph}, on the other, also remains the same for the corresponding coefficients for solutions of He^3 in helium II (this fact can be confirmed also by direct calculation). This relation was established by Khalatnikov[4] and has the form

$$\eta_{0r} = \varkappa_{0r}p_0^2T/5\Delta_r^2; \qquad \varkappa_{0r} = \Delta_r^2 t_{rr}N_r/3mT, \tag{5}$$

$$\eta_{0ph} = \frac{T}{5s^2}\left(1 + \frac{\bar{\theta}_{phr}}{5\theta_{ph}\tau_{ph}}\right)^{-1}\left(1 - \frac{S_0T}{\rho_{n0}s^2}\right)^{-1}\varkappa_{0ph}, \quad \varkappa_{0ph} = N_{ph}k\theta_{phr}s^2\left(1 - \frac{S_0T}{\rho_{n0}s^2}\right)\begin{cases} 19\dfrac{1 + 0.75\theta_{phr}/\theta_{ph}}{1 + 8\theta_{phr}/\theta_{ph}} & (\text{for } T > 0.9°K) \\ 1.8 & (\text{for } T < 0.9°K). \end{cases} \tag{6}$$

where τ_{ph} is a characteristic time for the phonon-phonon scattering process, which according to Landau and Khalatnikov,[2] is equal to

$$\tau_{ph}^{-1} = \frac{3\cdot 13!(u+2)^6}{5\cdot 2^{16}(2\pi)^6\hbar^3\rho^2 s}\left(\frac{kT}{s}\right)^9\left(u = \frac{2\rho}{s}\frac{\partial s}{\partial \rho}\right). \tag{7}$$

Here $N_{ph} = 2.4 \times 4\pi\,(kT/2\pi\hbar s)^3$ is the number of phonons per unit volume, θ_{ph} is the characteristic time for the establishment of equilibrium with respect to the number of phonons in the phonon gas, and S_0 and ρ_{n0} are the entropy per unit volume and the normal density of pure helium. For the temperature region $T > 0.9°K$, $\theta_{phr}/56\tau_{ph} \ll 1$ and the second term in the parentheses in (6) can be dropped. The bar over the time θ_{phr} denotes that the time characterizing the scattering of phonons by rotons has been calculated with a different dependence of the deviations of the distribution function δn on the scattering angle than in the case of the thermal conductivity; namely, for calculations of the viscosity we have $\delta n \sim \cos\theta \sin\theta \cos\varphi$. In the case of a solution, τ_{ph}^{-1} can be set equal to zero for $c > 10^{-4}$. For concentrations $c < 10^{-4}$, $\theta/\theta_{ph} \ll 1$ for $T < 0.8°K$.

Taking all the above considerations into account and with the help of (5) and (6) we find the roton and phonon parts of the viscosity coefficient of a solution:

$$\eta_{ir} = t_r p_0^2 N_r/15m, \tag{8}$$

$$\eta_{iph} = \begin{cases} 3.8\,N_{ph}kT\bar{\theta}\dfrac{1 + 0.75\bar{\theta}/\theta_{ph}}{1 + 8\bar{\theta}/\theta_{ph}} & \begin{matrix}\text{for } T > 0.6°K;\ c > 10^{-4} \\ \text{for } T > 0.9°K;\ c < 10^{-4}\end{matrix} \\ 0.35\,N_{ph}kT\bar{\theta}\left(1 + \dfrac{\bar{\theta}}{56\tau_{ph}}\right) & \text{for } T < 0.8°K;\ c < 10^{-4}. \end{cases} \tag{9}$$

Here account has been taken on the fact that to determine the viscosity coefficients from the thermal conductivity coefficients it is necessary to replace the unbarred effective times by those with a bar. Such a substitution has little effect on the effective times; thus, $\bar{\theta}_{phr}$ and $\bar{\theta}_{phi}$ differ from θ_{phr} and θ_{phi} only because of insignificant changes of the constants A in (3) and δ in (4), which remain of order of magnitude unity.

A calculation of the impurity part of the viscosity coefficient η_i can be carried out in the same way as in the kinetic theory of gases in the two limiting cases $t_{ir} \ll t_{ii}$ and $t_{ir} \gg t_{ii}$. Here t_{ir} is an effective time characterizing the scattering of impurities by rotons:[3]

$$t_{ir}^{-1} = \sigma_{ir}\sqrt{3kT/\mu}\,N_r = 1\cdot 10^{13} T e^{-\Delta_r/kT}. \tag{10}$$

The effective time t_{ii} characterizing the scattering of impurities by each other is given by the equation

$$t_{ii}^{-1} = \overline{|v_{i1} - v_{i2}|\,\sigma_{ii}N} = \frac{a}{\pi}\frac{|V_{01}|^2\mu^2}{\hbar^6}\sqrt{\frac{kT}{\pi\mu}}\,N = 2.9\cdot 10^{11} a T^{1/2} c, \tag{11}$$

where μ is the effective mass of an impurity excitation, σ_{ii} is the effective cross-section for the scattering of impurities by impurities,[3] and V_{01} is a constant of the interaction between impurities. A constant a has been introduced in (11) since the magnitude of V_{01} is not known. A numerical value for (11) is obtained by taking $|V_{01}|^2 \sim 10^{-76}$ erg^2 cm^6. It can be assumed that the quantity a is on the order of unity. With the aid of the interpolation formula $t_i^{-1} = t_{ir}^{-1} + t_{ii}^{-1}$ we determine the effective time characterizing the scattering of impurities in the solution, and then after elementary calculations obtain

$$\eta_i = (15\pi/32)(kT/m_3)\,c p t_i. \tag{12}$$

After collecting the expressions obtained above, substituting numerical values for the parameters and making use of the final data given by Khalatnikov in his review article,[5] we obtain for the viscosity of the solution

$$\eta = \frac{1.15\cdot 10^{-6}}{1+0.23\cdot c e^{8.9/T}} + \frac{2.1\cdot T^{3/2}\cdot 10^{-8}}{a + 2.9\cdot 10^{7} T^{1/2} c^{-1} e^{-8.9/T}} + \frac{3.75\cdot 10^{-8} T^{-1/2} e^{8.9/T}}{1+3.5\cdot 10^{-28} T^{7} c e^{8.9/T}} \cdot \begin{cases} \dfrac{1+0.75\,\theta/\theta_{ph}}{1+8\,\theta/\theta_{ph}} & \text{for } T \gtrsim 0.6^\circ\text{K};\ c > 10^{-4} \\ & \text{for } T > 0.9^\circ\text{K};\ c < 10^{-4} \\ 0.095\,(1+\theta/56\tau_{ph})^{-1}, & \text{for } T < 0.8^\circ\text{K};\ c < 10^{-4}. \end{cases}$$

The temperature dependence of the viscosity for different concentrations is plotted in the figure. We see that above ~ 1.1°K the presence of impurities has slight effect in modifying the viscosity of pure helium II. Gradually, below 1.1°K, phonon-impurity scattering processes begin to play a predominant role, because of the abrupt decrease in the number of rotons, and lead to a sudden decrease in the phonon mean free path in the solution relative to its value in pure helium, and thus to a corresponding decrease in the viscosity of the solution relative to the viscosity of pure helium.

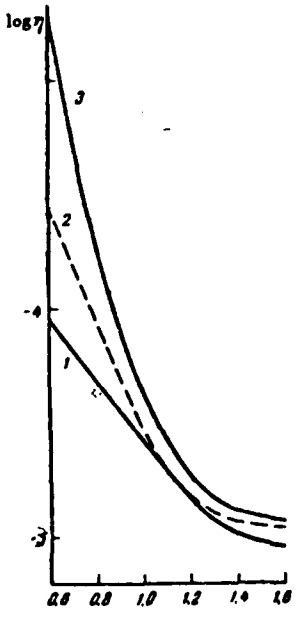

Temperature dependence of the viscosity of a solution (in poise). Theoretical curves: (1) c = 10^{-2}; (2) c = 10^{-3}; (3) c = 0 (viscosity of pure helium II).

In conclusion we take advantage of the opportunity to express our gratitude to Professor I. M. Khalatnikov for discussions of this work.

[1] L. D. Landau and I. Ia. Pomeranchuk, Dokl. Akad. Nauk SSSR 59, 669 (1948).
[2] L. D. Landau and I. M. Khalatnikov, J. Exptl. Theoret. Phys. (U.S.S.R.) 19, 637, 709 (1949).
[3] V. N. Zharkov and I. M. Khalatnikov, J. Exptl. Theoret. Phys. (U.S.S.R) 32, 1108 (1957), Soviet Phys. JETP 5, 905 (1957).
[4] I. M. Khalatnikov, J. Exptl. Theoret. Phys. (U.S.S.R.) 23, 21 (1952).
[5] I. M. Khalatnikov, Usp. Fiz. Nauk 59, 674 (1956).

Translated by W. M. Whitney
188

APPENDIX B

GERMANIUM RESISTANCE THERMOMETER CALIBRATION DATA

GERMANIUM RESISTANCE THERMOMETER CALIBRATION DATA

Temperature K	Ger #3 Conductance mMho	Ger #2 Conductance mMho
.050	.01036	
.062	.03185	
.070	.05935	
.080	.1068	
.100	.2532	1.11
.125	.5974	1.98
.150	.9876	2.81
.175	1.425	3.60
.200	1.958	4.36
.250	2.835	5.77
.300	3.610	7.12
.350	4.407	8.50
.400	5.430	9.80
.500	7.079	12.20
.603	8.657	14.40
.805	11.338	18.02
1.006	13.648	21.10
1.201	15.684	23.62
1.407	17.510	26.20
1.606	19.270	28.42
1.802	20.785	30.40
2.007	22.158	32.10
2.200	23.542	
2.416	24.953	
2.602	26.069	
2.809	27.288	
3.000	28.333	39.20

Calibration Current

.05K to .10K - .01
.125K to .250K .1
.30K to .603K 1.0
.805K to 3.20K 10.0

Model No. S-He^3A by Scientific Instruments, Inc., Lakeworth, Florida
Ger. #3 calibrated by Gilbert Halverson of SI
Ger. #2 calibrated from Ger. #3 and He^3 vapor pressure

APPENDIX C

EXPERIMENTAL DATA

EXPERIMENTAL SERIES I

LIQUID VISCOSITY DATA

BERYLLIUM INNER CYLINDER

Motor Freq f_o	Rotor Dir	Gain G	e_{ex} Volts	Thermom #2 Ohm	e^+ or e^- Volts	η Micro-Poise	Temp K	v cm/sec	
.05	F	100	7.1532	203.5	- 0.65		.219		
.05	R	100	"	209.0	+ 0.11	1.8152	.215		
.05	F	100	"	208.0	- 0.56	1.6002	.216		
.05	R	100	"	205.5	+ 0.16	1.7197	.217		
.05	F	100	"	202.0	- 0.70	2.0540	.220		
.05	R	100	"	208.0	+ 0.09	1.8868	.220		
.05	F	100	"	208.0	- 0.70	1.8868	.216		
.05	F	100	"	120.4	- 3.12		.345		
.05	R	100	"	122.0	+ 2.17	12.635	.338		
.05	F	100	"	123.5	- 3.08	12.539	.328		
.05	R	100	"	123.5	+ 2.14	12.467	.338	.10472	
.025	F	100	"	126.5	+ 0.69		.328	.05236	
.025	R	100	"	126.0	- 1.99	12.802	.328	.05236	
.025	F	100	"	123.0	+ 0.59	12.324	.338	.05236	
.025	R	100	"	124.5	- 1.99	12.324	.332	.05236	
.070	F	100	"	125.0	- 5.59		.332	.14661	
.070	R	100	"	125.0	+ 2.02	12.983	.332	.14661	
.070	F	100	"	124.5	- 5.84	13.409	.332	.14661	
.070	R	100	"	124.5	+ 1.96	13.307	.332	.14661	
.100	R	100	"	124.0	+ 3.55		.333	.20944	
.100	F	100	"	124.0	- 7.62	13.339	.333	.20944	
.100	R	100	"	121.0	+ 3.46	13.232	.340	.20944	
.250	R	10	"	122.0	+ 1.71		.338	.52360	
.250	F	10	"	122.5	- 2.41	15.024	.337	.52360	
.250	R	10	"	121.0	+ 1.73	15.135	.341	.52360	

EXPERIMENTAL SERIES I

LIQUID VISCOSITY DATA

BERYLLIUM INNER CYLINDER

Motor Freq f_o	Rotor Dir	Gain G	e_{ex} Volts	Thermom #2 Ohm	e^+ or e^- Volts	η Micro-Poise	Temp K	v cm/sec	
1.40	F	1	7.1532	123.8	- 1.47		.334	2.93215	
1.40	R	1	"	125.22	+ 1.416	18.629	.330	2.93215	
1.40	F	1	"	125.55	- 1.458	18.552	.330	2.93215	
.60	F	10	"	123.0	- 5.24		.337	1.25664	
.60	R	10	"	121.0	+ 4.94	15.494	.341	1.25664	
.60	F	10	"	121.05	- 5.24	15.494	.341	1.25664	
2.2	F	1	"		- 2.706			4.6077	
2.2	R	1	7.1507		+ 2.614	16.84682		4.6077	
.17	F	10	"		- 1.306			0.35605	
.17	R	10	"		+ 1.174	13.302		0.35605	
,17	F	10	"		- 1.302	13.283		0.35605	
.07	F	100	"		- 4.07			0.14661	
.07	R	100	"		+ 3.47	12.868		0.14661	
.07	F	100	"		- 4.03	12.799		0.14661	
.07	R	100	"		+ 3.47	12.799		0.14661	
.04	F	100	"		- 2.53			0.08378	
.04	R	100	"		+ 1.62	12.391		0.08378	
.04	F	100	"		- 2.53	12.391		0.08378	
.04	R	100	"		+ 1.70	12.630		0.08378	
.04	F	100	"		- 2.56	12.719		0.08378	
.02	F	100	"	664.5	- 0.33			0.04188	
.02	R	100	"		- 0.29	0.358	.110 - .130	0.04188	
.02	R	100	"	523.5	- 0.216		.124	0.04188	
.02	F	100	"	465.5	- 0.288	0.550	.130	0.04188	
.02	R	100	"	417.0	- 0.220	0.556	.138	0.04188	

EXPERIMENTAL SERIES I

LIQUID VISCOSITY DATA

BERYLLIUM INNER CYLINDER

Motor Freq f_o	Rotor Dir	Gain G	e_{ex} Volts	Thermom #2 Ohm	e^+ or e^- Volts	η Micro-Poise	Temp K	v cm/sec	
.05	R	100	7.1507		+ 8.24			0.10472	
.05	F	100	"		- 7.20	36.89		0.10472	
.05	R	100	"	95.05	+ 8.26	36.94	.430	0.10472	
.05	R	10	"	86.4	- 1.926		.472	0.10472	
.05	F	10	"		- 1.794	67.85		0.10472	
.05	R	10	"		+ 1.936	68.03		0.10472	
.05	R	10	"	76.2	+ 3.434		.541	0.10472	
.05	F	10	"	75.05	- 3.326	123.30	.541	0.10472	
.05	R	10	"		+ 3.414	122.94		0.10472	
.05	R	10	"	68.58	+ 5.200		.612	0.10472	
.05	F	10	"		- 5.09	187.69		0.10472	
.05	R	10	"	68.5	+ 5.18	187.32	.613	0.10472	
.05	F	10	"	65.08	+ 5.38	203.56	.652	0.10472	
.05	F	10	"		- 5.97	217.97		0.10472	
.05	R	10	"	65.36	+ 5.99	218.15	.650	0.10472	
.05	R	10	"		+ 6.13			0.10472	
.05	F	10	"	61.6	- 6.10	223.25	.700	0.10472	
.05	R	10	"	61.64	+ 6.11	222.71		0.10472	
.05	R	10	"	58.12	+ 4.89		.756	0.10472	
.05	F	10	"	58.54	- 4.87	178.02	.750	0.10472	
.05	R	10	"		+ 4.89	178.02		0.10472	
.05	R	10	"	59.8	+ 5.67		.730	0.10472	
.05	F	10	"		- 5.67			0.10472	
.05	R	10	"	59.84	+ 5.67	206.84	.721	0.10472	
.05	R	10	"	60.91	+ 5.94	206.84	.711	0.19472	

EXPERIMENTAL SERIES I

LIQUID VISCOSITY DATA

BERYLLIUM INNER CYLINDER

Motor Freq f_o	Rotor Dir	Gain G	e_{ex} Volts	Thermom #2 Ohm	e^+ or e^- Volts	η Micro-Poise	Temp K	v cm/sec	
.05	R	10	7.1507	54.98	+ 2.99		.816	0.10472	
.05	F	10	"		- 2.99	109.07		0.10472	
.05	F	10	"	51.4	- 1.652		.922	0.10472	
.05	R	10	"	51.4	+ 1.666	60.520		0.10472	
.05	R	100	"	47.8	+ 7.01		.992	0.10472	
.05	F	100	"		- 6.61	32.541		0.10472	
.05	F	100	7.1485	45.4	- 1.28		1.08	0.10472	
.05	R	100	"	45.32	+11.28	31.309		0.10472	
.05	F	100	"		- 1.84	32.647		0.10472	
.05	R	100	"		+11.97	33.006		0.10472	
.05	F	100	"		- 1.60	32.432		0.10472	
.05	R	100	"	45.48	+ 8.96	25.238	1.06	0.10472	
.05	F	100	"		- 1.76	25.621		0.10472	
.05	R	100	"		+ 8.98	25.668		0.10472	
.05	R	100	"		+ 3.02				
.05	F	100	"		- 3.94	16.634		0.10472	
.05	R	100	"	42.37	+ 4.26	19.598	1.18	0.10472	
.05	F	100	"		- 3.88	19.454		0.10472	
.05	R	100	"		+ 4.15	19.192		0.10472	
.05	R	100	"	42.36	+ 3.65			0.10472	
.05	F	100	"		- 3.59	17.303		0.10472	
.05	R	100	"		+ 3.73	17.495		0.10472	
.05	F	100	"	40.34	- 3.50	17.280	1.28	0.10472	
.05	R	100	7.1445	36.74	+ 3.425		1.5	0.10472	
.05	F	100	"		- 2.73	14.707		0.10472	

EXPERIMENTAL SERIES I

LIQUID VISCOSITY DATA

BERYLLIUM INNER CYLINDER

Motor Freq f_o	Rotor Dir	Gain G	e_{ex} Volts	Thermom #2 Ohm	e^+ or e^- Volts	η Micro-Poise	Temp K	v cm/sec	
.05	R	100	7.1445		+ 3.57	15.065		0.10472	
.05	F	100	"		- 2.58	14.707		0.10472	
.05	R	100	"		+ 3.64	14.874		0.10472	

EXPERIMENTAL SERIES II

LIQUID VISCOSITY DATA

GLASS INNER CYLINDER

Motor Freq f_o	Rotor Dir	Gain G	e_{ex} Volts	Thermom #2 m MHO	e^+ or e^- Volts	η Micro-Poise	Temp K	v cm/sec	
.05	F	10	7.15	17.33	+ 2.15		1.381	.534	
.05	R	10	"	17.27	- 1.4	15.03	1.372	"	
.05	F	10	"	17.17	+ 2.8	17.79	1.363	"	
.10	F	10	"	17.11	+ 5.84		1.356	1.068	
.10	R	10	"	16.75	- 5.14	23.25	1.317	"	
.10	F	10	"	16.39	+ 5.72	23.00	1.277	"	
.10	R	10	7.1625	15.97	- 4.96	22.67	1.229	"	
.05	F	10		14.88	- .90			.534	
.05	R	10	7.1588	"	+ 5.9	21.17	1.124	"	
.3	R	10		3.617	-12.9		.300	3.204	
.3	F	10		4.000	+13.0	18.3	3.24	"	
.3	R	1		"	- 1.75			"	
.3	F	1	7.147	3.752	+ 1.11	20.28	.309	"	
.12	R	10	"	3.623	- 4.74		.281	1.28	
.12	F	10	"	"	+ 2.06	12.01	"	"	
.12	R	10	"	"	- 4.72	11.97	"	"	
.12	F	1	7.068	8.406	+ 7.05		.586	"	
.12	R	1	"		- 7.082	250.5	"	"	
.12	F	1	"	"	+ 6.984	249.4	"	"	
.24	F	1	4.179	"	+ 8.474		"	2.56	
.24	R	1	"	"	- 8.548	258.2	"	"	
.24	F	1	"	"	+ 8.40	257.0	"	"	
.44	F		2.105	8.471	+ 7.96		.584	4.70	
.44	R		"	"	- 8.252	265.0	"	"	
.44	F		"	8.428	+ 7.882		.588	"	

EXPERIMENTAL SERIES II

LIQUID VISCOSITY DATA

GLASS INNER CYLINDER

Motor Freq f_o	Rotor Dir	Gain G	e_{ex} Volts	Thermom #2 m MHO	e^+ or e^- Volts	η Micro-Poise	Temp K	v cm/sec	
.1	F	10	7.113	17.89	+ 4.97		1.43	1.068	
.1	R	10	"	"	- 4.88	21.62		"	
.1	F	10	"	"	+ 4.97	21.62		"	
.05	F	10	"	17.90	+ 1.79			.534	
.05	R	10	"	"	- 1.77	15.63		"	
.05	F	10	"	"	+ 1.75	15.45		"	
.005	F	100	"	17.86	+ 2.2	13.0		.0534	
.005	R	100	"	"	- 3.2	19.0		"	
.005	F	100	"	"	+ 1.6	9.5		"	
.005	R	100	"	"	- 2.4	14.0		"	
.005	F	100	"	"	+ 1.6	9.5		"	
.02	R	100	"	"	- 8.0	11.9		.214	
.02	F	100	"	"	+ 7.5	11.1		"	
.02	R	100	"	"	- 7.3	10.8		"	
.02	F	100	"	"	+ 8.0	11.9		"	
.02	R	100	"	"	- 8.0	11.9		"	
.02	F	100	"	"	+ 8.0	11.9		"	
.02	R	100	"	"	- 8.8	13.0		"	
.04	R	100	"	"	11.0			.427	
.04	F	100	"	17.81	- 9.6			"	
.04	R	100	"	"	+10.6	14.9		"	
.04	F	100	"	"	- 9.2	14.65		"	
.075	F	10	"	"	+ 3.42			.0801	
.075	R	10	"	"	- 3.18	19.38		"	
.075	F	10	"	"	+ 3.40	19.33		"	

EXPERIMENTAL SERIES II

LIQUID VISCOSITY DATA

GLASS INNER CYLINDER

Motor Freq f_o	Rotor Dir	Gain G	e_{ex} Volts	Thermom #2 m MHO	e^+ or e^- Volts	η Micro-Poise	Temp K	v cm/sec	
.2	R	1.0	7.113	17.80	- 1.128			.214	
.2	F	1.0	"	"	+ 1.156	25.16		"	
.2	R	1.0	"	"	- 1.17	25.62		"	
.2	F	1.0	"	"	+ 1.08	24.79		"	
.4	F	1.0	"		+ 4.00			4.27	
.4	R	1.0	"	"	- 4.36	45.69		"	
.4	F	1.0	"	"	+ 4.06	46.01		"	
.4	R	1.0	"	"	- 4.12	44.70		"	
1.0	F	1.0	2.485		+ 8.63			10.18	
1.0	R	1.0	"		- 8.86	110.3		"	
1.0	F	1.0	"		+ 8.812	111.4		"	
.03	F	100	7.107	17.77	+ 7.6		1.43	.320	
.03	R	100	"	"	- 6.2	13.7		"	
.03	F	100	"	"	+ 7.8	13.9		"	
.03	R	100	"	"	- 5.3	13.0		"	
.01	F	100	"	"	+ 3.0			.1068	
.01	R	100	"	"	- 1.6	13.7		"	
.01	F	100	"	"	+ 1.6	9.5		"	
.01	R	100	"	"	- 1.6	9.5		"	
.025	R	100	"	17.74	- 3.7			.267	
.025	F	100	"	"	-15.0	10.34		"	
.025	R	100	"	"	- 3.7	10.34		"	
.025	F	100	"	"	+ 5.1	10.46		"	
.025	R	100	"	"	- 3.6	10.34		"	
.0275	R	100	"	17.73	- 4.6			.294	

EXPERIMENTAL SERIES II

LIQUID VISCOSITY DATA

GLASS INNER CYLINDER

Motor Freq f_o	Rotor Dir	Gain G	e_{ex} Volts	Thermom #2 m MHO	e^+ or e^- Volts	η Micro-Poise	Temp K	v cm/sec	
.0275	F	100	7.107	17.73	+ 5.3	10.74		.294	
.0275	R	100	"	"	- 5.1	11.27		"	
.0275	F	100	"	"	+ 4.9	10.84		"	
.0290	F	100	"	"	+ 5.0			.310	
.0290	R	100	"	"	- 5.2	10.48		"	
.0290	F	100	"	"	+ 5.3	10.79		"	
.0290	R	100	"	"	- 5.2	10.79		"	
.031	R	100	"	"	- 5.6			.331	
.031	F	100	"	"	+ 5.8	10.94		"	
.031	R	100	"	"	- 5.4	10.75		"	
.06	R	10	"	"	- 1.72			.641	
.06	F	10	"	"	+ 2.08			"	
.06	R	10	"	"	- 1.72			"	
.06	F	10	7.107	12.24	+ 7.44		.88	.641	
.06	R	10	"	12.16	- 8.40	58.13	.87	"	
.06	F	10	"	12.07	+ 7.90	58.16	.86	"	
.06	R	10	"	12.02	- 9.0	62.0	.86	"	
.06	F	1	"	10.74	+ 2.71		.76		
.06	R	1	"	10.39	- 2.07	176.0	.75	"	
.06	F	1	"	10.74	+ 3.47	200.3	.725	"	
.06	R	1	"	9.653	- 3.38	252.2	.700	"	
.06	F	1	"	9.452	+ 3.90	21.80	.685	"	
.06	R	1	"	9.276	- 3.54	273.9	.652	"	
.06	F	1	"	9.170	+ 3.88	273.2	.642	"	
.06	R	1	"	8.606	- 3.5	271.7	.621	"	

EXPERIMENTAL SERIES II

LIQUID VISCOSITY DATA

GLASS INNER CYLINDER

Motor Freq f_o	Rotor Dir	Gain G	e_{ex} Volts	Thermom #2 m MHO	e^+ or e^- Volts	η Micro-Poise	Temp K	v cm/sec	
.06	F	1	7.107	8.299	+ 3.24	248.1	.59	.641	
.06	R	1	"	8.140	- 2.88	225.3	.575	"	
.06	F	1	"	8.016	+ 2.94	214.3	.565	"	
.06	R	1	"	7.946	- 2.68	206.9	.560	"	
.06	F	1	"	7.896	+ 2.806	202.0	.557	"	
.06	R	1	"	7.946	- 2.715	203.3	.558	"	
.06	F	1	"	7.701	+ 2.62				
.06	R	1	"	7.637	- 2.46	187.0	.525		
.06	F	1	"	6.651	+ 1.67			"	
.06	R	1	"	6.536	- 1.40	113.0	.470	"	
.06	F	1	"	6.313	- 1.36	106.6	.460	"	
.06	R	1	"	5.693	- .840				
.06	F	1	"	5.511	+ .83	61.49	.412	"	
.06	F	10	"	4.880	+ 5.48				
.06	R	10	"	4.695	- 3.90	34.29	.365	"	
.06	F	10	"	4.537	+ 4.1	29.34	.355		
.06	F	10	"	4.095	+ 3.20				
.06	R	10	"	3.981	- 2.22	19.88	"	"	
.06	R	10	"	3.502	- .8				
.06	F	10	"	3.388	+ 1.93	10.01	.289	"	
.06	F	100	"	2.848	+ 5.91				
.06	R	"	"	2.650	- 5.39	5.60	.246	"	
.15	R	10	7.11	.1403	- 1.38		.085	1.602	
.15	F	10	"	"	+ .2	2.24		"	
.15	R	10	"	"	- 1.40			"	

EXPERIMENTAL SERIES II

LIQUID VISCOSITY DATA

GLASS INNER CYLINDER

Motor Freq f_o	Rotor Dir	Gain G	e_{ex} Volts	Thermom #2 m MHO	e^+ or e^- Volts	η Micro-Poise	Temp K	v cm/sec	
.15	F	10	7.11	.1403	+ .55	2.76		1.602	
.05	R	100	"	.01637	- .20		.055	.534	
.05	F	100	"	.01988	+ 2.20	1.38	.057	"	
.05	R	100	"	.02168	+ .08	1.22	.058	"	
.05	F	100	"	.02710	+ 2.30	1.28	.060	"	
.05	R	100	"	.03283	- .34	1.52	.062	"	
.05	F	100	"	.04195	2.20	1.46	.066	"	
.05	R	100	"	.04762	- .30	1.44	.068	"	
.05	F	100	"	.09132	+ 1.70	1.15	.078	"	
.05	R	100	"	.1800	- .50	1.26	.091	"	
.05	F	100	"	.2334	+ 2.10	1.50	.097	"	
.05	R	100	"	.2075	- .83	1.68	.094	"	
.05	F	100	"	.2000	+ 2.00	1.63	.093	"	
.05	R	100	"	.6689	- 1.12	1.79	.131	"	
.05	F	100	"	.6780	+ 2.08	1.84		"	
.05	R	100	"	.6803	- 1.08	1.82		"	
.05	F	100	"	.6779	+ 1.40	1.43	.130	"	
.05	R	100	"	.6826	- 1.50	1.67		"	
.05	F	100	"	1.163	+ 2.04	2.04	.161	"	
.05	R	100	"	1.153	- 1.30	1.92	.159	"	
.05	F	100	"	1.161	+ 1.70	1.72	.160	"	
.05	R	100	"	1.157	- 1.86	2.04	.160	"	
.03	F	100	"	.01297	+ 1.12			.320	
.03	R	100	"	.01509	+ 0.04	1.03	.054	"	
.03	F	100	"	.01626	+ .96	.88		"	

EXPERIMENTAL SERIES II

LIQUID VISCOSITY DATA

GLASS INNER CYLINDER

Motor Freq f_o	Rotor Dir	Gain G	e_{ex} Volts	Thermom #2 m MHO	e^+ or e^- Volts	η Micro-Poise	Temp K	v cm/sec	
.03	F	100	7.11	.01789	+ 1.96			.320	
.03	R	100	"	.02107	+ .68	.83	.056	"	
.03	R	100	"	.02347	+ .50		.059	"	
.03	R	100	"		+ .04			"	
.03	F	100	"	1.331	+ 2.50	2.43		"	
.03	R	100	"		+ .80	1.68	.168	"	
.03	F	100	"		+ 2.44	1.62		"	
.03	R	100	"	1.318	+ .60	1.82		"	
.03	R	100	"		+ .50			"	
.03	F	100	"	1.761	+ 2.50	1.98		"	
.03	R	100	"		- .06	2.54	.192	"	
.03	F	100	"		+ 2.56	2.60		"	
.03	R	100	"		+ .60	2.60		"	
.03	F	100	"	2.564	+ .40			"	
.03	R	100	"		- 1.20	5.15		"	
.03	F	100	"		+ 3.66	4.81	.236	"	
.03	R	100	"		- 1.20	4.81		"	
.03	F	100	"		+ 3.66			"	
.03	R	100	"	2.165	+ .30	2.33	.215	"	
.03	F	100	"		+ 3.50	3.17		"	
.03	R	100	"		+ .30	3.17		"	
.03	F	100	"		+ 3.60	3.27		"	
.03	F	100	"	2.963	+ 6.04		.262	"	
.03	R	100	"		- 1.40	7.37		"	
.03	F	100	"		+ 5.70	7.03		"	

EXPERIMENTAL SERIES II

LIQUID VISCOSITY DATA

GLASS INNER CYLINDER

Motor Freq f_o	Rotor Dir	Gain G	e_{ex} Volts	Thermom #2 m MHO	e^+ or e^- Volts	η Micro-Poise	Temp K	v cm/sec	
.03	F	100	7.11	3.130	+ 1.30		.300	.320	
.03	R	100	"	3.696	- .52	13.3	.305	"	
			Added 7.0	x 10^{-5} STP	liters of He^3	to instrument package			
.06	F	100	7.11		+ 4.30			.641	
.06	R	100	"		+ .40	1.93			
.06	F	100	"	.2427	+ 3.94	1.75	.098		
.06	R	100	"		+ .10	1.90			
			Added additional 1.48 x 10^{-3} STP liters of He^3 to instrument package						
.06	F	100	7.11	.0962	+ .6		.078	.641	
.06	R	100	"		- 3.3	1.93		"	
.06	F	100	"	.1093	+ .3	1.78	.081	"	
.06	R	100	"		- 3.76	2.01		"	
.06	F	100	"	.1125	+ .16	1.94	.081	"	
.06	F	100	"	.1122	+ .60			"	
.06	R	100	"	.1119	- 4.50	2.53	.081	"	
.06	F	100	"		+ .2	2.33		"	
.06	R	100	"		- 4.70	2.43		"	
			Added an additional 5.15 x 10^{-3} STP liters of He^3 to instrument package						
.06	F	100	7.11	.03968	+ 2.0		.065	.641	
.06	R	100	"	.05038	- 1.8	1.9	.068	"	
.03	F	100	"	.07407	+ .48		.074	.320	
.03	R	100	"	.06126	- 1.20	1.66	.071	"	
.03	F	100	"		+ .16	1.35		"	
.03	R	100	"		- 1.40	1.54		"	
.03	F	100	"		+ .32			"	

EXPERIMENTAL SERIES II

LIQUID VISCOSITY DATA

GLASS INNER CYLINDER

Motor Freq f_o	Rotor Dir	Gain G	e_{ex} Volts	Thermom #2 m MHO	e^+ or e^- Volts	η Micro-Poise	Temp K	v cm/sec	
.03	R	100	7.11	.2141	- 1.10	1.41	.095	.320	
.03	R	100	"	.2999	- 2.8	2.38	.103	"	
.03	F	100	"		+ 1.2	1.20			
.03	F	10	"	22.34	- 1.388				
.03	R	10	"		- 3.644	16.52	2.04	"	
.03	F	10	"	22.43	- 1.328	16.95	2.05	"	
.03	R	10	"		- 3.510	15.97			
.06						55.9	.402		
						75.4	.43		
						86.8	.445		
						93.9	.452		
						101.5	.460		
						114.6	.468		
						119.6	.471		
						121.5	.465		
						126.2	.469		
						131.3	.476		
						138.7	.485		
						149.7	.493		
						166.6	.502		
						177.6	.510		
						193.8	.523		
						242.8	.575		
						279.9	.608		
						289.6	.623		

EXPERIMENTAL SERIES II

LIQUID VISCOSITY DATA

GLASS INNER CYLINDER

Motor Freq f_o	Rotor Dir	Gain G	e_{ex} Volts	Thermom #2 m MHO	e^+ or e^- Volts	η Micro-Poise	Temp K	v cm/sec	
.06						297.0	.652		
						289.4	.680		
						271.6	.705		
						247.7	.726		
						21.06	.337		
						35.0	.337		
						87.8	.442		
						269.7	.615		
						284.3			
						196.4	.755		
						88.88	.85		
						36.01	1.01		
						17.51	1.31		

EXPERIMENTAL SERIES III

LIQUID VISCOSITY DATA

GLASS INNER CYLINDER

Motor Freq f_o	Rotor Dir	Gain G	e_{ex} Volts	Ger Therm #2 m MHO	e^+ or e^- Volts	η Micro-Poise	Temp K	v cm/sec	
.085	R	100	6.458	5.725 ←	+ 7.90	7.858	0.248	.913	
"	F	"	6.435		- 8.50				
"	R	"	"	5.751	+ 7.76				
"	F	"	"	5.745	- 8.04	8.02	"	"	
"	R	"	6.441	"	+ 8.22				
"	R	"	6.427	5.104 ←	+ 4.40				
"	F	"	"	5.120	- 7.92	5.75	0.226	"	
"	F	"	"	5.271	- 8.16				
.010	F	"	"	4.912	- 1.68	1.632	0.218	.1074	
"	R	"	"	4.872 ←	- 1.28				
.005	R	10	6.444	12.758 ←	+ 1.380	234.0	0.524	.0537	
"	F	"	6.420	12.760	- 1.488				
.010	F	"			- 2.92	236.6	"	.1074	
"	R	"	6.407	12.762	+ 2.86				
.020	R	"		12.765	+ 5.797	237.5	"	.215	
"	F	"	6.410	12.760	- 5.82				
.040	F	1	6.042	12.760	- 1.121	235.5	"	.429	
"	R	"	6.048	"	+ 1.050				
.080	R	"		"	+ 2.155	235.5	"	.859	
"	F	"	6.053	"	- 2.192				
.160	F	"	5.426	"	- 3.980	237.8	"	1.718	
"	R	"	5.424	12.762	+ 3.892				
.320	R	"	4.718	12.760	+ 6.764	238.1	"	3.44	
"	F	"	4.707	12.761	- 6.910				
.600	F	"	3.594	12.760	- 9.260	186.8 ?	"	6.44	

EXPERIMENTAL SERIES III

LIQUID VISCOSITY DATA

GLASS INNER CYLINDER

Motor Freq f_o	Rotor Dir	Gain G	e_{ex} Volts	Ger Therm #2 m MHO	e^+ or e^- Volts	η Micro-Poise	Temp K	v cm/sec	
.600	F	1	3.593	12.760	+ 6.104				
.02	R	100	6.500	4.130	+ 1.16	1.13	0.192	.215	
"	F	"	"	"	+ 0.60				
.015	R	"	6.494	"	+ 1.26				
"	F	"		"	+ 0.58	1.94	"	.161	
"	R	"	6.467	"	+ 1.34				
.005	R	100	6.490	4.095 ←	+ 0.14				
"	F	"	"	"	0.00	1.13	.192	.0537	
"	R	"	"	4.098	+ 0.14				
"	R	"	6.515	4.096	0.00	.33	"	"	
"	F	"	"	"	- .04				
.020	F	"	6.513	4.217 ←	+ 1.64	1.21 (2 pts)	0.195	.215	
"	R	"	"	4.244	+ 1.08				
.10	R	"	6.498	4.534 ←	+ 5.64	4.41	0.206	1.074	
"	F	"	"	4.557	- 5.40				
"	F	"	"	4.769	- 6.26	4.71	0.214	"	
"	R	"	6.492	4.763	+ 5.40				
.20	R	10	6.490	5.701	+ 2.62	9.64	.245	2.147	
"	F	"	6.621	5.621 ←	- 2.16				
.5	R	1	5.004	8.295	+ 2.028	41.7 ?	0.337	5.36	
"	F	"	"	8.137 ←	- 2.136				
.85	F	"	"	10.242	- 9.52	113.7	0.417	9.13	
"	R	"	"	10.194 ←	+ 9.12				
2.0	R	"	4.002	16.854 ←	-38.14	249.5	0.736	21.47	
"	F	"	"	16.896	+38.44				

EXPERIMENTAL SERIES III

LIQUID VISCOSITY DATA

GLASS INNER CYLINDER

Motor Freq f_o	Rotor Dir	Gain G	e_{ex} Volts	Ger Therm #2 m MHO	e^+ or e^- Volts	η Micro-Poise	Temp K	v cm/sec	
1.2	R	1	4.002	12.738	-24.32				
"	F	"	"	12.755	-21.72	249.5	.522	12.88	
"	F	"	"	12.774	-21.95				
.5	F	"	"	"	- 8.92	226.3	"	5.36	
"	R	"	"	12.717	+ 8.34				
.7	R	"	"	12.746	-14.15	240.4	.528	7.52	
"	F	"	"	12.727	-11.72				
.4	F	"	"	12.736	- 7.17	233.0	"	4.29	
"	R	"	"	12.715 ←	+ 7.10				
1.4	R	1	4.002	12.803	+28.51	253.8	.525	15.03	
"	F	"	"	12.791	-26.23				
1.3	F	"	"	12.738	-23.83	254.0	"	13.96	
"	R	"	"	12.729	+26.18				
.3	R	"	"	12.780	+ 5.67	238.4	"	3.22	
"	F	"	"	12.771	- 5.26				
1.4	F	"	"	12.802	-26.28	253.7	"	15.03	
"	R	"	"	12.801	+28.54				
.8	R	"	"	12.784	+16.27	242.0	"	8.59	
"	F	"	"	12.776	-13.37				
.9	F	"	"	12.795	-15.64	243.2	"	9.66	
"	R	"	"	12.772	+17.91				
1.0	R	"	"	12.796	+20.26	246.7	"	10.74	
"	F	"	"	12.784	-17.64				
1.1	F	"	"	12.786	-19.86	250.6	"	11.81	
"	R	"	"	12.770 ←	+22.28				

EXPERIMENTAL SERIES III

LIQUID VISCOSITY DATA

GLASS INNER CYLINDER

Motor Freq f_o	Rotor Dir	Gain G	e_{ex} Volts	Ger Therm. #2 m MHO	e^+ or e^- Volts	η Micro-Poise	Temp K	v cm/sec	
.1	R	1	4.002	12.793	+ 2.026				
"	F	"	"	12.787	- 1.623	238.1	.525	1.074	
"	F	"	"	"	- 1.640				
1.7	R	"	"	12.841	+34.08	258.9			
"	F	"	"	12.798	-33.88	257.5	"	18.25	
"	R	"	"	12.785	+33.78				
.05	R	100	4.004	6.716←	+ 5.44	13.56	.285	.537	
"	F	"	"	6.708	- 4.96				
"	R	"	"	7.113	+ 6.02				
"	F	"	4.003	7.106←	- 7.94	18.10	.300	"	
"	R	"	"	7.117	+ 5.80				
"	R	10	4.002	8.275	+ 1.38				
"	F	"	4.003	8.273	- 1.54	38.54	.341	"	
"	F	"	"	"	- 1.58				
.2	F	1	4.003	10.668←	- 1.98	127.9	.435	2.15	
"	R	"	"	10.671	+ 1.87				
"	R	"	"	10.681	+ 1.98				
"	R	"	"	12.880	+ 3.364	243.4	.530	"	
"	F	"	"	12.879	- 3.794				
"	F	"	"	17.878	- 2.120	135.5	.794	"	
"	R	"	"	17.865	+ 2.015				
"	R	"	"	16.141	+ 4.035	266.2	.696	"	
"	Fq	"	"	16.143	- 4.090				
.1	F	"	"	16.154	- 2.060	265.1	"	1.074	
"	R	"	"	16.137	+ 1.986				

EXPERIMENTAL SERIES III

LIQUID VISCOSITY DATA

GLASS INNER CYLINDER

Motor Freq f_o	Rotor Dir	Gain G	e_{ex} Volts	Ger Therm #2 m MHO	e^+ or e^- Volts	η Micro-Poise	Temp K	v cm/sec	
.05	R	1	4.003	16.165	+ 0.970	263.4	.696	.537	
"	F	"	"	16.162	- 1.04				
.01	F	10	"	16.1[illegible]	- [illegible].17	3[illegible].1	"	.107[illegible]	
"	F	"	"	16.167	1.83				
.005	R	100	"	16.167	+ [illegible].20	23[illegible].[illegible]	"	.0537	
"	F	"	"	16.171	-1[illegible].86				
.10	F	1	"	16.[illegible]53	- [illegible].787	229.3	.734	.107[illegible]	
"	R	"	"	16.631	+ 1.702				
"	R	"	"	17.384	+ 1.236	166.2	.765	"	
"	F	"	"	"	- 1.315				
"	F	10	"	18.314	- [illegible].19	105.3	.823	"	
"	R	"	"	18.317	+ 7.88				
.01	R	100	"	18.313	+ [illegible].90	102.[illegible]	"	.1074	
"	F	"	4.003	18.310	- [illegible].83				
"	F	"	6.506	19.86	- [illegible].90	51.0	.920	"	
"	R	"	"	19.87	+ 3.74				
"	R	"	"	24.22	+ 0.44	20.2	1.21	"	
"	F	"	"	24.37	- 4.58				
.02	F	"	"	24.10	- 7.08	20.7	"	.215	
"	R	"	"	24.15	+ 3.17				
.04	R	"	"	24.13	+ 9.17	22.16	"	.429	
"	F	"	"	24.10	-12.82				
.06	F	10	"	24.00	- 2.08	25.0	"	.644	
"	R	"	"	23.92	+ 1.64				
.005	R	100	"	24.30	- 0.79	19.[illegible]	"	.0537	
"	F	"	"	"	- 3.26				

APPENDIX D

COMPUTER PROGRAMS

APPENDIX D

COMPUTER PROGRAMS

D1 Introduction

The computer used to develop the theory of the effective viscosity of liquid helium II in Section 3 and to plot the theoretical curves was an Apple II microcomputer with 48K byte memory, with a disk II floppy disk system, and a IDS-440 impact printer with graphic capability.

These programs are written in the Applesoft version of the BASIC computer language. Explanatory remarks have been amply inserted in the programs which should facilitate modifications of the programs to other microcomputer systems.

The programs presented in Appendix D are the ones used to make Figures 5.5 through 5.8. Even though these programs represent only a small part of the programs developed for this report, they represent the main substance from which the other programs can be readily developed.

To use the programs for the Apple II system described, two copyrighted programs are required. The "Hires Playground" available from Systems Design Lab and the "Paper Tiger Graphics Software" from Computer Stations, Inc.

Program #1 creates a log-log graph set of coordinate axes which is titled and labeled with the "Hires Playground" program, which is called in at statement 480 in Program #1. This log-log graph is then given a file name and stored on disk for use in Program #3. Program #2 creates a data file of the experimental data points which is given a file name

and stored on disk to be used in Program #3. A data file was created for each Experimental Series. Program #3 calls from the disk the previously created log-log graph and plots on this graph the experimental data points called from the data file. Following this, the program plots the theoretical curve for the selected parameters and then prints out the resulting graph on the IDS-440 graphic printer using the "Paper Tiger Graphic Software" at statement 1020 of Program #3.

APPENDIX D2

DEFINITION OF COMPUTER PROGRAM SYMBOLS

A = a = d/1: the ratio of the fluid gap to the mean free path.

D = d: the fluid gap (cm).

E = $E_1(a)$: the exponential integral, Equation (3.26).

F1 = $f(\delta_1)$: the fraction of diffuse scattered phonons from surface (1) Equation (3.25)

F2 = $f(\delta_2)$: the fraction of diffuse scattered phonons from surface (2) Equation (3.25)

G1 = γ_1: the surface smoothness ratio for surface (1), Equation (3.32).

G2 = γ_2: the surface smoothness ratio for surface (2), Equation (3.32).

G3 = γ_3: the specular reflection-slip factor for He^3 atoms.

G4 = γ_r: the specular reflection-slip factor for the rotons.

L1 = δ_1: the surface roughness factor for surface (1), (Å).

L2 = δ_2: the surface roughness factor for surface (2), (Å).

N = η_o: the velocity independent effective viscosity, (poise). Equation (3.137)

NH = $\eta_{ph} = \eta_{ph\text{-}ph,\ r,\ w,\ 3}$: the phonon component of the effective viscosity due to interaction with other phonons, rotons, the surface walls and the He^3 impurity, Equation (3.138)

NO = $\eta_{ph\text{-}ph,\ r,\ w}$: the phonon component of the effective viscosity due to interaction with other phonons, rotons, and surface wall, Equation (3.135).

NP = $\eta_{ph\text{-}ph,\ r}$: the coefficient of first viscosity, Equations (3.49) and (3.50).

NR = $\eta_r = \eta_{r\text{-}r,\ w,\ 3}$: the roton component of the effective viscosity due to the interaction with other rotons, surface walls and the He^3 impurity atoms, Equation (3.54).

N3 = η_3 = $\eta_{3\text{-r, w, }3}$: the He^3 impurity atoms component of the effective viscosity due to interaction with rotons, surface walls and other He^3 atoms, Equation (3.69).

T = T: the Kelvin temperature.

W = W(a): the viscosity "switching" function, Equation (3.134).

X3 = X_3: the concentration of He^3 impurity atoms.

Z = Z(a): the effective viscosity "switching" function, Equation (3.134).

PROGRAM # 1

```
10  REM  CATALOG FILE NAME: LOG GRAPH PLOT FOR TITLE
20  PRINT "LOG-LOG GRAFT PLOT WITH THE X AXIS RANGING FROM X1 TO
      X2 AND WITH THE Y AXIS RANGING FROM Y1 TO Y2"
30  REM  THIS PROGRAM PLOTS A LOG LOG GRAPH AXIS AND RESERVES 5
     SPACES TO THE LEFT OF THE Y AXIS FOR PRINTING NUMBERS AND T
     ITLE AND 2 LINES AT THE BOTTON OF THE X AXIS FOR PRINTING N
     UMBER DIVISIONS AND TITLE.
40  REM  USE THE HIRES PLAYGROUND PROGRAM TO EDIT THE GRAPH PLOT
      WITH NUMBERS AND TITLES.
50  INPUT "X1,X2,Y1,Y2:";X1,X2,Y1,Y2
55  PRINT
60  REM  CONSTANTS FOR RELATING COMPUTER AXIS TO LOG GRAPH AXIS
70  LET A1 = 174 / ( LOG (Y2) -  LOG (Y1)):B1 = 174 *  LOG (Y2) /
     ( LOG (Y2) -  LOG (Y1))
80  LET A2 = 244 / ( LOG (X1) -  LOG (X2)):B2 = 244 *  LOG (X1) /
     ( LOG (X1) -  LOG (X2))
82  PRINT "FOR THE X AXIS IF YOU WANT NUMERICALLY CONSECUTIVE NI
     MOR DIVISIONS MARKS BETWEEN THE MAJOR DIVISION MARKS : SELE
     CT (1) ; OR IF EVERY OTHER MINOR DIVISION IS TO BE MARKED S
     ELECT (2) ";: INPUT K
83  PRINT
84  IF K = 1 THEN D1 = 1:D2 = 8
85  IF K = 2 THEN D1 = 2:D2 = 6
86  IF K > 2 THEN  GOTO 82
88  PRINT "FOR THE Y AXIS IF YOU WANT NUMBERICALLY CONSECUTIVE M
     INOR DIVISION MARKS BETWEEN THE MAJOR DIVISIONS MARKS : SEL
     ECT (1) ;OR IF EVERY OTHER MINOR DIVISIONS ARE TO BE MARKED
      SELECT (2)";: INPUT K
89  PRINT
90  IF K = 1 THEN E1 = 1:E2 = 8
92  IF K = 2 THEN E1 = 2:E2 = 6
94  IF K > 2 THEN  GOTO 88
98  REM   FULL PAGE GRAPHICS
100  HGR : POKE  - 16302,0: HCOLOR= 7
110  REM  PLOT OUTER MARGINS
120  HPLOT 35,0 TO 279,0 TO 279,174 TO 35,174 TO 35,0
130  REM  PLOT MAJOR DIVISIONS ALONG X AXIS
140  LET N1 =  INT (1 +  LOG (X1) /  LOG (10)):N2 =  INT ( LOG (
     X2) /  LOG (10))
150  FOR N = N1 TO N2
160  LET W2 = 35 + B2 - A2 *  LOG (10 ↑ N)
170  HPLOT W2,0 TO W2,5: HPLOT W2,174 TO W2,169
180  REM  PLOT MINOR DIVISIONS ALONG X AXIS
190  NEXT N
200  FOR N = N1 - 1 TO N2
210  FOR J = 0 TO D2 STEP D1
220  LET X = (D1 + J) * 10 ↑ N:W2 = 35 + B2 - A2 *  LOG (X)
230  REM  TO LIMIT RANGE OF MINOR AXIS TO PLOT
240  IF X < X1 THEN 270
250  IF X > X2 THEN 280
260  HPLOT W2,0 TO W2,2: HPLOT W2,174 TO W2,172
270  NEXT J: NEXT N
280  LET N1 =  INT (1 +  LOG (Y1) /  LOG (10)):N2 =  INT ( LOG (
     Y2) /  LOG (10))
290  REM  PLOT MAJOR DIVISIONS ALONG Y AXIS
300  FOR N = N1 TO N2
310  LET W1 = B1 - A1 *  LOG (10 ↑ N)
320  HPLOT 35,W1 TO 40,W1: HPLOT 274,W1 TO 279,W1
```

```
330  NEXT N
340  REM  PLOT MINOR DIVISIONS ALONG Y AXIS
350  FOR N = N1 - 1 TO N2
360  FOR J = 0 TO E2 STEP E1
370  LET Y = (E1 + J) * 10 ↑ N:W1 = B1 - A1 *  LOG (Y)
380  REM   TO LIMIT MINOR DIVISIONS TO RANGE OF GRAPH
390  IF Y < Y1 THEN 420
400  IF Y > Y2 THEN 430
410  HPLOT 35,W1 TO 37,W1: HPLOT 277,W1 TO 279,W1
420  NEXT J: NEXT N
425  REM  AFTER VIEWING GRAPH PICTURE HIT ANY KEY TO CONTINUE PR
     AGRAM
430  GET A$
435  REM  SET TEXT WINDOW
440  POKE  - 16301,0
450  PRINT " DO YOU WANT A DIFFERENT LOG-LOG GRAPH (Y/N) ";: INPUT
     B$:B = B$ = "Y"
460  IF B THEN  TEXT : HOME : GOTO 20
470  PRINT "DO YOU WANT TO PRINT TITLES AND NUMBER DIVISIONS ON
     LOG-LOG GRAPH ? (Y/N).  IF YES (Y),INSERT * HIRES PLAYGROUN
     D * DISK TYPE 'Y' AND HIT RETURN";: INPUT B$:B = B$ = "Y"
480  TEXT : HOME :D$ =  CHR$ (4): IF B THEN  PRINT D$;"RUN HIRES
      PLAYGROUND"
485  PRINT
490  PRINT "DO YOU WANT TO SAVE GRAPH ON DISK (Y/N) ";: INPUT B$
     :B = B$ = "Y"
500  IF B THEN  GOTO 520
510  PRINT " GOOD BYE ": END
520  INPUT "FILE NAME OF GRAPH :";F$
530  PRINT D$;"BSAVE";F$;",A8182,L8192"
540  GOTO 510
```

PROGRAM #2

```
10  REM    CATALOG FILE NAME : CREATE FILE FROM DATA PTS.3
20  REM   IN ADDITION TO CREATING A DATA FILE THIS PROGRAM CAN D
     ISPLAY AND AMEND AN EXISTING FILE
30  REM  PROGRAM TO INPUT EXPERIMENTAL DATA INTO AN ARRAY AND TH
     EN INTO A SEQUENCIAL TEXT FILE ON DISK
40  REM  J IS THE NUMBER OF EXPERIMENTAL POINTS . T(I) AND N(I)
     FORM THE I TH EXPERIMENTAL POINT.
50  PRINT "STATE NAME OF DATA FILE";: INPUT A$
60  PRINT
90  INPUT "NUMBER OF DATA POINTS ?";J
100 K = J + 5: DIM T(K): DIM N(K)
105  REM  INPUT DATA POINTS INTO ARRAYS N(I) AND T(I) FOR I=1 TO
      J.
107  IF S = 2 THEN  GOTO 450
110  FOR I = 1 TO J
120  PRINT "T(";I;: PRINT ")=";: INPUT T(I)
130  PRINT "N(";I;: PRINT ")=";: INPUT N(I)
140  PRINT
150  NEXT I
160  PRINT "I"; SPC( 5);"T","N"
170  FOR I = 1 TO J
175  REM  DISPLAY DATA POINTS INPUTED AT SLOW SPEED
180  SPEED= 10
190  PRINT I; SPC( 5);T(I),N(I)
200  NEXT I
210  SPEED= 255
220  PRINT
230  PRINT "FOR CORRECTIONS TYPE AS 'T(2)=#;AND POINTS J=#.*****
     **THEN 'CONT' PLUS RETURN."
240  REM  THE BREAK PERMITS THE USER TO MAKE CORRECTIONS IN DATA

250  STOP
260  PRINT
270  PRINT "WANT EXPERIMENTAL POINTS PRINTED OUT AGAIN (Y/N)";: INPUT

     B$:B = B$ = "Y": IF B THEN  GOTO 160
280  PRINT
290  REM  CREATE A SEQUENTIAL TEXTFILE
300 D$ =  CHR$ (4)
310  PRINT D$;"OPEN";A$
320  PRINT D$;"DELETE";A$
330  PRINT D$;"OPEN";A$
340  PRINT D$;"WRITE";A$
350  PRINT J
360  FOR I = 1 TO J
370  PRINT T(I)
380  PRINT N(I)
390  NEXT I
400  PRINT D$;"CLOSE";A$
410  PRINT
420  PRINT "DATA FILE ";A$;: PRINT " COMPLETED"
430  PRINT
440  PRINT "FIRST FIELD CONTAINS NUMBER OF DATA POINTS J=";J;: PRINT
     ". THE REMAINING (2 * J) FIELDS CONTAIN THE DATA POINTS.
```

```
450  REM  VERIFY CONTENTS IN FILE
460 D$ =  CHR$ (4)
470  PRINT D$;"OPEN";A$
480  PRINT D$;"READ";A$
490  INPUT J
500  FOR I = 1 TO J
510  INPUT T(I)
520  INPUT N(I)
530  NEXT I
540  PRINT D$;"CLOSE";A$
550  PRINT
560  PRINT "CONTENTS OF DATA FILE"
570  PRINT "I"; SPC( 5);"T","N"
580  SPEED= 10
590  FOR I = 1 TO J
600  PRINT I; SPC( 5);T(I),N(I)
610  NEXT I
620  SPEED= 255
630  REM  BREAK SO THAT CORRECTIONS CAN BE MADE
640  PRINT "FOR CORRECTIONS TYPE AS 'T(2)=#;AND POINTS J=#.*****
     **THEN 'CONT' PLUS RETURN."
650  STOP
660  PRINT "DID YOU MAKE CORRECTION IN J,T(I) OR N(I, ? (Y/N) ";
     : INPUT B$:B = B$ = "Y"
670  IF B THEN  GOTO 300
680  PRINT
690  PRINT "DATA FILE IS COMPLETED; ** BYE ** "
700  END
```

PROGRAM #3

```
5  REM   CATALOG FILE NAME: HE-4 PLOT DTPO 5
10  REM  THIS PROGRAM PLOTS EXPERIMENTAL DATA FROM DATA FILE
20  REM   THIS PROGRAM PLOTS  THE HE-4 VISCOSITY USING THE EQUAT
     ION OF KHLATNIKOV, ZARKOV, WOODS AND HOLLIS HALLET AND THE
     EQUATIONS DEVELOPED BY PANDORF FOR THE WALL EFFECT AND THE
     TRANSITION REGION.
30  REM  THIS VERSION IS IN THE FORM USED IN THE FINAL REPORT
50  REM  RUN PARAMETERS WILL BE SET SO THAT  L1<=L2 SEE STATEMEN
     T 835
60  PRINT "INPUT D,G1,L1,G2,L2,X3"
70  INPUT D,G1,L1,G2,L2,X3
75  REM  TO CHANGE G3 OR G4 ENTER STATMENT 80
80 G4 = 1:G3 = 1
90  PRINT
110  PRINT "D="D;",G1="G1;", L1="L1;", X3="X3;", G2="G2;", L2="L
     2;", G4="G4;",G3="G3
115  PRINT
120  PRINT "ARE THESE OK ?": INPUT "(Y/N)?";B$:B = B$ = "Y": IF
      NOT B GOTO 60
125  PRINT
130  PRINT "NAME OF EXPERIMENTAL DATA FILE TO BE PLOTTED";: INPUT
     A$
140  PRINT
150  PRINT "IF DATA POINTS ARE TO APPEAR AS CROSSES SELECT 1, OR
      IF SQUARES SELECT 2 ";: INPUT K
160  REM  PLOTS DATA ON GRAFT PLOT PICTURE; X1,X2,Y1,AND Y2 ARE
     RANGE OF COORDINATES.
165  REM   G$ IS DISK FILE NAME OF LOG-LOG GRAPH PICTURE FROM PR
     OGRAM #1
167  REM  LIMITS OF X AXIS ARE X1 TO X2 ;LIMITS ON Y AXIS ARE Y1
      TO Y2
170 G$ = "LOG GRAFT FOR DATA 1.PIC":X1 = .06:X2 = 2:Y1 = 0.1:Y2 =
     400
180  REM   CONSTANTS FOR TRANSFORMATION EQUATION FOR COORDINATES

190 A1 = 174 / ( LOG (Y2) -  LOG (Y1)):B1 = 174 *  LOG (Y2) / ( LOG
     (Y2) -  LOG (Y1))
200 A2 = 244 / ( LOG (X1) -  LOG (X2)):B2 = 244 *  LOG (X1) / ( LOG
     (X1) -  LOG (X2))
210  HGR : HCOLOR= 7:D$ =  CHR$ (4)
220  REM   LOADING PRECOMPUTED LOG-LOG GRAPH PICTURE
230  PRINT D$;"BLOAD";G$;",A8192": POKE  - 16302,0
235  REM   READ DATA FILE INTO COMPUTER ;FILE CREATED BY PROGRAM
      #2
240  PRINT D$;"OPEN";A$
250  PRINT D$;"READ";A$
260  INPUT J
265 U = J + 5: DIM T(U): DIM N(U)
270  FOR I = 1 TO J
280  INPUT T(I)
285  INPUT N(I)
290  NEXT I
300  PRINT D$;"CLOSE";A$
310  FOR I = 1 TO J
```

```
320  REM  TRANSFORMATION EQUATION RELATING COORDINATES OF EXPERI
     MENTAL POINT TO COMPUTER COORDINATES
330 Y = B1 - A1 *  LOG (N(I)):X = 35 + B2 - A2 *  LOG (T(I))
335  REM  RANGE LIMITS TO LIMIT POINT TO GRAPH
340  IF X > 276 OR X < 38 THEN  GOTO 390
345  IF Y < 3 OR Y > 173 THEN  GOTO 390
350  IF K = 1 THEN 380
355  REM  SQUARE POINTS
360  HPLOT X + 2,Y + 2 TO X + 2,Y - 2 TO X - 2,Y - 2 TO X - 2,Y +
     2 TO X + 2,Y + 2: GOTO 390
370  GOTO 290
375  REM  CROSS POINTS
380  HPLOT X - 2,Y TO X + 2,Y: HPLOT X,Y - 2 TO X,Y + 2
390  NEXT I
400  REM   PLOT THEORETICAL VISCOSITY
410 XO = 35:YO = 174
420  REM  NEW COMPUTER COORDINATES W2,W1
430  FOR W2 = 35 TO 279 STEP 3
440 T =  EXP ((B2 - W2 + 35) / A2)
445  REM  FOR TEMP. T COMPUTE VISCOSITY N. (N IN UNITS OF POISE)

450  GOSUB 640
460 W1 = B1 - A1 *  LOG (N * 10 ↑ 6)
470  REM  TO KEEP COORDINATES WITHIN PLOT
480  IF W1 > 174 THEN W1 = 174
490  IF W1 < 0 THEN W1 = 0
500  HPLOT W2,W1
520  NEXT W2
530  REM   OPEN TEXT WINDOW ON SCREEN
540  POKE  - 16301,0
545  PRINT
550  PRINT "DO YOU WANT DIFFERENT INPUT  PARAMETERS ?";: INPUT "
     (Y/N)?";B$:B = B$ = "Y": IF B GOTO 60
555  PRINT
560  PRINT "DO YOU WANT A PRINT OUT ?": INPUT "(Y/N)?";B$:B = B$
      = "Y": IF B GOTO 980
570  PRINT "DO YOU WANT TO SAVE THIS PLOT ON DISK ?": INPUT "(Y/
     N)?";B$:B = B$ = "Y": IF B GOTO 590
580  TEXT : HOME : PRINT "GOOD BYE": END
585  REM   TO SAVE GRAPH ON DISK
590  INPUT "FILE NAME FOR PLOT :";F$
600  PRINT  CHR$ (4);"BSAVE";F$;", A8192,L8192"
610  TEXT : HOME : PRINT "GOOD BYE": END
620  REM  SUBROUTINE TO COMPUTE THEORETICAL VISCOSITY
630  REM  TO PREVENT OVERFLOW
640  IF T < .12 THEN Y = 10 ↑ 34: GOTO 690
650 Y =  EXP (8.65 / T)
660  REM  SELECT THE 5 PHONON EQUATION FOR T>0.8K OTHERWISE THE
     4 PHOKON EQUATION
670  IF T > 0.8 THEN 710
680  REM  KHALATNIKOV'S 4 PHONON EQUATION WITH NO ADJUSTMENTS
690 NP = 3.50 * 10 ↑  - 9 * T ↑  - .5 * Y / (1 + 2.15 * 10 ↑  -
     5 * T ↑ 4.5 * Y):A = .03 * T ↑ 4 * D / NP: GOTO 730
700  REM  THE 5 PHONON EQUATION
710 NP = 3.5 * 10 ↑  - 8 * T ↑  - .5 * Y * (1 + 2.66 * 10 ↑  - 4
      * T ↑ 4.5 * Y) / (1 + 4.26 * 10 ↑  - 3 * T ↑ 4.5 * Y):A =
     .030 * T ↑ 4 * D / NP
720  REM  COMPUTE THE EXPONENTIAL INTEGRAL
730 S = A: GOSUB 740:E = E0: GOTO 770
740  IF S > 1 THEN 760
```

```
750 E0 =  - .57722 -  LOG (S) + S - .24991 * S ↑ 2 + .0552 * S ↑
    3 - .00976 * S ↑ 4 + .00108 * S ↑ 5: RETURN
760 E0 =  EXP ( - S) * (S ↑ 2 + 2.3347 * S + .2506) / (S ↑ 3 + 3
    .3307 * S ↑ 2 + 1.6815 * S): RETURN
770 W = 1 - (A + 1) *  EXP ( - A) + A ↑ 2 * E
780 Z = (1 - A) *  EXP ( - A) + A ↑ 2 * E
790  REM   COMPUTE THE SPECULAR REFLECTION FUNCTION, F
800 X1 = 114 / (L1 * T):X2 = 114 / (L2 * T):Q1 = .1633 * X1 ↑ 2:
    Q2 = .1633 * X2 ↑ 2
810 S = Q1: GOSUB 740:E1 = E0:S = Q2: GOSUB 740:E2 = E0
820 F1 = .079 * ( EXP ( - Q1) - Q1 * E1) + 2 * X1 ↑ 3 *  EXP ( -
    X1) * (1 + 5 / X1 + 12 / X1 ↑ 2 + 12 / X1 ↑ 3) / 25.98
830 F2 = .079 * ( EXP ( - Q2) - Q2 * E2) + 2 * X2 ↑ 3 *  EXP ( -
    X2) * (1 + 5 / X2 + 12 / X2 ↑ 2 + 12 / X2 ↑ 3) / 25.98
835  IF L1 <  = L2 THEN F = F1
840  IF L2 < L1 THEN F = F2
845  REM   TO PREVENT OVERFLOW
850  IF T < .08 THEN 880
860  REM  COMPUTE THE PHONON COMPONENT
870 N0 = NP * W / (1 + 4 / (3 * A) * (W / (1 - Z)) * (.21 * ((G1
     * F1 + G2 * F2) / (G1 * F1 * F2 * G2) - 1))) + .106 * F *
    T ↑ 4 * D * Z * G1 * G2 * (G1 + G2 - G1 * G2) ↑  - 1: GOTO
    890
880 N0 = .106 * F * D * Z * G1 * G2 * T ↑ 4 * (G1 + G2 - G1 * G2
    ) ↑  - 1
890 NH = (1 / N0 + 3.0 * 10 ↑ 7 * X3) ↑  - 1
900  REM  COMUTE THE ROTON COMPONENT
910 NR = (7.94 * 10 ↑ 4 + 2.0 * 10 ↑ 4 * X3 * Y + 2.8 * 10 ↑  -
    4 * Y / (G4 * D * T ↑ .5)) ↑  - 1
920  REM  COMPUTE THE HE-3 COMPONENT
930 N3 = (1.87 * 10 ↑ 5 / T ↑ .5 + 1.4 * 10 ↑ 6 / (Y * X3) + 1.6
     * 10 ↑  - 3 / (G3 * X3 * D * T ↑ .5)) ↑  - 1
940  REM  COMPUTE THE EFFECTIVE VISCOSITY
950 N = NH + NR + N3
960  RETURN
970  REM  SUBROUTINE TO PRINT OUT PLOT ON IDS 440 PRINTER
980 IP = 7936:SA = IP + 10:SB = SA + 8:HP = SB + 5:F = IP:W = 17
    84
990  GOSUB 1000: GOTO 1040
1000 X = 0: FOR I = HP TO I + 227:X = X +  PEEK (I): NEXT
1010  IF X = 17402 THEN  RETURN
1015  REM    MACHINE LANGUAGE SUBROUTINE WHICH PRINT HIRES PICTU
    RE ON IDS 440 GRAPHIC PRINTER. A 7936; AVAILABLE FROM COMPU
    TER STATION,INC.
1017  PRINT "INSERT GRAPHIC DISK, HIT RETURN THEN RE-INSERT DATA
     DISK": INPUT Y$
1020  PRINT "BLOAD IDS440P4.OBJ,A";IP
1030  RETURN
1040 S = 1
1050  POKE SA,192 + S
1060  POKE SB,128 + S * 16
1070  GR : POKE  - 16297,0
1080  POKE F,0: GR : POKE  - 16297,0
1090  INPUT "EXPAND SCREEN (Y/N) ?";B$:B = B$ = "Y":FB = 64
1100  IF B THEN  POKE F, PEEK (F) + FB
1105  REM  ADDS SPACES BETWEEN GRAPH PRINT OUTS
1110  FOR I = 1 TO 6
1120  PRINT "PR#1": PRINT : PRINT "PR#0"
1130  NEXT I
1140  POKE  - 16302,0
```

```
1150  CALL HP
1160  POKE  - 16301,0
1165  REM  PRINT TITLE AND PARAMETERS
1170  PRINT "NAME TITLE OF FIGURE";: INPUT T$
1180  PR# 1
1185  PRINT
1190  PRINT
1195  PRINT
1200  PRINT  SPC( 3);T$;", D="D;", G1="G1;", L1="L1
1210  PRINT  SPC( 3);"X3="X3;", G2="G2;", L2="L2
1220  PR# 0
1230  PRINT "DO YOU WANT ANOTHER PRINT OUT OF THE GRAPH (Y/N) ";
      : INPUT B$:B = B$ = "Y"
1240  IF B THEN  GOTO 980
1250  GOTO 570
```

DISTRIBUTION LIST

Defense Documentation Center Cameron Station Alexandria, VA 22314	12#
Office of Naval Research (Code 221) 800 North Quincy Street Arlington, VA 22217	1* 6**
Office of Naval Research (Code 420) 800 North Quincy Street Arlington, VA 22217	2**
Director (Code 2627) Naval Research Laboratory 4555 Overlook Avenue, S.W. Washington, DC 20375	1**
Strategic Systems Projects (SP-24) Department of the Navy Washington, DC 20376	1**
Commander, Naval Sea Systems Command Attn: Code 0341 Department of the Navy Washington, DC 20360	1**
Defense Advanced Research Projects Agency/STO 1400 Wilson Boulevard Arlington, VA 22209	1*
Office of Naval Research Branch Office Building 114, Section D 666 Summer Street Boston, MA 02210	1**
Commander, Defense Contract Administration Services District 666 Summer Street Boston, MA 02210	1**

\# To be forwarded with DDC Form 50
* To be forwarded w/o AD number
** Distribution to await assignment of AD number

END

DATE
FILMED
6-81

DTIC